

ISSN 1881-7815 Online ISSN 1881-7823

BST

BioScience Trends

Volume 10, Number 6
December, 2016



www.biosciencetrends.com

BST

BioScience Trends



ISSN: 1881-7815
Online ISSN: 1881-7823

CODEN: BTIRCZ

Issues/Year: 6

Language: English

Publisher: IACMHR Co., Ltd.

BioScience Trends is one of a series of peer-reviewed journals of the International Research and Cooperation Association for Bio & Socio-Sciences Advancement (IRCA-BSSA) Group and is published bimonthly by the International Advancement Center for Medicine & Health Research Co., Ltd. (IACMHR Co., Ltd.) and supported by the IRCA-BSSA and Shandong University China-Japan Cooperation Center for Drug Discovery & Screening (SDU-DDSC).

BioScience Trends devotes to publishing the latest and most exciting advances in scientific research. Articles cover fields of life science such as biochemistry, molecular biology, clinical research, public health, medical care system, and social science in order to encourage cooperation and exchange among scientists and clinical researchers.

BioScience Trends publishes Original Articles, Brief Reports, Reviews, Policy Forum articles, Case Reports, News, and Letters on all aspects of the field of life science. All contributions should seek to promote international collaboration.

Editorial Board

Editor-in-Chief:

Norihiro KOKUDO
The University of Tokyo, Tokyo, Japan

Co-Editors-in-Chief:

Xue-Tao CAO
Chinese Academy of Medical Sciences, Beijing, China
Rajendra PRASAD
University of Delhi, Delhi, India
Arthur D. RIGGS
Beckman Research Institute of the City of Hope, Duarte, CA, USA

Chief Director & Executive Editor:

Wei TANG
The University of Tokyo, Tokyo, Japan

Senior Editors:

Xunjia CHENG
Fudan University, Shanghai, China
Yoko FUJITA-YAMAGUCHI
Beckman Research Institute of the City of Hope, Duarte, CA, USA
Na HE
Fudan University, Shanghai, China
Kiyoshi KITAMURA
The University of Tokyo, Tokyo, Japan
Misao MATSUSHITA
Tokai University, Hiratsuka, Japan
Munehiro NAKATA
Tokai University, Hiratsuka, Japan
Takashi SEKINE

Toho University, Tokyo, Japan
Ri SHO
Yamagata University, Yamagata, Japan
Yasuhiko SUGAWARA
Kumamoto University, Kumamoto, Japan
Ling WANG
Fudan University, Shanghai, China

Managing Editor:

Jianjun GAO
Qingdao University, Qingdao, China

Web Editor:

Yu CHEN
The University of Tokyo, Tokyo, Japan

Proofreaders:

Curtis BENTLEY
Roswell, GA, USA
Christopher HOLMES
The University of Tokyo, Tokyo, Japan
Thomas R. LEBON
Los Angeles Trade Technical College, Los Angeles, CA, USA

Editorial Office

Pearl City Koishikawa 603,
2-4-5 Kasuga, Bunkyo-ku, Tokyo 112-0003, Japan
Tel: +81-3-5840-8764 Fax: +81-3-5840-8765
E-mail: office@biosciencetrends.com

BioScience Trends

Editorial and Head Office

Pearl City Koishikawa 603, 2-4-5 Kasuga, Bunkyo-ku,
Tokyo 112-0003, Japan

Tel: +81-3-5840-8764, Fax: +81-3-5840-8765
E-mail: office@biosciencetrends.com
URL: www.biosciencetrends.com

Editorial Board Members

Girdhar G. AGARWAL (Lucknow, India)	(Daejeon, Korea)	Yutaka MATSUYAMA (Tokyo, Japan)	(Tokyo, Japan)
Hirosugu AIGA (Geneva, Switzerland)	Takahiro HIGASHI (Tokyo, Japan)	Qingyue MENG (Beijing, China)	Sumihito TAMURA (Tokyo, Japan)
Hidechika AKASHI (Tokyo, Japan)	De-Xing HOU (Kagoshima, Japan)	Mark MEUTH (Sheffield, UK)	Puay Hoon TAN (Singapore, Singapore)
Moazzam ALI (Geneva, Switzerland)	Sheng-Tao HOU (Ottawa, Canada)	Satoko NAGATA (Tokyo, Japan)	Koji TANAKA (Tsu, Japan)
Ping AO (Shanghai, China)	Yong HUANG (Ji'ning, China)	Miho OBA (Odawara, Japan)	John TERMINI (Duarte, CA, USA)
Hisao ASAMURA (Tokyo, Japan)	Hirofumi INAGAKI (Tokyo, Japan)	Fanghua QI (Ji'nan, Shandong)	Usa C. THISYAKORN (Bangkok, Thailand)
Michael E. BARISH (Duarte, CA, USA)	Masamine JIMBA (Tokyo, Japan)	Xianjun QU (Beijing, China)	Toshifumi TSUKAHARA (Nomi, Japan)
Boon-Huat BAY (Singapore, Singapore)	Kimitaka KAGA (Tokyo, Japan)	John J. ROSSI (Duarte, CA, USA)	Kohjiro UEKI (Tokyo, Japan)
Yasumasa BESSHO (Nara, Japan)	Ichiro KAI (Tokyo, Japan)	Carlos SAINZ-FERNANDEZ (Santander, Spain)	Masahiro UMEZAKI (Tokyo, Japan)
Generoso BEVILACQUA (Pisa, Italy)	Kazuhiro KAKIMOTO (Osaka, Japan)	Yoshihiro SAKAMOTO (Tokyo, Japan)	Junming WANG (Jackson, MS, USA)
Shiuan CHEN (Duarte, CA, USA)	Kiyoko KAMIBEPPU (Tokyo, Japan)	Erin SATO (Shizuoka, Japan)	Xiang-Dong Wang (Boston, MA, USA)
Yuan CHEN (Duarte, CA, USA)	Haidong KAN (Shanghai, China)	Takehito SATO (Isehara, Japan)	Hisashi WATANABE (Tokyo, Japan)
Naoshi DOHMAE (Wako, Japan)	Bok-Luel LEE (Busan, Korea)	Akihito SHIMAZU (Tokyo, Japan)	Lingzhong XU (Ji'nan, China)
Zhen FAN (Houston, TX, USA)	Mingjie LI (St. Louis, MO, USA)	Zhifeng SHAO (Shanghai, China)	Masatake YAMAUCHI (Chiba, Japan)
Ding-Zhi FANG (Chengdu, China)	Shixue LI (Ji'nan, China)	Judith SINGER-SAM (Duarte, CA, USA)	Aitian YIN (Ji'nan, China)
Xiaobin FENG (Chongqing, China)	Ren-Jang LIN (Duarte, CA, USA)	Raj K. SINGH (Dehradun, India)	George W-C. YIP (Singapore, Singapore)
Yoshiharu FUKUDA (Ube, Japan)	Xinqi LIU (Tianjin, China)	Peipei SONG (Tokyo, Japan)	Xue-Jie YU (Galveston, TX, USA)
Rajiv GARG (Lucknow, India)	Daru LU (Shanghai, China)	Junko SUGAMA (Kanazawa, Japan)	Benny C-Y ZEE (Hong Kong, China)
Ravindra K. GARG (Lucknow, India)	Hongzhou LU (Shanghai, China)	Hiroshi TACHIBANA (Isehara, Japan)	Yong ZENG (Chengdu, China)
Makoto GOTO (Tokyo, Japan)	Duan MA (Shanghai, China)	Tomoko TAKAMURA (Tokyo, Japan)	Xiaomei ZHU (Seattle, WA, USA)
Demin HAN (Beijing, China)	Masatoshi MAKUUCHI (Tokyo, Japan)	Tadatoshi TAKAYAMA (Tokyo, Japan)	(as of December 30, 2016)
David M. HELFMAN	Francesco MAROTTA (Milano, Italy)	Shin'ichi TAKEDA	

Reviews

- 424 - 432 **Current status of genome editing in vector mosquitoes: A review.**
Appadurai Daniel Reegan, Stanislaus Antony Ceasar, Michael Gabriel Paulraj, Savarimuthu Ignacimuthu, Naif Abdullah Al-Dhabi
- 433 - 444 **The interconnected role of chemokines and estrogen in bone metabolism.**
Yingping Xu, Nan Chu, Xuemin Qiu, Hans-Jürgen Gober, Dajin Li, Ling Wang

Original Articles

- 445 - 453 **Anemia in combined antiretroviral treatment-naive HIV-infected patients in China: A retrospective study of prevalence, risk factors, and mortality.**
Guorui Dai, Jiang Xiao, Guiju Gao, Xuejing Chong, Fang Wang, Hongyuan Liang, Liang Ni, Di Yang, Fengting Yu, Ling Xu, Di Wang, Junyan Han, Hui Zeng, Hongxin Zhao
- 454 - 459 **The expression of miR-124 increases in aged skin to cause cell senescence and it decreases in squamous cell carcinoma.**
Miho Harada, Masatoshi Jinnin, Zhongzhi Wang, Ayaka Hirano, Yukiko Tomizawa, Tomomi Kira, Toshikatsu Igata, Shinichi Masuguchi, Satoshi Fukushima, Hironobu Ihn
- 460 - 466 **Effects of STAT3 inhibitors on neural functional recovery after spinal cord injury in rats.**
Meng Cui, Xinlong Ma, Jie Sun, Jinquan He, Lin Shen, Fangguo Li
- 467 - 476 **Induction of apoptosis by ethanol extract of *Evodia rutaecarpa* in HeLa human cervical cancer cells via activation of AMP-activated protein kinase.**
Seon Young Park, Cheol Park, Shin-Hyung Park, Su-Hyun Hong, Gi-Young Kim, Sang Hoon Hong, Yung-Hyun Choi
- 477 - 481 **The fractal based analysis of human face and DNA variations during aging.**
Hamidreza Namazi, Amin Akrami, Jamal Hussaini, Osmar N. Silva, Albert Wong, Vladimir V. Kulish
- 482 - 488 **MiR-15a-5p regulates viability and matrix degradation of human osteoarthritis chondrocytes via targeting VEGFA.**
Hongwei Chen, Yun Tian
- 489 - 495 **TGP attenuates endoplasmic reticulum stress and regulates the expression of thioredoxin-interacting protein in the kidneys of diabetic rats.**
Yunxia Shao, Xiangming Qi, Xinxing Xu, Kun Wang, Yonggui Wu, Lingling Xia

Brief Reports

- 496 - 499 **Ledipasvir and sofosbuvir for recurrent hepatitis C after liver transplantation.**
Yuki Oya, Yasuhiko Sugawara, Takehisa Watanabe, Yoko Yoshimaru, Masaki Honda, Shintaro Hashimoto, Daiki Yoshii, Kaori Isono, Shintaro Hayashida, Hidekazu Yamamoto, Motohiko Tanaka, Yutaka Sasaki, Yukihiro Inomata
- 500 - 506 **A novel angiogenic peptide, Δ ADT: A truncated adrenotensin peptide revealed by secretory peptidome analysis of human retinal pericytes.**
Akinori Okumura, Eri Takahashi, Hiroyuki Unoki-Kubota, Yasushi Kaburagi
- 507 - 511 **Endoscopic and surgical ampullectomy for non-invasive ampullary tumors: Short-term outcomes.**
Margaux Dubois, Ismail Labгаа, Gian Dorta, Nermin Halkic

Guide for Authors

Copyright

Current status of genome editing in vector mosquitoes: A review

Appadurai Daniel Reegan^{1,2}, Stanislaus Antony Ceasar³, Michael Gabriel Paulraj¹, Savarimuthu Ignacimuthu^{1,3,4,*}, Naif Abdullah Al-Dhabi⁵

¹ Division of Vector Control, Entomology Research Institute, Loyola College, Tamil Nadu, India;

² Department of Zoology, Madras Christian College, Tamil Nadu, India;

³ Division of Molecular Biology, Entomology Research Institute, Loyola College, Tamil Nadu, India;

⁴ International Scientific Partnership Program, Deanship of Research, King Saud University, Saudi Arabia;

⁵ Department of Botany and Microbiology, Addiriyah chair for Environmental Studies, College of Science, King Saud University, Saudi Arabia.

Summary

Mosquitoes pose a major threat to human health as they spread many deadly diseases like malaria, dengue, chikungunya, filariasis, Japanese encephalitis and Zika. Identification and use of novel molecular tools are essential to combat the spread of vector borne diseases. Genome editing tools have been used for the precise alterations of the gene of interest for producing the desirable trait in mosquitoes. Deletion of functional genes or insertion of toxic genes in vector mosquitoes will produce either knock-out or knock-in mutants that will check the spread of vector-borne diseases. Presently, three types of genome editing tools viz., zinc finger nuclease (ZFN), transcription activator-like effector nucleases (TALEN) and clustered regulatory interspaced short palindromic repeats (CRISPR) and CRISPR associated protein 9 (Cas9) are widely used for the editing of the genomes of diverse organisms. These tools are also applied in vector mosquitoes to control the spread of vector-borne diseases. A few studies have been carried out on genome editing to control the diseases spread by vector mosquitoes and more studies need to be performed with the utilization of more recently invented tools like CRISPR/Cas9 to combat the spread of deadly diseases by vector mosquitoes. The high specificity and flexibility of CRISPR/Cas9 system may offer possibilities for novel genome editing for the control of important diseases spread by vector mosquitoes. In this review, we present the current status of genome editing research on vector mosquitoes and also discuss the future applications of vector mosquito genome editing to control the spread of vector-borne diseases.

Keywords: Gene alteration, mosquito borne disease control, zinc finger nuclease (ZFN), transcription activator-like effector nuclease (TALEN), clustered regulatory interspaced short palindromic repeats (CRISPR)/CRISPR associated protein 9 (Cas9)

1. Introduction

Mosquitoes are arthropod vectors responsible for the transmission of several disease causing pathogens. Dengue, chikungunya, malaria, filariasis and Japanese encephalitis are the major mosquito borne diseases

responsible for thousands of deaths each year (1,2). A recent outbreak of Zika is also caused by a vector mosquito *Aedes aegypti*. The World Health Organization declared a Public Health Emergency of International Concern due the outbreak of Zika in South America (3). So mosquitoes pose a great threat to public health and affect the economy of several countries. For the past several decades, synthetic insecticides were being used to control vector mosquitoes. Unfortunately, synthetic insecticides cause environmental pollution and kill many beneficial insects (4,5). Further, continuous use of synthetic insecticide has also resulted in the development of resistance in vector mosquitoes (6).

Recent advances in the field of genetic technologies

Released online in J-STAGE as advance publication December 18, 2016.

*Address correspondence to:

Dr. Savarimuthu Ignacimuthu, Division of Vector Control, Entomology Research Institute, Loyola College, Chennai-600034, Tamil Nadu, India.

E-mail: eriloyola@hotmail.com

have strengthened our understanding on creation of anti-pathogenic mosquito strains (7-10), sterile mosquito strains (11,12) and genetically modified strains (13-15). Especially the discovery of modern genome editing technologies provide many opportunities to edit new target genes, to analyze the functions of target genes more accurately and to modify the expression levels of target genes (upregulation or downregulation). As per Criscione *et al.*, 12 different classes of genetic-based technologies have been used as functional genomic tools for the control of insect vectors (16). Genome editing technology is one among them and it has been emerging as a powerful tool that can alter the genome more precisely.

Three types of genome editing tools are widely used for engineering the genomes of diverse species including vector mosquitoes. These are zinc finger nuclease (ZFN), transcription activator-like effector nucleases (TALEN) and clustered regulatory interspaced short palindromic repeats (CRISPR) and CRISPR associated protein 9 (Cas9). The ZFN based genome editing technique was initially applied in *Drosophila melanogaster* (17,18). This approach stimulated diverse ideas to carry out modifications in the genome of any insect. Following this, researchers have reported the successful application of ZFN and TALEN based genome editing technology in plants (19-22) and other animals (23,24). However after the discovery of CRISPR/Cas9 in 2012 (25), many researchers have successfully applied this technique to diverse organisms including mosquitoes and cell lines for precise genome editing. These genome editing technologies enable the alteration of target genes in insect pest, particularly useful for the control of vector-borne diseases caused by mosquitoes. Although excellent reviews are available on mosquito genome editing with these techniques (26-32), we present the recent application of these techniques in vector mosquito gene manipulation for the control mosquito borne diseases especially by CRISPR/Cas9, off-target effects of these tools, ethical issues and current problems in application of genome editing techniques in vector mosquitoes.

2. Major genome editing tools

Three major genome editing tools are currently applied for target specific alteration of genomes of diverse organisms. These are ZFN, TALEN and CRISPR/Cas9, although other techniques like meganuclease-mediated genome editing are proposed. ZFNs are one of the genome editing tools developed initially which was based on the specificity of DNA binding protein ZFN. ZFN is a target-specific endonuclease designed to bind and cleave DNA at desired positions of the genome. ZFN consists of DNA binding domain with zinc finger which recognizes the specific sequence on the genome and nuclease domain made up of *FokI*

enzyme which cleaves the specific site of DNA. DNA-binding domains of individual ZFNs typically contain three to six individual zinc finger repeats and each finger can recognize 3 base pairs. Through this strategy it is possible for ZFN to induce double-stranded breaks (DSB) at a specific region on the genome and with the help of endogenous DNA repair this technique was used by several groups to accurately alter the genome sequence of higher organisms (33-36). TALEN based genome editing is easy to engineer compared to ZFN and it is also more specific to target sequence (37). DNA binding domain of TALEN contains a highly conserved repeat of 33-34 amino acid sequence with difference at 12th and 13th amino acids. These two positions are highly variable and show a strong correlation with specific nucleotide recognition in the genome. This relationship between amino acid sequence and DNA recognition enabled the engineering of specific DNA-binding domains. DNA binding domain is fused with the *FokI* nuclease enzyme which confers extreme site specificity and has expanded the possibility of specific editing in a number of genomes (38,39).

CRISPR/Cas9 is a RNA-guided endonuclease technology that has been considered as a highly versatile tool for making breaks in the genomes of bacteria, yeast, plants and animals. CRISPR/Cas9 is the latest addition in the genome editing tool box. Compared to ZFN and TALEN, the creation of CRISPR/Cas9 constructs is several times easier and it is also more convenient to handle. CRISPR/Cas9 was found to function as an acquired immune system against viruses and phages through CRISPR RNA (crRNA)-guided DNA binding and Cas9 nucleases-mediated DNA breakage in bacteria and archaea (40). In genome editing, CRISPR/Cas9 works with the help of the single guide RNA (sgRNA) which recognises the target sequence (protospacer) in the genome of host organism through complementary base pairing (25). Then the Cas9 nuclease specifically makes a double-stranded break (DSB) at a region near to the PAM (Protospacer Adjacent Motif) sequence. The invention of sgRNAs was the major breakthrough in this field which was initially used along with Cas9 to create breaks in various DNA sites *in vitro* (25). Following this, several papers have been published utilizing this technology for precise genome engineering in cell lines and in diverse organisms (reviewed in 41-43).

3. Application of genome editing in vector mosquitoes

The invention and rapid development of tools like CRISPR/Cas9 have significantly expanded the scope of genome editing research that can be achieved in a broad range of organisms including vector mosquitoes. Further, the well established procedures are additional advantages which increase our ability to work on manipulation of mosquito genome. As per Franz *et al.* genome editing

Table 1. Details on various genome editing studies undertaken in mosquitoes using ZFN, TALEN and CRISPR/Cas9 systems

Mosquito species	Genome editing tool	Targeted genes	Application	Ref.
<i>Ae. aegypti</i>	ZFN	<i>AaegGr3</i>	Disruption of sensory pathways-dengue control	2014 (61)
<i>Ae. aegypti</i>	ZFN	<i>Orco</i>	Disruption of odorant receptor pathways-dengue control	2013 (14)
<i>Ae. aegypti</i>	ZFN	<i>npylr1</i>	Disruption of blood feeding behavior-dengue control	2013 (60)
<i>Ae. aegypti</i>	TALEN	<i>Kmo</i>	Lack of eye pigmentation-dengue control	2013 (13)
<i>An. gambiae</i>	TALEN	<i>TEP1</i>	Immune pathways-malaria control	2013 (15)
<i>Ae. aegypti</i>	CRISPR/Cas9	<i>ECFP</i>	Functional genomics	2015 (65)
<i>Ae. aegypti</i>	CRISPR/Cas9	<i>Nix</i>	Conversion of females into harmless males	2015 (66)
<i>Ae. aegypti</i>	CRISPR/Cas9	<i>Aaeg-wtrw</i>	Site-specific mutations	2015 (63)
<i>Ae. aegypti</i>	TALEN	<i>dcr2</i> and <i>ago2</i>	Transgenic strains and gene drive	2015 (64)
<i>Ae. aegypti</i>	CRISPR/Cas9	<i>Kmo</i> , <i>loqs</i> , <i>r2d2</i> , <i>ku70</i> , <i>lig4</i> and <i>nix</i> genes	Transgenic strains and gene drive	2015 (64)
<i>An. stephensi</i>	CRISPR/Cas9	<i>M1C3</i> and <i>m2A10</i>	<i>P. falciparum</i> resistance strains - malaria control	2015 (67)
<i>An. gambiae</i>	CRISPR/Cas9	<i>AGAP005958</i> , <i>AGAP007280</i> and <i>AGAP011377</i>	<i>An. gambiae</i> population suppression - malaria control	2016 (68)
<i>An. gambiae</i>	CRISPR/Cas9	<i>X-linked rDNA sequence</i>	Sex-distortion in <i>An. gambiae</i> - malaria control	2016 (69)

Abbreviations of genes: *AaegGr3*: *Ae. aegypti* gustatory receptors, *orco*: odorant receptor coreceptor, *npylr1*: neuropeptide Y-like receptors 1, *kmo*: kynurenine 3-monoxygenase, *TEP1*: thioester-containing protein, *ECFP*: enhanced cyan fluorescent protein, *Nix*: male-determining factor gene, *Aaeg-wtrw*: *Ae. aegypti* water witch locus, *dcr2*: dicer2, *ago2*: argonaute2, *loqs*: loquacious, *r2d2*: *r2d2* protein, *ku70*: ku heterodimer protein gene, *lig4*: ligase4, *m1C3* and *m2A10*: antiparasite effector genes, *AGAP005958*, *AGAP007280* and *AGAP011377*: *An. gambiae* female-fertility genes. In all these methods, the constructs were delivered through embryonic microinjection.

of vector mosquitoes is aimed for three major purposes: *i*) vector and pathogen control, *ii*) study of target gene function and *iii*) to improve genetic manipulation (44). We have summarized the successful reports of genome editing in vector mosquitoes in Table 1.

3.1. Application of ZFN in genome editing of vector mosquitoes

ZFN has been applied by a few researchers for the customized genome editing of vector mosquitoes. DeGennaro *et al.* targeted the *odorant receptor coreceptor (orco)* gene of *Aedes aegypti* to investigate the role of *orco* gene and the odorant receptor pathway in host identification and sensitivity to chemical repellent *N,N*-diethyl-meta-toluamide (DEET) (14). In this experiment, the designed ZFN was injected into *Ae. aegypti* embryos. The *orco* mutants generated through this study showed reduced spontaneous activity and reduced odour-evoked responses when compared to wild type. Behaviorally, *orco* mutant mosquitoes did not respond to human scent in the absence of CO₂. In another study, the ZFN was used to generate *neuropeptide Y-like receptors 1 (npylr1)* null mutants to study the functional genomics. ZFN construct was injected into *Ae. aegypti* embryos at a concentration of 200 ng/μL and a homologous recombination vector at 850 ng/μL. The tested *npylr1* mutants did not inhibit the host-seeking behavior and the study concluded that other peptides may act with *npylr1* and regulate this host-seeking behavior (45). McMeniman *et al.* mutated the *Ae. aegypti* gustatory receptors (*AaegGr3*) gene, a subunit of the heteromeric CO₂ receptor by injecting ZFNs into pre-blastoderm stage embryos and reported that *Gr3* mutant of *Ae. aegypti* lacked electrophysiological and behavioral responses to CO₂ (46). These studies have confirmed that in spite of

its complexity, ZFN could be successfully used for generating knock-out mutants in a major vector *Ae. aegypti*. Maybe the foundation laid with these studies could be utilized for further studies to advance the genome based control of mosquito-borne diseases using more convenient genome editing tools like CRISPR/Cas9.

3.2. Application of TALEN in genome editing of vector mosquitoes

In addition to ZFN mentioned above, TALEN has also been used as a potent genome editing tool to mutate the targeted genes in disease causing mosquitoes. Aryan *et al.* designed the TALEN to target the *kynurenine 3-monoxygenase (kmo)* gene of *Ae. aegypti* whose protein product was essential for the production of eye pigmentation (13). They injected the *kmo*-targeting TALEN construct into pre-blastoderm embryos of the black-eyed *Ae. aegypti*. Their assay resulted in 20-40% fertile survivors and most of them produced more than 20% white eyed progeny, with some producing up to 75% eye pigmentation mutants. Further, a detailed procedure for target selection (*kmo* gene), assessing the activity of TALEN, embryonic microinjection and detection of target site mutations in *Ae. aegypti* genome was described by the same group in the following year (47). In another reverse genetics study, Smidler *et al.* reported the targeted disruption of the *thioester-containing protein1 (TEP1)* gene using TALEN in *Anopheles gambiae* mosquitoes which spreads malaria. *TEP1* is reported to be an immunity gene in *An. gambiae* against plasmodium infection (15). The induced mutations showed reduced protein production and the resulted *TEP1* mutants were hyper-susceptible to *Plasmodium berghei* infections. These studies have demonstrated the TALEN based genome alterations

in vector mosquitoes. As the designing of TALEN is easier than ZFN, the former may be utilized in future for customized editing of more potent genes in mosquito to control the spread of vector-borne diseases.

3.3. Application of CRISPR/Cas9 in genome editing of vector mosquitoes

As CRISPR/Cas9 has emerged as a most popular and user friendly genome editing tool, it has opened new avenues for the editing of mosquito genomes with little effort. Several labs have already attempted this technique to engineer the genome of vector mosquitoes. Kistler *et al.* investigated the efficiency of CRISPR/Cas9-mediated gene editing system with *Aaeg-wtrw* locus to generate mutations via disparate repair mechanisms and achieved different types of mutations in several genomic loci of *Ae. aegypti* mosquitoes (48). Multiplexed effect of CRISPR/Cas9 was utilized by Basu *et al.* targeting 6 different (*kmo*, *loqs*, *r2d2*, *ku70*, *lig4* and *nix*) genes using CRISPR/Cas9 tool in *Ae. aegypti* mosquito (49). They considered that editing rate may vary across the genome. Hence they designed 40 additional sgRNAs and evaluated their editing potential in transient embryo assays and achieved generating different types of somatic and germline mutations in *Ae. aegypti* mosquitoes. These reports opened a new avenue for mosquito genome editing utilizing CRISPR/Cas9 system. In another study, Dong *et al.* used the CRISPR/Cas9-mediated system to modify *enhanced cyan fluorescent protein (ECFP)* gene in *Ae. aegypti* mosquito line expressing two different eye markers (50). Along with Cas9, two sgRNAs were used to target different regions of *ECFP* gene with *in vitro* transcribed mRNAs for germline transformation and obtained four different G1 pools with 5.5% knockout efficiency. The PCR amplification, cloning and sequencing experiments revealed indels (insertion or deletion) in the *ECFP* target gene ranging from 2-27 nucleotides and their results demonstrated that CRISPR/Cas9-mediated gene editing could be achievable in *Ae. aegypti* (50).

Another report in the same year by Hall *et al.* demonstrated that knockout of male determining (*Nix*) gene has resulted in feminized genetic males with successful application of CRISPR/Cas9-mediated gene editing system (51). Further, their investigation on ectopic expression of *Nix* gene in genetic females confirmed that *Nix* is sufficient to initiate male development and thus has given a path to convert the female mosquitoes into harmless male (51). This study may offer the possibilities of utilizing CRISPR/Cas9 for the customized editing of vector carrying female mosquito genomes. Studies like this could definitely lead to more meaningful inventions that will help combat the spread of deadly diseases especially in less developed countries. A recent review by Adelman and Tu also emphasized the importance of exploiting *Nix* gene for the control of mosquito borne

infectious diseases (31).

Gantz *et al.* developed a CRISPR/Cas9-mediated gene editing system in the Asian malaria vector *An. stephensi* (52). This system produced progeny for a small number of generations that were derived from transgenic males exhibiting a high frequency of gene alteration that were consistent with homology-directed repair (HDR). It has been confirmed that CRISPR/Cas9 system copied a ~17-kb construct from its site of insertion to its homologous chromosome in a site-specific manner. The authors used dual anti-*Plasmodium falciparum* effector genes with a marker gene for this study and the gene-drive components were introgressed into ~99.5% of the progeny following outcrosses of transgenic lines to wild-type mosquitoes. This study provided evidence for a highly efficient gene-drive system that can spread anti-malarial genes such as *m1C3*, *m2A10* into the *An. stephensi* population (52). This could be utilized in future for efficient genome editing of *An. stephensi* which spreads malaria in less developed countries in Asia.

Hammond *et al.* targeted three female-fertility genes viz. *AGAP005958*, *AGAP007280*, *AGAP011377* of *An. gambiae* which were ortholog with *Drosophila* genes and made an attempt to disrupt the coding sequence of these genes using CRISPR/Cas9. They found that reproductive phenotypes (fertility) of the generated mutants suppressed mosquito population to levels that did not support malaria transmission. The role of these genes occurs at distinct stages of egg production and embryo development. The fertility assays in G₂ progeny showed that the homozygous mutant females were sterile, whereas heterozygous females showed normal rates of egg laying and larval emergence. Homozygous mutant females carrying disrupted genes either *AGAP005958* or *AGAP011377* failed to lay eggs, whereas *AGAP007280* gene disrupted homozygous females laid eggs that failed to hatch (53). Further, the team advanced their study and described the first functional CRISPR/Cas9 sex-distortion system (CRISPR^{SD}) in the malaria mosquito *An. gambiae*. They designed a germline transformation construct where Cas9 endonuclease coding sequence was placed in a spermatogenesis-specific β 2 tubulin promoter and the CRISPR^{SD} construct was enclosed in *piggyBac* transformation vector. Among four transgenic lines tested, all the lines showed a strong sex-ratio distortion, with a male bias progeny ranging from 86.1% to 94.8% of males and the hatching rates varied between 83.6% and 93.2% (54).

As the CRISPR/Cas9 has been popularized and considered as a go to technique for genome editing, we can expect many more studies with CRISPR/Cas9 to produce knock-out and knock-in mutants in vector mosquitoes. The production of mutant strains like nonpathogenic mosquitoes, host seeking disturbed mosquitoes, production of only male mosquitoes and production of wingless mosquitoes using CRISPR/Cas9 would be the near future approaches that might

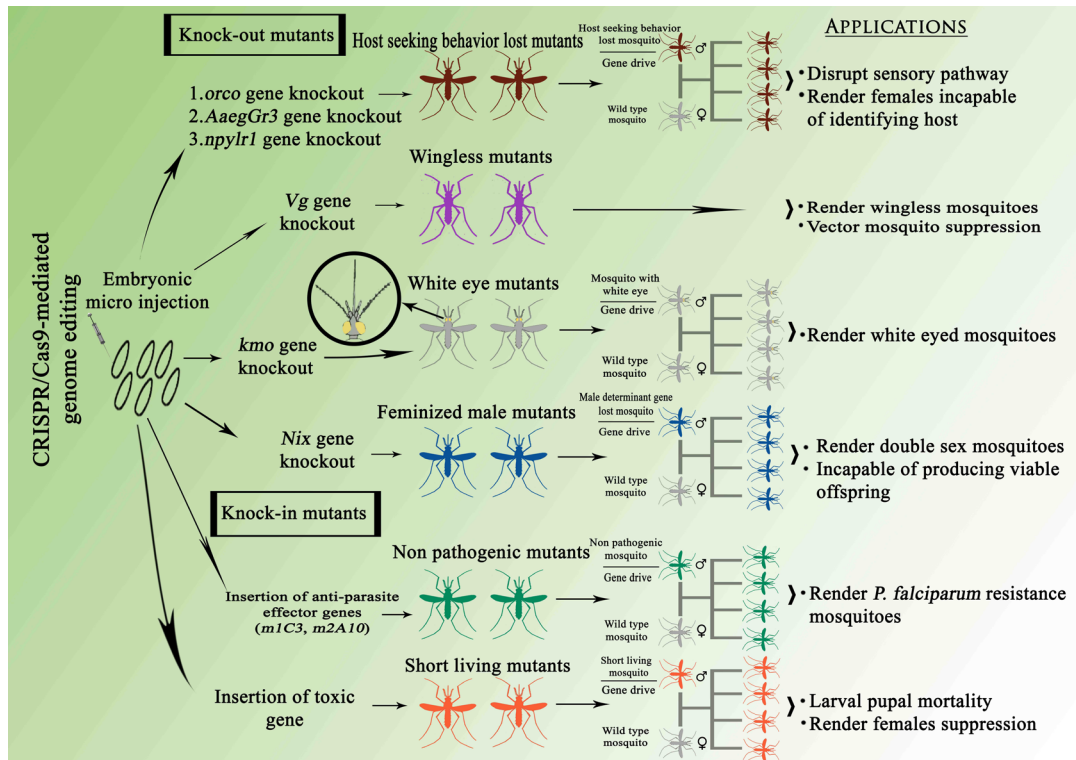


Figure 1. CRISPR-Cas9-mediated genetic modifications in mosquitoes. The figure shows two kinds of mutants such as knock-out and knock-in mutants produced by CRISPR/Cas9-mediated genome editing. It could be crossed with a wild type mosquito in a gene drive system to disrupt the particular activity/functions of the vector mosquito and population suppression that leads to disease eradication. The altered genes could be preferentially inherited by all offsprings when crossed with a wild type mosquito. A Gene drive technology would quickly spread the altered gene in the target mosquito population with nearly 100% chance. *Vg* - vestigial gene.

control/eradicate the spread of deadly diseases by vector mosquito species (Figure 1). Multiplexing feature of this tool also offers more possibilities to study the genes involved in mosquito-parasite interactions.

4. Off-target effects

Off-target mutations and unnecessary chromosomal translocations are the biggest issues with the genome editing tools. Especially with CRISPR/Cas9, specificity of sgRNA caused by off-target binding site mutations and co-inheritance caused by off-target mutations still need to be addressed to improve the specificity of genome editing tools for the successful application in mosquito control programmes (55,56). Furthermore, the off-target impacts of phylogenetic similarity, biogeographic overlap, and ecology, ecological resemblance with other non-target organisms and behavior of the mutants should be addressed in controlled small scale field trials (46).

Even though CRISPR/Cas9 is cost effective, the initial versions of CRISPR/Cas9 system had key issues due to off-target effects (57,58). Cas9 nickase (Cas9D10A mutant) was capable of creating single strand nicks (59,60), which when paired by targeting a site with two sgRNAs, resulted in a DSB which helped to overcome off target effects. More recently, Kleinstiver *et al.* developed a high-fidelity version of the Cas9 from *Streptococcus pyogenes* (SpCas9-HF1)

which was an engineered variant of wild type Cas9 to reduce non-specific DNA contacts. This novel enzyme has greatly reduced the off-target effects in human cells when tested (61). This enzyme could be employed in genome editing of vector mosquitoes too in the near future to produce more specific gene alterations. Unlike ZFN and TALEN, software tools are available to predict the off-target effects of CRISPR/Cas9 system for each experiment. A software tool in the name of Digenome-seq was developed by South Korean scientists recently (62). This *in vitro* digest yielded sequence reads with the same 5' ends at cleavage sites that could be computationally identified. The group had validated off-target sites at which mutations were induced with frequencies below 0.1%, near the detection limit of targeted deep sequencing. These recent developments on tools to predict the off-target effects will be helpful to avoid any undesirable effect of genome editing.

5. Ethical concerns

A great breakthrough was seen in UK recently in the era of genome editing. Developmental biologist Kathy Niakan of Francis Crick Institute in London has received permission from UK authorities to modify human embryos using the CRISPR/Cas9 gene-editing technology. Niakan applied for permission to use the technique to better understand the role of key genes

during the first few days of human embryo development (63). This has affirmed the promising results offered by CRISPR/Cas9 within a short period of its introduction. However it is really difficult to escape from critics and the protesters of genome editing. Although the genome editing is proved to be effective and useful, the editing rates may vary across the genome and also depend on the type of tool used. Each method has various disadvantages in terms of cost, sequence-specificity and off-target effects (64,65). Hence, genome editing raises many ethical issues and concerns to humans, other organisms and environment. Altering a gene in vector mosquitoes and releasing it in the environment could result in unknown and undesirable outcomes in the ecosystem. Many insect ecologists are deeply worried about the risk of mutated organisms and emergence of new insect pest. Ledford has also predicted the consequences and unpredictable effects of genome editing. Thus, the spread of genome edited strains through wild populations, would be extremely difficult to detect and would be challenging to biosecurity measures to prevent the spread of mutated mosquitoes, if they create unwanted effects (66). Similarly, the targeted removal of vector mosquito populations or spreading a genetic element to wild mosquito populations with CRISPR/Cas9-mediated gene drive technology may result in indirect ecological consequences and may raise various societal and regulatory concerns (67,68). Other concerns like survival rate of edited mosquitoes in the natural environment, effects on predatory insects and fishes who eat genetically edited mosquito larvae and ecological imbalance caused by vector mosquito population and eradication are still under debate. It should be carefully analyzed to produce only positive outcomes in the ecosystem.

6. The current problems in application of genome editing techniques in vector mosquitoes

Although user friendly genome editing tool CRISPR/Cas9 has enabled more rapid and efficient editing of mosquito genome with little effort, it has also caused some problems with off-target effects. Several studies have reported that Cas9 is prone to cutting off-target sequences that are similar to the target (58,69-71). Any such off-target effect may cause serious problems in vector mosquito genome editing. Mosquitoes such as *Ae. aegypti* have a very large genome of 1.38 Gb which may require more precise target site selection due to the increased number of potential off-target sequences present. Although many software tools are available to predict the off-target effects (reviewed in 43), it was not possible to apply these tools for all mosquito species due to lack of complete genome in many species. Further, highly efficient mutation systems need to be explored; in many studies, only half of the treated populations receive the desired changes (success rate varies).

There is a serious problem that exists in the gene drive strategy to eradicate or suppress the vector mosquito populations using HDR. We have to ensure that the cut sequence should be repaired using HDR rather than NHEJ to copy the drive, to have a successful gene drive. Also, the gene drives should be activated only in germline cells and only at developmental stages with a high rate of HDR, but this may be challenging in some species of vector mosquitoes.

There is also an appropriate concern that spread of the gene drive in vector mosquitoes will be difficult to control, and may result in unwanted consequences beyond the expected level (56,72,73). Releasing genome edited strain in the environment could result in undesirable effects in the ecosystem. Further, there is no method available so far to detect the mutated mosquitoes in the field condition (66). Even a very efficient endonuclease gene drive may be vulnerable to the evolution of drive resistance in the natural population. If a cut is repaired using the NHEJ pathway instead of HDR, by error, the result will be typically a drive-resistant allele which will bring about undesirable effects. It has also been predicted that some natural sequence polymorphisms in the mosquito population may also prevent the precise cutting. Further, the gene drives require many generations to spread through populations to eliminate or suppress the population of mosquitoes.

In practice, after designing the gene drive in transgenic mosquitoes, they must be allowed to mate with wild-type individuals in order to begin the process of spreading the drive through the wild population. Several critical factors are involved in the successful spread of gene drive in the ecosystem with wild populations. The total time required to spread to all wild mosquitoes depends on several important factors including the number of drive carrying mosquitoes released into the ecosystem and efficiency of gene drive.

7. Future directions

Genome editing tools have been shown to have a great impact on vector mosquito genome modification and these tools can potentially be used further to study the functions of target gene, gene indels, inversions, duplications, genetic network system, polymorphisms and also to investigate the mosquito-pathogen gene interactions. In particular, CRISPR/Cas9-mediated gene editing system may emerge as an efficient tool and may occupy a predominant position with high frequency of target specificity to modify genes of vector mosquitoes. We also need to consider that the CRISPR/Cas9-based introduction of mosquitoes with modified gene may lead to alteration in the wild mosquito population and can result in extinction of the target mosquito species within a short period. However, it is more important to follow all the guidelines and strict biosafety measures to prevent unexpected and undesirable outcome of genome editing.

According to Webber *et al.* researchers, resource managers and policymakers must carefully weigh the risks of implementation of genome editing technologies like CRISPR/Cas9 that could threaten rather than assist a given ecosystem. For example CRISPR/Cas9 approach can be used as a "silver bullet" to manage highly threatening invasive alien species. They also suggest that there are several important factors to take into account especially compared with classical biological control methods which offer important insights in this context (74). The genome editing technology especially like CRISPR/Cas9 which has been invented recently and being much popularized has already started raising debates among the policy makers, governments, non-governmental organizations (NGOs) and public, like GM era in the past. However scientists around the world have the opportunity to make the best use of it to improve the process and product in their field of research for the betterment of humankind especially in the control of vector mosquitoes.

Acknowledgements

The authors extend their appreciation to the International Scientific Partnership Program (ISPP), Deanship of research, King Saudi University Riyadh, Saudi Arabia for funding this research work through ISPP#0020. The authors are grateful to Mr. S. Sylvester Darwin, Senior Research Fellow, Entomology Research Institute for his assistance and contribution in preparing the figures.

References

1. Reegan AD, Gandhi MR, Paulraj MG, Balakrishna K, Ignacimuthu S. Effect of niloticin, a protolimonoid isolated from *Limonia acidissima* L.(Rutaceae) on the immature stages of dengue vector *Aedes aegypti* L.(Diptera: Culicidae). *Acta Trop.* 2014; 139:67-76.
2. WHO. World malaria report. World Health Organization. http://www.who.int/malaria/publications/world_malaria_report_2014/report/en/ 2014 (accessed September 22, 2016).
3. WHO. WHO Director-General summarizes the outcome of the Emergency Committee regarding clusters of microcephaly and Guillain-Barré syndrome. <http://www.who.int/mediacentre/news/statements/2016/emergency-committee-zika-microcephaly/en/> 2016 (accessed September 22, 2016).
4. Bayen S. Occurrence, bioavailability and toxic effects of trace metals and organic contaminants in mangrove ecosystems: A review. *Environ Int.* 2012; 48:84-101.
5. Madhu SK, Shaikath AK, Vijayan VA. Efficacy of bioactive compounds from *Curcuma aromatica* against mosquito larvae. *Acta Trop.* 2010; 113:7-11.
6. Tikar S, Kumar A, Prasad G, Prakash S. Temephos-induced resistance in *Aedes aegypti* and its cross-resistance studies to certain insecticides from India. *Parasitol Res.* 2009; 105:57-63.
7. Catteruccia F, Nolan T, Loukeris TG, Blass C, Savakis C, Kafatos FC, Crisanti A. Stable germline transformation of the malaria mosquito *Anopheles stephensi*. *Nature.* 2000; 405:959-962.
8. Coates CJ, Jasinskiene N, Miyashiro L, James AA. Mariner transposition and transformation of the yellow fever mosquito, *Aedes aegypti*. *Proc Natl Acad Sci.* 1998; 95:3748-3751.
9. Grossman GL, Rafferty CS, Clayton JR, Stevens TK, Mukabayire O, Benedict MQ. Germline transformation of the malaria vector, *Anopheles gambiae*, with the piggyBac transposable element. *Insect Mol Biol.* 2001; 10:597-604.
10. Jasinskiene N, Coates CJ, Benedict MQ, Cornel AJ, Rafferty CS, James AA, Collins FH. Stable transformation of the yellow fever mosquito, *Aedes aegypti*, with the Hermes element from the housefly. *Proc Natl Acad Sci.* 1998; 95:3743-3747.
11. Gabrieli P, Smidler A, Catteruccia F. Engineering the control of mosquito-borne infectious diseases. *Genome Biol.* 2014; 15:1-9.
12. Knippling E. Possibilities of insect control or eradication through the use of sexually sterile males. *J Econ Entomol.* 1955; 48:459-462.
13. Aryan A, Anderson MAE, Myles KM, Adelman ZN. TALEN-based gene disruption in the dengue vector *Aedes aegypti*. *Plos One.* 2013; 8:e60082.
14. DeGennaro M, McBride CS, Seeholzer L, Nakagawa T, Dennis EJ, Goldman C, Jasinskiene N, James AA, Vosshall LB. *orco* mutant mosquitoes lose strong preference for humans and are not repelled by volatile DEET. *Nature.* 2013; 498:487-491.
15. Smidler AL, Terenzi O, Soichot J, Levashina EA, Marois E. Targeted mutagenesis in the malaria mosquito using TALE nucleases. *PLoS One.* 2013; 8:e74511.
16. Criscione F, O'Brochta DA, Reid W. Genetic technologies for disease vectors. *Curr Opin Insect Sci.* 2015; 10:90-97.
17. Bibikova M, Beumer K, Trautman JK, Carroll D. Enhancing gene targeting with designed zinc finger nucleases. *Science.* 2003; 300:764-764.
18. Bibikova M, Golic M, Golic KG, Carroll D. Targeted chromosomal cleavage and mutagenesis in *Drosophila* using zinc-finger nucleases. *Genetics.* 2002; 161:1169-1175.
19. Boch J, Bonas U. Xanthomonas AvrBs3 family-type III effectors: Discovery and function. *Annu Rev Phytopathol.* 2010; 48:419-436.
20. Curtin SJ, Zhang F, Sander JD, Haun WJ, Starker C, Baltus NJ, Reyon D, Dahlborg EJ, Goodwin MJ, Coffman AP, Dobbs D, Joung JK, Voytas DF, Stupar RM. Targeted mutagenesis of duplicated genes in soybean with zinc-finger nucleases. *Plant Physiol.* 2011; 156:466-473.
21. Sander JD, Dahlborg EJ, Goodwin MJ, Cade L, Zhang F, Cifuentes D, Curtin SJ, Blackburn JS, Thibodeau-Beganny S, Qi Y, Pierick CJ, Hoffman E, Maeder ML, Khayter C, Reyon D, Dobbs D, Langenau DM, Stupar RM, Giraldez AJ, Voytas DF, Peterson RT, Yeh JR, Joung JK. Selection-free zinc-finger-nuclease engineering by context-dependent assembly (CoDA). *Nat Methods.* 2011; 8:67-69.
22. Shukla VK, Doyon Y, Miller JC, DeKolver RC, Moehle EA, Worden SE, Mitchell JC, Arnold NL, Gopalan S, Meng X, Choi VM, Rock JM, Wu YY, Katibah GE, Zhifang G, McCaskill D, Simpson MA, Blakeslee B, Greenwalt SA, Butler HJ, Hinkley SJ, Zhang L, Rebar EJ, Gregory PD, Urnov FD. Precise genome

- modification in the crop species *Zea mays* using zinc-finger nucleases. *Nature*. 2009; 459:437-441.
23. Carlson DF, Tan W, Lillico SG, Stverakova D, Proudfoot C, Christian M, Voytas DF, Long CR, Whitelaw CBA, Fahrenkrug SC. Efficient TALEN-mediated gene knockout in livestock. *Proc Natl Acad Sci*. 2012; 109:17382-17387.
 24. Cermak T, Doyle EL, Christian M, Wang L, Zhang Y, Schmidt C, Baller JA, Somia NV, Bogdanove AJ, Voytas DF. Efficient design and assembly of custom TALEN and other TAL effector-based constructs for DNA targeting. *Nucleic Acids Res*. 2011; 39:e82.
 25. Jinek M, Chylinski K, Fonfara I, Hauer M, Doudna JA, Charpentier E. A programmable dual-RNA-guided DNA endonuclease in adaptive bacterial immunity. *Science*. 2012; 337:816-821.
 26. Carroll D. Genome Engineering with Zinc-Finger Nucleases. *Genetics*. 2011; 188:773-782.
 27. Callaway E. Mosquitoes engineered to pass down genes that would wipe out their species. *Nature | News* 2015.
 28. Ledford H, Callaway E. Gene drive' mosquitoes engineered to fight malaria. *Nature | News*. 2015.
 29. Overcash JM, Aryan A, Myles KM, Adelman ZN. Understanding the DNA damage response in order to achieve desired gene editing outcomes in mosquitoes. *Chromosome Res*. 2015; 23:31-42.
 30. Champer J, Buchman A, Akbari OS. Cheating evolution: Engineering gene drives to manipulate the fate of wild populations. *Nat Rev Genet*. 2016; 17:146-159.
 31. Adelman ZN, Tu Z. Control of mosquito-borne infectious diseases: Sex and gene drive. *Trends Parasitol*. 2016; 32:219-229.
 32. Chakradhar S. Buzzkill: Regulatory uncertainty plagues rollout of genetically modified mosquitoes. *Nat Med*. 2016; 21:416-418.
 33. Bibikova M, Carroll D, Segal DJ, Trautman JK, Smith J, Kim YG, Chandrasegaran S. Stimulation of homologous recombination through targeted cleavage by chimeric nucleases. *Mol Cell Biol*. 2001; 21:289-297.
 34. Kim YG, Cha J, Chandrasegaran S. Hybrid restriction enzymes: Zinc finger fusions to Fok I cleavage domain. *Proc Natl Acad Sci*. 1996; 93:1156-1160.
 35. Miller J, McLachlan AD, Klug A. Repetitive zinc-binding domains in the protein transcription factor IIIA from *Xenopus* oocytes. *EMBO J*. 1985; 4:1609-1614.
 36. Wolfe SA, Nekludova L, Pabo CO. DNA recognition by Cys2His2 zinc finger proteins. *Annu Rev Biophys Biomol Struct*. 2000; 29:183-212.
 37. Reyon D, Tsai SQ, Khayter C, Foden JA, Sander JD, Joung JK. FLASH assembly of TALENs for high-throughput genome editing. *Nat Biotechnol*. 2012; 30:460-465.
 38. Mussolino C, Cathomen T. TALE nucleases: Tailored genome engineering made easy. *Curr Opin Biotechnol*. 2012; 23:644-650.
 39. Sakuma T, Woltjen K. Nuclease-mediated genome editing: At the front-line of functional genomics technology. *Dev Growth Differ*. 2014; 56:2-13.
 40. Grissa I, Vergnaud G, Pourcel C. The CRISPRdb database and tools to display CRISPRs and to generate dictionaries of spacers and repeats. *BMC Bioinformatics*. 2007; 8:1-10.
 41. Doudna JA, Charpentier E. The new frontier of genome engineering with CRISPR-Cas9. *Science*. 2014; 346:1-9.
 42. Barrangou R, Doudna JA. Applications of CRISPR technologies in research and beyond. *Nat Biotech*. 2016; 34:933-941.
 43. Ceasar A, Rajan V, Prykhodzhiy SV, Berman JN, Ignacimuthu S. Insert, remove or replace: A highly advanced genome editing system using CRISP/Cas9. *BBA Mol Cell Res*. 2016; 1863:2333-2344.
 44. Franz AW, Clem RJ, Passarelli AL. Novel genetic and molecular tools for the investigation and control of dengue virus transmission by mosquitoes. *Curr Trop Med Rep*. 2014; 1:21-31.
 45. Liesch J, Bellani LL, Vosshall LB. Functional and genetic characterization of neuropeptide Y-like receptors in *Aedes aegypti*. *PLoS Negl Trop Dis*. 2013; 7:e2486.
 46. McMeniman CJ, Corfas RA, Matthews BJ, Ritchie SA, Vosshall LB. Multimodal integration of carbon dioxide and other sensory cues drives mosquito attraction to humans. *Cell*. 2014; 156:1060-1071.
 47. Aryan A, Myles KM, Adelman ZN. Targeted genome editing in *Aedes aegypti* using TALENs. *Methods*. 2014; 69:38-45.
 48. Kistler KE, Vosshall LB, Matthews BJ. Genome engineering with CRISPR-Cas9 in the mosquito *Aedes aegypti*. *Cell Reports*. 2015; 11:51-60.
 49. Basu S, Aryan A, Overcash JM, Samuel GH, Anderson MAE, Dahlem TJ, Myles KM, Adelman ZN. Silencing of end-joining repair for efficient site-specific gene insertion after TALEN/CRISPR mutagenesis in *Aedes aegypti*. *Proc Natl Acad Sci*. 2015; 112:4038-4043.
 50. Dong S, Lin J, Held NL, Clem RJ, Passarelli AL, Franz AW. Heritable CRISPR/Cas9-mediated genome editing in the yellow fever mosquito, *Aedes aegypti*. *Plos One*. 2015; 10:e0122353.
 51. Hall AB, Basu S, Jiang X, Qi Y, Timoshevskiy VA, Biedler JK, Sharakhova MV, Elahi R, Anderson MA, Chen XG, Sharakhov IV, Adelman ZN, Tu Z. A male-determining factor in the mosquito *Aedes aegypti*. *Science*. 2015; 348:1268-1270.
 52. Gantz VM, Jasinskiene N, Tatarenkova O, Fazekas A, Macias VM, Bier E, James AA. Highly efficient Cas9-mediated gene drive for population modification of the malaria vector mosquito *Anopheles stephensi*. *Proc Natl Acad Sci*. 2015; 112:E6736-E6743.
 53. Hammond A, Galizi R, Kyrou K, Simoni A, Siniscalchi C, Katsanos D, Gribble M, Baker D, Marois E, Russell S, Burt A, Windbichler N, Crisanti A, Nolan T. A CRISPR-Cas9 gene drive system targeting female reproduction in the malaria mosquito vector *Anopheles gambiae*. *Nat Biotechnol*. 2016; 34:78-83.
 54. Galizi R, Hammond A, Kyrou K, Taxiarchi C, Bernardini F, O'Loughlin SM, Papathanos PA, Nolan T, Windbichler N, Crisanti A. A CRISPR-Cas9 sex-ratio distortion system for genetic control. *Scientific Reports*. 2016; 6:1-5.
 55. Briese DT. Weed biological control: Applying science to solve seemingly intractable problems. *Aust J Entomol*. 2004; 43:304-317.
 56. Esvelt KM, Smidler AL, Catteruccia F, Church GM. Concerning RNA-guided gene drives for the alteration of wild populations. *Elife*. 2014; 3:e03401.
 57. Cradick TJ, Fine EJ, Antico CJ, Bao G. CRISPR/Cas9 systems targeting β -globin and CCR5 genes have substantial off-target activity. *Nucleic Acids Res*. 2013; 41:9584-9592.
 58. Fu Y, Foden JA, Khayter C, Maeder ML, Reyon D, Joung JK, Sander JD. High-frequency off-target

- mutagenesis induced by CRISPR-Cas nucleases in human cells. *Nat Biotechnol.* 2013; 31:822-826.
59. Mali P, Yang L, Esvelt KM, Aach J, Guell M, DiCarlo JE, Norville JE, Church GM. RNA-guided human genome engineering via Cas9. *Science.* 2013a; 339:823-826.
 60. Ran FA, Hsu PD, Lin CY, Gootenberg JS, Konermann S, Trevino AE, Scott DA, Inoue A, Matoba S, Zhang Y, Zhang F. Double nicking by RNA-guided CRISPR Cas9 for enhanced genome editing specificity. *Cell.* 2013; 154:1380-1389.
 61. Kleinstiver BP, Pattanayak V, Prew MS, Tsai SQ, Nguyen NT, Zheng Z, Joung JK. High-fidelity CRISPR-Cas9 nucleases with no detectable genome-wide off-target effects. *Nature.* 2016; 529:490-495.
 62. Kim D, Bae S, Park J, Kim E, Kim S, Yu HR, Hwang J, Kim JI, Kim JS. Digenome-seq: Genome-wide profiling of CRISPR-Cas9 off-target effects in human cells. *Nat Methods.* 2015; 12:237-243.
 63. Vogel G. U.K. researcher receives permission to edit genes in human embryos. *Science News.* <http://www.sciencemag.org/news/2016/02/uk-researcher-receives-permission-edit-genes-human-embryos> (accessed September 22, 2016).
 64. DeFrancesco L. Move over ZFNs. *Nature Biotechnol.* 2012; 29:681-684.
 65. Gaj T, Gersbach CA, Barbas CF. ZFN, TALEN, and CRISPR/Cas-based methods for genome engineering. *Trends Biotechnol.* 2013; 31:397-405.
 66. Ledford H. CRISPR, the disruptor. *Nature.* 2015; 522:20-24.
 67. Alpey L. Can CRISPR-Cas9 gene drives curb malaria? *Nat Biotechnol.* 2016; 34:149-150.
 68. Paulraj MG, Ignacimuthu S, Reegan AD. Gene silencing and gene drive in dengue vector control: A review. *Indian J. Nat Prod Res.* 2016; 7:1-8.
 69. Hsu PD, Scott DA, Weinstein JA, Ran FA, Konermann S, Agarwala V, Li Y, Fine EJ, Wu X, Shalem O, Cradick TJ, Marraffini LA, Bao G, Zhang F. DNA targeting specificity of RNA-guided Cas9 nucleases. *Nat Biotechnol.* 2013; 31:827-832.
 70. Mali P, Aach J, Stranges PB, Esvelt KM, Moosburner M, Kosuri S, Yang L, Church GM. CAS9 transcriptional activators for target specificity screening and paired nickases for cooperative genome engineering. *Nat Biotechnol.* 2013b; 31:833-838.
 71. Pattanayak V, Lin S, Guilinger JP, Ma E, Doudna JA, Liu DR. High-throughput profiling of off-target DNA cleavage reveals RNA-programmed Cas9 nuclease specificity. *Nat Biotechnol.* 2013; 31:839-843.
 72. Burt A. Site-specific selfish genes as tools for the control and genetic engineering of natural populations. *Proc Biol Sci.* 2003; 270:921-928.
 73. Oye KA, Esvelt K, Appleton E, Catteruccia F, Church G, Kuiken T, Lightfoot SB, McNamara J, Smidler A, Collins JP. Regulating gene drives. *Science.* 2014; 345:626-628.
 74. Webber BL, Raghu S, Edwards OR. Opinion: Is CRISPR-based gene drive a biocontrol silver bullet or global conservation threat? *Proc Natl Acad Sci.* 2015; 112:10565-10567.

(Received September 22, 2016; Revised November 25, 2016; Accepted December 5, 2016)

The interconnected role of chemokines and estrogen in bone metabolism

Yingping Xu^{1,2,3,4,*}, Nan Chu^{1,2,3,*}, Xuemin Qiu^{1,2,3,4}, Hans-Jürgen Gober⁵, Dajin Li^{1,2,3,4}, Ling Wang^{1,2,3,4,**}

¹Obstetrics and Gynecology Hospital of Fudan University, Shanghai, China;

²Shanghai Key Laboratory of Female Reproductive Endocrine-related Diseases, Shanghai, China;

³Laboratory for Reproductive Immunology, Hospital & Institute of Obstetrics and Gynecology, IBS, Shanghai Medical College, Fudan University, Shanghai, China;

⁴The Academy of Integrative Medicine of Fudan University, Shanghai, China;

⁵Department of Pharmacy, Kepler University Clinic, Neuromed Campus, Linz, Austria.

Summary

Over the past few decades, researchers have paid considerable attention to the relationship between estrogen and bone metabolism. Nevertheless, few studies have examined the potential role of chemokines in estrogen regulation of bone metabolism. Chemokines are members of a superfamily of low-molecular-weight chemoattractant cytokines. Various chemokines and their corresponding transmembrane G protein-coupled receptors play distinct roles in the functional regulation and homeostasis of the immune and skeletal systems. This review summarizes the evidence that chemokines and estrogen display cooperative behavior in the skeletal system, with a focus on the mechanisms by which estrogen regulates the chemotactic factors that affect bone metabolism. Chemokines appear to represent a novel area for further examination in order to develop new therapeutics to treat disorders of bone metabolism.

Keywords: Chemokines, estrogen, bone metabolism, osteoblast, osteoclast, networks of the reproductive, endocrine, and immune systems and metabolic processes

1. Introduction

Bone homeostasis requires a balanced relationship between bone resorption and bone formation. An upset in bone homeostasis leads to a series of diseases including osteoporosis, osteomalacia, and osteosclerosis. Osteoblasts (OBs) and osteoclasts (OCs) are two distinct cell types that are mainly involved in bone homeostasis; both are influenced by many factors, such as cytokines, hormones, and growth factors. The receptor activator of nuclear factor- κ B (RANK), RANK ligand (RANKL)

and osteoprotegerin (OPG) are the central cytokines involved in this process and they also affect several steps in the inflammatory response (1). Estrogen is a well-known regulator of bone metabolism and is also involved in immune function. Seventy-five years ago, Fuller-Albright noted that estrogen deficiency after menopause is associated with a decline in bone mineral density (BMD) and osteoporosis (2,3). Estrogen regulates bone metabolism through various pathways. Estrogen depletion involves a change in the levels of cytokines such as TNF- α , IL-1, IL-6, and IL-17, thus influencing the functioning of OBs, OCs, and T cells and consequently affecting bone metabolism (4,5).

The effect of cytokines on bone remodeling, especially those related to estrogen, has been examined and reviewed in other works, but little is known about the relationship between chemokines and estrogen in bone metabolism. This review will focus on the role and mechanism of chemokines on estrogen-regulated bone metabolism.

Released online in J-STAGE as advance publication October 4, 2016.

*These authors contributed equally to this works.

**Address correspondence to:

Dr. Ling Wang, Obstetrics & Gynecology Hospital of Fudan University, 413 Zhaozhou Road, Shanghai 200011, China.

E-mail: Dr.wangling@fudan.edu.cn

2. Chemokines and chemokine receptors

Chemokines belong to a large family of small cytokines with a low molecular weight ranging from 7 to 15kDa, and chemokines are named according to their ability to induce directed chemotaxis of immune cells throughout the body under physiological and pathological conditions (6). Chemokines have been divided into four subfamilies, C, CC, CXC, and CX3C, according to the presence of four cysteine residues in the NH₂-terminal part of the protein. The function of chemokines is mediated by the G protein-coupled receptor superfamily (GPCR) with seven transmembrane domains. Chemokines belonging to the CC- and CXC-subfamily are the best known chemokines thus far. The CC chemokine subfamily is mainly related to monocyte, lymphocyte, and natural killer cell chemotaxis, while CXC chemokines take part in the chemotaxis of neutrophils. The best known function of chemokines is their role in immune cell homeostasis and in the pro-inflammatory process. Homeostatic chemokines are generally involved in lymphocyte trafficking and localization and are usually produced constitutively. Pro-inflammatory chemokines are produced during infection, stimulating leukocyte chemotaxis and inducing the migration of leukocytes to injured or infected sites or activating cells to enhance the host inflammatory response (6). However, these two functions often overlap. Different chemokines play various roles in immunoreaction *via* their specific transmembrane G protein-coupled receptors. For example, CXCL1(KC) and CXCL2(MIP-2) participate in the first line of innate immunity by attracting neutrophils, and CCL5(RANTES) act on monocytes and macrophagocytes (7). In addition, chemokines play roles in cell proliferation, differentiation, activation, immunological tolerance, cell movement, haematopoiesis, viral or cell interactions, neovascularization, cancer metastasis, and other activities (8,9).

Nearly 50 chemokines and 20 chemokine receptors have been identified thus far. Some chemokines are able to interact with multiple chemokine receptors while others interact with one distinct chemokine receptor. A series of downstream signals emerge after chemokines bind with their receptors, such as the activation of extracellular signal-regulated kinases 1 and 2 (ERK1 and ERK2), p21-activated kinase (PAK), and nuclear factor kappa-light-chain-enhancer of activated B cells (NF- κ B). Depending on the type of inflammatory response and the nature of the pathogen and due to the dynamic pattern of expression of chemokine receptors in a temporal and spatial sense, chemokines are able to mediate complex biological functions with exquisite specificity (10-37). The receptors and immune functions of chemokines are summarized in Table 1.

3. Chemokines and bone

3.1. Chemokines and OB

Numerous chemokines have been found to be involved in the process of bone metabolism (38-49), as summarized in Table 2. OBs are derived from bone marrow mesenchymal stem cells (BMMSCs). Along with other factors, chemokines play a crucial role in the process of BMMSCs differentiating into OBs. Ascorbate, b-glycerophosphate (b-GP), and dexamethasone (DEX) profoundly influence the differentiation of OBs. The synthetic glucocorticoid dexamethasone (DEX) increases the production of CXCL8 and CXCL1 by human mesenchymal stem cells (hMSCs) during differentiation into an osteoblastic lineage. ERK and p38 mitogen-activated protein kinase (MAPK) pathways are involved in subsequent activation of G-coupled receptors. A study has reported that OBs may also secrete CXCL8 and CXCL1, stimulating the differentiation of OBs and thus playing an autocrine role in bone metabolism (50). Chemokine and cytokine expression in MSCs were analyzed with a protein array during the differentiation of OBs. The levels of IL-6, MCP-1 (CCL2), and MIP-1B(CCL4) decreased and the levels of IL-10, IL-12, FGF-basic, and VEGF all increased with a lineage commitment towards mature OBs (51).

CXCL10 and CXCL13 were highly expressed in bone biopsies of patients following trauma. At the same time, high levels of their corresponding receptors-CXCR3 and CXCR5 were expressed in human OBs. While CXCR3/CXCL10 and CXCR5/CXCL3 have little effect on the proliferation of OBs, this finding suggests their involvement in the maturation of OBs and bone formation (52).

The receptors for CXCL8, CXCL9, CXCL10, and CCL20 have been found to be expressed in human primary OBs. Interestingly, those four chemokines are found to be elevated in the blood serum of patients with rheumatoid arthritis (RA) and expression of CCL20 and CCR6 increases in their OBs (53). However, a study by Pathak *et al.* found that CXCL8 and CCL20 did not significantly inhibit OB proliferation or gene expression of matrix proteins. Although these chemokines did not directly enhance osteoclastogenesis, they did enhance IL-6 gene expression and protein production by OBs that in turn enhanced OB-mediated osteoclastogenesis (54). Experimental data suggests that the chemokines CXCL12 and CXCL13 increase the proliferation of OBs isolated from patients with osteoarthritis (OA) and that the expression of these chemokines is found mainly in areas of bone remodeling, providing another clue to their function. These chemokines also up-regulate the expression of collagen type I (a marker of OB differentiation) mRNA but they have no effect on alkaline phosphatase in OBs from patients with OA (55).

Table 1. The roles of chemokines in the immune system*(continued on next page)*

Chemokines	Other Name	Receptor	Receptors/Distribution in immune cells	Functions in immunity	Ref.
CXCL1	GRO α	CXCR1, CXCR2	Neutrophils, monocytes, mast cells, basophils, dendritic cells, CD8 T cells, natural killer cells	Neutrophil trafficking	(7)
CXCL2	GRO β	CXCR2	Neutrophils, monocytes, mast cells, basophils, dendritic cells, natural killer cells	Neutrophil trafficking	(7)
CXCL3	GRO γ	CXCR2	Neutrophils, monocytes, mast cells, basophils, dendritic cells, natural killer cells	Neutrophil trafficking	(11)
CXCL4	PF4	CXCR3	Basophils, Th1 cells, CD8 T cells, natural killer cells, Treg cells	Monocyte activation	(12)
CXCL5	ENA-78	CXCR2	Neutrophils, monocytes, mast cells, basophils, dendritic cells, natural killer cells	Neutrophil trafficking	(7)
CXCL6	GCP-2	CXCR1, CXCR2	Neutrophils, monocytes, mast cells, basophils, dendritic cells, CD8 T cells, natural killer cells	Neutrophil trafficking	(13)
CXCL7	NAP-2	CXCR2	Neutrophils, monocytes, mast cells, basophils, dendritic cells, natural killer cells	Neutrophil trafficking	(7)
CXCL8	IL-8	CXCR1, CXCR2	Neutrophils, monocytes, mast cells, basophils, dendritic cells, CD8 T cells, natural killer cells	Neutrophil trafficking	(14)
CXCL9	MIG	CXCR3	Basophils, Th1 cells, CD8 T cells, natural killer cells, Treg cells	Th1 response, Th1, CD8 and NK trafficking	(15)
CXCL10	IP-10	CXCR3	Basophils, Th1 cells, CD8 T cells, natural killer cells, Treg cells	Th1 response, Th1, CD9 and NK trafficking	(15)
CXCL11	I-TAC	CXCR3, CXCR7	Basophils, Th1 cells, CD8 T cells, natural killer cells, Treg cells	Th1 response, Th1, CD10 and NK trafficking	(15)
CXCL12	SDF-1	CXCR4, CXCR7	Widely expressed	Bone marrow homing	
CXCL13	BCA-1	CXCR5	Basophils, CD8 T cells	B cell and Tfh positioning in lymph nodes	(16)
CXCL14	BRAK	Unknown		Macrophage homing to the skin	(17)
CXCL15		Unknown			
CXCL16	SR-PSOX	CXCR6	Th1 cells, Th17 cells, natural killer cells, plasma cells	NKT and ILC migration and survival	(18)
CXCL17	DMC	Unknown			
CCL1	I-309	CCR8	Dendritic cells, monocytes, macrophages, Th2 cells, Treg cells	Th2 and Treg trafficking	(19)
CCL2	MCP-1	CCR2	Monocytes, macrophages, Th1 cells, basophils, natural killer cells	Monocyte trafficking	(20)
CCL3	MIP-1 α	CCR1, CCR5	Dendritic cells, monocytes, macrophages, natural killer cells, Th1 cells, TH17 cells, Treg cells, neutrophils, basophils	Macrophage-NK migration; T cell/DC interaction	(21)
CCL4	MIP-1 β	CCR5	Dendritic cells, monocytes, macrophages, natural killer cells, Th1 cells, TH17 cells, Treg cells	Macrophage-NK migration; T cell/DC interaction	(21)
CCL5	RANTES	CCR1, CCR3, CCR5	Dendritic cells, monocytes, macrophages, natural killer cells, Th1 cells, Th2 cells, TH17 cells, Treg cells, neutrophils, basophils, eosinophils, mast cells	Macrophage-NK migration; T cell/DC interaction	(22)
CCL7	MCP-3	CCR1, CCR2, CCR3	Neutrophils, monocytes, macrophages, Th1 cells, basophils, dendritic cells, eosinophils, Th2 cells, mast cells, natural killer cells	Monocyte mobilization	(23)
CCL8	MCP-2	CCR1, CCR2, CCR3, CCR5	Neutrophils, monocytes, macrophages, Th1 cells, basophils, dendritic cells, eosinophils, Th2 cells, mast cells, natural killer cells, TH17 cells, Treg cells	Th2 response	(24)
CCL9	MIP-1 γ	CCR1	Neutrophils, monocytes, macrophages, Th1 cells, basophils, dendritic cells	T cell, NK cell, and myeloid cell migration	(25)
CCL11	Eotaxin	CCR3	Eosinophils, basophils, Th2 cells, mast cells, dendritic cells	Eosinophil and basophil migration, Th2 response	(26)
CCL12	MCP-5	CCR2	Monocytes, macrophages, Th1 cells, basophils, natural killer cells	Monocyte trafficking	(20)

Table 1. The roles of chemokines in the immune system*(continued)*

Chemokines	Other Name	Receptor	Receptors/Distribution in immune cells	Functions in immunity	Ref.
CCL13	MCP-4	CCR1, CCR2, CCR3	Neutrophils, monocytes, macrophages, Th1 cells, basophils, dendritic cells, eosinophils, Th2 cells, mast cells, natural killer cells	Th2 response	(26)
CCL14	HCC-1	CCR1	Neutrophils, monocytes, macrophages, Th1 cells, basophils, dendritic cells		(26)
CCL15	HCC-2	CCR1, CCR3	Neutrophils, monocytes, macrophages, Th1 cells, basophils, dendritic cells, eosinophils, Th2 cells, mast cells	Hematopoietic progenitor cell adhesion and migration	(27)
CCL16	HCC-4	CCR1, CCR3	Neutrophils, monocytes, macrophages, Th1 cells, basophils, dendritic cells, eosinophils, Th2 cells, mast cells	Macrophage activator	(28)
CCL17	TARC	CCR4	Th2 cells, Th17 cells, Treg cells, monocytes, basophils, CD4 & CD8 T cells	Th2 response, Th2 cell migration, Treg, homing to the lungs and skin	(26)
CCL18	PARC	Unknown		Th2 response, marker of AAM, homing to the skin	(26)
CCL19	ELC	CCR7	Dendritic cells (mature), T cells, basophils	T cell and DC homing to lymph nodes	(29)
CCL20	MIP-3 α	CCR6	Th17 cells, natural killer cells, Treg cells	Th17 response, B cell and DC homing to gut-associated lymphoid tissue	(30)
CCL21	SLC	CCR7	Dendritic cells (mature), T cells, basophils	T cell and DC homing to lymph nodes	(29)
CCL22	MDC	CCR4	Th2 cells, Th17 cells, Treg cells, monocytes, basophils, CD4 & CD8 T cells	Th2 response, Th2 cell migration, Treg migration	(10)
CCL23	MPIF-1	CCR1	Neutrophils, monocytes, macrophages, Th1 cells, basophils, dendritic cells	Monocyte and macrophage trafficking	(31)
CCL24	Eotaxin-2	CCR3	Eosinophils, basophils, Th2 cells, mast cells, dendritic cells	Eosinophil and basophil migration	(32)
CCL25	TECK	CCR9	Basophils, dendritic cells	T cell homing to the gut, thymocyte migration	(33)
CCL26	Eotaxin-3	CCR3	Eosinophils, basophils, Th2 cells, mast cells, dendritic cells	Eosinophil and basophil migration	(32)
CCL27	CTAK	CCR10	T cells, IgA+ plasma cells	T cell homing to the skin	(34)
CCL28	MEC	CCR10	T cells, IgA+ plasma cells	T cell and IgA plasma cell homing to the mucosa	(21)
XCL1	Lymphotactin	XCR1	Dendritic cells, CD4+ T cells, NK cells	CD8(+) T cell cytotoxicity	(35)
XCL2	SCM-1 β	XCR1	Dendritic cells	Cross-presentation by CD8+ DC	(36)
CX3CL1	Fractaline	CX3CR1	Monocytes, macrophages, Th1 cells, dendritic cells, natural killer cells	NK, monocyte, and T cell migration	(37)

3.2. Chemokines and OCs

In vitro, OCs differentiate from bone marrow cells and they require co-incubation with macrophage-colony stimulating factor (M-CSF) and receptor-activator of NF- κ B ligand (RANKL) (56). A systematic study by Chambers *et al.* found that the chemokine ligands CCL9, CCL22, CXCL13, and CCL25 and the chemokine receptors CCR1, CCR3, and CX3CR1 were highly expressed in OCs and that RANKL strongly induced the expression of CCL9, CCR1, and CCR3 while inhibiting the expression of CCR2, CCR5, and CCR7 in OCs (57).

Inflammatory cytokines may stimulate OBs or other types of active cells and release CCR1 chemokines, including CCL3, CCL5, and CCL7. These chemokines

stimulate the recruitment and development of pre-OCs and promote the migration of premature OCs (58). CCL3 also prolongs the survival of mature OCs through NF- κ B signals (59). CCR5 is also a chemokine receptor for CCL3, CCL5, CCL7, and CCL8. The amount of tartrate-resistant acid phosphatase (TRAP)-positive OCs and the expression of OC markers - cathepsin K, metalloprotease 13 (MMP13), and RANKL - were significantly higher in CCR5-deficient mice (CCR5^{-/-}) treated for orthodontic tooth movement than in wild-type mice (WT). The expression of two osteoblastic differentiation markers - runt-related transcription factor 2 (RUNX2) and OCN - and the expression of interleukin 10 (IL-10), bone resorption regulators, and OPG was lower in CCR5^{-/-} mice. Thus, CCR5

Table 2. The functions of chemokines in bone metabolism

Chemokines	Receptors	Main functions in bone metabolism	Ref.
CXCL1	CXCR1, CXCR2	Recruits osteoclast precursors	(38)
CXCL2	CXCR2	Generates osteoclasts (OCs)	(39)
CXCL5	CXCR2	Mobilizes HSCs	(40)
CXCL7	CXCR2	Stimulates the formation of OCs	(41)
CXCL8	CXCR1, CXCR2	Mediates the differentiation of hMSCs into OBs, enhances osteoblast-mediated osteoclastogenesis	(50,53)
CXCL9	CXCR3	Stimulates the formation of OCs	(42)
CXCL10	CXCR3	Mediates the differentiation of OCs	(65)
CXCL11	CXCR3, CXCR7	Reduces osteoclastogenesis	(43)
CXCL12	CXCR4, CXCR7	Increases the proliferation of OBs, promotes osteoclastogenesis, mediates the differentiation of OCs, recruits OC precursors, facilitates the homing of HSC	(50,54,65,68,80)
CXCL13	CXCR5	Increases the proliferation of OBs	(54)
CXCL16	CXCR6	Osteoblast migration	(44)
CCL2	CCR2	Mediates the differentiation of OBs, recruits OC precursors, promotes osteoclastogenesis	(51,64)
CCL3	CCR1, CCR5	Stimulates the recruitment and migration of premature OCs, prolongs the survival of OCs, augments the differentiation of osteoclasts, inhibits the differentiation of OBs	(57,58,72)
CCL4	CCR5	Mediates the differentiation of OBs	(51)
CCL5	CCR1, CCR3, CCR5	Stimulates the recruitment and migration of premature OCs	(57)
CCL7	CCR1, CCR2, CCR3	Stimulates the migration of premature OCs	(57)
CCL8	CCR1, CCR2, CCR3, CCR5	Stimulates the migration of premature OCs	(45)
CCL9	CCR1	Mediates the differentiation of OCs	(56)
CCL17	CCR4	Recruits osteoclast precursors	(46)
CCL18	Unknown	Recruits osteoclast precursors	(47)
CCL19	CCR7	Reduces osteoclastogenesis	(43)
CCL20	CCR6	Enhances osteoblast-mediated osteoclastogenesis	(53)
CCL21	CCR7	Recruits osteoclast precursors	(48)
CCL22	CCR4	Recruits osteoclast precursors	(46)
CCL23	CCR1	Recruits osteoclast precursors	(49)
CX3CL1	CX3CR1	Stimulates the formation of OCs	(41)

might be an inhibitor of alveolar bone resorption by down-regulating OC function during orthodontic tooth movement (60). A study reported finding CCR5 in osteolysis (61), while treatment with a CCR5 antagonist resulted in the abrogation of osteolysis induced by multiple myeloma (62) and improvement of arthritis-related bone loss (63,64). CCR2 binds to CCL2, CCL7, CCL8, and CCL13 and is down-regulated during the differentiation of OCs. The OCs in CCR2-knockout mice decreased in both quantity and quality, so osteoporosis did not occur in CCR2-knockout mice after ovariectomy. After activation of CCR2 in OC progenitor cells, nuclear factor- κ B (NF- κ B) and extracellular signal-related kinase 1 and 2 (ERK1/2) signaling were activated while more RANK was expressed by progenitor cells, making them more susceptible to RANK ligand-induced osteoclastogenesis (65).

During the differentiation of OCs, the expression of CXCL10 and CXCL12 and their receptors CXCR3 and CXCR4 increased significantly (66). Stromal cell-derived factor 1a (SDF-1a), also known as CXCL12, is also produced by stromal cells, OBs, and OCs in multiple myeloma (MM) (66-68), and its receptor CXCR4 is a regulator of bone resorption. A study found that gambogic acid (GA) down-regulated CXCR4 mRNA expression in MM cells by suppressing the binding of NF- κ B to a CXCR4 promoter. GA inhibits osteoclastogenesis mediated by

MM by suppressing SDF1a/CXCR4 signaling pathways (69). A study by Diamond *et al.* suggested that the expression of SDF-1a increased in a murine model of myeloma, inducing a marked increase in OCs and bone loss (70). The chemokine CXCL12 may recruit OC precursors and increase the production of MMP-9 and increase the bone function of OCs in bone resorption (71) while CXCL10 in bone plays an important role in OBs and the recruitment and proliferation of T cells (66).

3.3. Different chemokine axes and bone metabolism

CCR1-CCL3-related signaling pathways (axes) play a crucial role in bone metabolism. Up-regulated levels of Runx2, Atf4, Osteopontin, and Osteonectin in Ccr1^{-/-} mice resulted in less potential for OB differentiation. The co-culturing of CCR1^{-/-} OBs with OC precursors failed to induce OCs. CCR1^{-/-} mice had impaired differentiation and functioning of OBs and OCs mainly as a result of the modulation of RANK-RANKL-mediated interaction (72). Mice treated with Met-RANTES, an antagonist of CCR1, displayed alveolar bone remodeling. CCR1 expression by OBs is significantly greater in patients with myeloma bone diseases (MBD) compared to healthy controls. The chemokine cytokine ligand 3 (CCL3), a pro-inflammatory protein named macrophage inflammatory protein 1-alpha (MIP-1 α), binds to CCR1 and it inhibits

the differentiation, proliferation, and osteogenic potential of OBs by impairing mineralization activation, it decreases levels of OCN, Runx2, and osterix (Osx), and it stimulates OC activity in MBD. Stimulation with CCL3 antibody can increase the levels of OCN, Runx2, and Osx, partially restoring the activity of OBs (73). CCL3 suppresses the activity of OBs mediated by ERK activation and a decrease in the osteogenic transcription factor osterix (74). CCL3 (MIP-1 α) is an osteoclastogenic C-C chemokine, and bone resorption in CCL3^{-/-} mice decreased with low levels of RANK, RANKL, and TNF- α after mechanical loading (75). CCL3 up-regulates the expression of RANKL by OBs, it increases the transcription of TNF- α , it induces OC-OB interaction, it augments the differentiation of OCs, and it consequently increases bone resorption (76). Mechanical loading, such as orthodontic force, up-regulated the expression of CCL3 and CCR1 in alveolar bone and soft periodontal tissues, thus affecting the recruitment, differentiation, and activation of OC precursor cells and OBs and resulting in bone remodeling (58,77). However, CCL3 had no effect on bone loss associated with periodontal disease (78). CCR5 is another receptor for CCL3 and is related to up-regulation of infection-related bone loss in periodontal disease and the prevention of bone resorption induced by mechanical loading (79,80).

CXCL12/CXCR4 is another important pathway that plays a key role in maintaining skeletal homeostasis. CXCR4 and its only ligand SDF-1/CXCL12 are expressed by many cells types, including stromal cells, OCs, and OBs. CXCR4 is a type of OB-specific chemokine receptor. CXCR4/CXCL12 facilitates the homing of HSC to bone marrow; disruption of CXCR4/CXCL12 results in a decrease in HSC homing that is lethal in embryos (81). When CXCR4 is deleted by Cre-Loxp technology in mature OBs in mice, bone mass decreases and alterations appear in cancellous bone structure. In mature OBs, CXCL12-CXCR4 signaling regulates osteoprogenitor and OC precursor populations, but it also plays a multifunctional role in regulating bone formation and resorption in mature OBs (82). In a model of bone metastasis, mice with CXCR4 null hematopoietic cells had an increase in bone resorption, the perimeter of OCs, and bone loss. After the disruption of CXCR4, the differentiation of OCs accelerated and the resorption of bone increased (83). The functions of chemokines in bone remodeling processes differ depending on the agent or disease that induced their production.

4. Estrogen modulates the expression of chemokines

4.1. C chemokines

A study found that ER- α ^{-/-} human breast cancer does not respond to hormonal therapy and that it generally has a poor prognosis. Epigenetic regulation, including DNA methylation and histone deacetylation, is a

common mechanism resulting in ER gene silencing. The pharmacologic inhibitors 5-aza 2'deoxyctidine (AZA) and Trichostatin A (TSA) alter this mechanism by stimulating ER mRNA and expression of its functional protein. A study by Keen *et al.* found that the expression of two genes - lymphotactin (XCL1) and protein phosphatase 2A (PP2A) - appeared to be related to ER expression. PP2A is an upstream determinant of ER expression, while XCL1 is downstream and responsive to ER expression. A study found that the expression of XCL1 was down-regulated in the presence of AZA/TSA and ICI 182,780 (84). In conclusion, estrogen receptors suppress XCL1 expression.

4.2. CC chemokines

Estrogen is known to significantly affect immunity and inflammatory autoimmune-mediated diseases. Estrogen regulates immunity and inflammatory autoimmune-mediated diseases by altering the secretion of chemokines from activated splenocytes or other lymphocytes. However, the roles of estrogen differ in different tissues and cells. Estrogen significantly promotes the expression of spleen MCP-1 (CCL2), MCP-3 (CCL7), MCP-5 (CCL12), eotaxin (CCL11), and stromal cell-derived factor-1(SDF-1; CXCL12) by endothelial cells but has little effect on dermal endothelial cells (85). However, estrogen reduces the levels of MCP-1 in human coronary artery endothelial cells (HCAECs) (86). Estrogen significantly increased the levels of some specific chemokines such as MIP-1 α and MCP-1/JE in mammary cells *in vivo* and *in vitro* (87), while the expression of chemokines MCP-1/JE and MIP-1 α did not change in murine monocytes co-cultured with estrogen or tamoxifen (88). A study has found that both estrogen and tamoxifen significantly down-regulate the expression of CCR2 by murine monocytes and that they down-regulate the expression of CXCR3 by murine monocytes to a lesser extent at the same time (88). Estradiol inhibited CCL20 secretion at 48 hr in freshly isolated and polarized uterine epithelial cells of BALB/c mice, regardless of whether keratinocyte growth factor (KGF) was present or not (89). Raloxifene is a selective estrogen receptor modulator (SERMs) and a promising treatment for experimental autoimmune encephalomyelitis (EAE). In animals with EAE, raloxifene decreased IL-1 β and it induced the expression of CCL20 in reactive astrocytes, thus promoting Th17 cell migration (90).

4.3. CXC chemokines

Estrogen and epidermal growth factor (EGF) significantly promote the release of the angiogenic chemokine CXCL8 in human breast carcinoma MCF-7 cells. When MCF-7 breast carcinoma cells were co-cultured with EGF and estrogen, the expression of CXCL8 increased up to two-fold in comparison with

culturing with estrogen or EGF alone, indicating the additive effects of estrogen and EGF (91). Estrogen is thought to be a key regulator of CCL20 and CXCL1 in the upper female reproductive tract since it decreases the secretion of CCL20 but it directly increases the levels of CXCL1 in uterine epithelial cells (92). Estrogen enhances KGF-induced CXCL1 secretion in freshly isolated and polarized uterine epithelial cells at 24 hr (89). In Foxp3-deficient mice with EAE, estrogen (17 β -estradiol, E2) suppressed the expression and proliferation of CCL2 and CXCL2 but it enhanced the secretion of interleukin-10 (IL-10) and IL-13 by myelin oligodendrocyte glycoprotein (MOG)-35-55-specific spleen cells. E2 treatment suppresses the expression of CCR6 in spleen and lymph node T cells while it increases the levels of IL-17, interferon- γ , and TNF- α , suggesting that E2 could provide protection against EAE even in the absence of Foxp3+ Treg cells. E2 treatment increased the expression of several chemokines and receptors, including CXCL13 and CXCR5 (93). Theiler's murine encephalomyelitis virus (TMEV) induces demyelination in susceptible strains of mice (SJL/J). In this immunopathological process, increased expression of CXCL10 by astrocytes is induced by the inflammatory cytokines IL-1 α , IFN- γ , and TNF- α , causing demyelination. However, 17 β -estradiol or selective estrogen receptor modulators (SERMs) combined with estrogen receptor- α inhibited the expression of CXCL10 in astrocytes (94).

4.4. CX3C chemokines

In order to examine the effect of estrogen on the cytotoxic response to an early-stage infection with the bronchitis (IB) virus in hen oviducts, Nii *et al.* designed an experiment in which they inoculated the oviductal magnum lumen of White Leghorn hens with attenuated IB virus (aIBV group) in the egg-laying phase and with its vehicle (control group) in the molting phase (95). Twenty-four hours later, the oviductal isthmus and uterus were collected to examine the expression of cytokines, including CXCL12, CX3CL1, and IFN- γ . The level of expression of CXCL12, CX3CL1, and IFN- γ was significantly higher in the aIBV group in the egg-laying phase and M-EB hens compared to the control group. Nii *et al.* concluded that estrogen enhanced the expression of CX3CL1 in hen oviducts infected with the IB virus. Another study suggested that genistein, a polyphenolic nonsteroidal isoflavonoid with estrogen-like activity, strongly suppressed TNF- α -induced expression of CX3CR1 in monocytes (96).

5. The mechanism by which estrogen modulates chemokines

In experiments where spleen endothelial cells were cultured with estradiol, estradiol up-regulated the

level of estrogen receptor alpha (ER- α) 2.9-fold and it down-regulated the level of estrogen receptor beta (ER- β) 2.1-fold. In dermal endothelial cells, however, levels of both ER- α and ER- β decreased. When spleen endothelial cells were co-cultured with tamoxifen (one of ER antagonists) or ICI 182,780, none of these estradiol-mediated effects on splenic chemokines were noted, indicating that estrogen selectively regulates chemokines through estrogen receptors (85,97). In HCAECs, estrogen at a concentration of 10-8M reduced the levels of MCP-1, down-regulating MCP-1 mRNA and protein expression 30% (86). Raloxifene and tamoxifen also inhibited the expression of MCP-1 mRNA and protein. They induced a concentration-dependent inhibition of MCP-1 expression and production in cultured HCAECs. Treatment with estrogen or raloxifene and tamoxifen was ineffective at changing levels of MCP-1 expression in human umbilical vein endothelial cells (HUVECs) (86). In cultured mammary cells and murine mammary tissue, estrogen significantly down-regulates the levels of specific chemokines - MIP-1a and MCP-1/JE - compared to baseline levels, and estrogen also suppresses expression of JE/monocyte chemoattractant protein 1(MCP-1/JE) mRNA in murine macrophage cells (87). A study by Janis *et al.* reported no change in the expression of the chemokines MCP-1/JE and MIP-1a in murine monocytes, regardless of whether those cells were co-cultured with estrogen or tamoxifen (88). However, estrogen may affect the functioning of chemokines by decreasing the chemotaxis of monocytes to MCP-1/JE (88). The effects of estrogen on chemokines, including MCP-1/JE and MIP-1a, seem to be cell line-dependent. CXCL8 (interleukin-8), a member of the CXC family, is overexpressed in ER α -negative breast cancer cell lines while a high level of CXCL8 expression in tumors is closely correlated with the activating protein-1 (AP-1) pathway and somewhat correlated with the NF- κ B pathway (98). The inhibitory effect of estradiol or raloxifene on CCL20 secretion and function was reversed by administration of an estrogen receptor antagonist designated ICI 182,780 (89,90). ER α antagonists mediate CCL20 and CXCL1 secretion while ER β does not. Several studies have indicated that treatment of uterine epithelial cells with Y134 (ER α and ER β -SERMS) markedly enhanced CCL20 production and inhibited CXCL1 production, while treatment with PHTPP (ER β specific SERMS) had no effect on either CCL20 or CXCL1 (92). The findings above indicate that estradiol plays an important role in mediating chemokine secretion.

6. The relationship between chemokines and estrogen in regulation of bone metabolism

Estrogen has been found to down-regulate the expression of cytokines that are known to enhance

osteoclastogenesis, such as IL-1 and IL-6. Estrogen deficiency also increases the amount of TNF- α producing T cells, thus promoting the expression of RANKL in OBs and facilitating osteoclastogenesis (99).

Ovariectomized (OVX) mice are a model that can be used to examine the effect of estrogen on bone metabolism. Fat from OVX mice was found to secrete high levels of MCP-1 (CCL2) and an ovariectomy was found to induce increased formation of OCs (100). CCR2 is a receptor for CCL2 that is expressed by various hematopoietic cells. In OVX mice, CCR2 was up-regulated in preosteoclasts; when estrogen was deficient, CCR2 induced the expression of RANK, thus promoting osteoclastogenesis that led to bone loss. In contrast, bone loss was inhibited in CCR2^{-/-} mice after an ovariectomy. The absence of CCR2 increased the number of preosteoclasts, but these preosteoclasts did not counteract the protection provided by CCR2, so CCR2 plays a crucial role in the differentiation of OCs (65). Estrogen down-regulated the expression of CCR2 in monocytes and the levels of CCL2, but CCL2 increased after menopause (101,102). An estrogen deficiency up-regulated the expression of CCR2 preosteoclasts through both nuclear factor- κ B (NF- κ B) and extracellular signal-related kinase 1 and 2 (ERK1/2) signaling and an estrogen deficiency promoted osteoclastogenesis.

Estrogen is an important immunomodulatory agent that regulates the immune system, thus affecting bone metabolism. Regulatory T cells (Treg cells) suppress bone resorption and the differentiation of OCs in bone marrow. The CXCL12-CXCR4 pathway is critical to Treg cells migrating to and staying in bone marrow. An estrogen deficiency decreases the expression of CXCR4 in Treg cells and it significantly reduces the Treg cell population in bone marrow in OVX mice with little effect on CXCL12. An estrogen deficiency down-regulates the Treg cell population in bone marrow by inhibiting CXCR4 expression in Treg cells and Treg cell trafficking, thereby preventing Treg cells from suppressing the differentiation of OCs and eventually leading to bone loss in OVX mice (103).

In EAE, estrogen down-regulates IL-17 production and it inhibits Th17 differentiation through estrogen receptor α (ER α) in T cells (102,104-106). An estrogen deficiency increases the amount of Th17 cells in bone marrow and IL-17 levels. IL-17 promotes the expression of RANKL, TNF- α , and IL-6 and TRAP-positive cells while blocking IL-17 pathways, resulting in little bone loss in OVX mice (107). IL-17 plays a crucial role in inflammation-induced bone loss by stimulating osteoclastogenesis, so IL-17 is thus the driving force in some autoimmune diseases that involve bone metabolism, such as RA in particular. IL-17 up-regulates synovial fibroblasts to produce CXCL8, which attracts neutrophils to the joints and thus enhances joint inflammation in RA (108,109). The CCR6-CCL20 pathway is expressed in

Th17 cells, and this pathway facilitates the migration of Th17 cells to the site of inflammation (110). Estrogen augments the expression of CCR6 and CCL20 by Th17 cells in lymph nodes (LNs) through ER α , preventing the migration of Th17 cells to joints in established arthritis and resulting a higher level of Th17 cells in LNs and a lower level in joints (111). Estrogen affects the migration of Th17 cells *via* the CCR6 and CCL20 pathways while Th17 cells produce IL-17 to stimulate the expression of CXCL8, thus affecting the migration of neutrophils.

7. Conclusion

Chemokines play an important role in estrogen-regulated bone metabolism and may serve as a novel area for further examination in order to develop new therapeutics to treat diseases of bone metabolism.

Acknowledgements

This work was supported by the National Natural Science Foundation of China (grant no. 31571196 to Ling Wang), the Science and Technology Commission of Shanghai Municipality 2015 YIXUEYINGDAO project (grant no. 15401932200 to Ling Wang), the FY2008 JSPS Postdoctoral Fellowship for Foreign Researchers P08471 (to Ling Wang), the National Natural Science Foundation of China (grant no. 30801502 to Ling Wang), the Shanghai Pujiang Program (grant no. 11PJ1401900 to Ling Wang), the National Natural Science Foundation of China (grant no. 81401171 to Xue-Min Qiu), the Development Project of Shanghai Peak Disciplines-Integrative Medicine (grant no.20150407), and the Program for Outstanding Medical Academic Leaders (Da-Jin Li).

References

1. Eghbali-Fatourehchi G, Khosla S, Sanyal A, Boyle WJ, Lacey DL, Riggs BL. Role of RANK ligand in mediating increased bone resorption in early postmenopausal women. *J Clin Invest.* 2003; 111:221-1230.
2. Cauley JA. Estrogen and bone health in men and women. *Steroids.* 2015; 99:11-15.
3. Hofbauer LC, Khosla S, Dunstan CR, Lacey DL, Boyle WJ, Riggs BL. The roles of osteoprotegerin and osteoprotegerin ligand in the paracrine regulation of bone resorption. *J Bone Miner Res.* 2000; 15:2-12.
4. Charatcharoenwitthaya N, Khosla S, Atkinson EJ, McCready LK, Riggs BL. Effect of blockade of TNF- α and interleukin-1 action on bone resorption in early postmenopausal women. *J Bone Miner Res.* 2007; 22:724-729.
5. Ryan MR, Shepherd R, Leavey JK, Gao Y, Grassi F, Schnell FJ, Qian WP, Kersh GJ, Weitzmann MN, Pacifici R. An IL-7-dependent rebound in thymic T cell output contributes to the bone loss induced by estrogen deficiency. *Proc Natl Acad Sci U S A.* 2005; 102:16735-16740.

6. Antonelli A, Ferrari SM, Ruffilli I, Fallahi P. Cytokines and HCV-related autoimmune disorders. *Immunol Res.* 2014; 60:311-319.
7. Sanz MJ, Kubes P. Neutrophil-active chemokines in *in vivo* imaging of neutrophil trafficking. *Eur J Immunol.* 2012; 42:278-283.
8. Mackay CR. Chemokines: Immunology's high impact factors. *Nat Immunol.* 2001; 2:95-101.
9. Szekanecz Z, Kim J, Koch AE. Chemokines and chemokine receptors in rheumatoid arthritis. *Semin Immunol.* 2003; 15:15-21.
10. Anz D, Rapp M, Eiber S, *et al.* Suppression of intratumoral CCL22 by type I interferon inhibits migration of regulatory T cells and blocks cancer progression. *Cancer Res.* 2015; 75:4483-4493.
11. Rainard P, Riollot C, Berthon P, Cunha P, Fromageau A, Rossignol C, Gilbert FB. The chemokine CXCL3 is responsible for the constitutive chemotactic activity of bovine milk for neutrophils. *Mol Immunol.* 2008; 45:4020-4027.
12. Schwartzkopff F, Petersen F, Grimm TA, Brandt E. CXC chemokine ligand 4 (CXCL4) down-regulates CC chemokine receptor expression on human monocytes. *Innate Immun.* 2012; 18:124-139.
13. Jovic S, Linge HM, Shikhagaie MM, Olin AI, Lannefors L, Erjefalt JS, Morgelin M, Egesten A. The neutrophil-recruiting chemokine GCP-2/CXCL6 is expressed in cystic fibrosis airways and retains its functional properties after binding to extracellular DNA. *Mucosal Immunol.* 2016; 9:112-123.
14. Tang FS, Van Ly D, Spann K, Reading PC, Burgess JK, Hartl D, Baines KJ, Oliver BG. Differential neutrophil activation in viral infections: Enhanced TLR-7/8-mediated CXCL8 release in asthma. *Respirology* 2016; 21:172-179.
15. Muller M, Carter S, Hofer MJ, Campbell IL. Review: The chemokine receptor CXCR3 and its ligands CXCL9, CXCL10 and CXCL11 in neuroimmunity – A tale of conflict and conundrum. *Neuropathol Appl Neurobiol.* 2010; 36:368-387.
16. Rupprecht TA, Plate A, Adam M, Wick M, Kastenbauer S, Schmidt C, Klein M, Pfister HW, Koedel U. The chemokine CXCL13 is a key regulator of B cell recruitment to the cerebrospinal fluid in acute Lyme neuroborreliosis. *J Neuroinflammation.* 2009; 6:42.
17. Lu J, Chatterjee M, Schmid H, Beck S, Gawaz M. CXCL14 as an emerging immune and inflammatory modulator. *J Inflamm (Lond).* 2016; 13:1.
18. Jiang X, Shimaoka T, Kojo S, Harada M, Watarai H, Wakao H, Ohkohchi N, Yonehara S, Taniguchi M, Seino K. Cutting edge: Critical role of CXCL16/CXCR6 in NKT cell trafficking in allograft tolerance. *J Immunol.* 2005; 175:2051-2055.
19. Hoelzinger DB, Smith SE, Mirza N, Dominguez AL, Manrique SZ, Lustgarten J. Blockade of CCL1 inhibits T regulatory cell suppressive function enhancing tumor immunity without affecting T effector responses. *J Immunol.* 2010; 184:6833-6842.
20. Gonzalo JA, Lloyd CM, Wen D, Albar JP, Wells TN, Proudfoot A, Martinez AC, Dorf M, Bjerke T, Coyle AJ, Gutierrez-Ramos JC. The coordinated action of CC chemokines in the lung orchestrates allergic inflammation and airway hyperresponsiveness. *J Exp Med.* 1998; 188:157-167.
21. Danilova E, Skrindo I, Gran E, Hales BJ, Smith WA, Jahnsen J, Johansen FE, Jahnsen FL, Baekkevold ES. A role for CCL28-CCR3 in T-cell homing to the human upper airway mucosa. *Mucosal Immunol.* 2015; 8:107-114.
22. Hussen J, Frank C, Duvel A, Koy M, Schuberth HJ. The chemokine CCL5 induces selective migration of bovine classical monocytes and drives their differentiation into LPS-hyporesponsive macrophages *in vitro*. *Dev Comp Immunol.* 2014; 47:169-177.
23. Bardina SV, Michlmayr D, Hoffman KW, Obara CJ, Sum J, Charo IF, Lu W, Pletnev AG, Lim JK. Differential roles of chemokines CCL2 and CCL7 in monocytosis and leukocyte migration during West Nile Virus infection. *J Immunol.* 2015; 195:4306-4318.
24. Islam SA, Chang DS, Colvin RA, Byrne MH, McCully ML, Moser B, Lira SA, Charo IF, Luster AD. Mouse CCL8, a CCR8 agonist, promotes atopic dermatitis by recruiting IL-5⁺ T_H2 cells. *Nat Immunol.* 2011; 12:167-177.
25. McColl A, Thomson CA, Nerurkar L, Graham GJ, Cavanagh J. TLR7-mediated skin inflammation remotely triggers chemokine expression and leukocyte accumulation in the brain. *J Neuroinflammation.* 2016; 13:102.
26. Zhang RX, Yu SQ, Jiang JZ, Liu GJ. Complementary DNA microarray analysis of chemokines and their receptors in allergic rhinitis. *J Investig Allergol Clin Immunol* 2007; 17:329-336.
27. Richter R, Ruster B, Bistran R, Forssmann WG, Seifried E, Henschler R. Beta-Chemokine CCL15 affects the adhesion and migration of hematopoietic progenitor cells. *Transfus Med Hemother.* 2015; 42:29-37.
28. Cappello P, Caorsi C, Bosticardo M, De Angelis S, Novelli F, Forni G, Giovarelli M. CCL16/LEC powerfully triggers effector and antigen-presenting functions of macrophages and enhances T cell cytotoxicity. *J Leukoc Biol.* 2004; 75:135-142.
29. van de Ven R, Reurs AW, Wijnands PG, van Wetering S, Kruisbeek AM, Hooijberg E, Scheffer GL, Scheper RJ, de Gruijl TD. Exposure of CD34⁺ precursors to cytostatic anthraquinone-derivatives induces rapid dendritic cell differentiation: Implications for cancer immunotherapy. *Cancer Immunol Immunother.* 2012; 61:181-191.
30. Yu Q, Lou XM, He Y. Preferential recruitment of Th17 cells to cervical cancer *via* CCR6-CCL20 pathway. *PLoS One.* 2015; 10:e0120855.
31. Puposki JA, Uzzaman A, Nagarkar DR, *et al.* Increased expression of the chemokine CCL23 in eosinophilic chronic rhinosinusitis with nasal polyps. *J Allergy Clin Immunol.* 2011; 128:73-81.e74.
32. Provost V, Larose MC, Langlois A, Rola-Pleszczynski M, Flamand N, Laviolette M. CCL26/eotaxin-3 is more effective to induce the migration of eosinophils of asthmatics than CCL11/eotaxin-1 and CCL24/eotaxin-2. *J Leukoc Biol.* 2013; 94:213-222.
33. Li J, Xiong T, Xiao R, Xiong A, Chen J, Altaf E, Zheng Y, Zhu G, He Y, Tan J. Anti-CCL25 antibody prolongs skin allograft survival by blocking CCR9 expression and impairing splenic T-cell function. *Arch Immunol Ther Exp (Warsz).* 2013; 61:237-244.
34. Sigmundsdottir H, Pan J, Debes GF, Alt C, Habtezion A, Soler D, Butcher EC. DCs metabolize sunlight-induced vitamin D3 to 'program' T cell attraction to the epidermal chemokine CCL27. *Nat Immunol* 2007; 8:285-293.
35. Hartung E, Becker M, Bachem A, Reeg N, Jakel A, Hutloff A, Weber H, Weise C, Giesecke C, Henn V, Gurka S, Anastassiadis K, Mages HW, Kroczeck RA. Induction

- of potent CD8 T cell cytotoxicity by specific targeting of antigen to cross-presenting dendritic cells *in vivo* via murine or human XCR1. *J Immunol.* 2015; 194:1069-1079.
36. Wang M, Windgassen D, Papoutsakis ET. Comparative analysis of transcriptional profiling of CD3+, CD4+ and CD8+ T cells identifies novel immune response players in T-cell activation. *BMC Genomics.* 2008; 9:225.
 37. Siddiqui I, Erreni M, van Brakel M, Debets R, Allavena P. Enhanced recruitment of genetically modified CX3CR1-positive human T cells into Fractalkine/CX3CL1 expressing tumors: Importance of the chemokine gradient. *J Immunother Cancer.* 2016; 4:21.
 38. Onan D, Allan EH, Quinn JM, Gooi JH, Pompolo S, Sims NA, Gillespie MT, Martin TJ. The chemokine Cxcl1 is a novel target gene of parathyroid hormone (PTH)/PTH-related protein in committed osteoblasts. *Endocrinology.* 2009; 150:2244-2253.
 39. Dapunt U, Maurer S, Giese T, Gaida MM, Hansch GM. The macrophage inflammatory proteins MIP1 α (CCL3) and MIP2 α (CXCL2) in implant-associated osteomyelitis: Linking inflammation to bone degradation. *Mediators Inflamm.* 2014; 2014:728619.
 40. Yoon KA, Cho HS, Shin HI, Cho JY. Differential regulation of CXCL5 by FGF2 in osteoblastic and endothelial niche cells supports hematopoietic stem cell migration. *Stem Cells Dev.* 2012; 21:3391-3402.
 41. Goto Y, Aoyama M, Sekiya T, Kakita H, Waguri-Nagaya Y, Miyazawa K, Asai K, Goto S. CXCR4+ CD45- Cells are niche forming for osteoclastogenesis via the SDF-1, CXCL7, and CX3CL1 signaling pathways in bone marrow. *Stem Cells.* 2016. doi: 10.1002/stem.2440.
 42. Paula-Silva FW, Petean IB, da Silva LA, Faccioli LH. Dual role of 5-lipoxygenase in osteoclastogenesis in bacterial-induced apical periodontitis. *J Endod.* 2016; 42:447-454.
 43. Kim HJ, Park J, Lee SK, Kim KR, Park KK, Chung WY. Loss of RUNX3 expression promotes cancer-associated bone destruction by regulating CCL5, CCL19 and CXCL11 in non-small cell lung cancer. *J Pathol.* 2015; 237:520-531.
 44. Ota K, Quint P, Weivoda MM, Ruan M, Pederson L, Westendorf JJ, Khosla S, Oursler MJ. Transforming growth factor β 1 induces CXCL16 and leukemia inhibitory factor expression in osteoclasts to modulate migration of osteoblast progenitors. *Bone.* 2013; 57:68-75.
 45. Chen W, Foo SS, Taylor A, Lulla A, Merits A, Hueston L, Forwood MR, Walsh NC, Sims NA, Herrero LJ, Mahalingam S. Bindarit, an inhibitor of monocyte chemotactic protein synthesis, protects against bone loss induced by chikungunya virus infection. *J Virol.* 2015; 89:581-593.
 46. Cadosch D, Gautschi OP, Chan E, Simmen HP, Filgueira L. Titanium induced production of chemokines CCL17/TARC and CCL22/MDC in human osteoclasts and osteoblasts. *J Biomed Mater Res A.* 2010; 92:475-483.
 47. Koulouvaris P, Ly K, Ivashkiv LB, Bostrom MP, Nestor BJ, Sculco TP, Purdue PE. Expression profiling reveals alternative macrophage activation and impaired osteogenesis in periprosthetic osteolysis. *J Orthop Res.* 2008; 26:106-116.
 48. Bugatti S, Caporali R, Manzo A, Vitolo B, Pitzalis C, Montecucco C. Involvement of subchondral bone marrow in rheumatoid arthritis: Lymphoid neogenesis and *in situ* relationship to subchondral bone marrow osteoclast recruitment. *Arthritis Rheum.* 2005; 52:3448-3459.
 49. Votta BJ, White JR, Dodds RA, James IE, Connor JR, Lee-Ryckaczewski E, Eichman CF, Kumar S, Lark MW, Gowen M. CK β -8 [CCL23], a novel CC chemokine, is chemotactic for human osteoclast precursors and is expressed in bone tissues. *J Cell Physiol.* 2000; 183:196-207.
 50. Lisignoli G, Toneguzzi S, Grassi F, Piacentini A, Tschon M, Cristino S, Gualtieri G, Facchini A. Different chemokines are expressed in human arthritic bone biopsies: IFN- γ and IL-6 differently modulate IL-8, MCP-1 and rantes production by arthritic osteoblasts. *Cytokine.* 2002; 20:231-238.
 51. Penolazzi L, Lambertini E, Tavanti E, Torreggiani E, Vesce F, Gambari R, Piva R. Evaluation of chemokine and cytokine profiles in osteoblast progenitors from umbilical cord blood stem cells by BIO-PLEX technology. *Cell Biol Int.* 2008; 32:320-325.
 52. Lisignoli G, Toneguzzi S, Piacentini A, Cattini L, Lenti A, Tschon M, Cristino S, Grassi F, Facchini A. Human osteoblasts express functional CXC chemokine receptors 3 and 5: Activation by their ligands, CXCL10 and CXCL13, significantly induces alkaline phosphatase and beta-N-acetylhexosaminidase release. *J Cell Physiol.* 2003; 194:71-79.
 53. Lisignoli G, Manferdini C, Codeluppi K, Piacentini A, Grassi F, Cattini L, Filardo G, Facchini A. CCL20/CCR6 chemokine/receptor expression in bone tissue from osteoarthritis and rheumatoid arthritis patients: Different response of osteoblasts in the two groups. *J Cell Physiol.* 2009; 221:154-160.
 54. Heymann D, Pathak JL, Bakker AD, Verschueren P, Lems WF, Luyten FP, Klein-Nulend J, Bravenboer N. CXCL8 and CCL20 enhance osteoclastogenesis *via* modulation of cytokine production by human primary osteoblasts. *PLoS One.* 2015; 10:e0131041.
 55. Lisignoli G, Toneguzzi S, Piacentini A, Cristino S, Grassi F, Cavallo C, Facchini A. CXCL12 (SDF-1) and CXCL13 (BCA-1) chemokines significantly induce proliferation and collagen type I expression in osteoblasts from osteoarthritis patients. *J Cell Physiol.* 2006; 206:78-85.
 56. Campbell JJ, Butcher EC. Chemokines in tissue-specific and microenvironment-specific lymphocyte homing. *Curr Opin Immunol.* 2000; 12:336-341.
 57. Lean JM, Murphy C, Fuller K, Chambers TJ. CCL9/MIP-1 γ and its receptor CCR1 are the major chemokine ligand/receptor species expressed by osteoclasts. *J Cell Biochem.* 2002; 87:386-393.
 58. Yu X, Huang Y, Collin-Osdoby P, Osdoby P. CCR1 chemokines promote the chemotactic recruitment, RANKL development, and motility of osteoclasts and are induced by inflammatory cytokines in osteoblasts. *J Bone Miner Res.* 2004; 19:2065-2077.
 59. Lee JE, Shin HH, Lee EA, Van Phan T, Choi HS. Stimulation of osteoclastogenesis by enhanced levels of MIP-1 α in BALB/c mice *in vitro*. *Exp Hematol.* 2007; 35:1100-1108.
 60. Andrade I, Taddei SRA, Garlet GP, Garlet TP, Teixeira AL, Silva TA, Teixeira MM. CCR5 down-regulates osteoclast function in orthodontic tooth movement. *J Dent Res.* 2009; 88:1037-1041.
 61. De Rossi A, Rocha LB, Rossi MA. Interferon-gamma, interleukin-10, intercellular adhesion molecule-1, and chemokine receptor 5, but not interleukin-4, attenuate the

- development of periapical lesions. *J Endod.* 2008; 34:31-38.
62. Menu E, De Leenheer E, De Raeve H, Coulton L, Imanishi T, Miyashita K, Van Valckenborgh E, Van Riet I, Van Camp B, Horuk R, Croucher P, Vanderkerken K. Role of CCR1 and CCR5 in homing and growth of multiple myeloma and in the development of osteolytic lesions: A study in the 5TMM model. *Clin Exp Metastasis.* 2006; 23:291-300.
 63. Vierboom MP, Zavodny PJ, Chou CC, Tagat JR, Pugliese-Sivo C, Strizki J, Steensma RW, McCombie SW, Celebi-Paul L, Remarque E, Jonker M, Narula SK, and Hart B. Inhibition of the development of collagen-induced arthritis in rhesus monkeys by a small molecular weight antagonist of CCR5. *Arthritis Rheum.* 2005; 52:627-636.
 64. Okamoto H, and Kamatani N. A CCR-5 antagonist inhibits the development of adjuvant arthritis in rats. *Rheumatology (Oxford).* 2006; 45:230-232.
 65. Binder NB, Niederreiter B, Hoffmann O, Stange R, Pap T, Stulnig TM, Mack M, Erben RG, Smolen JS, Redlich K. Estrogen-dependent and C-C chemokine receptor-2-dependent pathways determine osteoclast behavior in osteoporosis. *Nat Med.* 2009; 15:417-424.
 66. Grassi F, Piacentini A, Cristino S, Toneguzzi S, Cavallo C, Facchini A, Lisignoli G. Human osteoclasts express different CXC chemokines depending on cell culture substrate: Molecular and immunocytochemical evidence of high levels of CXCL10 and CXCL12. *Histochem Cell Biol.* 2003; 120:391-400.
 67. Semerad CL, Christopher MJ, Liu F, Short B, Simmons PJ, Winkler I, Levesque JP, Chappel J, Ross FP, Link DC. G-CSF potently inhibits osteoblast activity and CXCL12 mRNA expression in the bone marrow. *Blood.* 2005; 106:3020-3027.
 68. Le Y, Zhou Y, Iribarren P, Wang J. Chemokines and chemokine receptors: Their manifold roles in homeostasis and disease. *Cell Mol Immunol.* 2004; 1:95-104.
 69. Pandey MK, Kale VP, Song C, Sung S-s, Sharma AK, Talamo G, Dovat S, Amin SG. Gambogic acid inhibits multiple myeloma mediated osteoclastogenesis through suppression of chemokine receptor CXCR4 signaling pathways. *Exp Hematol.* 2014; 42:883-896.
 70. Diamond P, Labrinidis A, Martin SK, Farrugia AN, Gronthos S, To LB, Fujii N, O'Loughlin PD, Evdokiou A, Zannettino AC. Targeted disruption of the CXCL12/CXCR4 axis inhibits osteolysis in a murine model of myeloma-associated bone loss. *J Bone Miner Res.* 2009; 24:1150-1161.
 71. Yu X, Huang Y, Collin-Osdoby P, Osdoby P. Stromal cell-derived factor-1 (SDF-1) recruits osteoclast precursors by inducing chemotaxis, matrix metalloproteinase-9 (MMP-9) activity, and collagen transmigration. *J Bone Miner Res.* 2003; 18:1404-1418.
 72. Hoshino A, Iimura T, Ueha S, *et al.* Deficiency of chemokine receptor CCR1 causes osteopenia due to impaired functions of osteoclasts and osteoblasts. *J Biol Chem.* 2010; 285:28826-28837.
 73. Fu R, Liu H, Zhao S, Wang Y, Li L, Gao S, Ruan E, Wang G, Wang H, Song J, Shao Z. Osteoblast inhibition by chemokine cytokine ligand3 in myeloma-induced bone disease. *Cancer Cell Int.* 2014; 14:132.
 74. Vallet S, Pozzi S, Patel K, Vaghela N, Fulciniti MT, Veiby P, Hideshima T, Santo L, Cirstea D, Scadden DT, Anderson KC, Raje N. A novel role for CCL3 (MIP-1 α) in myeloma-induced bone disease *via* osteocalcin downregulation and inhibition of osteoblast function. *Leukemia.* 2011; 25:1174-1181.
 75. de Albuquerque Taddei SR, Queiroz-Junior CM, Moura AP, Andrade I, Garlet GP, Proudfoot AEI, Teixeira MM, da Silva TA. The effect of CCL3 and CCR1 in bone remodeling induced by mechanical loading during orthodontic tooth movement in mice. *Bone.* 2013; 52:259-267.
 76. Tsubaki M, Kato C, Manno M, Ogaki M, Satou T, Itoh T, Kusunoki T, Tanimori Y, Fujiwara K, Matsuoka H, Nishida S. Macrophage inflammatory protein-1 α (MIP-1 α) enhances a receptor activator of nuclear factor kappaB ligand (RANKL) expression in mouse bone marrow stromal cells and osteoblasts through MAPK and PI3K/Akt pathways. *Mol Cell Biochem.* 2007; 304:53-60.
 77. Yano S, Mentaverri R, Kanuparthi D, Bandyopadhyay S, Rivera A, Brown EM, Chattopadhyay N. Functional expression of β -chemokine receptors in osteoblasts: Role of regulated upon activation, normal T cell expressed and secreted (RANTES) in osteoblasts and regulation of its secretion by osteoblasts and osteoclasts. *Endocrinology.* 2005; 146:2324-2335.
 78. Repeke CE, Ferreira SB, Jr., Claudino M, Silveira EM, de Assis GF, Avila-Campos MJ, Silva JS, Garlet GP. Evidences of the cooperative role of the chemokines CCL3, CCL4 and CCL5 and its receptors CCR1+ and CCR5+ in RANKL+ cell migration throughout experimental periodontitis in mice. *Bone.* 2010; 46:1122-1130.
 79. Ferreira SB, Jr., Repeke CE, Raimundo FM, Nunes IS, Avila-Campos MJ, Ferreira BR, Santana da Silva J, Campanelli AP, Garlet GP. CCR5 mediates pro-osteoclastic and osteoclastogenic leukocyte chemoattraction. *J Dent Res.* 2011; 90:632-637.
 80. Andrade I, Jr., Taddei SR, Garlet GP, Garlet TP, Teixeira AL, Silva TA, Teixeira MM. CCR5 down-regulates osteoclast function in orthodontic tooth movement. *J Dent Res.* 2009; 88:1037-1041.
 81. Nagasawa T, Hirota S, Tachibana K, Takakura N, Nishikawa S, Kitamura Y, Yoshida N, Kikutani H, Kishimoto T. Defects of B-cell lymphopoiesis and bone-marrow myelopoiesis in mice lacking the CXC chemokine PBSF/SDF-1. *Nature.* 1996; 382:635-638.
 82. Shahnazari M, Chu V, Wronski TJ, Nissenson RA, Halloran BP. CXCL12/CXCR4 signaling in the osteoblast regulates the mesenchymal stem cell and osteoclast lineage populations. *FASEB J.* 2013; 27:3505-3513.
 83. Hirbe AC, Rubin J, Uluckan O, Morgan EA, Eagleton MC, Prior JL, Piwnica-Worms D, Weilbaecher KN. Disruption of CXCR4 enhances osteoclastogenesis and tumor growth in bone. *Proc Natl Acad Sci U S A.* 2007; 104:14062-14067.
 84. Keen JC, Garrett-Mayer E, Pettit C, Mack KM, Manning J, Herman JG, Davidson NE. Epigenetic regulation of protein phosphatase 2A (PP2A), lymphotactin (XCL1) and estrogen receptor α (ER) expression in human breast cancer cells. *Cancer Biol Ther.* 2004; 3:1304-1312.
 85. Lengi AJ, Phillips RA, Karpuzoglu E, Ahmed SA. Estrogen selectively regulates chemokines in murine splenocytes. *J Leukoc Biol.* 2007; 81:1065-1074.
 86. Seli E, Pehlivan T, Selam B, Garcia-Velasco JA, Arici A. Estradiol down-regulates MCP-1 expression in human coronary artery endothelial cells. *Fertil Steril.* 2002; 77:542-547.
 87. Fanti P, Nazareth M, Bucelli R, Mineo M, Gibbs K,

- Kumin M, Grzybek K, Raiber L, Poppenberg K, Janis K, Schwach C, Aronica SM. Estrogen decreases chemokine levels in murine mammary tissue - Implications for the regulatory role of MIP-1 α and MCP-1/JE in mammary tumor formation. *Endocrine*. 2003; 22:161-167.
88. Janis K, Hoeltke J, Nazareth M, Fanti P, Poppenberg K, Aronica SM. Estrogen decreases expression of chemokine receptors, and suppresses chemokine bioactivity in murine monocytes. *Am J Reprod Immunol*. 2004; 51:22-31.
 89. Haddad SN, Wira CR. Estradiol regulation of constitutive and keratinocyte growth factor-induced CCL20 and CXCL1 secretion by mouse uterine epithelial cells. *Am J Reprod Immunol*. 2014; 72:34-44.
 90. Linker RA, Li R, Xu W, Chen Y, Qiu W, Shu Y, Wu A, Dai Y, Bao J, Lu Z, Hu X. Raloxifene suppresses experimental autoimmune encephalomyelitis and NF- κ B-dependent CCL20 expression in reactive astrocytes. *PLoS One*. 2014; 9:e94320.
 91. Haim K, Weitzenfeld P, Meshel T, Ben-Baruch A. Epidermal growth factor and estrogen act by independent pathways to additively promote the release of the angiogenic chemokine CXCL8 by breast tumor cells. *Neoplasia*. 2011; 13:230-243.
 92. Hickey DK, Fahey JV, Wira CR. Estrogen receptor α antagonists mediate changes in CCL20 and CXCL1 secretions in the murine female reproductive tract. *Am J Reprod Immunol*. 2013; 69:159-167.
 93. Subramanian S, Yates M, Vandenbark AA, Offner H. Oestrogen-mediated protection of experimental autoimmune encephalomyelitis in the absence of Foxp3⁺ regulatory T cells implicates compensatory pathways including regulatory B cells. *Immunology*. 2011; 132:340-347.
 94. Rubio N, Arevalo M-A, Cerciat M, Sanz-Rodriguez F, Unkila M, Garcia-Segura LM. Theiler's virus infection provokes the overexpression of genes coding for the chemokine Ip10 (CXCL10) in SJL/J murine astrocytes, which can be inhibited by modulators of estrogen receptors. *J Neurovirol*. 2014; 20:485-495.
 95. Nii T, Isobe N, Yoshimura Y. The effect of estrogen on the early cytotoxic response to IB virus infection in hen oviduct. *Vet Immunol Immunopathol*. 2015; 164:56-66.
 96. Sung MJ, Kim DH, Davaatseren M, Hur HJ, Kim W, Jung YJ, Park SK, Kwon DY. Genistein suppression of TNF- α -induced fractalkine expression in endothelial cells. *Cell Physiol Biochem*. 2010; 26:431-440.
 97. Murphy HS, Sun Q, Murphy BA, Mo R, Huo J, Chen J, Chensue SW, Adams M, Richardson BC, Yung R. Tissue-specific effect of estradiol on endothelial cell-dependent lymphocyte recruitment. *Microvasc Res*. 2004; 68:273-285.
 98. Bieche I, Chavey C, Andrieu C, Busson M, Vacher S, Le Corre L, Guinebretiere JM, Burlincho S, Lidereau R, Lazennec G. CXC chemokines located in the 4q21 region are up-regulated in breast cancer. *Endocr Relat Cancer*. 2007; 14:1039-1052.
 99. Drake MT, Clarke BL, Lewiecki EM. The pathophysiology and treatment of osteoporosis. *Clin Ther*. 2015; 37:1837-1850.
 100. Kim YY, Kim SH, Oh S, Sul OJ, Lee HY, Kim HJ, Kim SY, Choi HS. Increased fat due to estrogen deficiency induces bone loss by elevating monocyte chemoattractant protein-1 (MCP-1) production. *Mol Cells*. 2010; 29:277-282.
 101. Janis K, Hoeltke J, Nazareth M, Fanti P, Poppenberg K, Aronica SM. Estrogen decreases expression of chemokine receptors, and suppresses chemokine bioactivity in murine monocytes. *Am J Reprod Immunol*. 2004; 51:22-31.
 102. Koh KK, Son JW, Ahn JY, Lee SK, Hwang HY, Kim DS, Jin DK, Ahn TH, Shin EK. Effect of hormone replacement therapy on nitric oxide bioactivity and monocyte chemoattractant protein-1 levels. *Int J Cardiol* 2001; 81:43-50.
 103. Fan XL, Duan XB, Chen ZH, Li M, Xu JS, Ding GM. Lack of estrogen down-regulates CXCR4 expression on Treg cells and reduces Treg cell population in bone marrow in OVX mice. *Cell Mol Biol (Noisy-le-grand)*. 2015; 61:13-17.
 104. Wang C, Dehghani B, Li Y, Kaler LJ, Vandenbark AA, Offner H. Oestrogen modulates experimental autoimmune encephalomyelitis and interleukin-17 production *via* programmed death 1. *Immunology*. 2009; 126:329-335.
 105. Lelu K, Laffont S, Delpy L, Paulet PE, Perinat T, Tschanz SA, Pelletier L, Engelhardt B, Guery JC. Estrogen receptor α signaling in T lymphocytes is required for estradiol-mediated inhibition of Th1 and Th17 cell differentiation and protection against experimental autoimmune encephalomyelitis. *J Immunol*. 2011; 187:2386-2393.
 106. Engdahl C, Borjesson AE, Forsman HF, Andersson A, Stubelius A, Krust A, Chambon P, Islander U, Ohlsson C, Carlsten H, Lagerquist MK. The role of total and cartilage-specific estrogen receptor α expression for the ameliorating effect of estrogen treatment on arthritis. *Arthritis Res Ther*. 2014; 16:R150.
 107. Zhao R. Immune regulation of bone loss by Th17 cells in oestrogen-deficient osteoporosis. *Eur J Clin Invest*. 2013; 43:1195-1202.
 108. Pelletier M, Maggi L, Micheletti A, Lazzeri E, Tamassia N, Costantini C, Cosmi L, Lunardi C, Annunziato F, Romagnani S, Cassatella MA. Evidence for a cross-talk between human neutrophils and Th17 cells. *Blood*. 2010; 115:335-343.
 109. van Hamburg JP, Asmawidjaja PS, Davelaar N, Mus AM, Colin EM, Hazes JM, Dolhain RJ, Lubberts E. Th17 cells, but not Th1 cells, from patients with early rheumatoid arthritis are potent inducers of matrix metalloproteinases and proinflammatory cytokines upon synovial fibroblast interaction, including autocrine interleukin-17A production. *Arthritis Rheum*. 2011; 63:73-83.
 110. Hirota K, Yoshitomi H, Hashimoto M, Maeda S, Teradaira S, Sugimoto N, Yamaguchi T, Nomura T, Ito H, Nakamura T, Sakaguchi N, Sakaguchi S. Preferential recruitment of CCR6-expressing Th17 cells to inflamed joints *via* CCL20 in rheumatoid arthritis and its animal model. *J Exp Med*. 2007; 204:2803-2812.
 111. Andersson A, Stubelius A, Karlsson M, Engdahl C, Erlandsson M, Grahnemo L, Lagerquist MK, Islander U. Estrogen regulates T helper 17 phenotype and localization in experimental autoimmune arthritis. *Arthritis Res Ther*. 2015; 17:32.

(Received April 18, 2016; Revised August 10, 2016; Accepted September 5, 2016)

Anemia in combined antiretroviral treatment-naive HIV-infected patients in China: A retrospective study of prevalence, risk factors, and mortality

Guorui Dai^{1,2,§}, Jiang Xiao^{1,§}, Guiju Gao¹, Xuejing Chong^{2,3}, Fang Wang¹, Hongyuan Liang¹, Liang Ni¹, Di Yang¹, Fengting Yu², Ling Xu^{1,2}, Di Wang^{2,3}, Junyan Han², Hui Zeng^{2,*}, Hongxin Zhao^{1,*}

¹ The National Clinical Key Department of Infectious Diseases, Beijing Ditan Hospital, Capital Medical University, Beijing, China;

² Institute of Infectious Diseases, Beijing Ditan Hospital, Capital Medical University, Beijing, China;

³ The National Clinical Key Department of Infectious Diseases, Peking University Ditan Teaching Hospital, Beijing, China.

Summary

Anemia is one of the most important complications of HIV infection. In China, the prevalence, risk factors, and association between anemia and prognosis in HIV-infected patients are poorly elucidated. We analyzed data from 3452 HIV-infected patients not yet on combined antiretroviral therapy (cART) attending Beijing Ditan Hospital from June, 2003 to December, 2015. The overall prevalence of anemia was 9.8% (7.6% mild, 1.9% moderate, and 0.2% severe anemia). Female sex (odds ratio [OR] = 3.71, 95% confidence interval [CI]: 1.46-6.51, $p = 0.003$), age 40-59 years (OR = 2.54, 95% CI: 1.59-4.05, $p < 0.001$), body mass index $< 18.5 \text{ kg/m}^2$ (OR = 2.23, 95% CI: 1.31-3.79, $p = 0.003$), baseline HIV RNA $> 10^5$ copies/mL (OR = 2.79, 95% CI: 1.85-4.20, $p < 0.001$), baseline CD4 count $\leq 50 \times 10^9/\text{L}$ (OR = 17.12, 95% CI: 7.70-38.06, $p < 0.001$) and CD4 count $51-199 \times 10^9/\text{L}$ (OR = 2.81, 95% CI: 1.32-5.99, $p = 0.007$) were risk factors for anemia. Age 40-59 years (adjusted hazard ratio [AHR] = 5.76, 95% CI: 1.62-20.55, $p = 0.007$), and anemia – mild (AHR = 7.46, 95% CI: 1.48-37.50, $p = 0.015$), moderate (AHR = 9.89, CI: 1.35-72.38, $p = 0.024$), and severe (AHR = 28.29, 95% CI: 2.75-290.54, $p = 0.005$) anemia – were associated with an increased hazard of death. In this cohort, mild anemia was most common. Anemia was associated with female sex, older age, lower body mass index, lower baseline CD4 count, and higher viral load. Moreover, anemia was associated with an increased risk of death. These findings should promote awareness among physicians to make a timely diagnosis of HIV and to help physicians prioritize prevention and intervention strategies for anemia in HIV-infected patients.

Keywords: HIV/AIDS, anemia, prevalence, mortality, risk factors

Released online in J-STAGE as advance publication November 26, 2016.

§These authors contributed equally to this works.

*Address correspondence to:

Dr. Hongxin Zhao, The National Clinical Key Department of Infectious Diseases, Beijing Ditan Hospital, Capital Medical University, No.8 Jingshun East Street, Chaoyang District, Beijing 100015, China.

E-mail: 13911022130@163.com

Dr. Hui Zeng, Department of Institute of Infectious Diseases, Beijing Ditan Hospital, Capital Medical University, No.8 Jingshun East Street, Chaoyang District, Beijing 100015, China.

E-mail: zenghui@ccmu.edu.cn

1. Introduction

Hematological abnormalities are one of the most important complications in HIV-infected patients. In those with advanced HIV infection, anemia is the most common manifestation (1). The prevalence of anemia in the HIV-infected population varies between 18.9% and 65.5%, dependent on setting and social-economic conditions (1-3); normocytic anemia is most common. Different pathogenic factors are associated with HIV-related anemia, including opportunistic infections such malaria (4) and parvovirus B19 (5) or *Penicilliosis*

marneffe (6) infection, administration of antiretroviral agents such as zidovudine (7), and myelosuppression by infiltrative malignancies (8) or infectious pathogens (6). Other mechanisms for HIV-related anemia included vitamin B12, folate, and iron deficiencies (9), and HIV-driven impairment of hematopoietic progenitor cells (10).

Anemia can cause negative physiological functioning, which results in poor quality of life. Some studies reported that in HIV-infected patients, anemia was associated with disease progression and poor prognosis (11). Moore *et al.* (12) demonstrated that treating anemia reduced the risk of death and improved prognosis, indicating the need for periodic screening for and treatment of anemia, especially among patients not yet started on combined antiretroviral therapy (cART). The prevalence of and risk factors for anemia vary remarkably in different regions in China due to different socioeconomic conditions. Shen *et al.* (13) reported that the overall prevalence of anemia among HIV-infected patients was 51.9% and that anemia was highly prevalent among Chinese adults newly diagnosed with HIV-infection, but that severe anemia was less prevalent in this population. Older age, lower CD4 count, and minority ethnicity are associated with an increased risk of anemia: Mijiti *et al.* (14) reported that 38.9% of HIV-infected patients in Xinjing Province, China, were anemic at the time of cART initiation, and that Uyghur ethnicity, female sex, lower CD4 count, lower body mass index (BMI), self-reported tuberculosis infection, and oral candidiasis were associated with a higher prevalence of anemia.

Despite the availability of cART in China (15), confirmatory anti-HIV antibody testing is often performed late, once HIV infection has progressed to AIDS and CD4 counts are low, as many people are unaware of HIV infection (16). Both clinically advanced disease and low CD4 counts are associated with an increased risk of anemia (17). In China, the prevalence of anemia varies markedly between different regions (3), and mild anemia is prone to be neglected in clinical work. The prevalence of and risk factors for anemia, and the association between anemia and prognosis in HIV-infected patients are not well documented in China. Therefore, in this study, we retrospectively studied the baseline, pre-cART prevalence of anemia; the risk factors associated with anemia; and its impact on mortality in HIV-infected patients in Beijing Ditan Hospital, the largest specialized hospital for HIV-infected patients in North China. Further, we analyzed the trends of anemia incidence over the study period, once patients were established on cART.

2. Materials and Methods

2.1. Ethical considerations

This retrospective observational cohort study was

approved by the institutional review board of Beijing Ditan Hospital, the Capital Medical University, and complies with principles of the Declaration of Helsinki. Existing routine clinical and therapeutic data were anonymously used and were abstracted from the electronic medical records in Ditan Hospital; hence, the need for informed consent was waived.

2.2. Patient selection

We conducted the retrospective study in Beijing Ditan Hospital, the largest designated tertiary care hospital for HIV/AIDS in North China, from June, 2003 to December, 2015. Eligible participants were HIV-infected, confirmed by enzyme-linked immunosorbent assay (ELISA) and Western Blot testing; cART-naïve, ready to initiate treatment; and aged ≥ 18 years. We excluded patients who received interferon or ribavirin, patients with cirrhosis, and pregnant women.

2.3. Definitions and outcome

Prior to receiving cART, routine baseline blood tests were performed. Anemia was diagnosed as a hemoglobin level < 110 g/L (women) or < 120 g/L (men). Anemia status was categorized as: mild (hemoglobin 90-109 g/L [women] or 90-119 g/L [men]), moderate (60-89 g/L), and severe (hemoglobin < 60 g/L). Baseline leucopenia was diagnosed as a white cell count < 4.0 cells $\times 10^9$ /L and thrombocytopenia as a platelet count $< 100 \times 10^9$ /L in peripheral blood.

After cART initiation, follow-ups were scheduled at 2nd week, 1st month, 2nd month, 3rd month and every 3 month thereafter. At the time of follow-up, CD4 cell counts were routinely tested every 3 months, and viral load was tested every 6 months. The detail data about enrollment, dead cases and lost to follow-up were shown in Table supplement 1 (Table S1).

The primary outcome was death. The date of death was recorded in the electronic medical record system in Ditan Hospital, which helped to provide time from initial diagnosis to death.

The National Free Antiretroviral Treatment Program (NFATP) provides antiretroviral therapy and follow-up for HIV-infected patients in China (18), and 1-month antiretroviral regimens are provided to HIV-infected patients during first 3 months after initiation of cART, and after that, 3-month regimens are provided to patients, which helps control periodic follow-up rate in HIV-infected patients in China.

Clinical data about baseline evaluation, follow-up, lost to follow-up and dead cases are recorded in electronic medical records and provided to database in NFATP. Ditan Hospital is an observational sentinel for NFATP, which serves HIV-infected population in Beijing. The patients in our cohort are outpatients, who initiate antiretroviral therapy and receive follow-up in Ditan

Hospital. Mortality was calculated due to unambiguous records in database in NFATP.

We also found some patients were withdrawal during follow-up, and Zhang *et al.* (19) reported that factors independently associated with a higher likelihood of missed visits included female gender, age > 60 years, HIV transmission via injection drug use or plasma donation, baseline alanine aminotransferase >100 IU/L, and having more symptoms at antiretroviral therapy initiation.

2.4. Data collection

Study participants completed scheduled structured questionnaires, eliciting data on sociodemographic and clinical characteristics including sex, age, height, weight, transmission routes, World Health Organization (WHO) clinical stage, and trimethoprim/sulfamethoxazole (SMX-TMP) co-administration. BMI was calculated as weight (kg) divided by the square of height (m). Baseline laboratory tests were performed to measure CD4 count, HIV viral load, hemoglobin, white cell count, and platelet levels, and to detect hepatitis B (HBV) or C (HCV) virus infection.

2.5. Statistical analysis

Descriptive analysis was conducted, using frequency and percentages. Bar charts were used to illustrate the proportion of patients with mild, moderate, and severe anemia, stratified by CD4 count and outcome. Incidence rates were calculated as the number of cases of anemia per 100 person-years, and line charts were used to illustrate the trends in incidence of anemia during the follow-up period.

In this study, univariate logistic regression models were used to determine associations between anemia and the following variables: sex; age; HIV transmission route; WHO clinical stage; BMI; baseline CD4, white cell, and platelet counts; baseline and follow-up HIV viral load; SMZ-TMP co-administration; and baseline HBV/HCV co-infection. Statistically significant variables were fitted into a subsequent multivariate logistic regression models.

Cox proportional hazards models were used to evaluate the impact of anemia on mortality in HIV-infected patients. Kaplan-Meier survival curves were computed to evaluate the survival of HIV-infected patients with and without anemia. Log-rank testing was conducted to evaluate differences in cumulative survival between the two groups. All statistical analyses were performed using SPSS version 19.0 (SPSS Institute, Chicago IL, USA). Alpha was set to 0.05, and 95% confidence intervals (CI) were used.

3. Results

3.1. Demographic and clinical characteristics

From June, 2003 to December, 2015, we enrolled 3452 HIV-infected patients into our study. Table 1 describes their demographic and clinical characteristics. The median age of study subjects was 33.7 (range, 18-83) years and 93.7% were men. Sexual contact was the most common route of transmission (3124 cases, 90.5%); 79.8% was due to homosexual contact (2756 cases) and 10.7% was due to extra-marital heterosexual contact (368 cases). Overall, 38.1% of study subjects had a baseline CD4 count < 200 cells × 10⁹/L.

3.2. Prevalence of anemia, overall and stratified by CD4 count category

The overall prevalence of anemia prior to initiating cART was 9.76% ($n = 337$), with mild, moderate, and severe anemia observed in 7.6% ($n = 263$), 1.9% ($n = 66$), and 0.2% ($n = 8$) of patients, respectively (Table 1). Among patients with CD4 cell counts of ≤ 50, 51-199, 200-349, and ≥ 350 × 10⁹/L the prevalence of anemia was 43.0%, 11.0%, 2.7%, and 2.1%, respectively (Figure 1 and Table 1).

3.3. Predictors of anemia in HIV-infected patients

As seen in Table 2, the multivariate logistic regression model indicated that female sex (odds ratio [OR]: 3.71, 95% CI: 1.46-6.51, $p = 0.003$), age 40-59 years (OR: 2.54, 95% CI: 1.59-4.05, $p < 0.001$), age > 60 years (OR: 2.80, 95% CI: 1.80-7.24, $p = 0.034$), and BMI < 18.5 kg/m² (OR: 2.23, 95% CI: 1.31-3.79, $p = 0.003$, compared with normal BMI and overweight), were associated with increased odds of anemia. Laboratory tests indicated that baseline HIV viral load > 10⁵ copies/mL (OR: 2.79, 95% CI: 1.85-4.20, $p < 0.001$), baseline CD4 count ≤ 50 × 10⁹/L (OR: 17.12, 95% CI: 7.70-38.06, $p < 0.001$), and CD4 count 51-199 × 10⁹/L (OR: 2.81, 95% CI: 1.32-5.99, $p = 0.007$) were risk factors for anemia. Anemia was not associated with route of HIV transmission, WHO clinical stage, baseline HIV viral load, SMZ-TMP co-administration, or baseline HBV/HCV co-infection status.

3.4. Mortality, stratified by CD4 count category and by anemia

Overall, 1.3% ($n = 44$) of the cohort died. Among patients with mild, moderate, and severe anemia, mortality was 7.2% (19 of 263), 10.6% (7 of 66), and 12.5% (1 of 8), respectively (Table 1). Figure 2 displays mortality stratified by level of immune suppression (CD4 count category).

3.5. Survival analysis

The multivariate Cox regression model indicated that age 40-59 years (adjusted hazard ratio [AHR]: 5.76,

Table 1. Baseline demographic, clinical, and laboratory characteristics of HIV-infected patients

Characteristic	Total	Deaths	With anemia	Without anemia
Total	3,452 (100)	44 (1.27)	337 (9.76)	3,115 (90.24)
Sex				
Male	3,233 (93.66)	42 (1.30)	299 (9.25)	2,934 (90.75)
Female	219 (6.34)	2 (0.91)	38 (17.35)	181 (82.65)
Age (years)				
18-39	2,673 (77.43)	12 (0.45)	208 (7.78)	2,465 (92.22)
40-59	676 (19.58)	22 (3.25)	103 (15.24)	573 (84.76)
≥ 60	103 (2.98)	10 (9.71)	26 (25.24)	77 (74.76)
Transmission route				
Sexual	3,124 (90.50)	30 (0.96)	284 (9.09)	2,870 (91.87)
Transfusion	98 (2.84)	8 (8.16)	27 (27.55)	71 (72.45)
Unknown	230 (6.63)	6 (2.61)	26 (11.30)	174 (75.65)
WHO clinical stage				
I	2,536 (73.46)	16 (0.63)	165 (6.51)	2,371 (93.49)
II	212 (6.14)	3 (1.42)	14 (6.60)	198 (93.40)
III	244 (7.07)	4 (1.64)	25 (10.25)	219 (89.75)
IV	460 (13.33)	21 (4.57)	133 (28.91)	327 (71.09)
BMI (kg/m ²) ^a				
18.5-24	1,823 (67.10)	15 (0.82)	182 (9.98)	1,641 (90.02)
< 18.5	300 (11.04)	6 (0.02)	98 (32.67)	202 (67.33)
≥ 24	594 (21.86)	5 (0.84)	27 (4.55)	567 (95.45)
CD4 count (× 10 ⁹ /L)				
≥ 350	813 (23.55)	1 (0.12)	17 (2.09)	796 (97.91)
200-349	1,325 (38.38)	7 (0.53)	36 (2.72)	1,289 (97.28)
51-199	879 (25.46)	16 (1.82)	97 (11.04)	782 (88.96)
≤ 50	435 (12.60)	20 (4.60)	187 (42.99)	248 (57.01)
HIV RNA level (copies/mL) ^a				
< 100,000	2,306 (74.75)	16 (0.69)	87 (3.77)	2,219 (96.23)
≥ 100,000	779 (25.25)	12 (1.54)	178 (22.85)	601 (77.15)
White cell count (× 10 ⁹ /L)				
≥ 4.0	2,894 (83.84)	28 (0.97)	180 (6.22)	2,714 (93.78)
< 4.0	558 (16.16)	16 (2.87)	157 (28.14)	401 (71.86)
Platelet count (× 10 ⁹ /L)				
≥ 100	3,315 (96.03)	33 (1.00)	292 (8.81)	3,023 (91.20)
< 100	137 (3.97)	11 (8.03)	45 (32.85)	92 (67.15)
SMZ-TMP co-administration				
No	3,122 (90.44)	39 (1.25)	241 (7.72)	2,881 (92.28)
Yes	330 (9.56)	5 (1.52)	96 (29.09)	234 (70.91)
HBV/HCV co-infection				
No	3,236 (93.74)	37 (1.14)	312 (9.64)	2,924 (90.36)
Yes	216 (6.26)	7 (3.24)	25 (11.57)	191 (88.43)
Anemia				
Mild	263 (7.62)	19 (7.22)	263 (100.0)	-
Moderate	66 (1.91)	7 (10.61)	66 (100.0)	-
Severe	8 (0.23)	1 (12.50)	8 (100.0)	-

Data are presented as n (%); WHO, World Health Organization; BMI, body mass index; SMZ-TMP, Trimethoprim/sulfamethoxazole; ^aVariable had missing values: BMI = 735; HIV RNA level = 367.

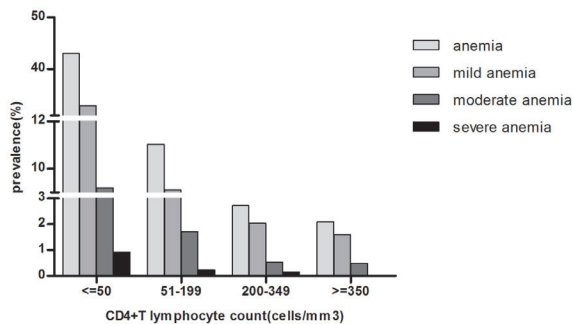


Figure 1. Prevalence of anemia in HIV-infected patients stratified by CD4 count category. The numbers of patients with CD4 counts of ≤ 50, 51-199, 200-349, and ≥ 350 × 10⁹/L were 435, 879, 1,325, and 813, respectively. The number of cases of anemia among CD4 counts of ≤ 50, 51-199, 200-349, and ≥ 350 × 10⁹/L were 187, 97, 36, and 17, respectively.

95% CI: 1.62-20.55, *p* = 0.007), mild anemia (AHR: 7.46, 95% CI: 1.48-37.50, *p* = 0.015), moderate anemia (AHR: 9.89, 95% CI: 1.35-72.38, *p* = 0.024), and severe anemia (AHR: 28.29, 95% CI: 2.75-290.54, *p* = 0.005) were associated with an increased hazard of mortality (Table 3). To clarify the effects of anemia on survival, Kaplan-Meier survival curves were plotted, stratified by presence or absence of anemia (Figure 3); log-rank testing demonstrated that there was a significant difference between the two groups (*p* < 0.05).

3.6. Incidence of anemia, stratified by sex

In this cohort, 79.8% of study participants were men infected with HIV through homosexual sexual contact.

Table 2. Risk factors for anemia by logistic regression analysis in HIV-infected patients

Characteristic	Anemia, n (%)	Univariate OR (95%CI)	p	Multivariate OR (95%CI)	p
Sex					
Male	299 (9.25)	1	-	1	-
Female	38 (17.35)	2.06 (1.42-2.98)	< 0.001	3.71 (1.46-6.51)	0.003
Age (years)					
18-39	208 (7.78)	1	-	1	-
40-59	103 (15.24)	2.13 (1.65-2.74)	< 0.001	2.54 (1.59-4.05)	< 0.001
≥ 60	26 (25.24)	4.00 (2.51-6.38)	< 0.001	2.801 (1.08-7.24)	0.034
Transmission route					
Sexual	284 (9.00)	1	-	1	-
Transfusion	27 (27.55)	3.99 (2.53-6.28)	< 0.001	1.59 (0.55-4.58)	0.395
Unknown	26 (13.07)	1.46 (0.94-2.26)	0.089	1.16 (0.52-2.56)	0.719
WHO stage					
I	165 (6.51)	1	-	1	-
II	14 (6.60)	1.02 (0.58-1.77)	0.942	0.58 (0.20-1.67)	0.310
III	25 (10.25)	1.52 (0.96-2.40)	0.075	0.80 (0.37-1.75)	0.579
IV	133 (28.91)	5.96 (4.60-7.72)	< 0.001	1.27 (0.79-2.06)	0.327
BMI (kg/m²)					
18.5-24	182 (9.98)	1	-	1	-
< 18.5	98 (32.67)	4.23 (3.06-5.84)	< 0.001	2.23 (1.31-3.79)	0.003
≥ 24	27 (4.55)	0.50 (0.32-0.78)	0.002	0.62 (0.35-1.10)	0.098
Baseline CD4 count (× 10⁹/L)					
≥ 350	17 (2.09)	1	-	1	-
200-349	36 (2.72)	1.31(0.73-2.34)	0.368	1.01 (0.47-2.15)	0.987
51-199	97 (11.04)	5.81 (3.44-9.82)	< 0.001	2.81 (1.32-5.990)	0.007
≤ 50	187 (42.99)	35.31 (21.06-59.18)	< 0.001	17.12 (7.70-38.06)	< 0.001
Baseline HIV RNA level (copies/mL)					
< 100,000	87 (3.77)	1	-	1	-
≥ 100,000	178 (22.85)	5.51 (4.19-7.23)	< 0.001	2.79 (1.85-4.20)	< 0.001
Baseline white cell count (× 10⁹/L)					
≥ 4.0	180 (6.22)	1	-	1	-
< 4.0	157 (28.14)	5.90 (4.65-7.49)	< 0.001	2.12 (1.33-3.37)	0.002
Baseline platelet count (× 10⁹/L)					
≥ 100	292 (8.81)	1	-	1	-
< 100	45 (32.84)	5.06 (3.48-7.38)	< 0.001	1.71 (0.79-3.72)	0.175
SMZ-TMP co-administration					
No	241 (7.72)	1	-	1	-
Yes	96 (29.09)	4.87 (3.72-6.39)	< 0.001	0.98 (0.60-1.60)	0.940
Baseline HBV/HCV co-infection					
No	312 (9.64)	1	-	1	-
Yes	25 (11.57)	0.74 (0.75-1.14)	0.173	0.68 (0.32-1.47)	0.329

OR, odds ratio; WHO, World Health Organization; BMI, body mass index; SMZ-TMP, Trimethoprim/sulfamethoxazole.

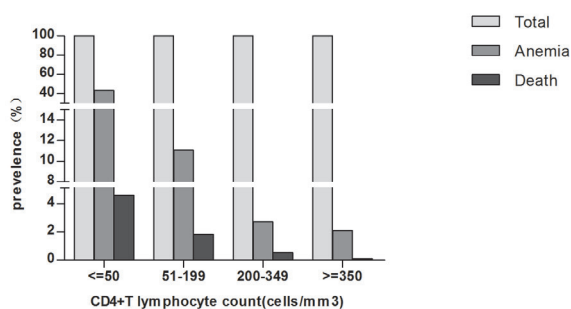


Figure 2. Mortality among HIV-infected patients stratified by CD4 count category. The number of deaths in the CD4 count categories ≤ 50, 51-199, 200-349, and ≥ 350 × 10⁹/L were 20, 16, 7, and 1, respectively.

Given that the risk factors for anemia differ by sex, we examined total and sex-specific incidence rates of anemia (Figure 4). The incidence of anemia in women was significantly higher than that in men ($p < 0.05$).

4. Discussion

Hematologic abnormalities are reportedly the most common complications of advanced HIV infection (20), with anemia being the most common hematologic abnormality. Anemia affects a large proportion of those with advanced-stage HIV-infection. Moreover, anemia is an independent risk factor for morbidity and mortality in HIV-infected patients (11,15). The prevalence and incidence of anemia varies in different socioeconomic conditions and clinical settings. In Europe and North America, anemia was found in 35-65% of HIV-infected patients pre-cART (21,22). Prevalence rates of 42.9% (3) and 18.9% (1) were reported in Ethiopia and in a rural Ugandan cohort, respectively. In a study conducted in China, Shen *et al.* (13) reported a prevalence of anemia of 51.9% in patients newly diagnosed with HIV infection. In our study, the prevalence of anemia was 9.76%, lower than

Table 3. Cox proportional hazard regression analysis of mortality in HIV-infected patients

Characteristics	Univariate analysis HR (95%CI)	<i>p</i>	Multivariate analysis AHR (95%CI)	<i>p</i>
Sex				
Male	1	-	1	-
Female	0.57 (0.14-2.38)	0.441	0.22 (0.03-1.63)	0.139
Age (years)				
18-39	1	-	1	0
40-59	6.17 (3.03-12.55)	< 0.001	5.76 (1.62-20.55)	0.007
≥ 60	13.34 (5.01-35.55)	< 0.001	4.50 (0.43-46.97)	0.208
WHO Stage				
I	1	-	1	-
II	0.91 (0.21-4.03)	0.904	0.81 (0.18-3.55)	0.774
III	1.93 (0.55-6.76)	0.303	1.36 (0.38-4.84)	0.663
IV	5.28 (2.47-11.29)	< 0.001	1.63 (0.78-3.75)	0.251
BMI (kg/m²)				
18.5-24	1	-	1	-
< 18.5	2.84 (1.03-7.86)	0.044	0.86 (0.16-4.66)	0.865
≥ 24	1.30 (0.33-3.20)	0.956	1.55 (0.36-6.65)	0.556
Baseline CD4 count (× 10⁹/L)				
≥ 350	1	-	1	-
200-349	1.22 (0.25-6.08)	0.806	1.15 (0.23-5.73)	0.747
51-199	5.64 (1.31-24.19)	0.020	3.35 (0.77-14.55)	0.569
≤ 50	7.71 (1.74-34.18)	0.007	2.05 (0.44-9.63)	0.112
Baseline HIV RNA level (copies/mL)				
< 100,000	1	-	1	-
≥ 100,000	1.58 (0.73-3.43)	0.249	0.71 (0.21-2.36)	0.575
Anemia				
Mild	13.50 (6.65-27.42)	< 0.001	7.46 (1.48-37.50)	0.015
Moderate	20.75 (8.35-51.59)	< 0.001	9.89 (1.35-72.38)	0.024
Severe	19.13 (2.50-149.34)	0.004	28.29 (2.75-290.54)	0.005

HR, hazard ratio; AHR, adjusted hazard ratio; WHO, World Health Organization; BMI, body mass index.

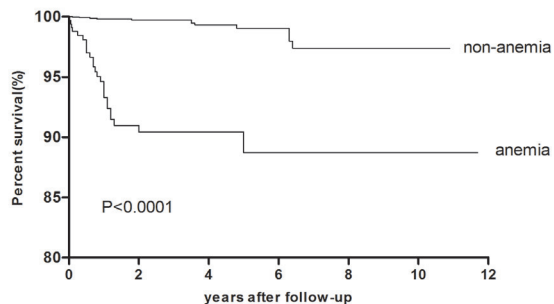


Figure 3. Survival curve for HIV-infected patients with or without anemia. Log-rank test *p* < 0.001.

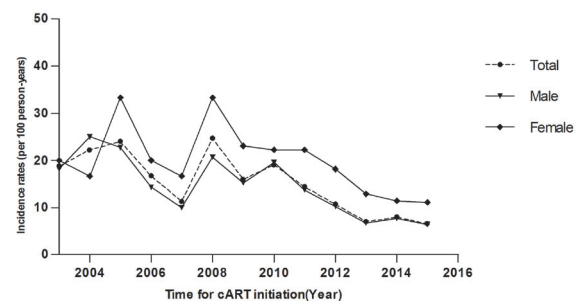


Figure 4. Incidence of anemia in HIV-infected patients, stratified by sex. Incidence rates of anemia in female HIV-infected patients were significantly higher than those in male patients (*p* < 0.05).

observed in previous studies. This low prevalence was remarkable, and may be explained by our study setting: First, patients were managed in a hospital-based setting (23). This has some advantages over community-based treatment models (24) that are commonly applied in China, including timely diagnosis of HIV infection and early detection of anemia. Healthcare workers in the hospital-based HIV treatment model formed a coordinated team to provide support to individuals with high-risk exposure or to cART-naïve patients (23), including counseling, earlier HIV testing of individuals at high-risk, periodic CD4 cell count measurement, routine blood tests, and timely cART initiation. These interventions significantly reduce morbidity

and mortality. Second, we included a high proportion of urban residents. Ditan Hospital, an observational sentinel for the National Free Antiretroviral Treatment Program (NFATP) in China (23), serves urban residents in Beijing. Urban study subjects may have received more adequate information about nutrition and routine blood testing than their rural counterparts. Third, cART was initiated at higher CD4 count thresholds than in previous studies. The guidelines for the use of antiretroviral agents in China (25) recommend initiation of cART at a CD4 count < 350 × 10⁹/L, or a CD4 count > 350 × 10⁹/L certain clinical criteria are met. Some studies documented that a CD4 count < 200 × 10⁹/L

was associated with myelosuppression and anemia (20). Thus, initiating cART at a higher CD4 count threshold reduces the risk of anemia.

Several mechanisms contribute to the pathophysiology of anemia in HIV-infected patients, including increased destruction and decreased or inadequate production of red blood cells (13,26). Alexaki *et al.* (27) documented that anemia occurred in the absence of opportunistic infections, malignancies, and chemotherapy in HIV-infected patients; hence, HIV itself must be involved in the pathophysiology of hematological abnormalities. Anemia may be associated with three HIV-driven mechanisms (10): *i*) impaired proliferation of hematopoietic progenitor cells, *ii*) inhibition of differentiation of hematopoietic progenitor cells into cell lineages, and *iii*) impairment of stromal cells. Moses *et al.* (28) demonstrated that stromal cells in the microenvironment of the bone marrow can be infected with HIV, resulting in dysregulation of cytokine expression and decreased red blood cell production. Erythropoietin is a glycoprotein hormone that controls erythropoiesis. Some studies demonstrated erythropoietin resistance as a pathophysiological phenomenon in HIV-infected patients (9), in which circulating auto-antibodies against endogenous erythropoietin blunted the normal physiological cytokine response to anemia. Vanasse *et al.* (29) reported that erythropoietin resistance was found in the hematopoietic stem cells of aging individuals, and that senescence was related to enhanced expression of inflammatory cytokines that positively regulated erythropoietin resistance, leading to anemia in older age. Older age was found to be an independent risk factor for anemia in this study.

The most statistically significant risk factors for anemia in HIV-infected patients in this study were age ≥ 40 years, female sex, BMI < 18.5 kg/m², and baseline CD4 count $\leq 199 \times 10^9$ /L. The higher prevalence of anemia in women might be due to menstrual blood loss that drains iron stores. Lower BMI is related to malnutrition and nutrient deficiencies, including deficiencies of vitamin B12, folate, and iron, which directly result in anemia. Similar to prior findings (3,20), our results found a strong independent association between CD4 count $\leq 199 \times 10^9$ /L and anemia; this association was most pronounced in those with a CD4 count $< 50 \times 10^9$ /L. We also demonstrated that higher baseline HIV viral loads were associated with anemia. Sullivan *et al.* (30) demonstrated that, as HIV infection progressed and immune status deteriorated, HIV viral loads increased, causing cytokine-mediated myelosuppression and anemia.

Although SMX-TMP administration may cause drug-induced aplastic anemia, several studies (30,31) failed to find this association. Keisu *et al.* (31) found that SMX-TMP induced anemia, but that this effect was sporadic. Conversely, Sullivan *et al.* (30) demonstrated a negative association between SMX-TMP use and

anemia, explained by the protective effect of SMX-TMP in preventing infections caused by some opportunistic pathogens (such as *Mycobacterium avium* complex) that can contribute to the development of anemia. In the present study, we failed to demonstrate an association between SMX-TMP administration and anemia. We also we failed to demonstrate an association between HIV/HCV or HIV/HBV co-infection and anemia. Such co-infections can cause anemia due to interferon-associated antiviral therapy or decompensated cirrhosis. That we did not observe this is most likely explained by our exclusion of those receiving interferon or ribavirin and of those diagnosed with cirrhosis.

In the multivariate Cox regression analysis, we found that anemia was the most statistically significant predictor of mortality in HIV-infected patients. Similarly, Santiago-Rodríguez *et al.* (17) reported that anemia was the strongest predictor of mortality in a cohort of HIV-infected Hispanics, and that the risk of mortality was proportional to the severity of anemia. In a study involving a large urban HIV clinical practice in the US, Moore *et al.* (32) indicated that the development of anemia was associated with decreased survival, independent of other prognostic factors. In addition, Mocroft *et al.* (33) demonstrated that a 10 g/L decrease in most recent hemoglobin level increased the hazard of death by 57%, implying that prophylactic measures against anemia should be instituted in HIV-infected patients with CD4 counts $< 200 \times 10^9$ /L or in patients with higher HIV viral loads. Such prophylactic measures would include vitamin B12, folate, and iron supplementation, and avoidance of myelosuppressive drugs such as zidovudine. The Chinese national HIV treatment guidelines (25) recommend the use of zidovudine in first-line cART regimens. However, zidovudine should be avoided when initiating cART in patients with the above-mentioned anemia-related risk factors, based on baseline evaluation prior to treatment initiation. Some studies have indicated (3) that use of cART improves anemia, suggesting that cART should be initiated as soon as possible in HIV-infected patients with anemia.

Our study has some limitations. First, this was a retrospective observational study; hence, it was subject to the potential biases inherent in the use of observational data. Second, the study sample selection influenced the findings. The study population comprised urban residents in Beijing, who were treated within a hospital-based HIV treatment model. This limits the generalizability of our findings, as the study sample does not represent the HIV-infected population in China more generally, many of whom are treated within community-based treatment models. Third, data were obtained from baseline evaluation prior to initiating cART. This impeded us from elucidating associations between anemia and variables that change over time.

In summary, the overall prevalence of anemia

in cART-naïve patients was 9.76% and mild anemia was most common. Anemia was associated with female sex, older age, lower BMI, lower baseline CD4 count, and baseline higher viral load, but was not associated with route of HIV transmission, WHO clinical stage, baseline HIV viral load, SMZ-TMP co-administration, or baseline HBV/HCV co-infection. Anemia was associated with an increased risk of mortality in cART-naïve patients. These findings should be used to promote awareness among physicians to identify anemia early and to prioritize prevention and intervention strategies for anemia in HIV-infected patients.

Acknowledgements

We acknowledge the work of HIV health care providers for their diagnosis, nursing, and treatment of HIV-infected patients in Ditan Hospital. We acknowledge the work of social workers and volunteers in Beijing Red Ribbon who provide counseling, adherence interventions and resolving psychosocial issues for HIV/AIDS patients.

Support for this work was provided by: 1) Healthcare Talent Training Program in Beijing Health System (grant 2015-3-105); 2) the National Natural Science Fund The study of T-cell repertoire diversity in AIDS patients based on the restoration of thymic function (grant 81371804); 3) The Capital Health Research and Development of Special (grant 2014-2-2173); and 4) Beijing Municipal Administration of Hospitals' Youth Programme (No. QML20151701)

The funders had no role in study design, data collection and analysis, decision to publish, or preparation of the manuscript.

References

- Mugisha JO, Shafer LA, Van der Paal L, Mayanja BN, Eotu H, Hughes P, Whitworth JA, Grosskurth H. Anaemia in a rural Ugandan HIV cohort: Prevalence at enrolment, incidence, diagnosis and associated factors. *Trop Med Int Health*. 2008; 13:788-794.
- Dikshit B, Wanchu A, Sachdeva RK, Sharma A, Das R. Profile of hematological abnormalities of Indian HIV infected individuals. *BMC Blood Disord*. 2009; 9:5.
- Assefa M, Abegaz WE, Shewamare A, Medhin G, Belay M. Prevalence and correlates of anemia among HIV infected patients on highly active anti-retroviral therapy at Zewditu Memorial Hospital, Ethiopia. *BMC Hematol*. 2015; 15:6.
- Naing C, Sandhu NK, Wai VN. The effect of malaria and HIV co-infection on anemia: A meta-analysis. *Medicine (Baltimore)*. 2016; 95:e3205.
- Ferry T, Hirschel B, Dang T, Meylan P, Delhumeau C, Rauch A, Weber R, Elzi L, Bernasconi E, Schmid P, Calmy A; Swiss HIV Cohort Study. Infrequent replication of parvovirus B19 and erythrovirus genotypes 2 and 3 among HIV-infected patients with chronic anemia. *Clin Infect Dis*. 2010; 50:115-118.
- Qiu Y, Zhang J, Liu G, Zhong X, Deng J, He Z, Jing B. Retrospective analysis of 14 cases of disseminated *Penicillium marneffei* infection with osteolytic lesions. *BMC Infect Dis*. 2015; 15:47.
- Akilimali PZ, Kashala-Abotnes E, Musumari PM, Kayembe PK, Tylleskar T, Mapatano MA. Predictors of persistent anaemia in the first year of antiretroviral therapy: A retrospective cohort study from Goma, the Democratic Republic of Congo. *PLoS One*. 2015; 10:e0140240.
- Bidmos MA, Joubert S, van Jaarsveld MF, Louw VJ. Plasma cell leukaemia and HIV co-infection: Profile of patients and experience at Universitas Academic Hospital in Bloemfontein, South Africa. *Int J Hematol*. 2013; 98:672-680.
- Redig AJ, Berliner N. Pathogenesis and clinical implications of HIV-related anemia in 2013. *Hematology Am Soc Hematol Educ Program*. 2013; 2013:377-381.
- Gibellini D, Clò A, Morini S, Misericocchi A, Ponti C, Re MC. Effects of human immunodeficiency virus on the erythrocyte and megakaryocyte lineages. *World J Virol*. 2013; 2:91-101.
- Moyle G. Anaemia in persons with HIV infection: Prognostic marker and contributor to morbidity. *AIDS Rev*. 2002; 4:13-20.
- Moore RD. Anemia and human immunodeficiency virus disease in the era of highly active antiretroviral therapy. *Semin Hematol*. 2000; 37(4 Suppl 6):18-23.
- Shen Y, Wang Z, Lu H, Wang J, Chen J, Liu L, Zhang R, Zheng Y. Prevalence of anemia among adults with newly diagnosed HIV/AIDS in China. *PLoS One*. 2013; 8:e73807.
- Mijiti P, Yuexin Z, Min L, Wubuli M, Kejun P, Upur H. Prevalence and predictors of anaemia in patients with HIV infection at the initiation of combined antiretroviral therapy in Xinjiang, China. *Int J STD AIDS*. 2015; 26:156-164.
- Zhang F, Dou Z, Ma Y, Zhang Y, Zhao Y, Zhao D, Zhou S, Bulterys M, Zhu H, Chen RY. Effect of earlier initiation of antiretroviral treatment and increased treatment coverage on HIV-related mortality in China: A national observational cohort study. *Lancet Infect Dis*. 2011; 11:516-524.
- Xiao J, Gao G, Li Y, Zhang W, Tian Y, Huang Y, Su W, Han N, Yang D, Zhao H. Spectrums of opportunistic infections and malignancies in HIV-infected patients in tertiary care hospital, China. *PLoS One*. 2013; 8:e75915.
- Santiago-Rodríguez EJ, Mayor AM, Fernández-Santos DM, Ruiz-Candelaria Y, Hunter-Mellado RF. Anemia in a cohort of HIV-infected Hispanics: Prevalence, associated factors and impact on one-year mortality. *BMC Res Notes*. 2014; 7:439.
- Zhang F, Haberer JE, Wang Y, Zhao Y, Ma Y, Zhao D, Yu L, Goosby EP. The Chinese free antiretroviral treatment program: Challenges and responses. *AIDS*. 2007; 21:S143-148.
- Zhang Y, Dou Z, Sun K, Ma Y, Chen RY, Bulterys M, Zhao Y, Zhu H, Liu Z, Zhang F. Association between missed early visits and mortality among patients of china national free antiretroviral treatment cohort. *J Acquir Immune Defic Syndr*. 2012; 60:59-67.
- Kyeyune R, Saathoff E, Ezeamama AE, Löscher T, Fawzi W, Guwatudde D. Prevalence and correlates of cytopenias in HIV-infected adults initiating highly active

- antiretroviral therapy in Uganda. *BMC Infect Dis.* 2014; 14:496.
21. Mocroft A, Kirk O, Barton SE, Dietrich M, Proenca R, Colebunders R, Pradier C, dArminio Monforte A, Ledergerber B, Lundgren JD. Anaemia is an independent predictive marker for clinical prognosis in HIV-infected patients from across Europe. *EuroSIDA study group. AIDS.* 1999; 13:943-950.
 22. Harris RJ, Sterne JA, Abgrall S, *et al.* Prognostic importance of anaemia in HIV type-1-infected patients starting antiretroviral therapy: Collaborative analysis of prospective cohort studies. *Antivir Ther.* 2008; 13:959-967.
 23. Xiao J, Han N, Yang D, Zhao HX. Lower mortality in persons infected with HIV receiving antiretroviral treatment in a hospital-based model: An observational cohort study. *Future Virol.* 2014; 9:363-372.
 24. Zhang F, Dou Z, Yu L, Xu J, Jiao JH, Wang N, Ma Y, Zhao Y, Zhao H, Chen RY. The effect of highly active antiretroviral therapy on mortality among HIV-infected former plasma donors in China. *Clin Infect Dis.* 2008; 47:825-833.
 25. Zhang F, editor. National free HIV antiretroviral treatment handbook. 3rd ed. Beijing, China: People's Medical Publishing House. 2012; p235. (in Chinese)
 26. Meidani M, Rezaei F, Maracy MR, Avijgan M, Tayeri K. Prevalence, severity, and related factors of anemia in HIV/AIDS patients. *J Res Med Sci.* 2012; 17:138-42.
 27. Alexaki A, Wigdahl B. HIV-1 infection of bone marrow hematopoietic progenitor cells and their role in trafficking and viral dissemination. *PLoS Pathog.* 2008; 4:e1000215.
 28. Moses A, Nelson J, Bagby GC. The influence of human immunodeficiency virus-1 on hematopoiesis. *Blood.* 1998; 91:1479-1495.
 29. Vanasse GJ, Berliner N. Anemia in elderly patients: An emerging problem for the 21st century. *Hematology Am Soc Hematol Educ Program.* 2010:271-275.
 30. Sullivan PS, Hanson DL, Chu SY, Jones JL, Ward JW. Epidemiology of anemia in human immunodeficiency virus (HIV)-infected persons: Results from the multistate adult and adolescent spectrum of HIV disease surveillance project. *Blood.* 1998; 91:301-308.
 31. Keisu M, Wiholm BE, Palmblad J. Trimethoprim-sulphamethoxazole associated blood dyscrasias. Ten years' experience of the Swedish spontaneous reporting system. *J Intern Med.* 1990; 228:353-360.
 32. Moore RD, Keruly JC, Chaisson RE. Anemia and survival in HIV infection. *J Acquir Immune Defic Syndr Hum Retrovirol.* 1998; 19:29-33.
 33. Mocroft A, Kirk O, Barton SE, Dietrich M, Proenca R, Colebunders R, Pradier C, dArminio Monforte A, Ledergerber B, Lundgren JD. Anaemia is an independent predictive marker for clinical prognosis in HIV-infected patients from across Europe. *EuroSIDA study group. AIDS.* 1999; 13:943-950.

(Received August 24, 2016; Revised November 8, 2016; Accepted November 18, 2016)

Supplemental Table

Table S1: Clinical data about enrollment, dead cases and lost to follow-up in our cohort

Time for cART initiation (year)	Enrollment (cases)	Deaths (cases)	Lost to follow-up (cases)
2003	16	0	0
2004	18	0	0
2005	25	0	0
2006	12	1	1
2007	62	2	0
2008	73	0	2
2009	138	2	5
2010	142	6	4
2011	312	7	16
2012	422	7	20
2013	598	9	37
2014	630	4	51
2015	1,004	6	126

cART, combination antiretroviral therapy.

The expression of miR-124 increases in aged skin to cause cell senescence and it decreases in squamous cell carcinoma

Miho Harada, Masatoshi Jinnin*, Zhongzhi Wang, Ayaka Hirano, Yukiko Tomizawa, Tomomi Kira, Toshikatsu Igata, Shinichi Masuguchi, Satoshi Fukushima, Hironobu Ihn

Department of Dermatology and Plastic Surgery, Faculty of Life Sciences, Kumamoto University, Kumamoto, Japan.

Summary

Skin senescence is induced by various factors including intrinsic aging and extrinsic aging. The current study compared the expression of microRNAs in young facial skin and senescent facial skin, and this study identified skin aging-related microRNAs. According to the results from a microRNA PCR Array, miR-124 was the microRNA that increased the most in senescent skin compared to young skin. Real-time PCR with a greater number of samples indicated that the increase in miR-124 levels in senescent facial skin was statistically significant. In situ hybridization was performed, and results indicated that the signal for miR-124 was evident in keratinocytes of senescent skin but not in those of young skin. The morphology of cultured normal human epidermal keratinocytes (NHEKs) transfected with a miR-124 mimic changed to an enlarged and irregular shape. In addition, the number of NHEKs positive for senescence-associated β -galactosidase (SA- β -gal) increased significantly as a result of the overexpression of the miR-124 mimic. The expression of miR-124 increased in UVB-irradiated NHEKs compared to controls in a dose-dependent manner. Expression of miR-124 in A431, a human cutaneous squamous cell carcinoma (SCC) cell line, decreased significantly compared to that in NHEKs. Forced overexpression of miR-124 as a result of the transfection of a miR-124 mimic in A431 resulted in the significant suppression of the proportion of cancer cells. The current results indicated that miR-124 increases as a result of cell senescence and that it decreases during tumorigenesis. The effect of supplementation of miR-124 in an SCC cell line suggests that senescence induction therapy with microRNA may be a new therapeutic approach for treatment of SCC.

Keywords: Skin senescence, microRNA, UVB

1. Introduction

Based on the characteristics of aging of the skin compared to aging of other organs, there appear to be two different types of aging: intrinsic aging and extrinsic aging. Intrinsic aging is caused by decreased cellular functioning of the skin, while extrinsic aging is mainly induced by UV irradiation. Other factors that affect skin senescence include smoking, eating habits, stress,

and oxygen radicals generated by air pollution, but the mediator of these various factors is still unknown.

The current study focused on the role of microRNAs (miRNAs) in skin senescence. miRNAs, short ribonucleic acid molecules an average of 22 nucleotides long, are small noncoding RNAs that lead to gene silencing of target mRNAs (1). miRNAs have been implicated in the pathogenesis of various human diseases such as cancers and inflammatory disorders. The current authors previously found that the miR-424 level in senile hemangioma, the most common vascular anomaly seen specifically in aged skin, was lower than levels in other vascular anomalies (2): Decreased miR-424 expression and increased levels of target molecules (MEK1 and cyclin E1) in endothelial cells of senile hemangioma may cause abnormal cell proliferation in the tumor.

The current study identified miRNAs that were

Released online in J-STAGE as advance publication November 5, 2016.

*Address correspondence to:

Dr. Masatoshi Jinnin, Department of Dermatology and Plastic Surgery, Faculty of Life Sciences, Kumamoto University, 1-1-1 Honjo, Chuo-ku, Kumamoto 860-8556, Japan.
E-mail: mjinn@kumamoto-u.ac.jp

dysregulated in senescent skin, and it attempted to clarify the role of miRNAs in skin senescence.

2. Materials and Methods

2.1. Patient samples

Skin samples were obtained from the facial skin of 6 elderly individuals (range: 80-100 years of age) and 3 young individuals (range: 0-10 years of age). Non-exposed parts of the skin of 3 young and elderly individuals were also collected. These samples were skin that was routinely discarded as "dog-ears" during skin surgery, and samples were processed immediately after removal. This study was approved by an institutional review board and written informed consent was obtained from patients in accordance with the Declaration of Helsinki.

2.2. Cell cultures

Normal human epidermal keratinocytes (NHEKs) were purchased from Lonza (Walkersville, MD) and were cultured in growth medium (KGM-Gold Bullet Kit, Lonza) in a 5% CO₂ incubator at 37°C. A human cutaneous squamous cell carcinoma (SCC) cell line, A431, was obtained from ATCC (Manassas, VA), and cells were cultured in DMEM (Lonza) with 10% fetal bovine serum (Hyclone, Logan, UT) and Antibiotic-Antimycotic (Invitrogen, Carlsbad, CA) in a 5% CO₂ incubator at 37°C.

2.3. PCR array analysis and real-time PCR analysis of miRNAs

Small RNAs were extracted from paraffin sections using the miRNeasy FFPE kit and from cultured cells using the RNeasy mini kit (Qiagen, Valencia, CA) as described previously (2,3). For the RT² Profiler PCR Array (SABiosciences, Frederick, MD), the RNAs were reverse-transcribed into first-strand cDNA using the RT² miRNA First Strand Kit (SABiosciences). The cDNA was mixed with RT² SYBR Green/ROX qPCR Master Mix, and the mixture was added to the 96-well RT² miRNA PCR Array (SABiosciences) that included primer pairs for 88 human miRNAs. PCR was performed on the Takara Thermal Cycler Dice (TP800) (Takara Bio Inc, Shiga, Japan) in accordance with the manufacturer's protocol. The threshold cycle (C_t) for each miRNA was determined using the Thermal Cycler Dice Real Time System ver2.10B. The raw C_t values were normalized using the values for small RNA housekeeping genes.

For quantitative real-time PCR, primers for miR-124 or U6 (Qiagen) and templates were mixed with SYBR Premix Ex TaqII (Takara Bio Inc). DNA was amplified for 50 cycles of denaturation for 5 s at 95°C and annealing for 30 s at 60°C. Transcript levels of

miR-124 were normalized to U6 levels.

2.4. In situ hybridization

In situ hybridization was performed using a representative sample with 5'-locked digoxigenin-labeled nucleic acid (LNA) probes complementary to human mature miR-124 and a scrambled negative control (Exiqon, Vedbaek, Denmark) (1,4). Sections of human skin were deparaffinized and deproteinized with protease K for 5 min. The slides were then washed in 0.2% glycine in PBS and fixed with 4% paraformaldehyde. Hybridization was performed at 57°C overnight followed by blocking with 2% fetal bovine serum and 2% bovine serum albumin in PBST for 1 h. The probe-target complex was immunologically detected with a digoxigenin antibody conjugated to alkaline phosphatase acting on the chromogen nitro blue tetrazolium/5-bromo-4-chloro-3-indolyl phosphate (Roche Applied Science, Mannheim, Germany). The slides were counterstained using nuclear fast red and examined under a light microscope (OLYMPUS BX50; Tokyo, Japan).

2.5. Transient transfection

miRNA mimics were obtained from Qiagen. Lipofectamine RNAiMAX (Invitrogen) was used as the transfection reagent. For reverse transfection, miRNA mimics were mixed with transfection reagent and then added when cells were plated (5).

2.6. Senescence-associated β -galactosidase (SA- β -Gal) activity

SA- β -Gal activity was examined using the Cellular Senescence Assay Kit (Chemicon International Inc, Billerica, MA). The cells were treated with fixing solution for 15 min at room temperature and then incubated with SA- β -gal Detection Solution at 37°C overnight. Senescent cells with green staining were counted under a light microscope (6).

2.7. Cell count

Cells were detached from the wells by trypsin treatment and counted using the Coulter[®] Particle Counter (Beckman Coulter, Fullerton, CA) (2,7).

2.8. Statistical analysis

Statistical analysis was performed with the Mann-Whitney test for comparison of medians. *p* values less than 0.05 were considered significant.

3. Results

3.1. miRNA expression in young and senescent facial skin

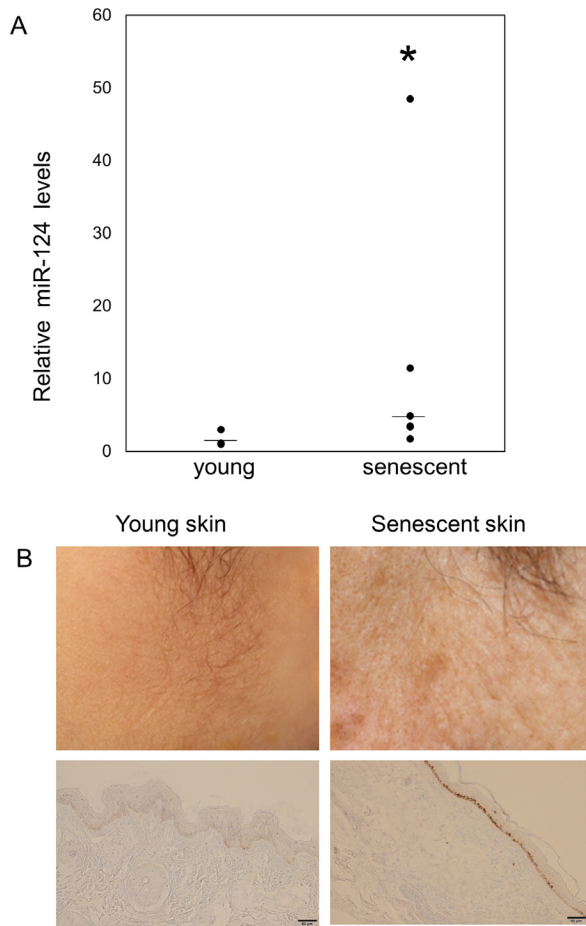


Figure 1. (A) Total miRNA was extracted from samples of young ($n = 3$) and senescent ($n = 6$) facial skin. miR-124 levels were measured with real-time PCR and normalized to U6 levels. Relative miR-124 levels are shown on the vertical axis. The minimum value in young skin was set at 1. Bars indicate medians. $p < 0.05$. **(B)** (upper panels) representative pictures of young and senescent facial skin. (lower panels) In situ detection of miR-124 in paraffin-embedded, formalin-fixed tissues from young skin and senescent skin. Nuclei were counterstained with nuclear fast red. The miR-124 stained brown.

As an initial experiment, to determine which miRNAs are involved in the senescence of facial skin, a mixture of equal amounts of miRNAs from 3 human facial skin samples from young individuals (0-10 years of age) or elderly individuals (80-100 years of age) were prepared (see Figure 1B). A miRNA PCR array was used to analyze 88 miRNAs involved in human cell differentiation and development.

There were several miRNAs that were specifically overexpressed in senescent facial skin (Table 1). The current study focused on one of those miRNAs, miR-124, since it increased the most in senescent skin compared to young skin (6.52-cycle difference in ΔCT method). Because the array was used in a single experiment, the results were verified with real-time PCR using specific primers for miR-124 and a greater number of samples (3 samples of young facial skin and 6 of senescent facial skin). As shown in Figure 1A, the increase in miR-124 levels in senescent facial skin was

Table 1. Up-regulated miRNAs in senescent facial skin compared to young facial skin according to a PCR array

ΔC_t	young	senescent
let-7a	- 0.33	- 3.63
miR-18b	3.80	- 0.29
miR-124	4.09	- 2.43
miR-192	2.30	- 1.37
miR-196a	4.87	- 0.14
miR-206	2.41	- 1.71
miR-208	4.09	0.21
miR-215	4.88	- 1.06
miR-219-5p	6.82	2.07
miR-302c	7.51	3.75
miR-488	5.75	2.00
miR-518b	7.35	2.96

A mixture of equal amounts of miRNAs from facial skin samples from 3 elderly individuals and 3 young individuals were prepared, and the miRNA expression profile in each group in vivo was evaluated using a PCR array. The raw threshold cycle (C_t) was normalized using the values for small RNA housekeeping genes. ΔC_t (the raw C_t for each miRNA - C_t for small RNA housekeeping genes) is shown.

statistically significant. In addition, in situ hybridization using a representative sample indicated that the signal for miR-124 was evident in keratinocytes of senescent skin but not in those of young skin (Figure 1B).

3.2. The role of miR-124 in the senescence of keratinocytes

Next, an attempt was made to determine the role of miR-124 in the senescence of NHEKs. Cells transfected with control miRNA had a cobblestone appearance, while the morphology of cells with overexpression of the miR-124 mimic changed to an enlarged and irregular shape, suggesting cell senescence (Figure 2A). SA- β -Gal staining indicated that the ratio of positive cells increased as a result of the overexpression of the miR-124 mimic compared to that in controls (Figure 2B), and this increase was statistically significant (Figure 2C). Taken together, the current results indicated that miR-124 may be associated with the senescence of keratinocytes.

3.3. The expression of miR-124 in keratinocytes with UVB irradiation

Based on above results, the expression of miR-124 was thought to increase in accordance with skin senescence, which means that miR-124 mediates skin senescence. An attempt was made to identify the mechanism by which expression of miR-124 is induced in senescent skin. As mentioned previously, skin senescence is mainly induced by both intrinsic factors and extrinsic factors. UV irradiation is known to be a main cause of extrinsic skin senescence.

The expression of miR-124 increased in UVB-irradiated cells compared to controls in a dose-dependent manner: The induction of miR-124 expression by 10 mJ of irradiation was statistically significant (Figure 3A). In contrast to the results for facial skin, miR-124 levels in non-exposed parts of the skin of elderly individuals

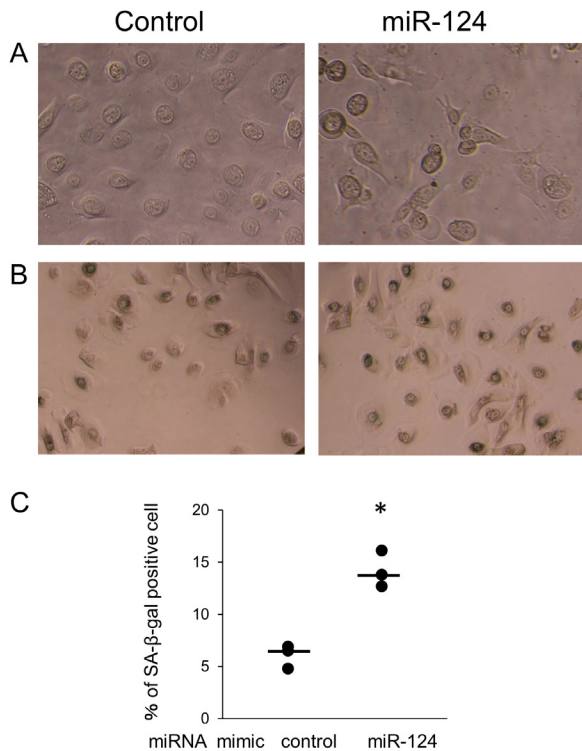


Figure 2. (A) Normal human epidermal keratinocytes (NHEKs) at a density of 6×10^4 cells/well in 24-well culture plates were transfected with a control miRNA mimic or a miR-124 mimic. The morphology of NHEKs was observed using phase-contrast microscopy. (B, C) NHEKs at a density of 6×10^4 cells/well in 24-well culture plates were transfected with a control miRNA mimic or an miR-124 mimic. Histochemical detection of SA β -gal in cells was assessed 7 days after transfection (B) The percentage of cells positive for SA- β -gal in 3 independent experiments is shown on the vertical axis. Bars indicate medians. $*p < 0.05$ compared to values in cells transfected with the control mimic (C).

varied and did not increase compared to those in young individuals (Figure 3B). Taking these findings together, miR-124 levels may increase as a result of UV irradiation rather than intrinsic aging.

3.4. The connection between miR-124 and SCC

SCC is a malignant skin tumor that is thought to be closely correlated with UVB. The expression of miR-124 in A431, a human cutaneous SCC cell line, decreased significantly compared to that in NHEKs (Figure 3C). Forced overexpression of miR-124 as a result of the transfection of a miR-124 mimic in A431 resulted in the significant suppression of the proportion of cancer cells (Figure 3D). Thus, the current results indicated that miR-124 increased as a result of cell senescence but it decreased during tumorigenesis. Furthermore, the supplementation of miR-124 may suppress tumor proliferation by inducing the senescence of tumor cells.

4. Discussion

To the extent known, no previous studies have examined miRNAs in relation to intrinsic or extrinsic aging. Xu

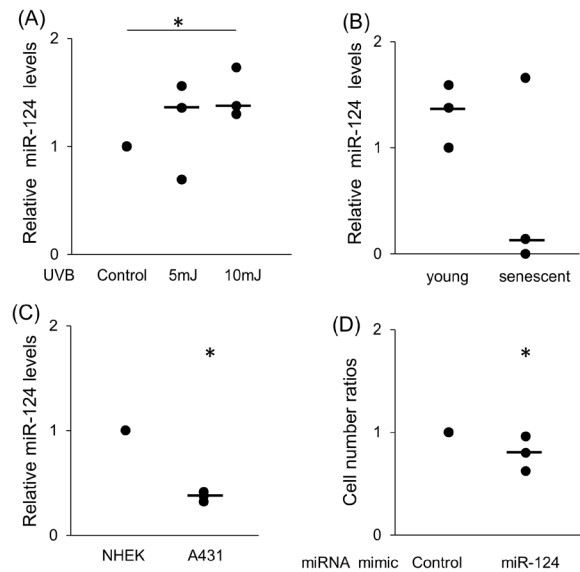


Figure 3. (A) Normal human epidermal keratinocytes (NHEKs) were exposed to UVB at 5 or 10mJ/cm² every day for 3 days. After 24 hours, total miRNA was extracted, and the relative level of miR-124 (normalized to U6) was determined with quantitative real-time PCR ($n = 3$). Bars show medians. The values in untreated cells were set at 1.0. $*p < 0.05$ compared to values in untreated cells. (B) Total miRNA was extracted from non-exposed parts of skin of young or elderly individuals ($n = 3$), and the relative level of miR-124 (normalized to U6) was determined using quantitative real-time PCR. Transcript levels in young skin were set at 1. The minimum value in young skin was set at 1. Bars show medians. (C) NHEKs and an SCC cell line (A431) were cultured independently under the same conditions until they became subconfluent. Total miRNA was extracted, and the relative level of miR-124 (normalized to U6) was determined using quantitative real-time PCR ($n = 3$). Bars show medians. $*p < 0.05$ compared to values in NHEKs (1.0). (D) A431 at a density of 5×10^3 cells/well in 24-well culture plates were transfected with a control miRNA mimic or a miR-124 mimic for 72 h. The proportion of cells is shown on the vertical axis ($n = 3$). Bars show medians. The values in control cells were set at 1.0.

et al. indicated that miR-22 plays roles both in cell senescence and tumorigenesis (8): the expression of miR-22 is induced by cell senescence while it is reduced in various malignant tumor cells. The authors also indicated that overexpression of miR-22 suppresses the development of breast cancer *in vivo*. The current authors considered the possibility that a similar phenomenon exists in relation to skin senescence. Based on this hypothesis, the current study correlated miRNAs with skin senescence and skin cancer, and this study yielded three major findings.

First, this study attempted to identify skin aging-related miRNAs. Analysis was performed with a miRNA PCR array consisting of 88 miRNAs involved in human cell differentiation and development, and miR-124 was identified as the most up-regulated miRNA in senescent skin compared to young skin. These results were verified by real-time PCR. Attention was then focused on miR-124, and overexpression of miR-124 in NHEKs was found to lead to cell senescence. Although miR-22 was included in the miRNA PCR array, it was similarly

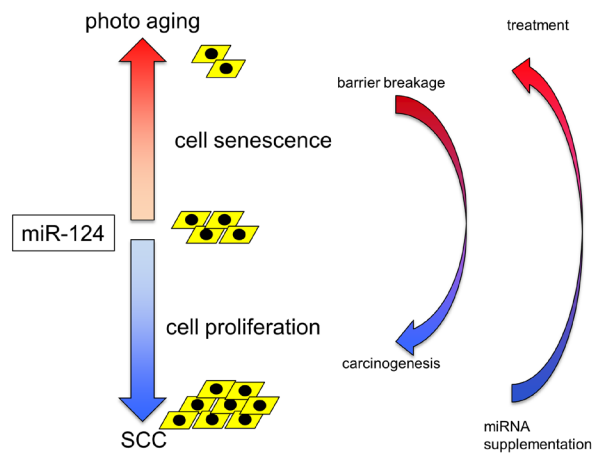


Figure 4. Diagrammatic representation of the function of miR-124 in skin senescence and tumorigenesis. In senescent skin, UVB increases the expression of miR-124, thus mediating cell senescence. In contrast, the expression of miR-124 decreases in SCC tumor cells, and this decrease may correlate with cell proliferation. miR-124 acts as a preventer of skin carcinogenesis, and miR-124 supplementation may have therapeutic value in inhibiting the progression of cancer.

expressed in senescent skin and young skin. This may be due to the tissue specificity of the pattern of miRNA expression.

Second, the expression of miR-124 in NHEKs increased as a result of UVB irradiation in a dose-dependent manner. UVB is a main extrinsic factor for the induction of skin senescence and seems to cause a phenomenon up-stream, resulting in increased miR-124 expression in senescent skin. The connection between UVB and miR-23a, -24, -98, -141 or -365 has previously been reported (9-13), but the current results indicated that miR-124 also mediates UVB-induced skin aging.

Third and last, the expression of miR-124 decreased in a human cutaneous SCC cell line in comparison to that in NHEKs, while the overexpression of miR-124 in those cells resulted in the significant suppression of the proportion of cell numbers. The current authors previously reported that the miR-124 expression was down-regulated in cutaneous SCC (14), which results in the overexpression of ERK as a target molecule and subsequent cell proliferation. miR-124 was also reported to be involved in the carcinogenesis of various cancers such as glioblastoma, gastric cancer, hepatocellular cancer, breast cancer, and prostate cancer (15-19), indicating that miR-124 is a key miRNA in carcinogenesis.

Based on these findings, a hypothetical model was devised as shown in Figure 4. The current results indicated the expression of miR-124 increases in aged skin, causing cell senescence. The effect of supplementation of miR-124 in an SCC cell line suggests that senescence induction therapy with miRNA may be a new therapeutic approach for the treatment of SCC. Limitations of this study are the small sample

size, the fact that a single experiment was performed, and the small number of cell lines examined, so further studies are needed in the future. Analysis with the array was performed in a single experiment and statistical analysis could not be performed, but the results were verified using real-time PCR. In addition, in situ hybridization was performed using a single sample of young and senescent skin due to the lack of available samples. Forced miR-124 overexpression in the SCC line reduced the proportion of cells, but this does not mean that decreased expression of miR-124 induces cell proliferation. The association between miR-124 and cell proliferation needs to be clarified in more detail in order to substantiate the hypothesis put forward here.

References

1. Friedman RC, Farh KKH, Burge CB, Bartel DP. Most mammalian mRNAs are conserved targets of microRNAs. *Genome Res.* 2009; 19:92-105.
2. Nakashima T, Jinnin M, Etoh T, Fukushima S, Masuguchi S, Maruo K, Inoue Y, Ishihara T, Ihn H. Down-regulation of mir-424 contributes to the abnormal angiogenesis *via* MEK1 and cyclin E1 in senile hemangioma: Its implications to therapy. *PLoS One.* 2010; 5.
3. Honda N, Jinnin M, Kajihara I, Makino T, Makino K, Masuguchi S, Fukushima S, Okamoto Y, Hasegawa M, Fujimoto M, Ihn H. TGF- β -mediated downregulation of microRNA-196a contributes to the constitutive upregulated type I collagen expression in scleroderma dermal fibroblasts. *J. Immunol.* 2012; 188:3323-3331.
4. Makino K, Jinnin M, Hirano A, Yamane K, Eto M, Kusano T, Honda N, Kajihara I, Makino T, Sakai K, Masuguchi S, Fukushima S, Ihn H. The downregulation of microRNA let-7a contributes to the excessive expression of type I collagen in systemic and localized scleroderma. *J. Immunol.* 2013; 190:3905-3915.
5. Honda N, Jinnin M, Kira-Etoh T, Makino K, Kajihara I, Makino T, Fukushima S, Inoue Y, Okamoto Y, Hasegawa M, Ihn H. MiR-150 down-regulation contributes to the constitutive type I collagen overexpression in scleroderma dermal fibroblasts *via* the induction of integrin β 3. *Am. J. Pathol.* 2013; 182:206-216.
6. Dimri GP, Lee X, Basile G, Acosta M, Scott G, Roskelley C, Medrano EE, Linskens M, Rubelj I, Pereira-Smith O. A biomarker that identifies senescent human cells in culture and in aging skin *in vivo*. *Proc. Natl. Acad. Sci. U. S. A.* 1995; 92:9363-9367.
7. Makino T, Jinnin M, Muchemwa FC, Fukushima S, Kogushi-Nishi H, Moriya C, Igata T, Fujisawa A, John T, Ihn H. Basic fibroblast growth factor stimulates the proliferation of human dermal fibroblasts *via* the ERK1/2 and JNK pathways. *Br. J. Dermatol.* 2010; 162:717-723.
8. Xu D, Takeshita F, Hino Y, Fukunaga S, Kudo Y, Tamaki A, Matsunaga J, Takahashi R, Takata T, Shimamoto A, Ochiya T, Tahara H. miR-22 represses cancer progression by inducing cellular senescence. *J. Cell Biol.* 2011; 193:409-424.
9. Guo L, Huang ZX, Chen XW, Deng QK, Yan W, Zhou MJ, Ou CS, Ding ZH. Differential expression profiles of microRNAs in NIH3T3 cells in response to UVB

- irradiation. *Photochem. Photobiol.* 2009; 85:765-773.
10. Li W, Di W, Hua L, Zhou B, Guo Z, Luo D. UVB suppresses PTEN expression by upregulating miR-141 in HaCaT cells. *J. Biomed. Res.* 2011; 25:135-140.
 11. Kraemer A, Chen I-P, Henning S, Faust A, Volkmer B, Atkinson MJ, Moertl S, Greinert R. UVA and UVB irradiation differentially regulate microRNA expression in human primary keratinocytes. *PLoS One.* 2013; 8:e83392.
 12. Zhou BR, Xu Y, Luo D. Effect of UVB irradiation on microRNA expression in mouse epidermis. *Oncol. Lett.* 2012; 3:560-564.
 13. Zhou BR, Xu Y, Permatasari F, Liu WL, Li W, Guo XF, Huang QH, Guo Z, Luo D. Characterization of the miRNA profile in UVB-irradiated normal human keratinocytes. *Exp. Dermatol.* 2012; 21:317-319.
 14. Yamane K, Jinnin M, Etoh T, Kobayashi Y, Shimozono N, Fukushima S, Masuguchi S, Maruo K, Inoue Y, Ishihara T, Aoi J, Oike Y, Ihn H. Down-regulation of miR-124/-214 in cutaneous squamous cell carcinoma mediates abnormal cell proliferation *via* the induction of ERK. *J. Mol. Med.* 2013; 91:69-81.
 15. Silber J, Lim DA, Petritsch C, Persson AI, Maunakea AK, Yu M, Vandenberg SR, Ginzinger DG, James CD, Costello JF, Bergers G, Weiss WA, Alvarez-Buylla A, Hodgson JG. miR-124 and miR-137 inhibit proliferation of glioblastoma multiforme cells and induce differentiation of brain tumor stem cells. *BMC Med.* 2008; 6:14.
 16. Xia J, Wu Z, Yu C, He W, Zheng H, He Y, Jian W, Chen L, Zhang L, Li Wen. MiR-124 inhibits cell proliferation in gastric cancer through down-regulation of SPHK1. *J. Pathol.* 2012; 227:470-480.
 17. Furuta M, Kozaki KI, Tanaka S, Arai S, Imoto I, Inazawa J. miR-124 and miR-203 are epigenetically silenced tumor-suppressive microRNAs in hepatocellular carcinoma. *Carcinogenesis.* 2009; 31:766-776.
 18. Liang YJ, Wang QY, Zhou CX, Yin QQ, He M, Yu XT, Cao DX, Chen GQ, He JR, Zhao Q. MiR-124 targets Slug to regulate epithelial-mesenchymal transition and metastasis of breast cancer. *Carcinogenesis.* 2013; 34:713-722.
 19. Shi X-B, Xue L, Ma A-H, Tepper CG, Gandour-Edwards R, Kung HJ, deVere White RW. Tumor suppressive miR-124 targets androgen receptor and inhibits proliferation of prostate cancer cells. *Oncogene.* 2013; 32:4130-4138.

(Received June 3, 2016; Revised September 12, 2016; Accepted October 19, 2016)

Effects of STAT3 inhibitors on neural functional recovery after spinal cord injury in rats

Meng Cui^{1,2}, Xinlong Ma^{1,*}, Jie Sun¹, Jinquan He¹, Lin Shen¹, Fangguo Li¹

¹Department of Orthopaedic Traumatology, Tianjin Hospital, Tianjin, China;

²Tianjin Medical University, Tianjin, China.

Summary Spinal cord injuries (SCIs) can induce primary and secondary injury, resulting in severe neurological damage and dysfunction in patients. Studies have reported that signal transducer and activator of transcription 3 (STAT3) plays an important role in the inflammatory immune response and neural stem cell differentiation. In order to examine whether a STAT3 inhibitor can prevent worsening of an SCI and promote neural stem cell differentiation, a rat model of surgically induced SCI was created and rats were treated with the STAT3 inhibitor S31-201. Tissue from the injured region was harvested and fixed in formalin and paraffin. H&E staining was used to look for morphological changes. The Basso, Beattie, and Bresnahan locomotor scale (BBB score), somatosensory evoked potentials (SEP), and motor evoked potentials (MEP) were examined. Western blotting was used to detect the expression of β -tubulin III, vimentin, GFAP, NF-200, and OX-42 protein. Results indicated that the STAT3 inhibitor S31-201 reduces the extent of SCI and it promotes neural stem cell differentiation.

Keywords: Signal transducer and activator of transcription 3 (STAT3), spinal cord injury, STAT3 inhibitor

1. Introduction

Spinal cord injuries (SCIs) are a problem worldwide. An SCI is known to cause direct mechanical damage and subsequent secondary injury cascades. An inflammatory immune response starts with an immediate influx of inflammatory cells into the injured spinal cord, and cytokines and neurotrophic factors hamper spinal cord regeneration (1,2). Other factors that affect regeneration of axons are reactive hyperplasia of astrocytes, microglia, and oligodendrocytes and the formation of a glial scar after spinal cord injury (1,2). Therefore, preventing the inflammatory process, decreasing secondary injury, and promoting neuron regeneration after an SCI are key areas in which to treat an SCI in its early stages (3). Although current clinical approaches to treating an SCI,

including the use of high doses of methylprednisolone, surgery, intensive multisystem medical management, and rehabilitative care, provide some benefits, novel approaches to treating SCIs need to be developed. Over the past few years, researchers have begun to use endogenous neural stem cells (NSCs) to treat SCIs. Recently, a study reported generating autologous pluripotent stem cells from skin fibroblasts, thus avoiding ethical problems and the problem of immune rejection (4). However, few studies have reported on regulation of the differentiation of NSCs.

In the early stage of an SCI, interleukin-6 (IL-6) rises rapidly, promoting and regulating the inflammatory response, inducing NSCs to selectively undergo astrocytic differentiation, and aggravating a secondary SCI (5,6). Signal transducer and activator of transcription 3 (STAT3) plays a crucial role in the inflammatory response of IL-6 (7). STAT3 inhibits the expression of Bim1 and Oct4 downstream of STAT3 and it promotes NSC differentiation (8).

Based on these previous findings, a murine model of SCI was used to investigate whether inhibiting STAT3 would modify the acute inflammatory response after an SCI and promote NSC differentiation.

Released online in J-STAGE as advance publication December 21, 2016.

*Address correspondence to:

Dr. Ma Xinlong, Department of Orthopaedics, Tianjin Hospital, Tianjin 300211, China.

E-mail: tjyymaxinlong@sina.com

2. Materials and Methods

2.1. Animals and groups

One hundred and twenty Sprague-Dawley rats (weight: 180-200 g) were purchased from the Laboratory Animal Center of the Military Academy of Medical Sciences (license: SCXK - (People's Liberation Army of China), 2012-0004) and were housed in individual cages in the Animal Facility of Tianjin Medical University with the approval of the Institutional Animal Care and Use Committee. These rats were randomly divided into three groups: a sham-operated (SO) group, an SCI group, and an SCI and treatment with the STAT3 inhibitor S31-201 (SCI+S31-201) group (40 rats in each group). Rats in each group were randomly sacrificed at five different points in time. At each time point, 8 rats from each group were sacrificed, and 3 outliers were eliminated. All rats were handled in accordance with the recommendations of the Guidelines for the welfare and use of animals in research.

2.2. Creation of a model of SCI

Rats in the SCI group were anesthetized with an intraperitoneal injection of 1% pentobarbital sodium (50 mg/kg). Using the T8 spinous process as the center, a median skin incision was made on the back and paravertebral muscle at T7-T9 was dissected under sterile surgical conditions. A laminectomy of the Th8 vertebra was performed. A model of acute SCI was produced with improved Allen's devices – a 30-g weight was dropped from a height of 5 cm onto the exposed dura of the spinal cord. An SCI was induced at T8. The skin and musculature were then sutured closed. Whether an SCI was successfully induced was determined by symptoms such as tail twitches, spinal cord bleeding and edema, contraction-like twitching of both hind limbs and the body, and delayed paralysis of both hind limbs after waking. After surgery, 1 million IU of penicillin was given daily *via* subcutaneous injection to prevent infections. The bladder was squeezed twice a day to assist voiding until the bladder reflex returned. All rats were housed in warm, separate cages. The rats were monitored daily. A laminectomy was performed on the SO group but an SCI was not induced.

2.3. Treatment with a specific STAT3 inhibitor

S31-201, a specific STAT3 inhibitor, was dissolved in dimethyl sulphoxide (DMSO) and injected into the abdominal cavity at 5 mg/Kg in rats in the SCI+S31-201 group. The other two groups were injected with DMSO as controls. All of the rats were injected once a day for a week.

2.4. Hematoxylin and eosin (H&E) staining

Specimens of spinal cord tissue were observed on day 14 and day 28 after surgically induced SCI. Tissue was fixed in 10% paraformaldehyde for 24 h, embedded in paraffin, and cut into sections 5 μ m in thickness. Hematoxylin and eosin (H&E) staining was performed to observe morphological changes.

2.5. Somatosensory evoked potentials (SEP) and motor evoked potentials (MEP)

Somatosensory evoked potentials (SEP) and motor evoked potentials (MEP) were examined on days 1, 7, 14, and 28 postoperatively.

2.6. Behavioral testing

Neurological function in the hind limbs was evaluated on days 1, 3, 7, 14, and 28 postoperatively using the Basso, Beattie, and Bresnahan locomotor scale (BBB score). Six rats per group were randomly selected for functional testing. Each rat was placed in an open field and was scored by two blind observers after an observation period of 5 min.

2.7. Western blotting

Spinal cord tissue was harvested on days 1, 3, 7, 14, and 28 postoperatively. One hundred mg of tissue was treated with 400 μ L of RIPA lysate containing PMSF and 1% protease inhibitor and placed on ice for 30 min. Produced proteins were stored at -80°C.

Proteins were transferred onto nitrocellulose membranes for 10% SDS-PAGE gel electrophoresis. Blots were blocked and incubated with a primary antibody. Western Lightning[®]-ECL, Enhanced Chemiluminescence Substrate (Perkin Elmer, NEL100001EA) was used to measure protein expression, with GAPDH serving as the internal control. Bands were imaged and analyzed using LABWORKS 4.0.

2.8. Statistical analysis

Data were collected and 3 outliers for each group were eliminated. Data were analyzed with SPSS.18 and are presented as the mean \pm standard deviation (M \pm S.D.). One-way analysis of variance (ANOVA) followed by the least significance difference (LSD)-multiple range test were used to analyze the differences between groups. $p < 0.05$ was considered statistically significant.

3. Results

3.1. Morphological changes

Macroscopic observation: In group 2 and group 3 with

a surgically induced SCI (SCI group and SCI+S31-201 group), diffuse hyperemia and edema in the dorsolateral spinal cord were observed. On day 14 and day 28 postoperatively, the formation of an epidural scar and epidural adhesions were evident. In group 1 (SO group), epidural scar formation and epidural adhesions were noted but hyperemia and edema were not noted.

Microscopic observation: On day 14 postoperatively, the structure of the spinal cord and nerve cells in the SCI group had been destroyed, liquefactive necrosis in damaged areas had resolved and was followed by the formation of a cystic space, and swollen axons and disordered nerve fibers were noted in white matter (Figure 1A). On day 28 postoperatively, a long, oval cavity had formed where the spinal cord was severed and the vertical axis of the cavity ran parallel to the long axis of the spinal cord. There are many foamy macrophages and glial scar in the cavity (Figure 1B). In the SCI+S31-201 group, the inflammatory response diminished and the cavity where the spinal cord was severed had shrunk; on day 28 postoperatively, the cavity where the spinal cord was severed and the glial

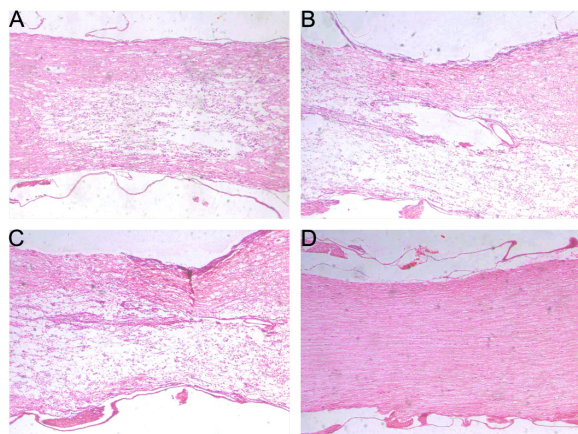


Figure 1. Microscopic observation. (A), Two weeks after surgically induced SCI, pathological changes indicative of liquefactive necrosis occurred in the area near the injured spinal cord, and the border of the cavity where the spinal cord was severed was not clear (SCI group); (B), Four weeks after surgically induced SCI, the border of the cavity where the spinal cord was severed was demarcated and the vertical axis of the cavity was consistent with the long axis of the spinal cord in the SCI group; (C), Four weeks after surgically induced SCI, demarcation was less evident in the SCI+S31-201 group than that in the SCI group; (D), After four weeks, there were no obvious changes in the structure of spinal cord in the SO group.

scar had shrunk (Figure 1C). In the SO group, the structure of the spinal cord was normal and there was no cavity in the spinal cord (Figure 1D).

3.2. BBB score

As Figure 2 and Table 1 show, the BBB scores for the SCI group and the SCI+S31-201 group were lower than that for the SO group. However, the BBB score for rats treated with S31-201 was higher than that for untreated rats with surgically induced SCI. Starting on day 14 postoperatively, the BBB scores for the SCI group and the SCI+S31-201 group differed significantly ($p < 0.001$).

3.3. SEP and MEP evaluation

As Figure 3 shows, both the MEP (Table 2) and SEP (Table 3) scores in the SCI group and the SCI+S31-201 group were significantly higher than those in the SO group. However, the MEP and SEP scores for rats treated with S31-201 were lower than those for untreated rats with surgically induced SCI. Starting on day 14 postoperatively, MEP and SEP scores for the SCI group and the SCI+S31-201 group differed significantly ($p < 0.001$).

3.4. Expression of proteins of interest

OX-42 was used to detect changes in morphology and the number of microglia. As Figure 4A and Table 4

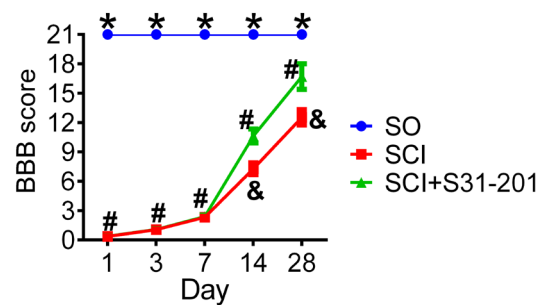


Figure 2. BBB scores for individual groups. The score for the SO group was significantly higher than that for the other two groups. * $p < 0.001$, vs. SCI groups. # $p < 0.001$, vs. SO group. & $p < 0.001$, vs. SCI+S31-201 groups ($n = 5$ points for each group; $n = 15$ points for 3 groups).

Table 1. BBB Score

day	group 1	group 2	group 3	F value	p	LSD group 1 vs. group 2	p	LSD group 1 vs. group 3	p	LSD group 2 vs. group 3	p
1	21 ± 0	0.36 ± 0.03	0.37 ± 0.02	1940061.82	*	t = 2955.71	*	t = 2953.70	*	t = 2.01	0.052
3	21 ± 0	1.05 ± 0.03	1.07 ± 0.05	535833.03	*	t = 1553.60	*	t = 1552.04	*	t = 1.56	0.128
7	21 ± 0	2.32 ± 0.09	2.39 ± 0.14	60142.17	*	t = 521.20	*	t = 519.25	*	t = 1.95	0.058
14	21 ± 0	7.28 ± 0.61	10.62 ± 0.71	789.31	*	t = 65.98	*	t = 49.92	*	t = 16.06	*
28	21 ± 0	12.53 ± 0.78	16.70 ± 1.30	105.83	*	t = 25.20	*	t = 12.79	*	t = 12.41	*

$n = 5$ points for each group; $n = 15$ points for 3 groups, * $p < 0.001$.

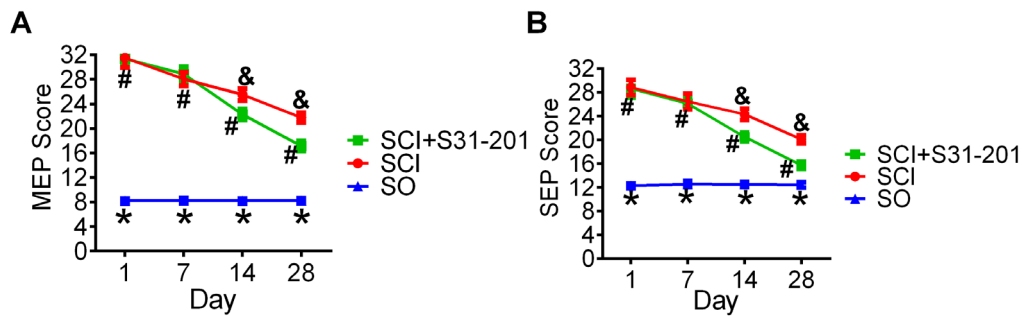


Figure 3. MEP (A) and SEP (B) were measured in rats on days 1, 7, 14, and 28 postoperatively. * $p < 0.001$, vs. SCI group. # $p < 0.001$, vs. SO group. & $p < 0.001$, vs. SCI+S31-201 group ($n = 5$ points for each group; $n = 15$ points for 3 groups).

Table 2. MEP

day	group 1	group 2	group 3	F value	p	LSD		LSD		LSD	
						group 1 vs. group 2	p	group 1 vs. group 3	p	group 2 vs. group 3	p
1	8.23 ± 0.35	31.51 ± 1.61	31.35 ± 1.00	656.70	*	$t = 54.55$	*	$t = 54.17$	*	$t = 0.38$	0.710
7	8.28 ± 0.40	28.06 ± 1.12	28.88 ± 1.16	671.08	*	$t = 53.80$	*	$t = 56.04$	*	$t = 2.23$	0.032
14	8.21 ± 0.32	25.52 ± 0.97	22.29 ± 0.87	639.32	*	$t = 58.24$	*	$t = 47.37$	*	$t = 10.87$	*
28	8.25 ± 0.37	21.77 ± 0.76	17.15 ± 0.82	459.17	*	$t = 51.63$	*	$t = 33.99$	*	$t = 17.64$	*

$n = 5$ points for each group; $n = 15$ points for 3 groups; group 1: SO group; group 2: SCI group; and group 3: SCI+S31-201 group; * $p < 0.001$.

Table 3. SEP

day	group 1	group 2	group 3	F value	p	LSD		LSD		LSD	
						group 1 vs. group 2	p	group 1 vs. group 3	p	group 2 vs. group 3	p
1	12.27 ± 0.40	28.85 ± 1.30	28.63 ± 1.52	295.97	*	$t = 36.74$	*	$t = 36.25$	*	$t = 0.49$	0.629
7	12.53 ± 0.53	26.46 ± 1.30	26.12 ± 0.91	306.75	*	$t = 37.60$	*	$t = 36.69$	*	$t = 0.92$	0.364
14	12.5 ± 0.48	24.33 ± 0.97	20.51 ± 0.78	277.90	*	$t = 40.01$	*	$t = 27.09$	*	$t = 12.92$	*
28	12.42 ± 0.43	20.09 ± 0.64	15.74 ± 0.61	205.13	*	$t = 34.98$	*	$t = 15.14$	*	$t = 19.84$	*

$n = 5$ points for each group; $n = 15$ points for 3 groups; group 1: SO group; group 2: SCI group; group 3: SCI+S31-201 group; * $p < 0.001$.

show, the level of OX-42 protein expression increased significantly as a result of SCI. S31-201 treatment decreased the level of OX-42 expression. The grayscale intensity of expression differed significantly ($p < 0.001$, Figure 4D).

Glial fibrillary acidic protein (GFAP) is a component of the cytoskeleton of astrocytes and vimentin is closely related to gliosis and glial recovery after brain injury. Western blotting indicated that on day 14 and day 28 postoperatively levels of both vimentin and GFAP expression were significantly higher in the SCI group and the SCI+S31-201 group. Moreover, S31-201 treatment significantly decreased the level of GFAP expression on day 28 postoperatively. The significant difference in vimentin expression caused by S31-201 treatment started on day 14 postoperatively (Figure 4B, $p < 0.001$).

Western blotting indicated that expression of the early neuronal specific marker β -tubulin III was downregulated as a result of surgically induced SCI and that S31-201 treatment upregulated the expression of β -tubulin III. The grayscale intensity of blots differed significantly (Figure 4E, $p < 0.001$).

The level of neurofilament-200 (NF-200) expression

was lower in the SCI group than in the SO group. The STAT3 inhibitor significantly upregulated the expression of NF-200 starting on day 14 postoperatively (Figures 4C and 4F, $p < 0.001$).

4. Discussion

SCI often results in devastating permanent neurological deficits. Glial scar tissue is considered to be a physical barrier that prevents axonal regeneration by producing axonal growth inhibitors (9). Pro-inflammatory cytokines such as IL-6, IL-1b, and tumor necrosis factor- α (TNF- α) initiate production of a number of specific molecules and contribute to secondary damage (10). Expression of IL-6 mRNA has also been observed in motoneurons 24-72 h after injury, indicating that these inflammatory cytokines may be involved in promoting axonal sprouting in the process of SCI. Studies have reported that STAT3 is a signal transducer of various cytokines and growth factors and that it plays an important role in IL-6 intercellular signaling after central nervous system (CNS) injury (which includes an SCI) (11-13). Activation of the JAK-STAT pathway has previously been reported in CNS injury and is directly associated with neurogenesis and

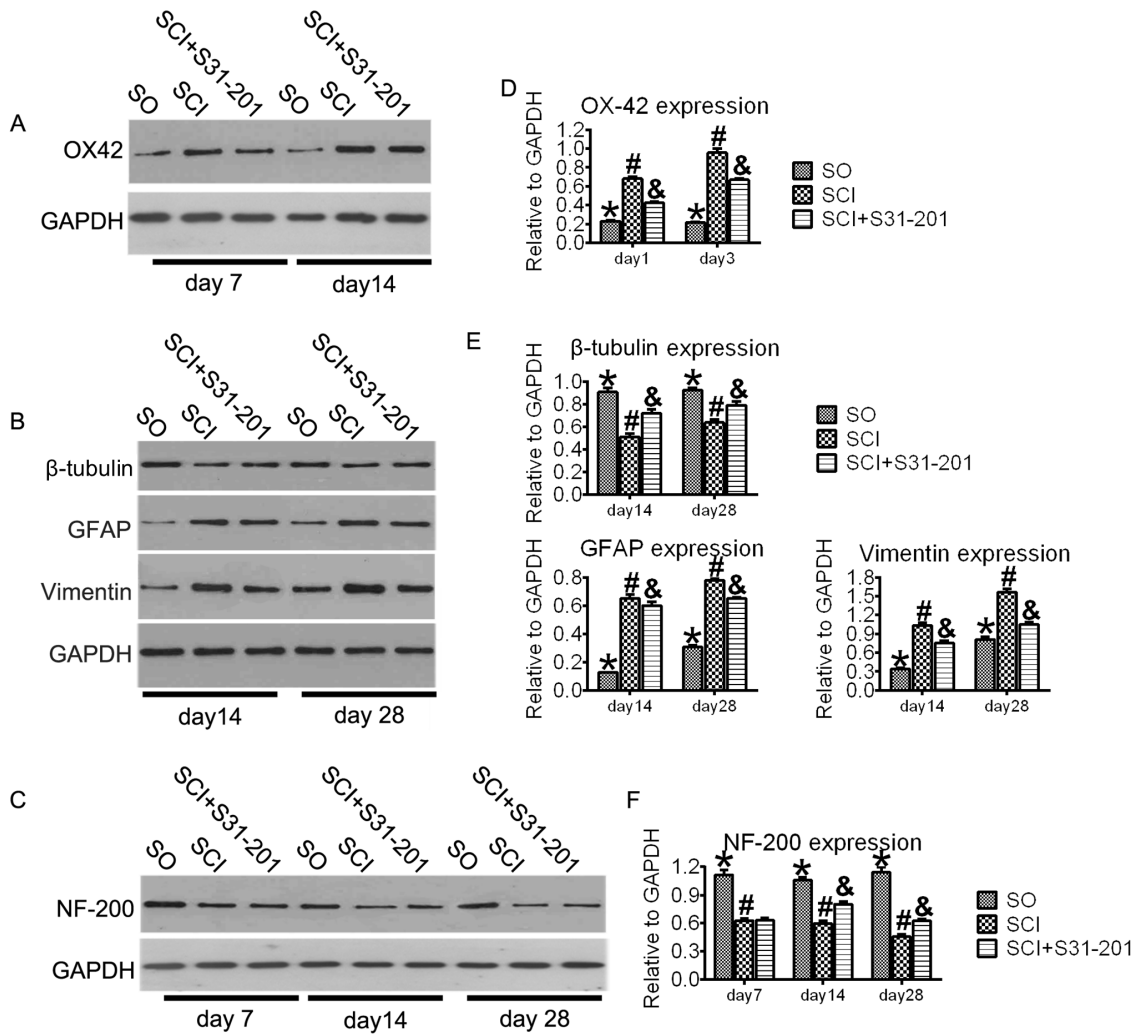


Figure 4. Western blotting and grayscale values for blots. **p* < 0.001, vs. SCI+S31-201 group. #*p* < 0.001, vs. SO group. &*p* < 0.001, vs. SCI group. (*n* = 5 points for each group; *n* = 15 points for 3 groups).

Table 4. Grayscale values for Western blots (relative to GAPDH)

indices	day	group 1	group 2	group 3	<i>F</i> value	<i>p</i>	LSD		LSD		LSD	
							group 1 vs. group 2	<i>P</i>	group 1 vs. group 3	<i>P</i>	group 2 vs. group 3	<i>P</i>
OX-42	1	0.23 ± 0.01	0.68 ± 0.02	0.43 ± 0.01	548.29	*	<i>t</i> = 57.19	*	<i>t</i> = 24.85	*	<i>t</i> = 32.34	*
	3	0.21 ± 0.00	0.96 ± 0.04	0.67 ± 0.02	490.39	*	<i>t</i> = 53.80	*	<i>t</i> = 32.92	*	<i>t</i> = 20.88	*
NF200	7	1.11 ± 0.05	0.63 ± 0.02	0.63 ± 0.03	148.31	*	<i>t</i> = 25.91	*	<i>t</i> = 25.76	*	<i>t</i> = 0.15	0882
	14	1.14 ± 0.05	0.46 ± 0.02	0.63 ± 0.02	290.80	*	<i>t</i> = 40.02	*	<i>t</i> = 30.38	*	<i>t</i> = 9.64	*
β-tubulin	14	0.91 ± 0.04	0.51 ± 0.02	0.72 ± 0.04	92.29	*	<i>t</i> = 23.52	*	<i>t</i> = 11.21	*	<i>t</i> = 12.31	*
	28	0.92 ± 0.02	0.64 ± 0.02	0.79 ± 0.03	77.56	*	<i>t</i> = 21.56	*	<i>t</i> = 10.10	*	<i>t</i> = 11.46	*
GFAP	14	0.13 ± 0.00	0.65 ± 0.03	0.60 ± 0.03	366.59	*	<i>t</i> = 42.45	*	<i>t</i> = 38.49	*	<i>t</i> = 3.96	*
	28	0.31 ± 0.01	0.78 ± 0.01	0.65 ± 0.01	1265.13	*	<i>t</i> = 84.30	*	<i>t</i> = 61.22	*	<i>t</i> = 23.08	*
Vimentin	14	0.34 ± 0.02	1.04 ± 0.04	0.76 ± 0.03	317.19	*	<i>t</i> = 43.35	*	<i>t</i> = 25.91	*	<i>t</i> = 17.44	*
	28	0.81 ± 0.04	1.56 ± 0.05	1.06 ± 0.03	206.24	*	<i>t</i> = 34.47	*	<i>t</i> = 11.18	*	<i>t</i> = 23.30	*

n = 5 points for each group; *n* = 15 points for 3 groups; **p* < 0.001.

glia scar formation in the injured region (14,15). The roles of STAT3 in SCI are not yet clear (16). Many pieces of evidence suggest that this family of cytokines plays important roles in regulating the immune response,

inflammation, and the CNS.

The current study investigated the effects of the STAT3 inhibitor S31-201 on the process of SCI. Results indicated that S31-201 reduced the inflammatory

response, it reduced secondary injury, and it promoted regeneration. Glial scar formation is considered to be major cause of poor regeneration of the adult CNS after injury (17). According to both macroscopic observation and microscopic examination, surgically induced SCI damaged the structure of the spinal cord, an epidural scar had formed, and there was a long, oval cavity where the spinal cord was severed. However, these morphological changes improved significantly as a result of S31-201 treatment. The extent of the decrease in the BBB score and the increase in SEP and MEP scores decreased as a result of treatment with the STAT3 inhibitor S31-201.

Western blotting indicated that S31-201 treatment decreased GFAP, vimentin, and OX-42 expression. The STAT3 inhibitor significantly upregulated the expression of NF-200 and β -tubulin III. A study has reported that IL-6 and the activity of its signaling partner establish a positive feedback mechanism with PAR1 that may promote IL-6-STAT3 signaling to levels sufficient to elicit fulminant astrogliosis, including increases in levels of the astroglial intermediate filament proteins GFAP and vimentin (18,19). The current results indicated that the STAT3 inhibitor S31-201 decreased the expression of GFAP and vimentin. In addition, S31-201 reduced the extent of the increase in OX-42. Thus, the STAT3 inhibitor S31-201 presumably attenuates the inflammatory response after SCI.

NF-200 is an indicator of neuronal differentiation and β -tubulin III indicates neural stem cell differentiation after an SCI in rats (5,20). Western blotting indicated that the STAT3 inhibitor S31-201 promoted the expression of NF-200 and β -tubulin III protein. The current study indicated that S31-201 stimulates neurogenesis in the region of an SCI.

In contrast to the current study, other studies have reported that STAT3 promotes motor neuron differentiation by collaborating with a motor neuron-specific LIM complex (21). STAT3 performs different roles during neural stem cell maintenance and motor neuron differentiation. In summary, the current mouse model of SCI suggests that early treatment with the STAT3 inhibitor S31-201 significantly improves functional recovery and reduces the posttraumatic inflammatory response and glial scar formation. The STAT3 inhibitor S31-201 inhibits the inflammatory action of IL-6 and neural stem cell differentiation, so S31-201 might be a potential treatment for SCI.

Acknowledgements

This study was supported by the Tianjin Natural Science Foundation (grant no. 16JCYBJC24900).

References

1. Karimi-Abdolrezaee S, Billakanti R. Reactive astrogliosis after spinal cord injury-Beneficial and detrimental effects. *Mol Neurobiol.* 2012; 46:251-264.
2. Gaudet AD, Popovich PG, Ramer MS. Wallerian degeneration: Gaining perspective on inflammatory events after peripheral nerve injury. *J Neuroinflammation.* 2011; 8:110.
3. Varma AK, Das A, Wallace Gt, Barry J, Vertegel AA, Ray SK, Banik NL. Spinal cord injury: A review of current therapy, future treatments, and basic science frontiers. *Neurochem Res.* 2013; 38:895-905.
4. Yu J, Vodyanik MA, Smuga-Otto K, Antosiewicz-Bourget J, Frane JL, Tian S, Nie J, Jonsdottir GA, Ruotti V, Stewart R, Slukvin II, Thomson JA. Induced pluripotent stem cell lines derived from human somatic cells. *Science.* 2007; 318:1917-1920.
5. Mukaino M, Nakamura M, Okada S, Toyama Y, Liu M, Okano H. Role of IL-6 in regulation of inflammation and stem cell differentiation in CNS trauma. *Nihon Rinsho Men'eki Gakkai Kaishi.* 2008; 31:93-98. (in Japanese)
6. Guerrero AR, Uchida K, Nakajima H, Watanabe S, Nakamura M, Johnson WE, Baba H. Blockade of interleukin-6 signaling inhibits the classic pathway and promotes an alternative pathway of macrophage activation after spinal cord injury in mice. *J Neuroinflammation.* 2012; 9:40.
7. Cao F, Hata R, Zhu P, Nakashiro K, Sakanaka M. Conditional deletion of Stat3 promotes neurogenesis and inhibits astrogliogenesis in neural stem cells. *Biochem Biophys Res Commun.* 2010; 394:843-847.
8. Nakajima Y, Osuka K, Seki Y, Gupta RC, Hara M, Takayasu M, Wakabayashi T. Taurine reduces inflammatory responses after spinal cord injury. *J Neurotrauma.* 2010; 27:403-410.
9. Wanner IB, Anderson MA, Song B, Levine J, Fernandez A, Gray-Thompson Z, Ao Y, Sofroniew MV. Glial scar borders are formed by newly proliferated, elongated astrocytes that interact to corral inflammatory and fibrotic cells *via* STAT3-dependent mechanisms after spinal cord injury. *J Neurosci.* 2013; 33:12870-12886.
10. Yamauchi K, Osuka K, Takayasu M, Usuda N, Nakazawa A, Nakahara N, Yoshida M, Aoshima C, Hara M, Yoshida J. Activation of JAK/STAT signalling in neurons following spinal cord injury in mice. *J Neurochem.* 2006; 96:1060-1070.
11. Na YJ, Jin JK, Kim JI, Choi EK, Carp RI, Kim YS. JAK-STAT signaling pathway mediates astrogliosis in brains of scrapie-infected mice. *J Neurochem.* 2007; 103:637-649.
12. Herrmann JE, Imura T, Song B, Qi J, Ao Y, Nguyen TK, Korsak RA, Takeda K, Akira S, Sofroniew MV. STAT3 is a critical regulator of astrogliosis and scar formation after spinal cord injury. *J Neurosci.* 2008; 28:7231-7243.
13. Dominguez E, Mauborgne A, Mallet J, Desclaux M, Pohl M. SOCS3-mediated blockade of JAK/STAT3 signaling pathway reveals its major contribution to spinal cord neuroinflammation and mechanical allodynia after peripheral nerve injury. *J Neurosci.* 2010; 30:5754-5766.
14. Kang MK, Kang SK. Interleukin-6 induces proliferation in adult spinal cord-derived neural progenitors *via* the JAK2/STAT3 pathway with EGF-induced MAPK phosphorylation. *Cell Prolif.* 2008; 41:377-392.
15. McFarland BC, Hong SW, Rajbhandari R, Twitty GB, Jr., Gray GK, Yu H, Benveniste EN, Nozell SE. NF- κ B-induced IL-6 ensures STAT3 activation and tumor aggressiveness in glioblastoma. *PLoS One.* 2013; 8:e78728.

16. Wang T, Yuan W, Liu Y, Zhang Y, Wang Z, Zhou X, Ning G, Zhang L, Yao L, Feng S, Kong X. The role of the JAK-STAT pathway in neural stem cells, neural progenitor cells and reactive astrocytes after spinal cord injury. *Biomed Rep.* 2015; 3:141-146.
17. Okada S, Nakamura M, Mikami Y, Shimazaki T, Mihara M, Ohsugi Y, Iwamoto Y, Yoshizaki K, Kishimoto T, Toyama Y, Okano H. Blockade of interleukin-6 receptor suppresses reactive astrogliosis and ameliorates functional recovery in experimental spinal cord injury. *J Neurosci Res.* 2004; 76:265-276.
18. Radulovic M, Yoon H, Wu J, Mustafa K, Scarisbrick IA. Targeting the thrombin receptor modulates inflammation and astrogliosis to improve recovery after spinal cord injury. *Neurobiol Dis.* 2016; 93:226-242.
19. Radulovic M, Yoon H, Wu J, Mustafa K, Fehlings MG, Scarisbrick IA. Genetic targeting of protease activated receptor 2 reduces inflammatory astrogliosis and improves recovery of function after spinal cord injury. *Neurobiol Dis.* 2015; 83:75-89.
20. Kim JB, Zehres H, Wu G, Gentile L, Ko K, Sebastiano V, Arauzo-Bravo MJ, Ruau D, Han DW, Zenke M, Scholer HR. Pluripotent stem cells induced from adult neural stem cells by reprogramming with two factors. *Nature.* 2008; 454:646-650.
21. Lee S, Shen R, Cho HH, Kwon RJ, Seo SY, Lee JW, Lee SK. STAT3 promotes motor neuron differentiation by collaborating with motor neuron-specific LIM complex. *Proc Natl Acad Sci U S A.* 2013; 110:11445-11450.

(Received August 17, 2016; Revised October 12, 2016; Accepted October 25, 2016)

Induction of apoptosis by ethanol extract of *Evodia rutaecarpa* in HeLa human cervical cancer cells *via* activation of AMP-activated protein kinase

Seon Young Park^{1,*}, Cheol Park^{2,*}, Shin-Hyung Park³, Su-Hyun Hong⁴, Gi-Young Kim⁵, Sang Hoon Hong^{1,**}, Yung-Hyun Choi^{4,6,**}

¹ Department of Internal Medicine, Donggeui University College of Korean Medicine, Busan, Korea;

² Department of Molecular Biology, College of Natural Sciences and Human Ecology, Donggeui University, Busan, Korea;

³ Department of Pathology, Donggeui University College of Korean Medicine, Busan, Korea;

⁴ Department of Biochemistry, College of Korean Medicine, Donggeui University, Busan, Korea;

⁵ Department of Marine Life Sciences, School of Marine Biomedical Science, Jeju National University, Jeju, Korea;

⁶ Anti-Aging Research Center, Donggeui University, Busan, Korea.

Summary

The fruit of *Evodia rutaecarpa* (Juss.) Benth has been used widely in traditional medicine therapy. Although it has been shown to possess many pharmacological activities, the molecular mechanisms of its anti-cancer activity have not been clearly elucidated. In the present study, we investigated the pro-apoptotic effects of an ethanol extract isolated from immature fruits of *E. rutaecarpa* (EEER) in HeLa human cervical cancer cells. EEER treatment decreased the cell viability of HeLa cells in a concentration-dependent manner, which was related to apoptotic cell death resulting from apoptotic body formation, DNA fragmentation, and an increased population of annexin V⁺-positive cells. EEER treatment significantly suppressed anti-apoptotic Bcl-2 expression, leading to subsequent loss of mitochondrial membrane potential (MMP), while it did not change expression levels of death receptor (DR)-related proteins. EEER treatment increased activity of caspase-3 and -9 but not caspase-8, and pretreatment of a caspase-3 inhibitor markedly attenuated EEER-induced apoptosis. Furthermore, EEER activated the AMP-activated protein kinase (AMPK) signaling pathway; however, inhibition of AMPK markedly abrogated EEER-induced apoptosis. Overall, the results suggest that the apoptotic activity of EEER may be associated with a caspase-dependent cascade through activation of the intrinsic signaling pathway connected with AMPK activation. *E. rutaecarpa* could be a prospective clinical application to treat human cervical cancer.

Keywords: *Evodia rutaecarpa*, cervical cancer, apoptosis, caspase, AMPK

1. Introduction

Apoptosis is a well-known type of programmed cell

death mediated by extrinsic and intrinsic pathways. The extrinsic pathway is activated by an interaction between DRs and their ligands at the plasma membrane, which causes subsequent activation of caspase-8 (1). The intrinsic pathway, also called the mitochondrial pathway, is initiated by the loss of MMP ($\Delta\psi_m$) and the release of pro-apoptotic proteins, such as cytochrome c, leading to the activation of caspase-9 and -3 (2). In particular, mitochondria are emerging as idealized targets for anti-cancer drugs. Whereas oncogenes are frequently mutated in cancers, leading to drug resistance, mitochondria have proved to be invariant targets working across all cancer types (3,4). Even though not absolutely essential for the induction of apoptosis, mitochondrial disruption results in excessive

Released online in J-STAGE as advance publication November 27, 2016.

*These authors contributed equally to this works.

**Address correspondence to:

Dr. Sang Hoon Hong, Department of Internal Medicine, Donggeui University College of Korean Medicine, Busan 47227, Republic of Korea.

E-mail: shhong@deu.ac.kr

Dr. Yung-Hyun Choi, Department of Biochemistry, College of Korean Medicine, Donggeui University, Busan, 47227, Republic of Korea.

E-mail: choiyh@deu.ac.kr

reactive oxygen species (ROS) production and therapy-activating apoptosis in cancer cells (4,5). In addition, cancer cells produce adenosine triphosphate (ATP) from mitochondria through oxidative phosphorylation (OXPHOS) in glucose-deprived conditions, implying that targeting the mitochondrial bioenergetic pathway could be an effective strategy to treat cancers (6).

AMPK is a metabolic-sensing protein kinase that plays a critical role as an energy sensor in ATP-deprived conditions (7,8). An increased ADP/ATP ratio leads to AMPK phosphorylation at Thr172, contributing to activation of ATP-generating catabolic processes, such as fatty acid oxidation and glycolysis, as well as suppression of ATP-utilizing anabolic pathways, including glycogen, protein, and lipid synthesis. Beyond these metabolic effects, interest in the potential involvement of AMPK in the regulation of cancer cell growth has gradually increased since the tumor suppressor liver kinase B1 (LKB1) was identified as the major upstream kinase of AMPK (9,10). A variety of studies have reported that AMPK regulates cell proliferation and apoptosis *via* multiple signaling pathways, such as phosphorylation and subsequent stabilization of tumor suppressor p53, upregulation of cyclin-dependent kinase inhibitors, and downregulation of the mammalian target of rapamycin complex-1 activity (7,11). In particular, it has been demonstrated that activation of AMPK is responsible for inducing apoptosis *via* the mitochondrial pathway (12,13). However, AMPK is also known to play a protective role in cancer cells under metabolic stressed conditions by maintenance of energy homeostasis and modulation of autophagy, making the influence of AMPK on cancer progression controversial (14,15).

The immature fruit of *Evodia rutaecarpa* (Juss.) Benth has traditionally been used in Oriental medicine to treat headaches, gastrointestinal disorders, and amenorrhea for thousands of years (16,17). It has been reported that the extracts of *E. rutaecarpa* and its alkaloids exhibit anti-obesity, anti-dementia, anti-inflammatory, and anti-oxidant effects (18,19). More recently, anti-cancer activities of *E. rutaecarpa* have been suggested. For instance, G2/M phase cell cycle arrest was involved in apoptosis of lung cancer cells induced by evodiamine, which is an *E. rutaecarpa* derived alkaloid based substance. The caspase activity accompanied by c-Jun N-terminal kinase (JNK) activity inhibition was involved in apoptosis induced in both ovarian and colonic cancer cells (20,21). In addition, there have been other reports indicating that inhibition of the activity of the mechanistic target of rapamycin (mTOR) signal systems, or insulin-like growth factor 1, is involved in apoptosis of human cancer cells exposed to evodiamine (22,23). Furthermore, it has been reported that the inhibition of human cancer cell proliferation by evodiamine is associated with overcoming of multidrug resistance related to nuclear factor-kappa B signaling pathway inhibition

and inhibition of invasive activity by calcium/JNK signaling-mediated autophagy induction and to increases in the activity of matrix metalloproteinase (24-26) However, to date no systematic study has been conducted on *E. rutaecarpa* extracts *per se*. In the current study, we explored the anti-cancer effects of the ethanol extract of *E. rutaecarpa* immature fruits (EEER) in HeLa human cervical cancer cells and investigated the underlying mechanism. We found that EEER triggered apoptosis in HeLa cells *via* the mitochondrial pathway, indicating that AMPK is a critical regulator of EEER-induced apoptosis. To our knowledge, this is the first study suggesting the involvement of AMPK in the anti-cancer activity of *E. rutaecarpa*.

2. Materials and Methods

2.1. Preparation of EEER

For the preparation of EEER, the dried immature fruits of *E. rutaecarpa* (100 g) were provided from Donggeui Korean Medical Center (Busan, Republic of Korea) and pulverized into a fine powder. The powder was then extracted in 1 L of 70% ethanol by sonication for 3 h. After filtering and concentrating the extracts, the remaining powder was dissolved in dimethyl sulfoxide (DMSO, Sigma-Aldrich Chemical Co., St. Louis, MO, USA) as a stock solution at a concentration of 100 mg/mL and stored at 4°C. The stock solution was diluted with medium to the desired concentration prior to use.

2.2. Cell culture

HeLa human cervical carcinoma cells were obtained from the American Type Culture Collection (Manassas, MD, USA) and cultured in Dulbecco's Modified Eagle Medium (DMEM, Gibco BRL, Grand Island, NY, USA) containing 10% heat-inactivated fetal bovine serum (FBS) and 1% penicillin streptomycin (Gibco BRL) at 37°C in a humidified atmosphere containing 5% CO₂.

2.3. Cell viability assay

To investigate cell viability, the HeLa cells were seeded in a 96-well plate at a density of 2×10^3 cells/well and stabilized for 24 h. The cells were treated with various concentrations of EEER for 24 h with or without 1 h pre-treatment with N-benzyloxycarbonyl-Asp-Glu-Val-Asp-fluoromethylketone (z-DEVD-fmk), a caspase-3 inhibitor (CalBiochem, San Diego, CA, USA), and compound C, an inhibitor of AMPK (Sigma-Aldrich Chemical Co.). 3-(4,5-dimethyl-2-thiazolyl)-2,5-diphenyl-2H-tetrazolium (MTT, Sigma-Aldrich Chemical Co.) working solution (0.5 mg/mL) was then added to the media and incubated for a further 4 h at 37°C. After incubation, the culture supernatant

was aspirated, and 100 μ L dimethyl sulfoxide (DMSO, Sigma-Aldrich Chemical Co.) was added to completely dissolve the formazan crystals. Absorbance of each well was measured at a wave length of 540 nm using an enzyme-linked immunosorbent assay (ELISA) reader (Molecular Devices, Sunnyvale, CA, USA) (27).

2.4. Nuclear staining with DAPI

The HeLa cells were treated with EEER at various concentrations for 24 h with or without 1 h pre-treatment with z-DEVD-fmk or compound C. The cells were then harvested, washed with phosphate-buffered saline (PBS), and fixed with 3.7% paraformaldehyde (Sigma-Aldrich Chemical Co.) for 30 min at room temperature. After washing twice with PBS, the cells were attached on glass slides using cytospin (Shandon, Pittsburgh, PA, USA) and stained with 2.5 μ g/mL 4,6-dianmidino-2-phenylindole (DAPI, Sigma-Aldrich Chemical Co.) solution for 20 min at room temperature. The stained cells were washed three times with PBS and analyzed using a fluorescence microscope (Carl Zeiss, Deisenhofen, Germany).

2.5. DNA fragmentation assay

Following EEER treatment for 24 h at various concentrations with or without 1 h pre-treatment using z-DEVD-fmk or compound C, the cells were lysed in a buffer [10 mM Tris-HCl (pH 7.4), 150 mM NaCl, 5 mM ethylenediaminetetra acetic acid (EDTA), and 0.5% Triton X-100] for 1 h at room temperature. After centrifugation at 14,000 rpm for 30 min, the supernatant was collected and incubated with proteinase K (Invitrogen, Carlsbad, CA, USA) for 3 h at 50°C. The fragmented DNA in the supernatant was purified using the same amount of neutral phenol:chloroform:isoamyl alcohol solution (Sigma-Aldrich Chemical Co.) by rotation for 30 min at room temperature. After centrifugation, the supernatant was added to 0.5 M NaCl (final concentration) and 1 volume of isopropanol to precipitate the fragmented DNA and was incubated overnight at 4°C. The DNA pellet obtained by centrifugation was then dissolved in TE buffer (10 mM Tris-HCl containing 1 mM EDTA) containing RNase A (Sigma-Aldrich Chemical Co.) and was separated on 1% agarose gels. The DNA fragmentation pattern was visualized by an ultraviolet light source after ethidium bromide (EtBr, Sigma-Aldrich Chemical Co.) staining.

2.6. Flow cytometry analysis

Changes in the MMP were measured by flow cytometry (Becton Dickinson, San Jose, CA, USA) using 5,5', 6,6'-tetrachloro-1,1',3,3'-tetraethyl-imidacarbocyanine iodide (JC-1, Sigma-Aldrich Chemical Co.) and a dual-emission potential-sensitive probe. The cells treated with

various concentrations of EEER for 24 h were collected, washed twice with PBS, and incubated with 10 μ M JC-1 for 20 min at 37°C in the dark. After centrifugation, the stained cells were washed once with PBS and were resuspended in PBS. Cells with normal MMP formed aggregates with a high FL-2 fluorescence after JC-1 treatment. However, the loss of MMP changes the FL-2 fluorescence into FL-1 fluorescence because the dye shifts from an aggregate to a monomeric state. Therefore, the increase of FL-1 fluorescence was determined to be the loss of MMP. For Annexin V-propidium iodide (PI) double staining, the cells were challenged with EEER for 24 h with or without 1 h pretreatment with z-DEVD-fmk or compound C. Apoptotic cells were quantitatively identified using an Annexin V-FITC Apoptosis Detection Kit (Becton Dickinson) containing FITC conjugated annexin V and PI, according to the protocols provided by the manufacturer (28). The data were converted to density plots for presentation using CellQuest software.

2.7. Determination of caspase activity

The activities of caspases were determined using colorimetric assay kits (R&D Systems, Minneapolis, MN, USA) containing the synthetic tetrapeptides [Asp-Glu-Val-Asp (DEAD) for caspase-3, Ile-Glu-Thr-Asp (IETD) for caspase-8, and Leu-Glu-His-Asp (LEHD) for caspase-9] labeled with p-nitroaniline (pNA), according to the manufacturer's instructions. Briefly, EEER-treated cells were harvested and lysed in the supplied lysis buffer. Supernatants were then collected and incubated at 37°C with the supplied reaction buffer, dithiothreitol (DTT), and respective substrates. Reaction activities were evaluated by measuring absorbance at 405 nm using an ELISA reader.

2.8. Western blotting analysis

To prepare whole cell lysate, cells treated under the indicated condition were lysed with ice-cold lysis buffer [25 mM Tris-Cl (pH 7.5), 250 mM NaCl, 5 mM EDTA, 1% Nonidet P-40, 1 mM phenylmethylsulfonyl fluoride (PMSF), 5 mM DTT], including a complete protease inhibitor cocktail tablet (Roche Diagnostics, Mannheim, Germany) and phosphatase inhibitors (1 mM Na₃VO₄, 100 mM NaF, 10 mM NaPP). After centrifugation at 13,000 rpm at 4°C for 30 min, the supernatants were collected and protein concentration was determined using a Bio-Rad protein assay (Bio-Rad Laboratories, Hercules, CA, USA), according to the manufacturer's instructions. Equivalent amounts of protein were resolved using sodium dodecyl sulfate (SDS)-polyacrylamide gels and transferred to polyvinylidene fluoride (PVDF) membranes (Millipore, Bedford, MA, USA). The membranes were probed with the specific primary antibodies and corresponding secondary antibodies. The protein-antibody complexes were

detected using SuperSignal West Pico Chemiluminescent Substrate (Thermo Scientific Pierce, Rockford, IL, USA), according to the manufacturer's protocol. All primary antibodies were purchased from Santa Cruz Biotechnology (Santa Cruz, CA, USA) except for the antibody against phospho-acetyl-coenzyme A carboxylase (ACC), which was obtained from Cell Signaling Technology (Beverly, MA, USA). The horseradish peroxidase (HRP)-conjugated secondary antibodies were obtained from Amersham Life Science Corp. (Arlington Heights, IL, USA).

2.9. Statistical analysis

Each result is expressed as the mean \pm standard deviation (S.D.) of data obtained from independent triplicate experiments. A statistical analysis was performed using a paired Student's *t*-test. A *p*-value $<$ 0.05 was considered statistically significant.

3. Results

3.1. EEER inhibits cell viability and induces apoptosis in HeLa cells

To investigate the effects of EEER on cell viability, HeLa cells were treated with various concentrations of EEER for 24 h. As shown in Figure 1A, EEER

treatment reduced cell viability in a concentration-dependent manner, with an IC_{50} of about 45 μ g/mL (Figure 1A). Morphological changes, including membrane blebbing, diminished cell density, and an increased number of floating cells were also observed (Figure 1B). Because several types of cell death, including necrosis, apoptosis, and autophagic cell death, have been reported, we next investigated which type of cell death is induced by EEER. The results showed that EEER treatment significantly increased the number of condensed or blebbing nuclei that generally appear in apoptosis before nuclear fragmentation (Figure 1C). DNA fragmentation was consistently observed with EEER treatment at 20 μ g/mL and gradually increased in a concentration-dependent manner (Figure 1D). EEER also enhanced the population of annexin V⁺/PI⁻ cells, which represent early apoptotic cells (Figure 1E). These data collectively suggest that EEER suppressed cell proliferation by inducing apoptosis in HeLa cells.

3.2. EEER modulates the intrinsic pathway leading to the loss of MMP in HeLa cells

Given that there are two classical pathways in apoptosis – the extrinsic and intrinsic pathways – we examined which pathway is involved in EEER-induced apoptosis. The extrinsic pathway is initiated by the interactions between the DRs and their corresponding ligands.

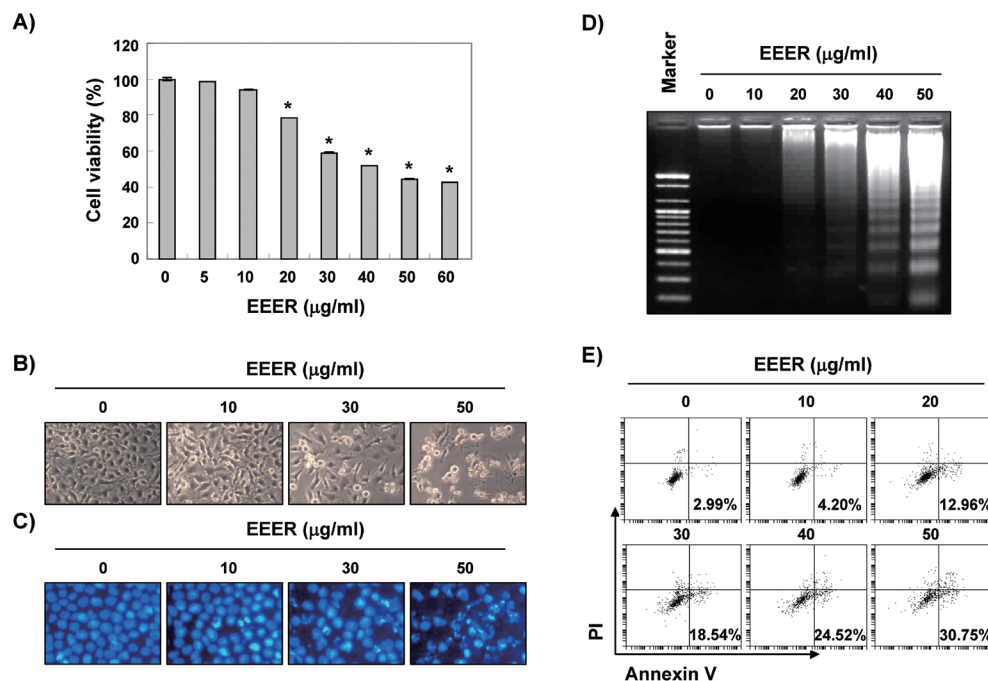


Figure 1. Inhibition of cell viability and induction of apoptosis by EEER in HeLa cells. Cells were treated with various concentrations of EEER for 24 h. (A) Cell viability was measured by an MTT assay. Data are expressed as the mean \pm S.D. of three independent experiments. Significance was determined by the Student's *t*-test ($*p <$ 0.05 vs. untreated control). (B) Morphological changes were visualized by an inverted microscope (Magnification, \times 200). (C) Nuclei were stained with DAPI solution and photographed with a fluorescent microscope (Magnification, \times 400). (D) Cells were collected and DNA was extracted. Fragmented DNA was separated on 1% agarose gel electrophoresis and visualized under UV light after staining with EtBr. (E) Cells were stained with FITC-conjugated annexin V and PI for DNA flow cytometry analysis. Percentages of apoptotic cells were determined by counting annexin V⁺/PI⁻ cells. Data are presented as mean \pm two independent experiments.

The most well recognized DRs are Fas, DR4, and DR5. They bind to Fas ligand (FasL) or TNF-related apoptosis-inducing ligand (TRAIL) to transfer death signals. Upon ligand binding, an adapter protein Fas-associated death domain (FADD) or TRAIL-associated death domain (TRADD) is recruited to the death receptor and forms a death-inducing signaling complex (DISC) to activate caspase-8 (1). Our results showed that the expressions of TRAIL, DR4, DR5, Fas, and FasL were hardly changed by EEER treatment, suggesting that EEER did not regulate the extrinsic pathway (Figure 2A).

Meanwhile, the intrinsic pathway is initiated through mitochondrial membrane permeabilization and release of pro-apoptotic proteins from mitochondria (2). Bcl-2 family proteins, including anti-apoptotic Bcl-2 and Bcl-xL, as well as pro-apoptotic Bax, BAD, and Bak, control this process tightly, and the ratio between pro-apoptotic and anti-apoptotic proteins determines the sensitivity to apoptosis (2). Our results clearly showed that anti-

apoptotic Bcl-2 was markedly downregulated by EEER treatment, even though the expression of pro-apoptotic Bax was not changed (Figure 2A). Accordingly, EEER treatment reduced MMP in a concentration-dependent manner (Figure 2B). Taken together, our results suggest that EEER induced apoptosis *via* the mitochondrial pathway but not *via* the DR-related pathway by an increase of the Bax/Bcl-2 ratio in HeLa cells.

3.3. EEER-induced apoptosis is regulated by the activation of caspases in HeLa cells

The extrinsic and intrinsic signaling pathways activate caspase cascades, which is a key hallmark of apoptosis. In particular, the disruption of mitochondria can trigger apoptosis through the activation of caspase-9 and -3, even if it can also induce caspase-independent apoptosis by the translocation of pro-apoptotic proteins, such as apoptosis-inducing factor (AIF) and endonuclease G (endoG), from the mitochondria into the nucleus (29,30). To examine whether EEER activates caspases, we investigated the expression and activity of two initiator caspases of the extrinsic and intrinsic apoptosis pathways, caspase-8 and -9, respectively, and caspase-3, a typical effector caspase. As shown in Figure 3A, EEER treatment apparently suppressed the expression of pro-caspase-9 and -3, while it hardly affected that

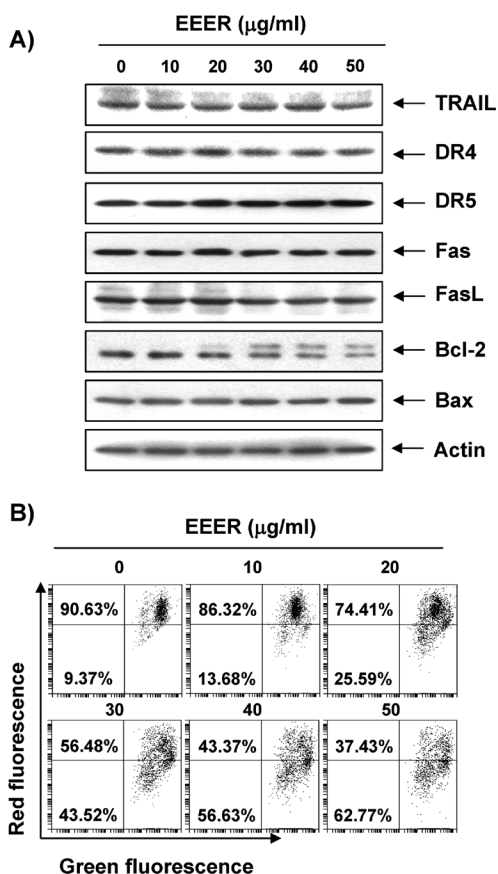


Figure 2. Effects of EEER on expression levels of apoptosis regulators and MMP values in HeLa cells. (A) After treatment with various concentrations of EEER for 24 h, cells were lysed and then equal amounts of cell lysates were separated on SDS-polyacrylamide gels and transferred to PVDF membranes. Membranes were probed with the indicated antibodies, and the proteins were visualized using an ECL detection system. Actin was used as an internal control. **(B)** To evaluate the changes of MMP, the cells grown under the same conditions as (A) were stained with JC-1 dye and were then analyzed on a DNA flow cytometer. Data are presented as mean \pm two independent experiments.

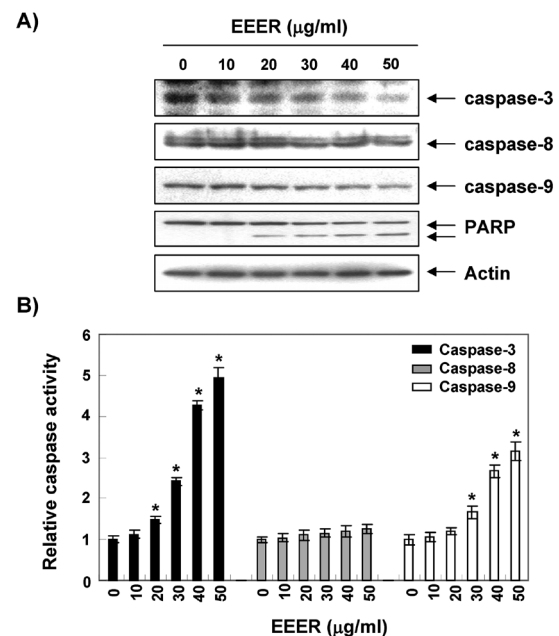


Figure 3. Activation of caspases by EEER treatment in HeLa cells. Cells were treated with various concentrations of EEER for 24 h. **(A)** Cells were lysed and then equal amounts of cell lysates were separated on SDS-polyacrylamide gels and transferred to membranes. Membranes were probed with the indicated antibodies against caspases, and the proteins were visualized using an ECL detection system. Actin was used as an internal control. **(B)** Activities of caspases were evaluated using caspase colorimetric assay kits. Data are expressed as the mean \pm S.D. of three independent experiments. Significance was determined by a Student's *t*-test (* p < 0.05 vs. untreated control).

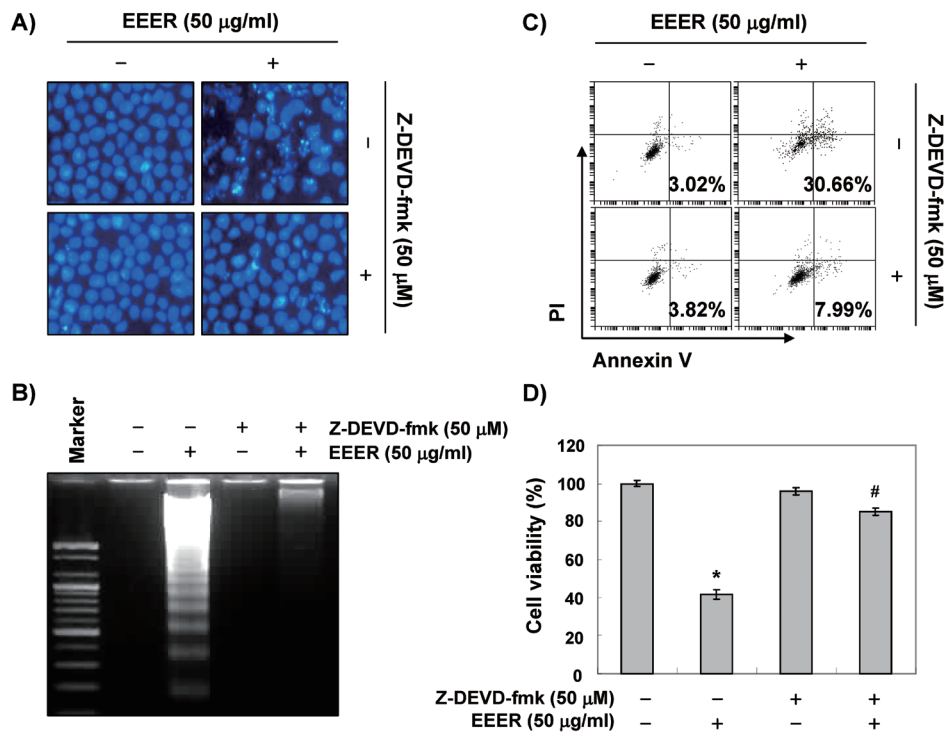


Figure 4. Suppression of EEER-induced apoptosis by inhibition of caspase-3 in HeLa cells. Cells were pre-treated with 50 μ M z-DEVD-fmk, a caspase-3 specific inhibitor, 1 h before treatment with 50 μ g/mL EEER for 24 h. **(A)** Nuclei were stained with DAPI solution and were photographed with a fluorescent microscope (Magnification, \times 400). **(B)** Fragmented DNA was separated on 1% agarose gel electrophoresis and visualized under UV light after staining with EtBr. **(C)** Percentages of apoptotic cells (annexin V⁺/PI⁺ cells) were measured using DNA flow cytometric analysis. Data are presented as mean \pm two independent experiments. **(D)** Cell viability was measured using an MTT assay. Data are expressed as the mean \pm S.D. of three independent experiments. Significance was determined by a Student's *t*-test (**p* < 0.05 vs. untreated control; #*p* < 0.05 vs. EEER-treated cells).

of pro-caspase-8. The subsequent increase of cleaved poly(ADP-ribose) polymerase (PARP), a well-known substrate of caspase-3 (31), was also observed (Figure 3A). The *in vitro* activity of caspase-3 and -9 but not of caspase-8 was consistently significantly enhanced by EEER treatment (Figure 3B). These results are in agreement with those in Figure 2, which suggest that EEER regulated the intrinsic pathway without control of the extrinsic pathway.

To verify whether EEER-induced apoptosis is caspase-dependent, we next inhibited the activity of caspase-3 using z-DEVD-fmk. Our results clearly showed that EEER-induced apoptotic body formation and DNA fragmentation were absolutely abrogated by z-DEVD-fmk pre-treatment (Figures. 4A and B). The increased population of annexin V⁺/PI⁻ cells and reduced cell viability were also reversed by the inhibition of caspase-3 activity (Figures. 4C and D). Taken together, our results demonstrate that the activation of caspase cascades following mitochondrial dysfunction is essential for EEER-induced apoptosis in HeLa cells.

3.4. EEER induces apoptosis through the activation of AMPK in HeLa cells

Given that mitochondria are the energy source, we

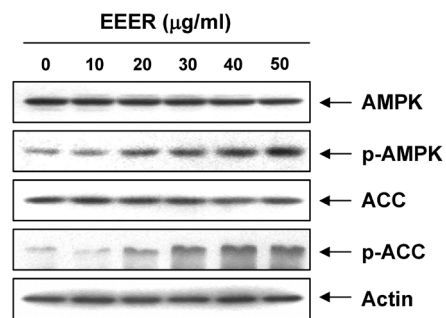


Figure 5. Activation of AMPK by EEER treatment in HeLa cells. Cells were treated with the indicated concentration of EEER for 24 h. Expression levels of p-AMPK, AMPK, p-ACC, and ACC were detected using Western blot analysis. Actin was used as a loading control.

hypothesized that the collapse of MMP would disturb energy homeostasis in HeLa cells. Because AMPK is a representative enzyme activated under low ATP states and is recognized as an emerging target of anti-cancer therapy (7,8), we checked activation of the AMPK signaling pathway. Interestingly, AMPK and its downstream target ACC were obviously phosphorylated by EEER treatment in a concentration-dependent manner, indicating that they were converted to the activated state (Figure 5). Previous research has demonstrated that activation of AMPK is responsible

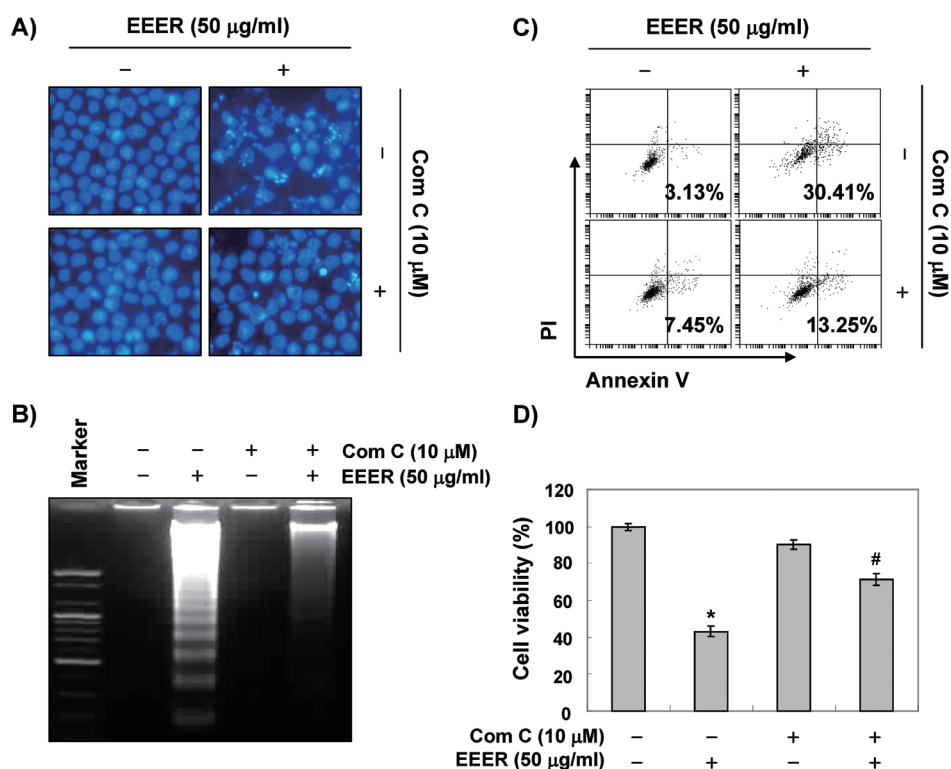


Figure 6. Suppression of EEER-induced apoptosis by inhibition of AMPK in HeLa cells. Cells were pre-treated with 10 µM compound C, an inhibitor of AMPK, 1 h before treatment with 50 µg/mL EEER for 24 h. **(A)** Nuclei were stained with DAPI solution and were photographed with a fluorescent microscope (Magnification, ×400). **(B)** Fragmented DNA was separated on 1% agarose gel electrophoresis and visualized under UV light after staining with EtBr. **(C)** Percentages of apoptotic cells (annexin V⁺/PI⁺ cells) were measured using DNA flow cytometric analysis. Data are presented as mean ± S.D. of two independent experiments. **(D)** Cell viability was measured using an MTT assay. Data are expressed as the mean ± S.D. of three independent experiments. Significance was determined by a Student's *t*-test (**p* < 0.05 vs. untreated control; #*p* < 0.05 vs. EEER-treated cells).

for mitochondria-mediated apoptosis (12,13). Therefore, we next investigated whether AMPK is involved in EEER-induced apoptosis. Our results showed that the markers of apoptosis increased by EEER treatment, including condensed and fragmented nuclei, DNA ladder, and the increased population of annexin V⁺/PI⁺ cells, which were reversed by pretreatment with compound C, an inhibitor of AMPK (Figure 6A-C). Accordingly, an EEER-induced decrease of cell viability was reversed by the addition of compound C (Figure 6D). These observations collectively suggest that AMPK activation played a crucial role in EEER-induced apoptosis in HeLa cells.

4. Discussion

In the current study, we investigated the anti-cancer activity of EEER and explored the underlying mechanism in HeLa human cervical carcinoma cells. Even though a variety of research has already reported the anti-proliferative effects of *E. rutaecarpa* and its alkaloids in various cancer cells, this is the first study, to our knowledge, to propose AMPK as a critical molecule mediating EEER-induced apoptosis.

Our results clearly show that EEER induced apoptotic cell death in HeLa cells. EEER treatment markedly suppressed the expression of Bcl-2, a

critical component of the mitochondrial pathway, and subsequently triggered the loss of MMP but did not modulate the DR-related pathway. The mediators of mitochondria-mediated apoptosis have been determined in various preceding reports. The first candidate released from the mitochondria upon apoptotic stimuli is cytochrome *c*, an essential component of the respiratory chain (2). It forms an apoptosome with apoptotic peptidase activating factor-1 (Apaf-1) and pro-caspase-9 to activate caspase-9 and the classical caspase cascade (30). Our results consistently showed that EEER activated caspase-9 and -3, while it did not influence the activity of caspase-8, thus supporting our idea that EEER induced mitochondria-mediated apoptosis. The other candidates released from the mitochondria to elicit apoptosis are AIF and endoG, which are especially involved in the caspase-independent pathway (29,30). However, based on our present data showing that z-DEVD-fmk completely blocked the apoptotic cell death induced by EEER, we suggest that the role of AIF and endoG in EEER-induced apoptosis might be slight. Notably, several preceding studies have also reported that evodiamine, an alkaloid isolated from *E. rutaecarpa*, induced mitochondria-mediated apoptosis in several cancer cell lines (20-26), which supports our current results.

Although the contribution of mitochondria in cancer

cell survival has been underestimated since Warburg suggested the significance of anaerobic glycolysis in cancers in overriding mitochondria as the source of energy (5,32), mitochondria are still idealized targets for anti-cancer therapy. When the cancer cells are in a glucose-depleted condition, they maintain ATP synthesis through OXPHOS and activate the catabolic pathways, including the oxidation of fatty acids and amino acids (6,33). In addition, cancer cells are more vulnerable to ROS generally generated from mitochondria compared to normal cells (5,34). Therefore, a broad range of physical and chemical stimuli causing mitochondrial dysfunction have been reported. First, the signals from the death receptor pathway are known to mediate the mitochondrial pathway. Caspase-8 connects the extrinsic pathway with the intrinsic pathway *via* cleavage of Bid, called truncated Bid (tBid). Binding of tBid to Bcl-2 proteins triggers release of Bax and Bak from Bcl-2, resulting in their indirect activation. In addition, tBid directly interacts with Bax located in the mitochondrial membrane to promote Bax oligomerization and subsequent loss of MMP (2,35). However, according to our present data, EEER treatment did not modulate the extrinsic pathway, which excludes tBid from the candidates causing mitochondrial disruption. Second, endoplasmic reticulum (ER) stress can induce permeabilization of the mitochondrial membrane *via* release of calcium into the cytoplasm (36). Liu *et al.* (25) demonstrated that evodiamine induced calcium/mitochondria-mediated apoptosis in human glioblastoma cells. In addition, cytosolic calcium is reported to activate AMPK *via* the Ca²⁺/calmodulin-dependent protein kinase kinase (CaMKK) pathway (37). As we observed that EEER treatment significantly activated the AMPK pathway, these studies strengthen the possibility that EEER-induced mitochondrial dysfunction might be the result of cytoplasmic calcium shifts. Third, accumulating research now indicates that oxidative stress also triggers apoptosis *via* the mitochondrial pathway. Oxidative stress causes severe damage to the electron transfer chain found in the inner mitochondrial membrane, leading to the explosive increase of ROS generation, referred to as ROS-induced ROS release, and resulting in the loss of MMP (38). Interestingly, ROS is also known to be an upstream signal of AMPK (39,40). Several studies have reported that oxygen deprivation induces autophagy *via* AMPK activation in human cancer cells (41,42). Therefore, the EEER-induced collapse of MMP might be the result of excessive generation of ROS.

Communication between mitochondria and AMPK has been suggested by various studies. When the cellular ATP level drops, AMPK is activated to inhibit mTOR signaling, leading to attenuation of protein synthesis (12,42). Because the mitochondrial electron transfer chain is the major source of ATP production,

mitochondrial dysfunction can drive reduction of ATP synthase, which results in activation of AMPK. Although AMPK might give cancer cells a survival advantage by conservation of energy in ATP-depleted conditions (14), it has been generally considered as a tumor suppressor based on the following points: *i)* AMPK deactivates mTOR, which is commonly activated in many cancers; *ii)* most of the tumor suppressor genes, including LKB1 and phosphatase and tensin homolog (PTEN), have been identified as upstream activators of AMPK (43,44); and *iii)* AMPK activators, such as 5-aminoimidazole-4-carboxamide ribonucleotide (AICAR) and metformin, are reported to inhibit tumorigenesis and tumor growth (45,46). Notably, metformin and antroquinonol have been reported to activate AMPK to induce apoptosis by inducing mitochondrial stress (47,48). Avicin D also disrupts mitochondrial metabolism, leading to decreased ATP levels and activation of AMPK, which is followed by autophagic cell death (41). These results are in agreement with our present data proposing AMPK as a key molecule inducing apoptosis in HeLa cells and supporting the possibility that EEER-induced loss of MMP leads to ATP depletion and the subsequent activation of AMPK. However, there are still other possible activators of AMPK, including ROS generated from the collapsed mitochondrial respiratory complex and CaMKK activated by increased cytosolic calcium, as mentioned above. Therefore, further studies are warranted to determine the precise upstream activator of AMPK.

In conclusion, our present results verified the anti-cancer effects of EEER in HeLa human cervical carcinoma cells. We suggest that AMPK plays a pivotal role in mitochondria-mediated apoptosis in response to EEER treatment. In support of our suggestion, recent clinical trials have demonstrated that metformin, an AMPK activator, decreased the incidence of cancer and cancer-related mortality and improved the disease control rate by itself or in combination with another drug (49). Although the active compound of EEER and the exact mechanism through which AMPK is activated should be further elucidated, our results suggest *E. rutaecarpa* is a prospective clinical option to treat human cervical cancer.

Acknowledgements

This research was supported by Basic Science Research Program through the National Research Foundation of Korea (NRF) funded by the Ministry of Science, ICT and Future Planning (2014R1A1A1008460 and 2015R1A2A2A01004633).

References

1. Okada H, Mak TW. Pathways of apoptotic and non-

- apoptotic death in tumour cells. *Nat Rev Cancer*. 2004; 4:592-603.
2. Hensley P, Mishra M, Kyprianou N. Targeting caspases in cancer therapeutics. *Biol Chem*. 2013; 394:831-843.
 3. Ralph SJ, Neuzil J. Mitochondria as targets for cancer therapy. *Mol Nutr Food Res*. 2009; 53:9-28.
 4. Modica-Napolitano JS, Weissig V. Treatment strategies that enhance the efficacy and selectivity of mitochondria-targeted anticancer agents. *Int J Mol Sci*. 2015; 16:17394-17421.
 5. Ralph SJ, Rodríguez-Enríquez S, Neuzil J, Moreno-Sánchez R. Bioenergetic pathways in tumor mitochondria as targets for cancer therapy and the importance of the ROS-induced apoptotic trigger. *Mol Aspects Med*. 2010; 31:29-59.
 6. Solaini G, Sgarbi G, Baracca A. *Biochim Biophys Acta*. Oxidative phosphorylation in cancer cells. Solaini. 2011; 1807:534-542.
 7. Gwinn DM, Shackelford DB, Egan DF, Mihaylova MM, Mery A, Vasquez DS, Turk BE, Shaw RJ. AMPK phosphorylation of raptor mediates a metabolic checkpoint. *Mol Cell*. 2008; 30:214-226
 8. Shackelford DB, Shaw RJ. The LKB1-AMPK pathway: Metabolism and growth control in tumour suppression. *Nat Rev Cancer*. 2009; 9:563-575.
 9. Shaw RJ, Bardeesy N, Manning BD, Lopez L, Kosmatka M, DePinho RA, Cantley LC. The LKB1 tumor suppressor negatively regulates mTOR signaling. *LC. Cancer Cell*. 2004; 6:91-99.
 10. Woods A, Johnstone SR, Dickerson K, Leiper FC, Fryer LG, Neumann D, Schlattner U, Wallimann T, Carlson M, Carling D. LKB1 is the upstream kinase in the AMP-activated protein kinase cascade. *Curr Biol*. 2003; 13:2004-2008.
 11. Monteverde T, Muthalagu N, Port J, Murphy DJ. Evidence of cancer-promoting roles for AMPK and related kinases. *FEBS J*. 2015; 282:4658-4671.
 12. Figarola JL, Singhal J, Tompkins JD, Rogers GW, Warden C, Horne D, Riggs AD, Awasthi S, Singhal SS. SR4 uncouples mitochondrial oxidative phosphorylation, modulates AMP-dependent kinase (AMPK)-mammalian target of rapamycin (mTOR) signaling, and inhibits proliferation of HepG2 hepatocarcinoma cells. *J Biol Chem*. 2015; 290:30321-30341.
 13. Chen H, Wang JP, Santen RJ, Yue W. Adenosine monophosphate activated protein kinase (AMPK), a mediator of estradiol-induced apoptosis in long-term estrogen deprived breast cancer cells. *Apoptosis*. 2015; 20:821-830.
 14. Laderoute KR, Amin K, Calaoagan JM, Knapp M, Le T, Orduna J, Foretz M, Viollet B. 5'-AMP-activated protein kinase (AMPK) is induced by low-oxygen and glucose deprivation conditions found in solid-tumor microenvironments. *Mol Cell Biol*. 2006; 26:5336-5347.
 15. Jeon SM. Regulation and function of AMPK in physiology and diseases. *Exp Mol Med*. 2016; 48:e245.
 16. Jiang J, Hu C. Evodiamine: A novel anti-cancer alkaloid from *Evodia rutaecarpa*. *Molecules*. 2009; 14:1852-1859.
 17. Kim D, Lee YH, Park SH, Lee MJ, Kim MJ, Jang HS, Lee JM, Lee HY, Han BS, Son WC, Seok JH, Lee JK, Jeong J, Kang JS, Kang JK. Subchronic oral toxicity of evodia fruit powder in rats. *J Ethnopharmacol*. 2014; 151:1072-1078.
 18. Ko HC, Wang YH, Liou KT, Chen CM, Chen CH, Wang WY, Chang S, Hou YC, Chen KT, Chen CF, Shen YC. Anti-inflammatory effects and mechanisms of the ethanol extract of *Evodia rutaecarpa* and its bioactive components on neutrophils and microglial cells. *Eur J Pharmacol*. 2007; 555:211-217.
 19. Tan MX, Liu YC, Luo XJ, Li DQ. Studies on the antioxidant activities of total alkaloids from the fruits of *Evodia rutaecarpa* (Juss.) Benth. *Adv Mater Res*. 2012; 396-398:52-55.
 20. Lin L, Ren L, Wen L, Wang Y, Qi J. Effect of evodiamine on the proliferation and apoptosis of A549 human lung cancer cells. *Mol Med Rep*. 2016; 14:2832-2838.
 21. Chen TC, Chien CC, Wu MS, Chen YC. Evodiamine from *Evodia rutaecarpa* induces apoptosis via activation of JNK and PERK in human ovarian cancer cells. *Phytomedicine*. 2016; 23:68-78.
 22. Li YL, Pan YN, Wu WJ, Mao SY, Sun J, Zhao YM, Dong JY, Zhang DY, Pan JP, Zhang C, Lin NM. Evodiamine induces apoptosis and enhances apoptotic effects of erlotinib in wild-type EGFR NSCLC cells via S6K1-mediated Mcl-1 inhibition. *Med Oncol*. 2016; 33:16.
 23. Huang J, Chen ZH, Ren CM, Wang DX, Yuan SX, Wu QX, Chen QZ, Zeng YH, Shao Y, Li Y, Wu K, Yu Y, Sun WJ, He BC. Antiproliferation effect of evodiamine in human colon cancer cells is associated with IGF-1/HIF-1 α downregulation. *Oncol Rep*. 2015; 34:3203-3211.
 24. Sui H, Zhou LH, Zhang YL, Huang JP, Liu X, Ji Q, Fu XL, Wen HT, Chen ZS, Deng WL, Zhu HR, Li Q. Evodiamine suppresses ABCG2 mediated drug resistance by inhibiting p50/p65 NF- κ B pathway in colorectal cancer. *J Cell Biochem*. 2016; 117:1471-1481.
 25. Liu AJ, Wang SH, Chen KC, Kuei HP, Shih YL, Hou SY, Chiu WT, Hsiao SH, Shih CM. Evodiamine, a plant alkaloid, induces calcium/JNK-mediated autophagy and calcium/mitochondria-mediated apoptosis in human glioblastoma cells. *Chem Biol Interact*. 2013; 205:20-28.
 26. Zhao LC, Li J, Liao K, Luo N, Shi QQ, Feng ZQ, Chen DL. Evodiamine induces apoptosis and inhibits migration of HCT-116 human colorectal cancer cells. *Int J Mol Sci*. 2015; 16:27411-27421.
 27. You MK, Kim MS, Jeong KS, Kim E, Kim YJ, Kim HA. Loquat (*Eriobotrya japonica*) leaf extract inhibits the growth of MDA-MB-231 tumors in nude mouse xenografts and invasion of MDA-MB-231 cells. *Nutr Res Pract*. 2016; 10:139-147.
 28. Eom DW, Lee JH, Kim YJ, Hwang GS, Kim SN, Kwak JH, Cheon GJ, Kim KH, Jang HJ, Ham J, Kang KS, Yamabe N. Synergistic effect of curcumin on epigallocatechin gallate-induced anticancer action in PC3 prostate cancer cells. *BMB Rep*. 2015; 48:461-466.
 29. Li LY, Luo X, Wang X. Endonuclease G is an apoptotic DNase when released from mitochondria. *Nature*. 2001; 412:95-99.
 30. Cregan SP, Dawson VL, Slack RS. Role of AIF in caspase-dependent and caspase-independent cell death. *Oncogene*. 2004; 23:2785-2796.
 31. Kaufmann SH, Desnoyers S, Ottaviano Y, Davidson NE, Poirier GG. Specific proteolytic cleavage of poly(ADP-ribose) polymerase: An early marker of chemotherapy-induced apoptosis. *Cancer Res*. 1993; 53:3976-3985.
 32. Warburg O. On the origin of cancer cells. *Science*. 1956; 123:309-14.
 33. Oronsky BT, Oronsky N, Fanger GR, Parker CW, Caroen SZ, Lybeck M, Scicinski JJ. Follow the ATP: Tumor energy production: A perspective. *Anticancer Agents Med Chem*. 2014; 14:1187-98.
 34. Zorov DB, Juhaszova M, Sollott SJ. Mitochondrial ROS-

- induced ROS release: An update and review. *Biochim Biophys Acta*. 2006; 1757:509-517.
35. Brenner D, Mak TW. Mitochondrial cell death effectors. *Curr Opin Cell Biol*. 2009; 21:871-877.
 36. Jimbo A, Fujita E, Kouroku Y, Ohnishi J, Inohara N, Kuida K, Sakamaki K, Yonehara S, Momoi T. ER stress induces caspase-8 activation, stimulating cytochrome c release and caspase-9 activation. *Exp Cell Res*. 2003; 283:156-166.
 37. Hawley SA, Pan DA, Mustard KJ, Ross L, Bain J, Edelman AM, Frenguelli BG, Hardie DG. Calmodulin-dependent protein kinase kinase-beta is an alternative upstream kinase for AMP-activated protein kinase. *Cell Metab*. 2005; 2:9-19.
 38. Pelicano H, Carney D, Huang P. ROS stress in cancer cells and therapeutic implications. *Drug Resistance Updates*. 2004; 7:97-110.
 39. Hwang JT, Lee M, Jung SN, Lee HJ, Kang I, Kim SS, Ha J. AMP-activated protein kinase activity is required for vanadate-induced hypoxia-inducible factor 1alpha expression in DU145 cells. *Carcinogenesis*. 2004; 25:2497-2507.
 40. Sid B, Verrax J, Calderon PB. Role of AMPK activation in oxidative cell damage: Implications for alcohol-induced liver disease. *Biochem Pharmacol*. 2013; 86:200-209.
 41. Papandreou I, Lim AL, Laderoute K, Denko NC. Hypoxia signals autophagy in tumor cells *via* AMPK activity, independent of HIF-1, BNIP3, and BNIP3L. *Cell Death Differ*. 2008; 15:1572-1581.
 42. Xu ZX, Liang J, Haridas V, Gaikwad A, Connolly FP, Mills GB, Gutterman JU. A plant triterpenoid, avicin D, induces autophagy by activation of AMP-activated protein kinase. *Cell Death Differ*. 2007; 14:1948-1957.
 43. Feng Z, Hu W, de Stanchina E, Teresky AK, Jin S, Lowe S, Levine AJ. The regulation of AMPK beta1, TSC2, and PTEN expression by p53: Stress, cell and tissue specificity, and the role of these gene products in modulating the IGF-1-AKT-mTOR pathways. *Cancer Res*. 2007; 67:3043-3053.
 44. Hardie DG. AMP-activated protein kinase as a drug target. *Annu Rev Pharmacol Toxicol*. 2007; 47:185-210.
 45. Buzzai M, Jones RG, Amaravadi RK, Lum JJ, DeBerardinis RJ, Zhao F, Viollet B, Thompson CB. Systemic treatment with the antidiabetic drug metformin selectively impairs p53-deficient tumor cell growth. *Cancer Res*. 2007; 67:6745-6752.
 46. Sui X, Xu Y, Yang J, Fang Y, Lou H, Han W, Zhang M, Chen W, Wang K, Li D, Jin W, Lou F, Zheng Y, Hu H, Gong L, Zhou X, Pan Q, Pan H, Wang X, He C. Use of metformin alone is not associated with survival outcomes of colorectal cancer cell but AMPK activator AICAR sensitizes anticancer effect of 5-fluorouracil through AMPK activation. *PLoS ONE*. 2014; 9:e97781.
 47. Zakikhani M, Dowling R, Fantus IG, Sonenberg N, Pollak M. Metformin is an AMP kinase-dependent growth inhibitor for breast cancer cells. *Cancer Res*. 2006; 66:10269-10273.
 48. Chiang PC, Lin SC, Pan SL, Kuo CH, Tsai IL, Kuo MT, Wen WC, Chen P, Guh JH. Antroquinonol displays anticancer potential against human hepatocellular carcinoma cells: A crucial role of AMPK and mTOR pathways. *Biochem Pharmacol*. 2010; 79:162-171.
 49. Groenendijk FH, Mellema WW, van der Burg E, Schut E, Hauptmann M, Horlings HM, Willems SM, van der Heuvel MM, Jonkers J, Smit EF, Bernards R. Sorafenib synergizes with metformin in NSCLC through AMPK pathway activation. *Int J Cancer*. 2015; 136:1434-1444.
- (Received September 7, 2016; Revised November 2, 2016; Accepted November 5, 2016)

The fractal based analysis of human face and DNA variations during aging

Hamidreza Namazi^{1,*}, Amin Akrami², Jamal Hussaini³, Osmar N. Silva⁴, Albert Wong⁵, Vladimir V. Kulish¹

¹ School of Mechanical and Aerospace Engineering, Nanyang Technological University, Singapore;

² Faculty of Mechanical Engineering, University of Tehran, Tehran, IRAN;

³ Faculty of Medicine, Universiti Teknologi MARA, Selangor, Malaysia;

⁴ S-Inova Biotech, Programa de Pós-Graduação em Biotecnologia, Universidade Católica Dom Bosco, Campo Grande, MS, Brazil;

⁵ Department of Radiotherapy, Oncology and Palliative care, Sarawak General Hospital, Sarawak, Malaysia.

Summary

Human DNA is the main unit that shapes human characteristics and features such as behavior. Thus, it is expected that changes in DNA (DNA mutation) influence human characteristics and features. Face is one of the human features which is unique and also dependent on his gen. In this paper, for the first time we analyze the variations of human DNA and face simultaneously. We do this job by analyzing the fractal dimension of DNA walk and face during human aging. The results of this study show the human DNA and face get more complex by aging. These complexities are mapped on fractal exponents of DNA walk and human face. The method discussed in this paper can be further developed in order to investigate the direct influence of DNA mutation on the face variations during aging, and accordingly making a model between human face fractality and the complexity of DNA walk.

Keywords: DNA mutation, face, complexity, fractal dimension, DNA walk.

1. Introduction

DNA is a molecule that carries most of the genetic instructions used in the development, functioning and reproduction of all known living organisms and many viruses. Eye color (1-2), skin tone (3-4) and face shape (5) are determined by our genes.

One of the areas of research that has aroused scientists' interest is to study the relation between human DNA and face. Liu *et al.* (6) conducted a genome-wide association study for facial shape phenotypes in multiple discovery and replication cohorts, considering almost ten thousand individuals of European descent from several countries. They identified five independent genetic loci associated with different facial phenotypes,

suggesting the involvement of five candidate genes (*PRDM16*, *PAX3*, *TP63*, *C5orf50*, and *COL17A1*) in the determination of the human face. In another research using bootstrapped response-based imputation modeling (BRIM), Claes *et al.* (7) uncovered the relationships between facial variation and sex, genomic ancestry, and a subset of craniofacial candidate genes. Results of their analysis on significant effect of a set of 20 genes on facial features supported their approach as a mean to identify genes affecting normal-range facial features and for approximating the appearance of a face from genetic markers. They also developed a software that sketch human face from his DNA. See also (8-9). By understanding the relation between human DNA and face, current attempts are going on prediction of human face using his DNA.

A mutation is a change that occurs in our DNA sequence. Different factors can cause DNA mutation that in general can be categorized in two parts. First, DNA fails to copy accurately. Secondly, external influences can also cause mutation. For instance, mutations can be caused by smoking or exposure to specific chemicals or radiation. These agents cause the

Released online in J-STAGE as advance publication October 29, 2016.

*Address correspondence to:

Dr. Hamidreza Namazi, School of Mechanical and Aerospace Engineering, Nanyang Technological University, 50 Nanyang Avenue, Singapore.

E-mail: hnamazi@ntu.edu.sg

DNA to break down. This is not necessarily unnatural, even in the most isolated and pristine environments, DNA breaks down. Nevertheless, when the cell repairs the DNA, it might not do a perfect job of the repair. Thus, the cell would end up with DNA slightly different than the original DNA and hence, a mutation occurs. In general, there are many different ways that DNA can be changed, resulting in different types of mutation (substitution, insertion, deletion, frameshift).

Since all cells in our body contain DNA, there are lots of places for mutation to occur. Mutation can have widely varying individual effects. In some cases, mutation proves beneficial to an organism by making it better able to adapt to the environmental factors. In other situations, mutations are harmful to an organism and for instance cause diseases such as cancer. In overall, human DNA is changing during his life due to mutations.

As was mentioned before, human DNA affects his face shape. Besides all efforts done on analysis of the variations of DNA and human face, no one has analyzed the DNA mutation and variations of human face simultaneously as human gets older. For this purpose, in this research we use fractal theory in order to analyze the variations of human DNA and face. Fractal theory has been used widely in biology and medicine for various cases such as eye movement (10), EEG signal (11-14), bone structure (15), respiration signal (16), human stride time series (17). A fractal dimension is an index for characterizing fractal patterns or sets by quantifying their complexity as a ratio of the change in detail to the change in scale.

Employing fractal dimension for analysis of human DNA and face was limited based on literatures. In case of fractal analysis of human face, most of works have focused on human face recognition using fractal theory (18-20). In an extensive work on analysis of fractal dimension of face according to the age, Yarlagadda *et al.* developed a method that classified facial images into four categories *i.e.* child image [0-15], young adult image [15-30], middle-aged adult image [31-50], and senior adult image (> 50) based on correlation fractal dimension value of a facial edge image (21).

In case of fractal analysis and modeling of DNA walk, almost all reported works in literatures focused on proving the multi fractal nature of DNA walk (22-26). In a different work on employing fractal theory for analysis of DNA walk, we analyzed the complexity of DNA walk in case of healthy subjects and subjects with skin cancer using fractal theory. We found out that DNA walk in case of patients shows higher fractal dimension than for normal DNA sequences (27). In another work, considering the diffusion of drugs in cancer cells and fractality of DNA walks, we developed a model which analyzed the effect of chemotherapy on cancer cells using Fractional Diffusion Equation (FDE) (28).

In this research for the first time we simultaneously analyze the variations of human DNA and face during

aging. In other words, we study the complexity of human DNA walk and face by computing the fractal dimension. We believe that we should see the simultaneous variations of human DNA and face during aging.

2. Materials and Methods

The goal of this study is to investigate the variations of human DNA and face during aging. In order to map the DNA mutation, we used DNA walk as the sequencing method. DNA walk as a fractal random walk shows the variations of purine-pyrimidine displacement along nucleotide distance. In (27) we showed that variations of DNA affect its DNA walk's fractal dimension. Then, in order to study the DNA walk and human face, we considered the complexity phenomenon and used fractal dimension.

Fractals can be defined as geometric objects whose scaling exponent (dimension) satisfies the Szpilrajn inequality:

$$\aleph \geq D_T \quad (1)$$

Where \aleph is the scaling exponent (dimension) of the object and D_T is its topological dimension, *i.e.*, Euclidean dimension of units from which the fractal object is built.

The fractal exponent is based on the entropy concept for a probability distribution. In case of a DNA walk with ξ_{max} and ξ_{min} , we can divide the total range into N bin, where each bin has the size of $\delta\xi$:

$$N = \frac{\xi_{max} - \xi_{min}}{\delta\xi} \quad (2)$$

So, the probability of a value to fall into the i 'th bin:

$$w_i = \lim_{N \rightarrow \infty} \frac{N_i}{N} \quad (3)$$

The fractal dimensions for a DNA walk are defined as:

$$\aleph_q = \lim_{\delta\xi \rightarrow 0} \frac{1}{q-1} \frac{\log \sum_{i=1}^N w_i^q}{\log \delta\xi} \quad (4)$$

where $-\infty < q < +\infty$.

We extracted the DNA sequence of gens in case of different subjects using a popular method that generates a planar trajectory of DNA sequences (DNA walk). Then, we computed the fractal exponent for the DNA walk. In another step, we computed the fractal dimension of subject's face. It is noteworthy in order to analyze the influence of aging we analyzed the complexity of DNA walk and human face in three and five age periods respectively, for each subject. So, we will be able to analyze the variations of DNA and face during aging.

2.1. Data collection

We did the data collection on 200 subjects (100 males

and 100 females), 30-31 years old. All subjects were healthy and non-smoker without any record of serious biological or psychological diseases, also never faced any radiation exposure such as radiology. These steps are considered to ensure no unwanted stimulus affects/damages human DNA. Also, subjects did not have any scar on their face and never did any operation on their face. As the environmental changes cause DNA mutation, we chose the subjects that grew in the same city during their life. Another important factor in selection of subjects was that they did not experience any emotional/psychological impact in their life which may affect their DNA.

At first, each subject was interviewed by a physician to describe the nature of study to him/her. Written informed consent was obtained from all subjects after the nature of the study was fully explained. All procedures (experiments, *etc.*) were approved by the Internal Review Board of the university and the approval for experimentation involving subjects was issued by the university. The methods used in this research were carried out in accordance with the approved guidelines. It is noteworthy that the identity of all subjects remains confidential.

As was mentioned before, we needed the data on the subjects' DNA and photo in different age periods. The main difficulty was the DNA of subjects in the age below one year old and the age of 14-15 years old. For this purpose, we found subjects that did normal DNA test in the age of 14-15 years old and the medical center/hospital stored their DNA sequence. We also found the hospital they born, and collected their DNA sequence from there by subjects' permission.

The collection of DNA sequence from subjects in their current age (30-31 years old) was done in this research. For this purpose, the subject's blood plasma was collected. We used 2 mL of the plasma. We prepared Proteinase K with two wash buffers (WBI) in DNA sample preparation kit. Then, we mixed the plasma with 260 μ L Proteinase K and 2.1 mL DNA PBB (binding buffer), and incubated it at room temperature for 25 min. After that, we mixed 500 μ L isopropanol with the lysate and then transferred it into the High Pure Extender Assembly. Then, these assemblies were centrifuged at 4,000 \times g for 1min. The DNA was eluted in 100 μ L DNA EB (elution buffer). The extraction yielded high quality DNA suitable for further analysis. Totally we had three DNA sequences in three age periods from each subject for further analysis.

In order to analyze the influence of aging on human face more effectively, we did the data collection from five age groups. As was mentioned before, due to the difficulty of DNA collection, the DNA data was only available in three age groups for all subjects. Subjects provided us with five photos. First to fifth photos belong to the age below 1 year old, 7-8 years old, 14-15 years old, 22-23 years old, and 30-31 years old respectively.

The photos were taken in front of a plain white background while full face view directly the camera with a neutral facial expression and both eyes open. Subjects did not wear glasses in photos and male subjects had shaved face. It should be noted that for further analysis, we re-sized the photos to have a same size.

2.2. Data analysis

In order to do the analysis, we wrote two sets of code in MATLAB. One set of code which used for the analysis of DNA walk, first generated a planar trajectory of DNA sequences (DNA walk) based on purine-pyrimidine binary rule (29), and then computed its average fractal dimension value. The second set of codes computed the fractal dimension for the subjects' photos. Please note that in this part, only human face without other parts of photo such as background and subject's shoulder was processed. It is noteworthy that computation of fractal dimension was based on box counting method which is widely used by researchers (30-31). As fractal dimension usually is considered for time series, and DNA walk is variations of purine-pyrimidine displacement along nucleotide distance, here we used the methodology we discussed in (29) in order to consider the box counting method in case of DNA walk.

2.3. Statistical analysis

Mean values for the dependent variables (fractal exponents of DNA walk and face) were compared across different age periods with a one-way fixed-effect ANOVA. Mauchly's test ($\alpha = 0.05$) was conducted in order to test for sphericity. Trend analysis was conducted based on the age increment. For a repeated measures design, we used Omega squared (ω^2) as an unbiased measure of effect size suitable for small samples; in order to do pairwise comparisons effect size, r , was used. All statistical analyses were performed using SPSS software.

3. Results

In this section we present the results obtained from fractal analysis of subjects' DNA and face. Mauchly's test indicated that the assumption of sphericity had not been violated for the outcome variables (fractal dimension in case of DNA walk and face). Figure 1 shows the variations of fractal dimension for DNA walk across three age periods. The results indicate the mean of all data governed from subjects in each age period.

Considering $F_{crit}(2,597) = 3.01$ at $\alpha = 0.05$, the result of statistical analysis [$F(2,597) = 418, p = 0.001$] indicates that there was a significant influence of aging on the fractal exponent of DNA walk, with an effect size $\omega^2 = 0.53$. In general, aging increase the fractal dimension of DNA walk. The effect size calculations between different age periods suggest that the third age

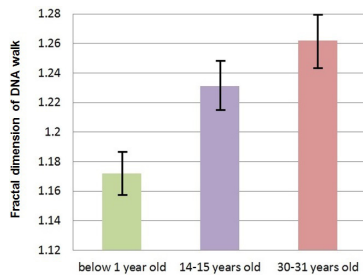


Figure 1. Fractal Analysis of the DNA walk across three age periods, for all subjects. Error bars are standard deviations.

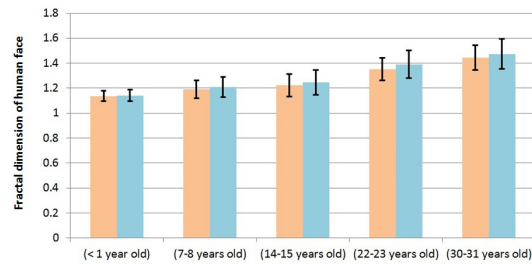


Figure 2. Fractal analysis of human face across five age periods, for all subjects. Error bars are standard deviations.

Table 1. Effect sizes for pairwise comparisons in case of fractal dimension of DNA walk

Condition	Effect size (<i>r</i>)
Below 1 year old vs. 14-15 years old	0.67
Below 1 year old vs. 30-31 years old	0.79
14-15 years old vs. 30-31 years old	0.39

period (30-31 years old) led to the greatest change in the fractal exponent of DNA walk observed across all comparisons (Table 1). As fractal dimension indicates the complexity of the process, the results indicate that human DNA gets more complex with aging.

Figure 2 shows the variations of fractal dimension for human face across five age periods. The results indicate the mean of all data governed from subjects in each age period. As it can be seen in this figure, male and female subjects were separated in this study for better understanding of the age influence on their face.

Considering $F_{crit}(4,995) = 2.38$ at $\alpha = 0.05$, the result of statistical analysis [$F(4,995) = 455.14, p = 0.001$] indicates that there was a significant influence of aging on the fractal dimension of human face, with an effect size $\omega^2 = 0.66$. In general, aging increase the fractal dimension of human face. Trend analysis showed the significant linear trend ($p = 0.001$) between different age groups. This linear trend indicates that the increment of the subjects' age from the first to the fifth group is mirrored on the increment of fractal exponent of human face from first to the fifth group. The effect size calculations between different age periods suggest that the fifth age period (30-31 years old) led to the greatest change in the fractal exponent of human face observed across all comparisons (Table 2). As fractal dimension indicates the complexity of process, the results indicate that human face gets more complex with aging.

Figure 2 also shows that aging has greater influence on fractal dimension of the female face than the male face. In other words, the females face gets more complex than males face, as they get older. It is noteworthy that the difference between fractal structures of males and females was not significant.

In summary, by increasing the age more mutations happen in DNA as the result of different kinds of stimulations. These mutations increase the complexity of the DNA. This increase is mapped on increasing the

Table 2. Effect sizes for pairwise comparisons in case of fractal dimension of human face

Condition	Effect size (<i>r</i>)
Below 1 year old vs. 7-8 years old	0.46
Below 1 year old vs. 14-15 years old	0.54
Below 1 year old vs. 22-23 years old	0.84
Below 1 year old vs. 30-31 years old	0.89
7-8 years old vs. 14-15 years old	0.18
7-8 years old vs. 22-23 years old	0.70
7-8 years old vs. 30-31 years old	0.82
14-15 years old vs. 22-23 years old	0.58
14-15 years old vs. 30-31 years old	0.75
22-23 years old vs. 30-31 years old	0.42

fractal exponent of the DNA walk. On the other hand, human face also gets more complex during aging. This complexity increment was concluded from studying the fractal structure of human face. We saw that human face gets more fractal as he/she gets older.

4. Discussion

In this paper we studied the variations of human DNA and face during aging by analyzing their fractal dimension. Based on the results we found out that as more mutations happen in human DNA its complexity increases. Also, our investigation showed the similar results in case of human face during aging. Based on the results, fractal dimension of human face increases as his/her age increases, which means the face gets more complex. Based on the work done by Kaur *et al.* (32), this face variation can be linked to facial soft tissue changes with aging. In comparison between male and female subjects, the results showed that women's face gets more affected by aging than men's face. This result agrees with the observed phenomenon in other research which states a woman's skin ages faster than a man's skin (33).

This analysis can be further applied in order to study the variations of DNA and face in case of subjects from different countries with different living conditions. If so, we will be able to concurrently analyze the influence of environmental changes and social living conditions on variations of human DNA (mutation) and face. In this case, we can discuss why the face of people in some countries looks younger.

We can also use this method for analysis of human face and DNA during aging in case of patients suffering from diseases which change their DNA and/or face. Also, the method discussed in this paper can be further developed in order to directly investigate the influence of DNA mutation on the face variations during aging. In the advanced level, by making a model between the DNA complexity and face complexity, scientists can work on changing the fractal pattern of human face by re-modeling of their DNA using stimulation. In this way we can benefit from different fractional models (14).

References

- Mengel J, Wong TH, Morling N, Rees JL, Jackson JJ. Genetic determinants of hair and eye colours in the Scottish and Danish populations. *BMC Genetics*. 2009; 10:1-13.
- Sturm RA, Duffy DL, Zhao ZZ, Leite FP, Stark MS, Hayward NK, Martin NG, Montgomery GW. A single SNP in an evolutionary conserved region within intron 86 of the *HERC2* gene determines human blue-brown eye color. *Am J Hum Genet*. 2008; 82:424-431.
- Visser M, Palstra RJ, Kayser M. Human skin color is influenced by an intergenic DNA polymorphism regulating transcription of the nearby *BNC2* pigmentation gene. *Hum Mol Genet*. 2014; 23:5750-5762.
- Parra EJ, Kittles RA, Shriver MD. Implications of correlations between skin color and genetic ancestry for biomedical research. *Nat Genet*. 2004; 36:S54-60.
- Goodman-Delahunty J, Taitb D. DNA and the Changing Face of Justice. *Aust J Forensic Sci*. 2006; 38:97-106.
- Liu F, van der Lijn F, Schurmann C, *et al*. A genome-wide association study identifies five loci influencing facial morphology in europeans. *PLoS Genet*. 2012; 8:1-13.
- Claes P, Liberton DK, Daniels K, *et al*. Modeling 3D facial shape from DNA. *PLoS Genet*. 2014; 10:1-14.
- Sheehan MJ, Nachman MW. Morphological and population genomic evidence that human faces have evolved to signal individual identity. *Nat Commun*. 2014; 5:1-10.
- Boehringer S, van der Lijn F, Liu F, *et al*. Genetic determination of human facial morphology: Links between cleft-lips and normal variation. *Eur J Hum Genet*. 2011; 19:1192-1197.
- Namazi H, Kulish VV, Akrami A. The analysis of the influence of fractal structure of stimuli on fractal dynamics in fixational eye movements and EEG signal. *Sci Rep*. 2016; 6:1-7.
- Namazi H, Kulish VV, Hussaini J, Hussaini J, Delaviz A, Delaviz F, Habibi S, Ramezanpoor S. A signal processing based analysis and prediction of seizure onset in patients with epilepsy. *Oncotarget*. 2016; 7:342-350.
- Namazi H, Khosrowabadi R, Hussaini J, Habibi S, Akhavan A, Kulish VV. Analysis of the influence of memory content of auditory stimuli on the memory content of EEG signal. *Oncotarget*. 2016; 7:56120-56128.
- Namazi H, Akrami A, Nazeri S, Kulish VV. Analysis of the influence of complexity and entropy of odorant on fractal dynamics and entropy of EEG signal. *BioMed Res Int*. 2016; 2016:1-5.
- Namazi H, Kulish VV. Fractional Diffusion Based Modelling and Prediction of Human Brain Response to External Stimuli. *Comput Math Methods Med*. 2015; 2015:1-11.
- Kyung-Hoe H, Jee-Seon B, Won-Jin Y, Min-Suk H, Sam-Sun L, Soon-Chul C, Sun-Bok L, Seung-Pyo L. Fractal analysis of mandibular trabecular bone: Optimal tile sizes for the tile counting method. *Imaging Sci Dent*. 2011; 41:71-78.
- Namazi H, Akrami A, Kulish VV. The Analysis of the Influence of Odorant's Complexity on Fractal Dynamics of Human Respiration. *Sci Rep*. 2016; 6:1-8.
- Namazi H, Kulish VV. Mathematical-based modeling and prediction of the effect of external stimuli on human gait. *Int J Numer Method Biomed Eng*. 2016; 32:1-10.
- Zhang Z, Zhuang P, Liu Y, Ding Q, Ye H. Face recognition based on wavelet-curvelet-fractal technique. *Chinese J Electron*. 2010; 27:206-211.
- Tang X, Qu C. Facial image recognition based on fractal image encoding. *Bell Labs Techn J*. 2010; 5:209-214.
- Karmakar D, Murthy CA. Face recognition using face-autocropping and facial feature points extraction. *Proceedings of the 2nd International Conference on Perception and Machine Intelligence*. 2015; 116-122.
- Yarlagadda A, Murthy JVR, Prasad MHMK. A novel method for human age group classification based on correlation fractal dimension of facial edges. *JKSU*. 2015; 27:468-476.
- Peng CK, Buldyrev SV, Goldberger AL, Havlin S, Sciortino F, Simons M, Stanley HE. Fractal landscape analysis of DNA walks. *Physica A*. 1992; 15:25-29.
- Abramson G, Cerdeira HA, Bruschi C. Fractal properties of DNA walks. *BioSystems*. 1999; 49:63-70.
- Oiwa NN, Glazier JA. Self-similar mitochondrial DNA. *Cell Biochem Biophys*. 2004; 41:41-62.
- Kinsner W, Zhang H. Multifractal analysis and feature extraction of DNA sequences. *Proceeding of 8th IEEE International Conference on Cognitive Informatics*. 2009; 29-37.
- Cattani C. Fractals and hidden symmetries in DNA. *Math probl eng*. 2010; 2010:1-31.
- Namazi H, Kulish VV, Delaviz F, Delaviz A. Diagnosis of skin cancer by correlation and complexity analyses of damaged DNA. *Oncotarget*. 2015; 6:42623-42631.
- Namazi H, Kulish VV, Wong A. Mathematical modelling and prediction of the effect of chemotherapy on cancer cells. *Sci Rep*. 2015; 5:1-8.
- Namazi H, Kiminezhadmalalaie M. Diagnosis of Lung Cancer by Fractal Analysis of Damaged DNA. *Comput Math Methods Med*. 2015; 2015:1-13.
- Popescu DP, Flueraru C, Mao Y, Chang S, Sowa MG. Signal attenuation and box-counting fractal analysis of optical coherence tomography images of arterial tissue. *Biomed Opt Express*. 2010; 1:268-277.
- Li J, Du Q, Sun C. An improved box-counting method for image fractal dimension estimation. *Pattern Recognition*. 2009; 42:2460-2469.
- Kaur M, Garg RK, Singla S. Analysis of facial soft tissue changes with aging and their effects on facial morphology: A forensic perspective. *Egyptian Journal of Forensic Sciences*. 2015; 5:46-56.
- Koehler MJ, König K, Elsner P, Bückle R, Kaatz M. In vivo assessment of human skin aging by multiphoton laser scanning tomography. *Opt Lett*. 2006; 31:2879-2881.

(Received October 5, 2016; Revised October 25, 2016; Accepted October 26, 2016)

MiR-15a-5p regulates viability and matrix degradation of human osteoarthritis chondrocytes *via* targeting VEGFA

Hongwei Chen^{1,*}, Yun Tian²

¹Department of Orthopedics, Yiwu Central Hospital Affiliated to Wenzhou Medical University, Yiwu, Zhejiang, China;

²Department of Orthopedic Trauma, Peking University Third Hospital, Beijing, China.

Summary

Previous studies demonstrated that miR-15a-5p was probably associated with human hepatocellular carcinoma, while the function of miR-15a-5p in OA (Osteoarthritis) still remains unknown. Here, we uncovered the potential role of miR-15a-5p on OA pathogenesis and confirmed its predicted target VEGFA (Vascular Endothelial Growth Factor A). Measured by RT-PCR, miR-15a-5p expression increased remarkably while VEGFA expression was significantly decreased in OA chondrocytes compared with normal conditions. According to Luciferase activity assay, miR-15a-5p directly targeted the 3'-UTR of VEGFA to inhibit its expression. Functional analysis including CCK-8 assay and flow cytometry revealed that overexpression of VEGFA or inhibition of miR-15a-5p promoted cell proliferation, suppressed cell apoptosis and reduced matrix degradation in OA chondrocytes. Moreover, rescue assays carried out with both expression of VEGFA and miR-15a-5p demonstrated that miR-15a-5p contributes to cell apoptosis and matrix degradation via inhibiting VEGFA. We further provided evidence that multiple proteins related to matrix synthesis were regulated by miR-15a-5p and VEGFA using Western blot and ELISA assays. Taken together, our findings elucidated an underlying mechanism by which miR-15a-5p regulates viability and matrix degradation of OA and indicated a new target for OA diagnosis and therapy.

Keywords: Osteoarthritis, miR-15a-5p, VEGFA

1. Introduction

Osteoarthritis (OA), the most prevalent disease of the articulating joints affecting millions of people worldwide is a chronic degenerative joint disease that is characterized by deterioration in the integrity of cartilage and is coupled with pain, tenderness, disability and inflammation without systemic effects (1). Although multiple factors are included in OA etiology, chondrocytes are crucial to tissue function and dominate the degenerative process of cartilage if the genes are expressed inappropriately when compared with adjacent tissues.

Small non-coding RNAs, namely MicroRNAs, are

highly conserved and prevalent in human cells. They are important in especially down-regulating target gene expression by binding to the 3' untranslated region of corresponding mRNAs. Meanwhile, they control significant basic biological functions, including cell cycle, cellular differentiation proliferation, apoptosis and so forth. Several recent studies demonstrated their importance in maintaining cartilage homeostasis and their effects on promoting the pathogenesis of OA. For instance, it was claimed in 2016 by Xu Cui and his group that by targeting PIK3R1, overexpression of miR-634 can suppress survival and matrix synthesis of human osteoarthritis chondrocytes (2). It is illustrated by Tadahiro Sakai and his colleagues that miR-125b plays a pivotal role in regulating expression of aggrecanase-1 (ADAMTS-4) in human osteoarthritic chondrocytes (3).

VEGFA (Vascular endothelial growth factor A) is important in regulating growth plate endochondral ossification. The VEGFA family consists of three different isoforms, including VEGFA120, VEGFA164, and VEGFA188, which possess different domains.

Released online in J-STAGE as advance publication December 3, 2016.

*Address correspondence to:

Dr. Hongwei Chen, Department of Orthopedics, Yiwu Central Hospital Affiliated to Wenzhou Medical University, No. 699 Jiangdong Road, Yiwu, Zhejiang, 322000, China.
E-mail: guoqian_wei@126.com

VEGFA120 and VEGFA 164 control heparin-binding domains, which permit interactions with heparin sulfate, whereas VEGFA120 only exists in mice. VEGFA seems to have a few functions during the process of bone formation. On the one hand, VEGFA is crucial in the early as well as late stages of cartilage angiogenesis, since VEGFA conditional knockout (CKO) mice illustrated both delayed blood vessel invasion and a delayed shift of terminal hypertrophic chondrocytes. On the other hand, VEGFA is important for chondrocyte survival, as the joint and epiphyseal regions of VEGFA CKO endochondral bones suffer substantially from abundant cell death (4). Given its important role in keeping the normal construction of the growth plate and endochondral ossification, VEGFA would be a potential target for remedies of Osteoarthritis (5).

MicroRNA signatures have been recently reported as useful diagnostic tools applied to the treatment of Osteoarthritis. Just take miR-15a-5p as an example. According to current research achievements, attention has been paid to the role of miR-15a-5p in human hepatocellular carcinoma, and the findings have shown that by targeting BDNF, miR-15a-5p suppresses cancer proliferation and division in human hepatocellular carcinoma (6). Little is known about the effect and function of miR-15a-5p in other diseases. For the first time, this article proposes to illustrate the impact of miR-15a-5p on cell proliferation and matrix synthesis of the OA chondrocyte and demonstrate the target-relationship between miR-15a-5p and VEGFA. It has been illuminated that by suppressing VEGFA, miR-15a-5p is able to promote degradation of matrix in OA chondrocytes. At the same time, miR-15a-5p also helps to inhibit the activities of the cell and finally leads to the apoptosis of OA chondrocytes.

2. Materials and Methods

2.1. Patients

Six normal cartilage tissues from patients without OA or RA (rheumatic arthritis) history and 15 cartilage tissues from OA patients were collected from Yiwu Central Hospital Affiliated to Wenzhou Medical University.

2.2. Immunohistochemistry (IHC)

Human cartilage tissues were fixed overnight with 4%

paraformaldehyde, decalcified, dehydrated, and then embedded in paraffin. Tissues were cut into sections 6 mm thick and deparaffinized with xylene, serially dehydrated in ethanol and washed in PBS. Endogenous peroxidases was blocked with 5% hydrogen peroxide in methanol and then digested with 100 mg/mL hyaluronidase. Nonspecific protein binding was blocked using a serum blocking solution. Sections were then incubated with primary antibodies against VEGFA (ab31745, Abcam, UK), Bcl-2 (ab59348, Abcam, UK), MMP13 (ab75606, Abcam, UK), TIMP1 (ab38978, Abcam, UK) and TIMP2 (ab180630, Abcam, UK) overnight at 4°C, followed by biotinylated secondary antibodies (ZSJB-BIO, China) joined with 3,3'-diaminobenzidine (Sigma-Aldrich, St. Louis, USA) for 15 min at room temperature. The immune stained sections were counterstained briefly with hematoxylin. Negative controls included the use of IgG isotype controls and secondary antibody only (omission of primary antibody) controls.

2.3. Cell culture

HEK293T cell lines were purchased from the Chinese Academy of Sciences (Shanghai, China). Human articular cartilage tissues were digested with 0.2% collagenase II in DMEM. Chondrocytes were cultured in DMEM with 10% FBS at 37, 5% CO₂ atmosphere.

2.4. Cell transfection

Lentivirus with human mature miR-15a-5p mimics (Lenti-miR-mimics), inhibitor (Lenti-miR-in) and negative control (Lenti-null), were obtained from SunBio (SunBio Medical Biotechnology, China). Recombinant eukaryotic expression vector pEGFP-VEGFA as well as its negative control (pEGFP-null) was constructed specifically.

2.5. Real-time Quantitative PCR (RT-PCR)

Total RNA was extracted with Trizol (Thermo Fisher Scientific, MA, USA). RNA extracts were reverse-transcribed into cRNA and then RT-PCR was performed (Related primers are listed in Table 1). The expression of VEGFA mRNA and miR-15a-5p was normalized with GAPDH mRNA and RNU6B respectively as endogenous control. Relative RNA levels were determined with the 2- $\Delta\Delta$ Ct method.

Table 1. Primer sequences

Items	Forward sequences	Reverse sequences
miR-15a-5p	5'-TAAGGCACGCGGTGAATGCC-3'	
VEGFA	5'-CGAGGGCCTGGAGTGTGT-3'	5'-GATCCGCATAATCTGCATGGT-3'
RNU6B	5'-ACGCAAATTCGTGAAGCGTT-3'	
GAPDH	5'-GGAAGGTGAAGGTCGGAGTCA-3'	5'-GTCATTGATGGCAACAATATCCAAT-3'

2.6. Luciferase reporter assay

MiRDB and TargetScan were employed to predict miR-15a-5p targets. The wild-type sequence of VEGFA-3'UTR containing miR-15a-5p binding sites was inserted into the pmiR-RB-Reporter vector (Ribobio, Guangzhou, China) and a mutant was used as control (named as pmiR-VEGFA-wt and pmiR-VEGFA-mut respectively). HEK293T cells were co-transfected with the pmiR-VEGFA-wt or pmiR-VEGFA-mut and Lenti-miR-mimics or Lenti-null using Lipofectamine 2000 (Invitrogen, CA, USA). Luciferase activity was measured 48 h after transfection.

2.7. Cell proliferation analysis

Cell vitality was evaluated with Cell Counting Kit-8 (CCK-8, Sigma-Aldrich, MO, USA) after cells were incubated for various periods of time (0 d, 3 d, 6 d, and 9 d). The OD values at 450 nm were measured with spectrophotometry.

2.8. Cell apoptosis assay

Forty eight hours after transfection, cells were collected and washed with PBS, and then re-suspended in binding buffer. Cell apoptosis was evaluated by flow cytometry with the Annexin V: FITC Apoptosis Detection Kit I (BD Biosciences, NJ, USA) according to the manufacturers' protocol.

2.9. Western blot analysis

Forty eight hours after transfection, cells were washed with cold PBS and lysed with the cell lysis buffer. Protein extracts were subjected to SDS-PAGE, transferred to PVDF membranes and blocked with 5% nonfat milk in TBST. The membranes were subsequently incubated with primary VEGFA (ab31745, Abcam, UK), Bcl-2 (ab59348, Abcam, UK), COL2A1 (ab21291, Abcam, UK), MMP13 (ab75606, Abcam, UK), β -actin (ab8227, Abcam, UK), and GAPDH (ab9483, Abcam, UK) antibodies overnight at 4°C.

Then, the secondary antibodies (ZSJB-BIO, China) were added and co-incubated with the membranes for 1 h. Chemiluminescent detection was performed using an ECL kit (Pierce Chemical, Rockford, IL, USA).

2.10. MMP13 ELISA assay

The MMP13 protein level in extracellular matrix was analyzed with the human MMP13 kit (Sciencell, CA, USA) according to the procedure supplied by the manufacturer. The OD values at 450 nm were measured with spectrophotometry.

2.11. Statistical analysis

The results were represented as means and differences between two groups were analyzed using the Student's *t*-test, otherwise by the One-Way ANOVA method. $p < 0.05$ indicates significant variation between groups.

3. Results

3.1. The expressions of miR-15a-5p, VEGFA and related cytokines in OA chondrocytes

According to the RT-PCR assay, Figure 1A showed that the expression level of miR-15a-5p in OA chondrocytes was significantly higher than that in normal chondrocytes ($*p < 0.05$). On the contrary, the expression of VEGFA mRNA was suppressed in OA chondrocytes (Figure 1B-C, $*p < 0.05$). Based on IHC results (Figure 1D), the numbers of cells that stained positively for VEGFA, Bcl-2, TIMP1 and TIMP2 respectively were significantly lower in OA chondrocytes compared with normal chondrocytes while the numbers of cells that are stained positively for MMP13 showed an opposite trend which is consistent because OA chondrocyte cells possessed a weak viability and a remarkable pathological apoptosis.

3.2. MiR-15a-5p directly targeted VEGFA

VEGFA 3'UTR contained the miR-15a-5p binding sites (Figure 2A). To make sure that miR-15a-5p actually

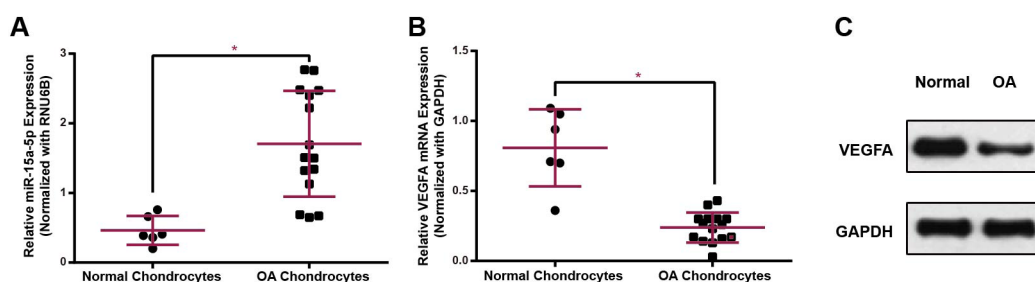


Figure 1. The expression of miR-15a-5p, VEGFA and related cytokines in OA chondrocytes were compared with normal chondrocytes. (A) MiR-15a-5p in normal and OA chondrocytes measured by RT-PCR. It was normalized by RNU6B. (B) VEGFA mRNA was detected with RT-PCR in normal and OA chondrocytes. It was normalized using GAPDH mRNA. (C) The VEGFA expression levels in normal and OA chondrocytes analyzed by Western blot with GAPDH as control. (D) Immunohistochemical activities of VEGFA, Bcl-2, MMP13, TIMP1 and TIMP2 in normal and OA chondrocytes. Scale bar = 50 μ m.

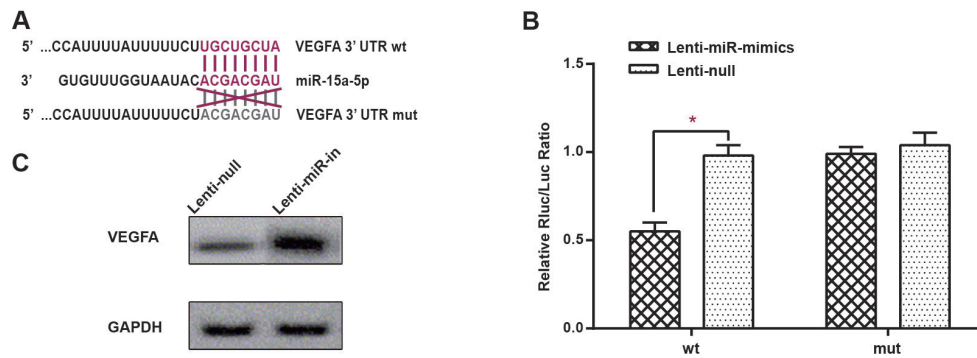


Figure 2. MiR-15a-5p targets VEGFA in human OA chondrocytes. (A) Schematic of the VEGFA 3'UTR containing the miR-15a-5p binding sites. **(B)** The results of Luciferase reporter assay. **(C)** VEGFA protein levels in OA chondrocytes evaluated by Western blot analysis with GAPDH as control.

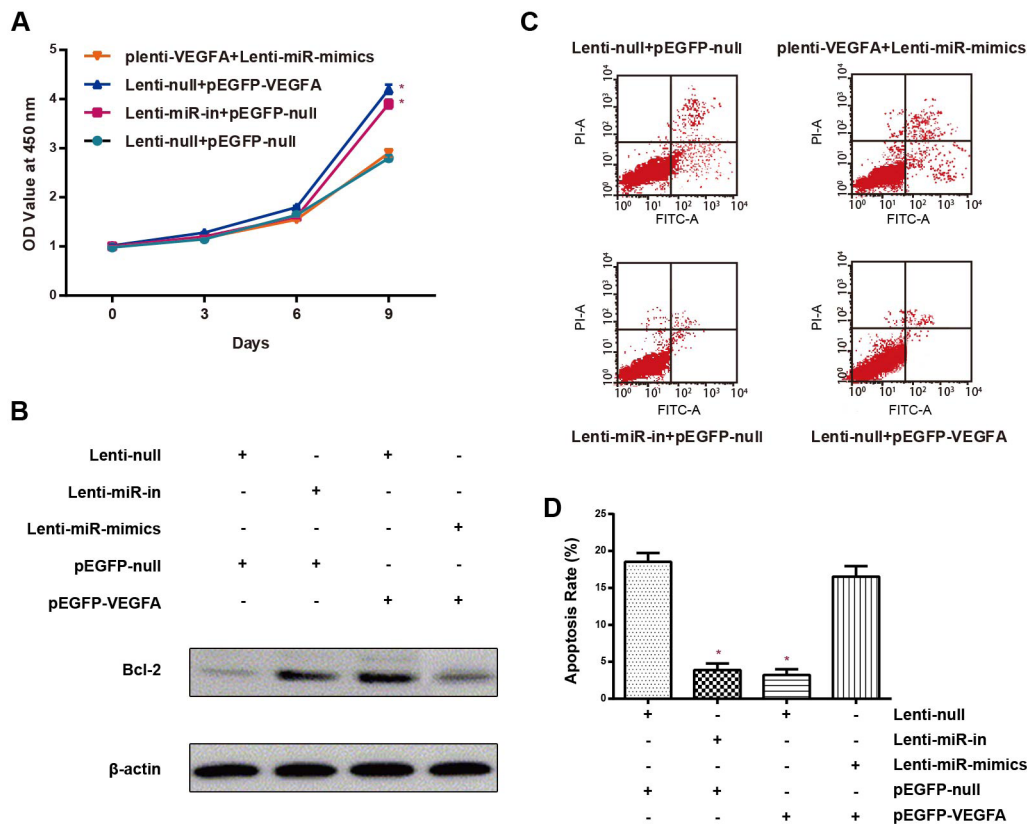


Figure 3. MiR-15a-5p suppressed OA chondrocytes vitality and anti-apoptosis. (A) The proliferation rate of cells measured by CCK8 assay. **(B)** The protein level of Bcl-2 was measured by Western blot with β -actin as control. **(C-D)** Apoptosis measured by flow cytometry.

targets VEGFA, dual-luciferase analysis was performed 48 h after HEK293 cells were transfected with pmir-VEGFA-wt or pmir-VEGFA-mut reporter vectors and Lenti-miR-mimics or Lenti-null, respectively. As presented in Figure 2B, cells co-transfected with miR-15a-5p and pmir-VEGFA-wt vector showed a significant decrease of luciferase activity in comparison with NC (negative control), showing that miR-15a-5p directly targeted VEGFA ($*p < 0.05$, versus NC). Furthermore, the protein levels of VEGFA were analyzed with Western blot analysis. Figure 2C displayed that miR-15a-5p inhibitor up-regulated VEGFA protein level. Consequently, miR-15a-5p

could directly bind the VEGFA mRNA 3'UTR region and regulate the VEGFA protein level, indicating that VEGFA could be one of miR-15a-5p targets.

3.3. MiR-15a-5p suppressed viability of OA chondrocytes by inhibiting expression of VEGFA

The effect of miR-15a-5p on chondrocyte viability was evaluated with CCK8 assays. The results suggested that miR-15a-5p inhibitor promoted cell viability of OA chondrocytes and overexpression of VEGFA exerted a similar effect (Figure 3A, $*p < 0.05$, versus NC). Moreover, the expression level of anti-apoptotic

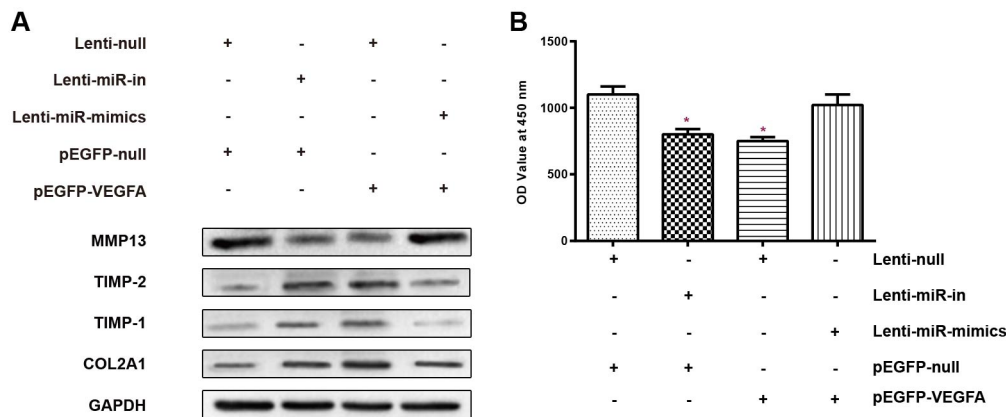


Figure 4. MiR-15a-5p promoted matrix degradation of OA chondrocytes. (A) The protein levels of MMP13, TIMP-2, TIMP-1 and COL2A1 were analyzed with Western blot (GAPDH as control). (B) The MMP13 protein level in extracellular matrix in OA chondrocytes was measured by ELISA.

protein Bcl-2 was analyzed by Western blot analysis to investigate the effect of miR-15a-5p on OA chondrocytes apoptosis. Figure 3B shows that compared with NC, Bcl-2 is overexpressed in OA chondrocytes transfected with miR-15a-5p inhibitor or pEGFP-VEGFA respectively while those transfected with both miR-15a-5p mimics and pEGFP-VEGFA appeared to have little difference. Meanwhile, the results of cell apoptosis assays by flow cytometry were consistent with the Western blot results (Figure 3C-D, $*p < 0.05$, versus NC). Both inhibition of miR-15a-5p and overexpression of VEGFA significantly reduced the apoptosis rate compared with NC. Overall, miR-15a-5p could suppress the viability of OA chondrocytes and induce cell apoptosis *via* targeting VEGFA.

3.4. MiR-15a-5p promoted matrix degradation of OA chondrocytes

The expression of matrix synthesis biomarkers COL2A1, MMP13, TIMP-1 and TIMP-2 in each group of cells were analyzed via Western blot analysis to look for the effect of miR-15a-5p on OA chondrocytes matrix synthesis (Figure 4A). The results indicated that both inhibition of miR-15a-5p and overexpression of VEGFA dramatically down-regulated MMP13 protein level, but on the contrary increased TIMP-1, TIMP-2 and COL2A1 expression, indicating suppression of matrix degradation. In addition, ELISA results also showed a decrease in MMP13 protein levels in the extracellular matrix of cells in the Lenti-miR-in group and pEGFP-null group (Figure 4B, $*p < 0.05$, versus NC). Together, we could draw a conclusion that miR-15a-5p promoted matrix degradation of OA chondrocytes by regulating VEGFA expression.

4. Discussion

OA is one of the most common joint diseases among senior citizens, which is characterized by degenerative

alteration of cartilage. Because the joint dysfunction interferes with daily living and work ability, OA is considered to be an enormous threat to human function (7). Recent studies demonstrated that abnormal expression of miRNAs played a crucial role during the development of OA, for example, Park *et al.* (2014) found that miR-127-5p could regulate MMP13 in human OA chondrocytes and might promote the progression of OA (8). Kang *et al.* (2016) demonstrated that miR-23a-3p was up-regulated in OA chondrocytes and could suppress ECM synthesis through targeting SMAD3, which accelerated the development of OA (9).

The aberrant expression of miR-15a has been reported in several types of human cancers. For example, abnormal overexpression of miR-15a-5p was reported to suppress cancer proliferation, induce cell cycle arrest in human HCC cells, and have a specific and negative regulating effect on BDNF (6). In addition, the protein levels of p27, GSK-3beta, Bax, procaspase3, and active caspase 3 were upregulated by the overexpression of miR-15a, which inhibited proliferation and induced apoptosis of CNE1 cells (10). There were other studies that investigated the role of miR-15a in OA. In our study, the results of RT-PCR indicated that miR-15a-5p was up-regulated in OA chondrocytes compared with normal chondrocytes.

VEGFA is a strong angiogenic protein with a selective mitogenic influence on vascular endothelial cells. It is an important cytokine in angiogenesis, and its circulating levels were associated with cell proliferation, migration and organization (11). As a pivotal element, VEGFA has been identified to act as an essential characteristic substance in many human cancers, for example, breast cancer, brain tumor, and cutaneous melanoma, to name just a few (12-14). On the other hand, VEGFA is a necessary factor for chondrocyte growth during skeletal development (4). Brew *et al.* (2010) found that VEGFA was downregulated in OA chondrocytes (15), which was consistent with the results of our study. The results of RT-PCR and Western blot

assays indicated that VEGFA was down-regulated in OA chondrocytes compared with normal chondrocytes.

The protein encoded by the Bcl-2 gene has been widely implicated in the prolongation of cell survival by blocking apoptosis and necrosis (16,17). Many observations confirmed that Bcl-2 in human articular chondrocyte prevents their apoptosis in osteoarthritis (18,19). A time-dependent relationship between p53, Bcl-2 and VEGF protein has been revealed in esophagus cancer cells (20). In this study, it was found that the association of VEGFA and Bcl-2 in osteoarthritis suggests a potential understanding of VEGFA's function on chondrocyte apoptosis.

Previous studies confirmed that MMP13 is a major enzyme targeting cartilage for degradation of type II, IV, IX collagen, proteoglycan, osteonectin and perlecan (21,22). Overexpression of MMP13 contributes to cartilage destruction among in both human OA patients and mice models (23,24). TIMP1 and TIMP2 are two members of Tissue inhibitors of metalloproteinases (TIMPs) and act as inhibitors of MMP13. A balance between MMPs and TIMPs is necessary for the physiological processes of OA (25). A relationship of VEGF and TIMP1 has been reported in the diagnosis of patients with breast cancer (26). To the best of our knowledge, it's a novel finding that overexpression of VEGFA promoted the expression of TIMP1 and TIMP2 and repressed the level of MMP13 which supported the idea that VEGFA fortified the viability of chondrocyte cells.

The results of RT-PCR and Western blots suggested that miR-15a-5p was up-regulated in the OA cells compared with adjacent normal cells, whereas VEGFA was down-regulated, which inspired us to think that there was probably a targeting relationship between miR-15a-5p and VEGFA. Previously, an analogous outcome has been confirmed in the study of Yang *et al.* (27). In our study, the targeting relation was further verified using luciferase reporter assays and Western blot assays. The results of the following experiments demonstrated that miR-15a-5p could significantly suppress the viability, promote apoptosis, suppress the synthesis of matrix and promote the degradation of matrix of the OA chondrocytes through targeting VEGFA, which was consistent with Nagata *et al.* (28) in miR-15a function.

Despite the fact that it is innovative to investigate the relationship between miR-15a-5p and VEGFA, as well as their roles in OA, there are still a few limitations and controversies. Whether there are other microRNAs that have the same function as miR-15a-5p of inhibiting VEGFA *via* a targeted relationship remains questionable, further investigation should be conducted. Also Li *et al.* (2012) found that miR-146a might promote OA pathogenesis by upregulating VEGF and by impairing the TGF-beta pathway through inhibiting Smad4 in chondrocytes (27), which are different views compared to our study of VEGF function. This needs

further research to explore the complicated mechanism. In addition, the possibility that miR-15a-5p targets other growth factors that are also essential for the formation of the matrix in OA chondrocytes can't be ruled out.

In a nutshell, on the basis of our newly-produced data, it has been revealed that an excess of miR-15a-5p can lead to the inhibition of VEGFA, resulting in OA progression and inhibiting apoptosis of OA chondrocytes. Therefore, miR-15a-5p may serve as a new target for OA therapy in the future to relieve the suffering of patients.

Acknowledgements

This work was supported by the Project of Zhejiang Province Science and Technology Hall (2013C33216), the Project of the Health Department of Zhejiang Province (2014KYB296) and Yiwu Programs for Science and Technology Development (2013-G3-02).

References

1. Pun YL, Moskowitz RW, Lie S, Sundstrom WR, Block SR, McEwen C, Williams HJ, Bleasel JF, Holderbaum D, Haqqi TM. Clinical correlations of osteoarthritis associated with a single-base mutation (arginine519 to cysteine) in type II procollagen gene. A newly defined pathogenesis. *Arthritis Rheum.* 1994; 37:264-269.
2. Cui X, Wang S, Cai H, Lin Y, Zheng X, Zhang B, Xia C. Overexpression of microRNA-634 suppresses survival and matrix synthesis of human osteoarthritis chondrocytes by targeting PIK3R1. *Sci Rep.* 2016; 6:23117.
3. Matsukawa T, Sakai T, Yonezawa T, Hiraiwa H, Hamada T, Nakashima M, Ono Y, Ishizuka S, Nakahara H, Lotz MK, Asahara H, Ishiguro N. MicroRNA-125b regulates the expression of aggrecanase-1 (ADAMTS-4) in human osteoarthritic chondrocytes. *Arthritis Res Ther.* 2013; 15:R28.
4. Zelzer E, Mamluk R, Ferrara N, Johnson RS, Schipani E, Olsen BR. VEGFA is necessary for chondrocyte survival during bone development. *Development.* 2004; 131:2161-2171.
5. Hamilton JL, Nagao M, Levine BR, Chen D, Olsen BR, Im HJ. Targeting VEGF and Its Receptors for the Treatment of Osteoarthritis and Associated Pain. *J Bone Miner Res.* 2016; 31:911-924.
6. Long J, Jiang C, Liu B, Fang S, Kuang M. MicroRNA-15a-5p suppresses cancer proliferation and division in human hepatocellular carcinoma by targeting BDNF. *Tumour Biol.* 2016; 37:5821-5828.
7. Roos EM, Arden NK. Strategies for the prevention of knee osteoarthritis. *Nat Rev Rheumatol.* 2016; 12:92-101.
8. Park SJ, Cheon EJ, Lee MH, Kim HA. MicroRNA-127-5p regulates matrix metalloproteinase 13 expression and interleukin-1beta-induced catabolic effects in human chondrocytes. *Arthritis Rheum.* 2013; 65:3141-3152.
9. Kang L, Yang C, Song Y, Liu W, Wang K, Li S, Zhang Y. MicroRNA-23a-3p promotes the development of osteoarthritis by directly targeting SMAD3 in chondrocytes. *Biochem Biophys Res Commun.* 2016; 478:467-473.
10. Zhu K, He Y, Xia C, Yan J, Hou J, Kong D, Yang Y, Zheng

- G. MicroRNA-15a Inhibits Proliferation and Induces Apoptosis in CNE1 Nasopharyngeal Carcinoma Cells. *Oncol Res.* 2016; 24:145-151.
11. Schlieve CR, Mojica SG, Holyoak KA, Hou X, Fowler KL, Grikscheit TC. Vascular Endothelial Growth Factor (VEGF) Bioavailability Regulates Angiogenesis and Intestinal Stem and Progenitor Cell Proliferation during Postnatal Small Intestinal Development. *PLoS One.* 2016; 11:e0151396.
 12. Luo M, Hou L, Li J, Shao S, Huang S, Meng D, Liu L, Feng L, Xia P, Qin T, Zhao X. VEGF/NRP-1 axis promotes progression of breast cancer *via* enhancement of epithelial-mesenchymal transition and activation of NF- κ B and beta-catenin. *Cancer Lett.* 2016; 373:1-11.
 13. Sanden E, Enriquez Perez J, Visse E, Kool M, Caren H, Siesjo P, Darabi A. Preoperative systemic levels of VEGFA, IL-7, IL-17A, and TNF-beta delineate two distinct groups of children with brain tumors. *Pediatr Blood Cancer.* 2016.
 14. Gacevic M, Jovic M, Zolotarevski L, Stanojevic I, Novakovic M, Miller K, Suljagic V, Mijuskovic Z, Vojvodic D. Association of vascular endothelial growth factor expression with pathohistological parameters of cutaneous melanoma. *Vojnosanit Pregl.* 2016; 73:449-457.
 15. Brew CJ, Clegg PD, Boot-Handford RP, Andrew JG, Hardingham T. Gene expression in human chondrocytes in late osteoarthritis is changed in both fibrillated and intact cartilage without evidence of generalised chondrocyte hypertrophy. *Ann Rheum Dis.* 2010; 69:234-240.
 16. Hockenbery DM, Oltvai ZN, Yin XM, Millman CL, Korsmeyer SJ. Bcl-2 functions in an antioxidant pathway to prevent apoptosis. *Cell.* 1993; 75:241-251.
 17. Kane DJ, Ord T, Anton R, Bredesen DE. Expression of bcl-2 inhibits necrotic neural cell death. *J Neurosci Res.* 1995; 40:269-275.
 18. Iannone F, De Bari C, Scioscia C, Patella V, Lapadula G. Increased Bcl-2/p53 ratio in human osteoarthritic cartilage: A possible role in regulation of chondrocyte metabolism. *Ann Rheum Dis.* 2005; 64:217-221.
 19. Wei R, Mahemuti D, Hu HH. [Effects of sand treatment in Uyghur medicine on caspase-3, Bcl-2, Bax, and the apoptotic expression in the cartilage of rabbit knee osteoarthritis model]. *Zhongguo Zhong Xi Yi Jie He Za Zhi.* 2012; 32:801-805.
 20. Wei W, Wang Y, Yu X, Ye L, Jiang Y, Cheng Y. Expression of *TP53*, *BCL-2*, and *VEGFA* Genes in Esophagus Carcinoma and its Biological Significance. *Med Sci Monit.* 2015; 21:3016-3022.
 21. Vincenti MP, Brinckerhoff CE. Transcriptional regulation of collagenase (*MMP-1*, *MMP-13*) genes in arthritis: Integration of complex signaling pathways for the recruitment of gene-specific transcription factors. *Arthritis Res.* 2002; 4:157-164.
 22. Shiomi T, Lemaitre V, D'Armiento J, Okada Y. Matrix metalloproteinases, a disintegrin and metalloproteinases, and a disintegrin and metalloproteinases with thrombospondin motifs in non-neoplastic diseases. *Pathol Int.* 2010; 60:477-496.
 23. Roach HI, Yamada N, Cheung KS, Tilley S, Clarke NM, Oreffo RO, Kokubun S, Bronner F. Association between the abnormal expression of matrix-degrading enzymes by human osteoarthritic chondrocytes and demethylation of specific CpG sites in the promoter regions. *Arthritis Rheum.* 2005; 52:3110-3124.
 24. Neuhold LA, Killar L, Zhao W, Sung ML, Warner L, Kulik J, Turner J, Wu W, Billingham C, Meijers T, Poole AR, Babij P, DeGennaro LJ. Postnatal expression in hyaline cartilage of constitutively active human collagenase-3 (*MMP-13*) induces osteoarthritis in mice. *J Clin Invest.* 2001; 107:35-44.
 25. Hayakawa T. Multiple functions of tissue inhibitors of metalloproteinases (TIMPs): A new aspect involving osteoclastic bone resorption. *J Bone Miner Metab.* 2002; 20:1-13.
 26. Sivchik VV, Grachova EV, Melnikov AS, Smirnov SN, Ivanov AY, Hirva P, Tunik SP, Koshevoy IO. Solid-State and Solution Metallophilic Aggregation of a Cationic [Pt(NCN)L](+) Cyclometalated Complex. *Inorg Chem.* 2016; 55:3351-3363.
 27. Yang RQ, Teng H, Xu XH, Liu SY, Wang YH, Guo FJ, Liu XJ. Microarray analysis of microRNA deregulation and angiogenesis-related proteins in endometriosis. *Genet Mol Res.* 2016; 15.
 28. Nagata Y, Nakasa T, Mochizuki Y, Ishikawa M, Miyaki S, Shibuya H, Yamasaki K, Adachi N, Asahara H, Ochi M. Induction of apoptosis in the synovium of mice with autoantibody-mediated arthritis by the intraarticular injection of double-stranded MicroRNA-15a. *Arthritis Rheum.* 2009; 60:2677-2683.

(Received October 12, 2016; Revised November 1, 2016; Accepted November 6, 2016)

TGP attenuates endoplasmic reticulum stress and regulates the expression of thioredoxin-interacting protein in the kidneys of diabetic rats

Yunxia Shao¹, Xiangming Qi¹, Xinxing Xu¹, Kun Wang¹, Yonggui Wu^{1,*}, Lingling Xia^{2,*}

¹ Department of Nephropathy, the First Affiliated Hospital of Anhui Medical University, Hefei, Anhui, China;

² Department of Infective Disease, the First Affiliated Hospital of Anhui Medical University, Hefei, Anhui, China.

Summary

Recent evidence suggests that the endoplasmic reticulum stress (ERS)-thioredoxin-interacting protein (TXNIP)-inflammation chain contributes to diabetic renal injury. The aim of the current study was to investigate whether total glucosides of peony (TGP) could inhibit ERS and attenuate up-regulation of TXNIP in the kidneys of rats with streptozotocin-induced diabetes. TGP was orally administered daily at a dose of 50, 100, or 200 mg/kg for 8 weeks. The expression of glucose-regulated protein 78 (GRP78), phospho-protein kinase RNA-like ER kinase (p-PERK), phospho-eukaryotic translation initiation factor 2 α (p-eIF2 α), C/EBP-homologous protein (CHOP), and TXNIP was assessed. Results indicated that TGP significantly decreased diabetes-induced albuminuria and it acted by down-regulating activation of the ERS-TXNIP-inflammation chain in the kidneys of diabetic rats. These findings indicate that renoprotection from TGP in diabetic rats possibly contributed to inhibition of ERS and decreased expression of TXNIP. These findings also offer a new perspective from which to study the molecular mechanisms of diabetic nephropathy and prevent its progression.

Keywords: Diabetic nephropathy, endoplasmic reticulum stress, thioredoxin-interacting protein, total glucosides of peony

1. Introduction

Diabetic nephropathy (DN) is currently prevalent around the world and accounts for nearly one-third of cases of end-stage renal disease. In clinical settings, treatments for DN usually consist of close monitoring of blood glucose and blood pressure and use of medications such as renin-angiotensin system (RAS) blockers. Nonetheless, DN worsens in many patients, increasing the need for dialysis

and eventually leading to organ failure (1,2).

Over the past few years, several studies have indicated that endoplasmic reticulum stress (ERS) plays a crucial role in the pathogenesis of diabetic vascular complications (3,4). An ERS response may be triggered by a stressful stimulus (e.g., hyperglycemia, oxidative stress, albuminuria, advanced glycation end products (AGEs), and activation of RAS (5-8)), that exhausts or disrupts normal protein folding by the endoplasmic reticulum, thus causing accumulation of misfolded and/or unfolded proteins. ERS may also activate the unfolded protein response (UPR) pathway that is initiated by glucose-regulated protein 78 (GRP78) and three endoplasmic reticulum transmembrane sensors - inositol requiring enzyme 1 α (IRE1 α), protein kinase RNA-like ER kinase (PERK), and activating transcription factor 6 (ATF6) (9). Therefore, the overexpression of IRE1 α , PERK, and ATF6 contribute to a modified endoplasmic reticulum or the continued presence of unfolded proteins, resulting in insufficient protein folding.

Inflammation plays a leading role in the pathogenesis

Released online in J-STAGE as advance publication December 24, 2016.

*Address correspondence to:

Dr. Yonggui Wu, Department of Nephropathy, the First Affiliated Hospital of Anhui Medical University, Hefei, Anhui 230022, China.

E-mail: wuyonggui@medmail.com.cn

Dr. Lingling Xia, Department of Infective Disease, the First Affiliated Hospital of Anhui Medical University, Hefei, Anhui 230022, China.

E-mail: wuyongguixialiang@163.com

of DN (10,11). A key molecule, thioredoxin-interacting protein (TXNIP, and also known as vitamin-D3 up-regulated protein-1 (VDUP1) or thioredoxin binding protein-2 (TBP-2)), has been found to link ERS to inflammation and cell death (12,13). ERS can induce TXNIP activation through the PERK and IRE1 pathways, it can provoke interleukin 1 β (IL-1 β) mRNA transcription, and it can mediate ERS-mediated β cell death (13). Microarray studies indicated that the expression of TXNIP mRNA was markedly elevated in human islet cells and renal tubular cells (14,15). More recently, studies have found that TXNIP can induce oxidative stress and increase extracellular matrix production, causing the development of DN (16). Thus, the prevention of TXNIP expression may inhibit the progression of DN (17). Accordingly, the ERS-TXNIP-inflammation chain may be a novel target for DN therapy.

Over the past few years, patients with DN have become increasingly interested in Chinese herbal therapies. The dried root of *Paeonia lactiflora* Pall. is often used in Chinese herbal remedies, where it is commonly referred to as white peony root (baishao in Chinese). Total glucosides of peony (TGP) are active compounds that can be extracted from the dried roots of *Paeonia lactiflora* Pall. Reversed-phase high-performance liquid chromatography (HPLC) has indicated that TGP contain eight principal components, namely paeoniflorin, oxypaeoniflorin, benzoylpaeoniflorin, benzoyloxypaeoniflorin, oxybenzoyl-paeoniflorin, albiflorin, paeoniflorigenone, and lactiflorin (Figure 1 (18)). TGP are considered to have antiinflammatory, antioxidative, hepatoprotective, and immunoregulatory actions (19-21). TGP are a disease-modifying medication for rheumatoid arthritis that was approved by the State Food and Drug Administration (SFDA) in 1998. Recently, TGP have been used to treat chronic nephritis in rats (22), and their action may involve the regulation of the expression of IL-1 and IL-1 α mRNA (23). In previous studies, the current authors experimentally induced DN, and results indicated that TGP prevented inflammation, oxidation, and macrophage activation, thus slowing the progression of DN (24-26). However, the effect of TGP on the ERS-TXNIP-inflammation chain in DN remains unclear. The aim of the current study was to determine how TGP averts renal injury in diabetic rats in terms of the ERS-TXNIP-inflammation chain.

2. Materials and Methods

2.1. Reagents

TGP was extracted from the roots of *P. lactiflora* Pall. using ethanol reflux, n-butanol extraction, and macroreticular absorption resin chromatography. HPLC fingerprinting analysis indicated that the

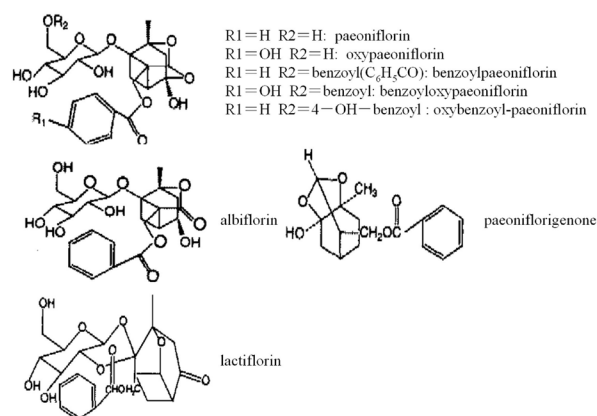


Figure 1. Chemical structures of the major components of total glucosides of peony.

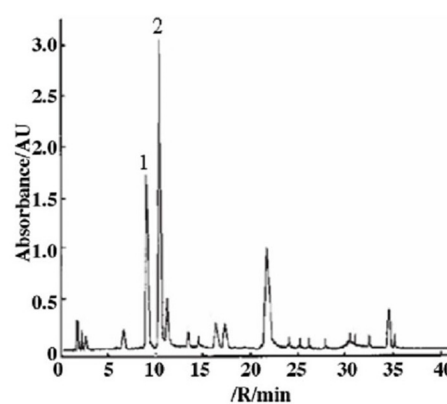


Figure 2. HPLC fingerprinting of total glucosides of peony. (1) Albiflorin; (2) Paeoniflorin. Column: Supelcosil LC-18 (5 mm, 150 mm \times 4.6 mm); Solvent A: Acetonitrile; Solvent B: H₂O (acidified to pH 3.0 with phosphoric acid); Gradient: 10%, 15%, 18%, 30%, 35%, 40%. And 40% of solvent A at 0, 5, 25, 27, 38, 40, and 50 min, respectively. Flow rate: 1.0 mL/min. Injection volume: 10 mL. Detection: 230 nm.

extract contained 41.1% paeoniflorin (Figure 2) (27). Streptozotocin (STZ) was obtained from Sigma Chemical Co. (St. Louis, MO, USA). A microalbumin assay kit was purchased from Abcam Biotechnology (Abcam, Cambridge, UK). An immunohistochemistry kit (PV-9000) was purchased from Beijing Zhongshan Biotechnology, Inc. (Zhongshan, China). TXNIP and a GAPDH primer were obtained from Shanghai Sangon Co. (Shanghai, China). A Trizol Kit was obtained from Invitrogen (Invitrogen, California, USA). M-MLV reverse transcriptase and an RNA enzyme inhibitor were purchased from Promega (Madison, WI, USA). A SYBR Green PCR Master Mix Kit was obtained from Bio-Rad Laboratories (Hercules, CA, USA). The following antibodies were used in this study: rabbit anti-GRP78 and anti-TXNIP antibodies were obtained from Santa Cruz Biotechnology (Santa Cruz, CA, USA), and anti-p-PERK, anti-p-eIF2 α , and anti-CHOP antibodies were purchased from Cell Signaling (USA). Anti- β -actin antibodies, anti-rabbit IgG, and anti-mouse IgG antibodies conjugated to horseradish peroxidase (HRP)

were purchased from Wuhan Sanying Biotechnology, Inc. (Wuhan, China). A bicinchoninic acid (BCA) kit was obtained from Beyotime Institute of Biotechnology (Jiangsu, China). A chemiluminescence kit was obtained from Amersham Life Science (Little Chalfont, UK).

2.2. Animals

Male Munich-Wistar rats ($n = 50$, weight: 180 to 200 g) were purchased from the Experimental Animal Center of Anhui Medical University. Each cage contained 5 animals with free access to food and water. Animals were housed in a constant environment (temperature of about $24 \pm 1^\circ\text{C}$, 60% humidity, 12:12-h light:dark cycle). This study was approved by the Animal Ethics Committees of the Faculty of Anhui Medical University and animals were treated in accordance with the "Principles of Laboratory Animal Care and Use in Research" (Ministry of Health, Beijing, China).

2.3. Experimental design

After ten days of acclimation, rats fasted overnight and were then injected with 65 mg/kg of streptozotocin in a citrate buffer (0.1 M, pH 4.5) based on their weight. Two days later, blood glucose and body weight were evaluated and only rats with blood glucose levels higher than 16.8 mmol/L were used in this study. Diabetic rats were randomly divided into four groups (a diabetic control group and TGP intervention groups) with no differences among the groups. TGP intervention groups were administered TGP daily at a dose of 50, 100, or 200 mg/kg *via* a stomach tube, while the non-diabetic control group and diabetic control group were administered an equivalent amount of 0.5% sodium carboxymethylcellulose (CMC-Na).

2.4. Urinary albumin excretion

Prior to sacrifice, 24-h urine samples were collected from rats housed in metabolic cages in order to measurement urinary albumin excretion. Samples were centrifuged at 10,000 g for 3 min at 4°C and final volumes were recorded. Albumin levels were detected using the Rat Albumin ELISA Kit in accordance with the manufacturer's instructions.

2.5. Blood samples and tissue collection

After 8 wk of follow-up, rats fasted 12 h, and 10 rats from each group were euthanized by intraperitoneal injection of sodium pentobarbital (50 mg/kg). Blood samples were immediately collected by catheterizing the right jugular artery and then the rats were perfused with normal saline at 4°C . After the rats were perfused, one kidney was fixed in a 10% formaldehyde solution for immunohistochemical experiments and another kidney

was stored at -80°C for further analysis.

2.6. Immunohistochemistry

Immunoperoxidase staining for GRP78 was performed on 10% formalin-fixed paraffin sections (2 μm). Three-percent hydrogen peroxide was used to block endogenous peroxidase and antigens were retrieved with microwave heating. Tissue sections were blocked with 10% normal goat serum for 10 min followed by incubation with anti-GRP78 antibodies (1:100) overnight at 4°C . The sections were washed in phosphate-buffered saline and incubated with the appropriate horseradish peroxidase-labeled secondary antibody for 30 min at 37°C . After sections were rinsed, reactions were visualized using 3,3-diaminobenzidine (DAB, Sigma), with a brown color indicating peroxidase activity. Sections were counterstained with hematoxylin. Immunostaining of GRP78 was evaluated using the Image-Pro Plus 6.0 image analysis system by quantifying the stained area of the sections and the entire field of view at the same light intensity used in microscopy (28). Five fields were randomly selected from each section for observation at a high magnification and the ratio of the stained area to the entire field was calculated.

2.7. Western blot analysis

Tissue samples from each of the 5 groups were homogenized in radio immunoprecipitation assay (RIPA) lysis buffer, and Western blot analysis was performed as described previously (26). Nitrocellulose membranes were blocked with 5% non-fat milk for 2 h and then incubated with the primary antibody at 4°C overnight. Membranes were then treated with horseradish peroxidase-labeled secondary antibody. Blots were developed with enhanced chemiluminescence. The signal intensity of each band was quantified and analyzed using the Leica Q500IW image analysis system, and the result was expressed as a ratio of GRP78, p-PERK, p-eIF2 α , CHOP, and TXNIP to housekeeping protein-actin in optical density units.

2.8. RNA extraction and real-time PCR

Total RNA was extracted from kidney tissue with the Trizol reagent in accordance with the manufacturer's instruction. Real-time PCR was performed using the SYBR Green PCR master mix kit as previously described (26). The primers used in this study were as follows: TXNIP, 5'-TCAGTCAGAGGCAATCACATTA-3', and 5'-GGAGCCAGGGACACTAACATAG-3 and GAPDH, 5'-ACAGCAACAGGGTGGTGGAC-3', and 5'-TTTGAGGGTGCAGCGAACTT-3'. The relative expression of mRNA was analyzed using $2^{-\Delta\Delta\text{Ct}}$, and expression of the mRNA of interest was normalized to GAPDH.

Table 1. Characteristics of the rats clinical and metabolic parameters

Groups	Dose (mg/kg*d)	Blood glucose (mg/dL)	Body weight (g)	Kidney weight/ body weight (g/100g BW)	Albumin excretion rate ^a (mg/24 h)
Normal		123.53 ± 29.19	458 ± 27.47	0.30 ± 0.04	0.38 ×/÷ 1.3
Diabetic control		469.07 ± 74.58**	271.75 ± 16.86**	0.56 ± 0.05*	1.87 ×/÷ 1.1**
Diabetic + TGP	50	445.04 ± 77.43	281.75 ± 25.01	0.52 ± 0.02	1.32 ×/÷ 1.1 [#]
	100	470.49 ± 75.47	266.4 ± 27.87	0.50 ± 0.06	1.15 ×/÷ 1.1 [#]
	200	484.16 ± 75.65	318.0 ± 17.8	0.50 ± 0.04	0.65 ×/÷ 1.1 ^{###}

Data are expressed as means ± S.E.M. ^aShown as geometric mean ×/÷ tolerance factor. Number of rats in each group was 10. **p* < 0.05, ***p* < 0.01, compared with normal group; [#]*p* < 0.05, ^{###}*p* < 0.01 compared with diabetic control group.

2.9. Statistical analysis

Data obtained from this study are expressed as the mean ± S.E.M. unless otherwise specified. For statistical analysis, ANOVA was performed using SPSS 16.0. The difference between groups was tested using the LSD test and Levene's test for homogeneity of variance, where *p* < 0.05 was considered to indicate a significant difference. Since the rate of urinary albumin excretion followed a skewed distribution, log transformation was used prior to statistical analysis of this parameter.

3. Results

3.1. TGP attenuated an increase in albuminuria in diabetic rats

TGP treatment did not cause any significant changes in body weight, blood glucose levels, and the ratio of the kidney weight to body weight among the diabetic groups. Accumulated evidence has indicated that albuminuria is a leading risk factor for the progression of renal disease (29,30). TGP significantly attenuated the high level of albuminuria in all of the diabetic groups (Table 1). Although that attenuation was dose-dependent, the levels of albuminuria were still higher than those in normal control rats. This finding suggests that TGP can potentially protect the kidneys and prevent the development of DN.

3.2. TGP inhibited the expression of GRP78 in the kidneys of rats with STZ-induced diabetes

GRP78 is a marker of ERS and has been implicated in the pathogenesis of diabetic complications (9). GRP78 was noted in the glomerulus and tubulointerstitium. There was minimal staining for GRP78 in the kidneys of normal rats, while GRP78 was abundantly expressed in the kidneys of diabetic rats. Overexpression of GRP78 was more limited in diabetic rats treated with TGP (Figure 3 and Table 2). Densitometric analysis of Western blots revealed that the level of GRP78 protein was markedly higher in control diabetic rats than in normal rats. As shown in Figure 4, TGP at a dose of 50, 100, or 200 mg/kg significantly down-regulated renal expression of GRP78 protein in diabetic rats according

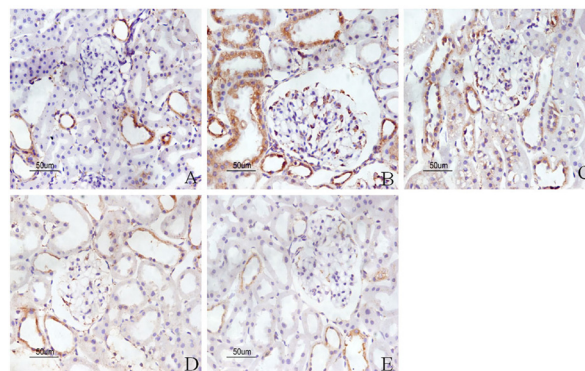


Figure 3. Immunostaining of GRP78 in the kidney. (A) normal; (B) control diabetic; (C) diabetic + TGP 50 mg/kg; (D) diabetic + TGP 100 mg/kg; (E) diabetic + TGP 200 mg/kg. Original magnification ×400.

Table 2. Semiquantitative assessment of GRP78 immunohistochemistry staining in five groups of rats

Groups	Dose (mg/kg*d)	Glomeruli (%) ^a	Tubulointerstitium (%) ^a
Normal		0.75 ± 0.53	5.05 ± 0.77
Diabetic control		12.42 ± 5.56**	18.93 ± 1.67**
Diabetic + TGP	50	9.46 ± 1.83 [#]	15.60 ± 2.07 ^{##}
	100	5.79 ± 1.89 ^{###}	12.33 ± 3.46 ^{###}
	200	4.89 ± 2.26 ^{###}	10.25 ± 3.27 ^{###}

Data are expressed as means ± S.E.M. ^aShown as the median. Number of rats in each group was 10. ***p* < 0.01, compared with the normal group; [#]*p* < 0.05, ^{###}*p* < 0.01, compared with the control diabetic group.

to Western blot analysis.

3.3. TGP reduced the expression of p-PERK and p-eIF2α in the kidneys of rats with STZ-induced diabetes

ERS caused abnormal levels of p-PERK and p-eIF2α expression. As indicated by densitometric analysis of Western blots, the levels of p-PERK and p-eIF2α expression were significantly higher in diabetic rats than in normal rats. However, TGP treatment caused the levels of p-PERK and p-eIF2α expression to decrease markedly (Figure 4).

3.4. TGP attenuated the expression of CHOP in the kidneys of rats with STZ-induced diabetes

CHOP (or GADD153) is an integral component of

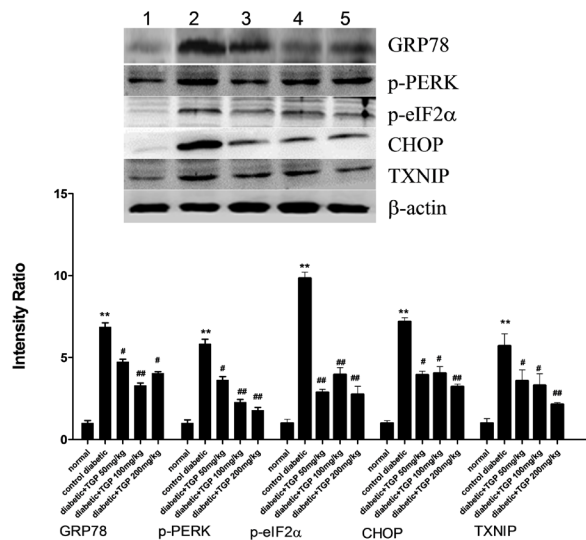


Figure 4. Western blot analysis of GRP78, p-PERK, p-eIF2 α , CHOP, and TXNIP in renal tissue from five groups of rats. (1) normal; (2) control diabetic; (3) diabetic + TGP 50 mg/kg; (4) diabetic + TGP 100 mg/kg; (5) diabetic + TGP 200 mg/kg. Densitometric data were normalized to β -actin levels and values for each control group were arbitrarily defined as 1. Results are expressed as the mean \pm S.E.M from at least three independent experiments. ** $p < 0.01$ vs. normal, # $p < 0.05$, ## $p < 0.01$ vs. control diabetic.

ERS-induced apoptosis; importantly, CHOP is also a component of the inflammatory response (10). In order to investigate whether TGP was involved in the pathogenesis of DN *via* the inflammatory response, the level of CHOP expression was determined using Western blot analysis. The level of CHOP protein was markedly higher in control diabetic rats than in normal rats. Like the findings mentioned earlier, the activation of CHOP diminished dramatically as a result of treatment with TGP at a dose of 50, 100, or 200 mg/kg (Figure 4).

3.5. TGP attenuated the expression of TXNIP in the kidneys of rats with STZ-induced diabetes

The current study focused on TXNIP, which is an important link between ERS and inflammation (12,13). The current results indicated that TXNIP tended to increase in rats with STZ-induced diabetes. As shown in Figure 4, the level of TXNIP expression decreased markedly with administration of TGP at a dose of 50, 100, or 200 mg/kg. The level of TXNIP mRNA expression in the renal tissues of rats with DN was significantly higher than that in the control group, and that level of expression decreased markedly as a result of treatment with TGP (Figure 5).

4. Discussion

Previous studies by the current authors indicated that the weight of the kidney, the glomerular volume, the tubulointerstitial damage index, and the rate of urinary albumin excretion improved markedly 8 weeks

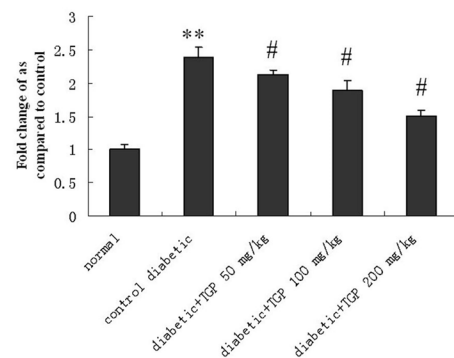


Figure 5. Quantitative real-time PCR of TXNIP in the kidney. Values are expressed as the mean \pm S.E.M from at least three independent experiments. ** $p < 0.01$ vs. normal, # $p < 0.05$ vs. control diabetic.

after diabetes was induced with STZ; however, TGP ameliorated albuminuria and it attenuated glomerular and tubulointerstitial injuries without changing blood glucose levels (24,25,31). This suggested that TGP might prove to be a useful therapy for DN. The current results suggested that type 1 diabetes mellitus induced with STZ was associated with activation of the renal ERS response and upregulation of TXNIP. Previous studies have indicated that the protective effects of TGP in diabetic rats were related to its antiinflammatory and antioxidative action. The current study further identified the effects of TGP on ERS and TXNIP in diabetic rats.

Diabetes has been characterized as a chronic inflammatory disease (31,32) and is associated with abnormal secretion of numerous inflammatory factors. The increased UPR in diabetes reveals the existence of ERS (33), including upregulation of nuclear transcription factors such as PERK. Fang *et al.* reported that ERS appeared to play an important part in albuminuria-provoked inflammasome activation and elimination of ERS *via* tauroursodeoxycholic acid (TUDCA), which might represent a novel avenue for attenuating kidney epithelial cell damage caused by albuminuria (34). The UPR is a homeostatic response that allows the cells to cope with stressful conditions associated with increased misfolded or unfolded protein loads; failure of this mechanism is referred to as the ERS response (9). The ERS response has been found to play a key role in a growing number of pathological conditions such as DN (10,34,35), and the ERS response is considered to be a cause of chronic inflammation (36). The current results verified the hypothesis that DN is related to ERS *via* dysregulated expression of GRP78, p-PERK, p-eIF2 α , and CHOP.

Recent experimental evidence suggests that TXNIP occupies a critical node in signaling that connects ERS and IL-1 β production. TXNIP expression was induced by ERS *via* the IRE1 α and PERK-eIF2 α pathways of the UPR. Carbohydrate response element binding protein (ChREBP) and activating transcription factor 5 (ATF5) regulate TXNIP expression at the

transcriptional level (12,13), while IRE1 α regulates TXNIP expression at the posttranscriptional level (12). Consequently, cell death is induced by IL-1 β production caused by TXNIP through the initiation of IL-1 β mRNA transcription. Transcriptional activation of IL-1 β might explain the upregulation of TXNIP caused by ERS (37). TXNIP is also considered to be as a crucial signaling molecule that connects oxidative stress and inflammasome activation (38). Studies of endothelial cells have indicated that activation of the ERS-TXNIP-inflammation chain was responsible for endothelial dysfunction (39,40). Suppressing ERS, regulating TXNIP expression, and inhibiting inflammation have proven beneficial in the management of cardiovascular disease in obese individuals and diabetics (39,41).

TGP are isolated from the roots of *P. lactiflora* Pall. and are used in clinical settings to alleviate an inflammatory reaction. The roots of *P. lactiflora* Pall. have long been used as a treatment for rheumatoid arthritis. Recent studies in China had reported that TGP cure nephritis, including Heymann nephritis and IgA nephropathy. Together with previous results indicating that TGP treatment reduces the expression of tumor necrosis factor α (TNF- α) and IL-1 β (26), the current results indicated that TXNIP might be a critical hub between ERS and IL-1 β . Numerous stress signaling pathways may converge at TXNIP, contributing to inflammasome activation and pro-inflammatory cytokine production. An important finding is that TGP may inhibit the upregulation of TXNIP and ERS in diabetic kidneys *via* the attenuation of pro-inflammatory cytokine production. Therefore, TGP could possibly play a pivotal role in the treatment of DN.

Together with the results of recent studies, the current findings indicated that there are close ties among ERS, glucose toxicity, oxidative stress, and inflammation in DN, suggesting that a therapeutic strategy targeting TXNIP might be effective in treating DN. However, the specific mechanism by which TGP acts on ERS and TXNIP is not yet fully understood. This topic will be examined in further studies in the future.

Acknowledgements

This research was funded by the National Natural Science Foundation of China (No. 81374034) and the Natural Science Foundation of Anhui Province (No.1408085MH183, No.1208085MH149).

References

1. Grace BS, Clayton P, McDonald SP. Increases in renal replacement therapy in Australia and New Zealand: Understanding trends in diabetic nephropathy. *Nephrology*. 2012; 17:76-84.
2. Taler SJ, Agarwal R, Bakris GL, Flynn JT, Nilsson PM, Rahman M, Sanders PW, Textor SC, Weir MR, Townsend RR. KDOQI US commentary on the 2012 KDIGO clinical

- practice guideline for management of blood pressure in CKD. *Am J Kidney Dis*. 2013; 62:201-213.
3. Khan MI, Pichna BA, Shi Y, Bowes AJ, Werstuck GH. Evidence supporting a role for endoplasmic reticulum stress in the development of atherosclerosis in a hyperglycaemic mouse model. *Antioxid Redox Signal*. 2009; 11:2289-2298.
4. Chen Y, Wang JJ, Li J, Hosoya KI, Ratan R, Townes T, Zhang SX. Activating transcription factor 4 mediates hyperglycaemia-induced endothelial inflammation and retinal vascular leakage through activation of STAT3 in a mouse model of type 1 diabetes. *Diabetologia*. 2012; 55:2533-2545.
5. Lindenmeyer MT, Rastaldi MP, Ikehata M, Neusser MA, Kretzler M, Cohen CD, Schlondorff D. Proteinuria and hyperglycemia induce endoplasmic reticulum stress. *J Am Soc Nephrol*. 2008; 19:2225-2236.
6. Liu G, Sun Y, Li Z, Song T, Wang H, Zhang Y, Ge Z. Apoptosis induced by endoplasmic reticulum stress involved in diabetic kidney disease. *Biochem Biophys Res Commun*. 2008; 370:651-656.
7. Inagi R, Nangaku M, Onogi H, Ueyama H, Kitao Y, Nakazato K, Ogawa S, Kurokawa K, Couser WG, Miyata T. Involvement of endoplasmic reticulum (ER) stress in podocyte injury induced by excessive protein accumulation. *Kidney Int*. 2005; 68:2639-2650.
8. Liu J, Huang K, Cai GY, Chen XM, Yang JR, Lin LR, Yang J, Huo BG, Zhan J, He YN. Receptor for advanced glycation end-products promotes premature senescence of proximal tubular epithelial cells *via* activation of endoplasmic reticulum stress-dependent p21 signaling. *Cell Signal*. 2014; 26:110-121.
9. Kitamura M. Endoplasmic reticulum stress in the kidney. *Clin Exp Nephrol*. 2008; 12:317-325.
10. Wu J, Zhang R, Torreggiani M, Ting A, Xiong H, Striker GE, Vlassara H, Zheng F. Induction of diabetes in aged C57B6 mice results in severe nephropathy: An association with oxidative stress, endoplasmic reticulum stress, and inflammation. *Am J Pathol*. 2010; 176:2163-2176.
11. Saraheimo M, Teppo AM, Forsblom C, Fagerudd J, Groop PH. Diabetic nephropathy is associated with low-grade inflammation in Type 1 diabetic patients. *Diabetologia*. 2003; 46:1402-1407.
12. Lerner AG, Upton JP, Praveen PV, *et al*. IRE1 α induces thioredoxin-interacting protein to activate the NLRP3 inflammasome and promote programmed cell death under irremediable ER stress. *Cell Metab*. 2012; 16:250-264.
13. Osowski CM, Hara T, O'Sullivan-Murphy B, Kanekura K, Lu S, Hara M, Ishigaki S, Zhu LJ, Hayashi E, Hui ST, Greiner D, Kaufman RJ, Bortell R, Urano F. Thioredoxin-interacting protein mediates ER stress-induced beta cell death through initiation of the inflammasome. *Cell Metab*. 2012; 16:265-273.
14. Shalev A, Pise-Masison CA, Radonovich M, Hoffmann SC, Hirshberg B, Brady JN, Harlan DM. Oligonucleotide microarray analysis of intact human pancreatic islets: Identification of glucose-responsive genes and a highly regulated TGF beta signaling pathway. *Endocrinology*. 2002; 143:3695-3698.
15. Qi W, Chen X, Gilbert RE, Zhang Y, Waltham M, Schache M, Kelly DJ, Pollock CA. High glucose-induced thioredoxin-interacting protein in renal proximal tubule cells is independent of transforming growth factor-beta1. *Am J Pathol*. 2007; 171:744-754.

16. Advani A, Gilbert RE, Thai K, *et al.* Expression, localization, and function of the thioredoxin system in diabetic nephropathy. *J Am Soc Nephrol.* 2009; 20:730-741.
17. Hamada Y, Fukagawa M. A possible role of thioredoxin interacting protein in the pathogenesis of streptozotocin-induced diabetic nephropathy. *Kobe J Med Sci.* 2007; 53:53-61.
18. Li J, Chen CX, Shen YH. Effects of total glucosides from paeony (*Paeonia lactiflora* Pall) roots on experimental atherosclerosis in rats. *J Ethnopharmacol.* 2011; 135:469-475.
19. Wang Y, Zhang H, Du G, Wang Y, Cao T, Luo Q, Chen J, Chen F, Tang G. Total glucosides of paeony (TGP) inhibits the production of inflammatory cytokines in oral lichen planus by suppressing the NF-kappaB signaling pathway. *Int Immunopharmacol.* 2016; 36:67-72.
20. Zhang LL, Wei W, Wang NP, Wang QT, Chen JY, Chen Y, Wu H, Hu XY. Paeoniflorin suppresses inflammatory mediator production and regulates G protein-coupled signaling in fibroblast-like synoviocytes of collagen induced arthritic rats. *Inflamm Res.* 2008; 57:388-395.
21. Liu DF, Wei W, Song LH. Protective effect of paeoniflorin on immunological liver injury induced by bacillus Calmette-Guerin plus lipopolysaccharide: Modulation of tumour necrosis factor-alpha and interleukin-6 mRNA. *Clin Exp Pharmacol Physiol.* 2006; 33:332-339.
22. Zhou DY, Xu XM, Dai H, Feng J. Effect of total glucosides of paeony on mesangial proliferative glomerulonephritis in rats. *Acta Universitatis Medicinalis Anhui.* 2006; 41:146-149. (in Chinese)
23. Zhang MO, Wang YW, Zhu XL, Yang RC, Zhang YH, Lu Y, Wang YJ. Total glucosides of peony reduces renal damage in rats with mesangial proliferative nephritis. *Zhe Jiang Medical Journal.* 2008; 30:1176-1179. (in Chinese)
24. Su J, Zhang P, Zhang JJ, Qi XM, Wu YG, Shen JJ. Effects of total glucosides of paeony on oxidative stress in the kidney from diabetic rats. *Phytomedicine.* 2010; 17:254-260.
25. Wang K, Wu YG, Su J, Zhang JJ, Zhang P, Qi XM. Total glucosides of paeony regulates JAK2/STAT3 activation and macrophage proliferation in diabetic rat kidneys. *Am J Chin Med.* 2012; 40:521-536.
26. Xu XX, Qi XM, Zhang W, Zhang CQ, Wu XX, Wu YG, Wang K, Shen JJ. Effects of total glucosides of paeony on immune regulatory toll-like receptors TLR2 and 4 in the kidney from diabetic rats. *Phytomedicine.* 2014; 21:815-823.
27. Zou ZM, Li-Zhen XU, Yang SL. HPLC fingerprinting of total glucosides of paeony. *Acta Pharmaceutica Sinica.* 2003; 38:46-49. (in Chinese)
28. Aoyama I, Shimokata K, Niwa T. An oral adsorbent downregulates renal expression of genes that promote interstitial inflammation and fibrosis in diabetic rats. *Nephron.* 2002; 92:635-651.
29. Bakris GL. Slowing nephropathy progression: Focus on proteinuria reduction. *Clin J Am Soc Nephrol.* 2008; 3 Suppl 1:S3-10.
30. de Zeeuw D, Remuzzi G, Parving HH, Keane WF, Zhang Z, Shahinfar S, Snapinn S, Cooper ME, Mitch WE, Brenner BM. Proteinuria, a target for renoprotection in patients with type 2 diabetic nephropathy: Lessons from RENAAL. *Kidney Int.* 2004; 65:2309-2320.
31. Wu Y, Ren K, Liang C, Yuan L, Qi X, Dong J, Shen J, Lin S. Renoprotective effect of total glucosides of paeony (TGP) and its mechanism in experimental diabetes. *J Pharmacol Sci.* 2009; 109:78-87.
32. Li J, Wang JJ, Yu Q, Wang M, Zhang SX. Endoplasmic reticulum stress is implicated in retinal inflammation and diabetic retinopathy. *FEBS Lett.* 2009; 583:1521-1527.
33. Hotamisligil GS. Endoplasmic reticulum stress and the inflammatory basis of metabolic disease. *Cell.* 2010; 140:900-917.
34. Fang L, Xie D, Wu X, Cao H, Su W, Yang J. Involvement of endoplasmic reticulum stress in albuminuria induced inflammasome activation in renal proximal tubular cells. *PloS one.* 2013; 8:e72344.
35. Baban B, Liu JY, Mozaffari MS. Endoplasmic reticulum stress response and inflammatory cytokines in type 2 diabetic nephropathy: Role of indoleamine 2,3-dioxygenase and programmed death-1. *Exp Mol Pathol.* 2013; 94:343-351.
36. Hasnain SZ, Lourie R, Das I, Chen AC, McGuckin MA. The interplay between endoplasmic reticulum stress and inflammation. *Immunol Cell Biol.* 2012; 90:260-270.
37. Koenen TB, Stienstra R, van Tits LJ, de Graaf J, Stalenoef AF, Joosten LA, Tack CJ, Netea MG. Hyperglycemia activates caspase-1 and TXNIP-mediated IL-1beta transcription in human adipose tissue. *Diabetes.* 2011; 60:517-524.
38. Zhou R, Tardivel A, Thorens B, Choi I, Tschopp J. Thioredoxin-interacting protein links oxidative stress to inflammasome activation. *Nat Immunol.* 2010; 11:136-140.
39. Li Y, Yang J, Chen MH, Wang Q, Qin MJ, Zhang T, Chen XQ, Liu BL, Wen XD. Ilexgenin A inhibits endoplasmic reticulum stress and ameliorates endothelial dysfunction via suppression of TXNIP/NLRP3 inflammasome activation in an AMPK dependent manner. *Pharmacol Res.* 2015; 99:101-105.
40. Zhao Y, Li Q, Zhao WJ, Li J, Sun Y, Liu K, Liu BL, Zhang N. Astragaloside IV and cycloastragenol are equally effective in inhibition of endoplasmic reticulum stress-associated TXNIP/NLRP3 inflammasome activation in the endothelium. *J Ethnopharmacol.* 2015; 169:210-218.
41. Song JN, Li J, Hou FJ, Wang XN, Liu BL. Mangiferin inhibits endoplasmic reticulum stress-associated thioredoxin-interacting protein/NLRP3 inflammasome activation with regulation of AMPK in endothelial cells. *Metabolism.* 2014; 64:428-437.

(Received October 14, 2016; Revised November 30, 2016; Accepted December 4, 2016)

Ledipasvir and sofosbuvir for recurrent hepatitis C after liver transplantation

Yuki Oya, Yasuhiko Sugawara*, Takehisa Watanabe, Yoko Yoshimaru, Masaki Honda, Shintaro Hashimoto, Daiki Yoshii, Kaori Isono, Shintaro Hayashida, Hidekazu Yamamoto, Motohiko Tanaka, Yutaka Sasaki, Yukihiro Inomata

Departments of Transplantation/Pediatric Surgery and Gastroenterology and Hepatology, Postgraduate School of Life Science, Kumamoto University, Kumamoto, Japan.

Summary Management of recurrent hepatitis C following liver transplantation still remains a challenge. Here, we report five patients who achieved viral responses following combined treatment with ledipasvir and sofosbuvir. All the patients received tacrolimus for immunosuppression. No dose adjustment was made before the ledipasvir and sofosbuvir therapy. All completed the intended 12-week treatment course with the full dose of ledipasvir and sofosbuvir. There were no significant adverse events greater than grade 2. During the study period, no acute rejection episodes were detected. The trough levels of tacrolimus were maintained stably. Hepatitis C virus RNA was not detected at week 12 in any of the patients. Based on the findings from this pilot study, combined ledipasvir and sofosbuvir therapy for 12 weeks is effective and safe for living - donor liver transplantation recipients with recurrence of hepatitis C virus.

Keywords: Liver transplantation, living donor, hepatocellular carcinoma

1. Introduction

In the United States, Europe, and Japan, cirrhosis following hepatitis C virus (HCV) infection is the most common indication for liver transplantation (1). Liver transplant recipients with HCV infection have a poorer prognosis than those without HCV infection (2) when the virological response is not enough (3). Up to 30% of HCV-infected living-donor liver transplantation (LDLT) recipients develop cirrhosis within 5 years after transplantation (4-6). The interferon-based therapy (pegylated interferon and ribavirin with/without HCV protease inhibitor, such as simeprevir or telaprevir) for recurrent HCV is less effective for inducing an antiviral response in liver transplant recipients.

A sustained virologic response (SVR), indicating

HCV eradication following anti-viral therapies, is associated with an improved clinical outcome in LDLT recipients (5,7). Treatment for HCV infection has been limited to pegylated interferon and ribavirin, which results in poor SVR rates (< 50%) and is accompanied by frequent adverse events, including flu-like symptoms, pancytopenia, hemolysis, and psychologic disorders (e.g., depression) (8).

New interferon - free direct-acting antiviral therapies, however, produce high SVR rates in patients after liver transplantation with a lower incidence of side effects and consequent improved tolerability (9). Direct-acting antiviral therapies, e.g., sofosbuvir (nucleotide NS5B polymerase inhibitor) plus ledipasvir (NS5A replication complex inhibitor) or daclatasvir (NS5A replication complex inhibitor), and ombitasvir (NS5A replication complex inhibitor) plus paritaprevir (NS3/4A protease inhibitor) and ritonavir have demonstrated higher safety and efficacy in patients with recurrent HCV after transplantation (10-12).

Here we report five post-transplant patients with recurrent HCV. They achieved an SVR for more than 12 weeks by ledipasvir and sofosbuvir treatment with minimum effect on trough levels of the immunosuppressive agents.

Released online in J-STAGE as advance publication December 18, 2016.

*Address correspondence to:

Dr. Yasuhiko Sugawara, Department of Transplantation/Pediatric Surgery, Postgraduate School of Life Science, Kumamoto University, 1-1-1 Honjo, Chuo-ku, Kumamoto 8603-8556, Japan.

E-mail: yasusuga-tyk@umin.ac.jp

2. Materials and Methods

2.1. Antiviral treatment regimen and patients

Between December 1998 and May 2016, adult-to-adult LDLT was performed in 315 patients at Kumamoto University Hospital. Of these 315 patients, the 93 patients were indicated for HCV cirrhosis. In the patients who underwent LDLT for HCV after the end of 2013 when the ledipasvir and sofosbuvir were available in Japan, the therapy was indicated for the first line therapy ($n = 1$). In the patients who underwent LDLT for HCV before the end of 2013, 41 patients were non -responders after interferon based therapy. Of these four were alive with sustainably positive HCV-RNA at the time of inclusion in this study. Totally 5 patients were the subjects of the study.

Liver biopsy was performed at 3, 6, 12, 24, and 36 months after transplantation. The combined ledipasvir and sofosbuvir therapy was started when hepatitis recurrence was diagnosed on biopsy, along with the HCV RNA and transaminase levels. Patients received 90 mg of ledipasvir and 400 mg of sofosbuvir as a fixed-dose combination tablet (ledipasvir-sofosbuvir) once a day for 12 weeks. No patients received ribavirin with ledipasvir and sofosbuvir. Patients with estimated glomerular filtration rate [eGFR] < 30 mL/min/1.73 m² were excluded from the treatment.

2.2. Blood analysis and histological assessment

Laboratory assessment for the patients with post-transplant hepatitis was performed when necessary. The eGFR was calculated using the following formula: $194 \times \text{serum creatinine}^{-1.094} \times \text{age}^{-0.287} \times 0.739$ (if female), Japanese equation (equation 4; 12). HCV RNA levels were measured using a COBAS TaqMan HCV assay (Roche Diagnostics K.K., Tokyo, Japan). The HCV genotype was determined before transplantation. The interleukin 28B (IL28B) genotype rs8099917 was checked with the Invader assay (Third Wave Technologies, Madison, WI) (13). The NS3 and NS5A regions of HCV were evaluated as resistance-associated variants using direct - sequencing methods before the induction of the therapy. Liver biopsy was done which was evaluated by a pathologist based on the Metavir score (14).

2.3. Immunosuppression

The strategy after the transplantation comprised steroid induction with tacrolimus or cyclosporine. The dose of each drug was gradually tapered over 6 months after LDLT. The methylprednisolone dose was tapered from 3 mg/kg on the first postoperative day to 0.05 mg/kg at the sixth postoperative month. All the five patients are continuing to use methylprednisolone with a maintenance dose (2-4 mg).

2.4. Ethics statement

The study protocol was approved by the Postgraduate School of Life Science at the Kumamoto University of Research Ethics Committee.

2.5. Statistical analysis

The SPSS 17.0 statistical software was used (SPSS Inc., Chicago, IL) to analyze the relevant data. The effect of treatment on eGFR and immunosuppressant trough levels were analyzed by the Mann-Whitney U test. A p -value < 0.05 was considered significant.

3. Results and Discussion

The characteristics of the recipients are shown in detail (Table 1). The model for end-stage liver disease score was 15 in median (range 9-23). One case received an ABO – incompatible liver graft. None were co-infected with HIV. Two (40%) had hepatocellular carcinoma which was satisfying the Milan criteria. The HCV profile are shown also in Table 1. All the patients completed the therapy. The HCV load became undetectable at week 2 ($n = 1$), 4 ($n = 3$), and 8 ($n = 1$; Table 1). No remarkable adverse events were observed. There was no significant change in eGFR before (median 68 [range 65~90] mL/min/1.73 m²) or after the therapy (median 70 [range 57~90] mL/min/1.73 m²; $p = 0.78$). No patients needed a dose reduction, blood transfusion, or granulocyte-colony stimulating factor. None exhibited increased bilirubin levels. Immunosuppression was not changed before the therapy, and the immunosuppressant trough levels did not change significantly before (median 5.8 [range 2.1~8.4] ng/mL) or after (median 5.8 [range 1.9~7.7] ng/mL) introduction of the therapy ($p = 0.24$). No episodes of acute or chronic rejection were recognized during the treatment.

The introduction of pegylated interferon and ribavirin improved the virological efficacy for recurrent HCV in post-transplant patients. Although the SVR rate for liver transplantation patients with a history of HCV genotype 1 infection was improved to 30-50% (5, 15, 16), more than 50% of the recipients suffered from recurrent HCV infection. The use of protease inhibitors in LDLT recipients is limited due to strong drug-to-drug interactions. Here we report the experience with five patients treated with combined ledipasvir and sofosbuvir for recurrent post-liver transplantation hepatitis caused by HCV genotype 1.

Ledipasvir is a potent inhibitor of HCV NS5A. NS5A is a viral protein with an important role in viral replication. Sofosbuvir is a nucleotide analog inhibitor of NS5B polymerase. NS5B is the key enzyme mediating HCV replication. Combined therapy with the two agents produces a high virological response in patients with

Table 1. Patinets' characteristics

Patients	1	2	3	4	5
Age (years)	57	57	50	66	58
Gender	Male	Female	Male	Female	Male
Height (cm)/weight (kg)	176/87	157/46	159/45	147/42	169/69
Donor age (years)	49	29	36	62	29
Donor relationship	Spouse	Child	The third party*	Spouse	Child
Calcineurin inhibitor	FK	FK	FK	FK	FK
MMF	Yes	No	Yes	No	No
Splenectomy at LT	Yes	Yes	Yes	Yes	No
Pretreatment activity [†]	A2	A1	A3	A1	A1
Pretreatment fibrosis [†]	F1	F1	F3	F1	F1
Baseline clinical chemistry at the therapy					
Total bilirubin (mg/dL)	2.1	1.3	0.4	1	1
Alanine aminotransferase (IU/mL)	631	888	306	690	257
Creatinine (mg/dL)	0.62	0.71	0.96	0.47	0.86
eGFR (mL/min)	> 90	65	66	> 90	68
Prothrombin time (International normalized ratio)	1.15	0.85	1.12	0.98	0.99
Hemoglobin (g/dL)	11.1	9.8	10	12	14
Leukocytes (/μL)	6,000	7,400	5,600	4,900	4,800
Platelets (/μL)	18.9	36.5	16.6	12	16
HCV genotype	1b	1b	1a	1b	1b
NS5A mutation	No	No	No	No	No
NS3 mutation	No	No	No	No	No
IL28B Recipient	TT	TT	GG	TG	TT
Pretransplant antiviral therapy	None	None	Relapse	Relapse	None
Baseline HCV RNA pre-LT (log ₁₀ IU/mL)	4.3	3.9	5.5	6.1	2.7
Pre-treatment (mo) since LT	4	3	83	81	109
HCV RNA at the therapy (log ₁₀ IU/mL)	6.5	7.5	5.9	6.2	6.1
HCV response for the therapy					
HCV RNA at w1	3.3	3.1	ND	ND	2.1
HCV RNA at w2	LLOQ	2.3	UD	1.5	LLOQ
HCV RNA at w4	UD	UD	UD	LLOQ	UD
HCV RNA at w8	UD	UD	UD	UD	UD
HCV RNA at w12	UD	UD	UD	UD	UD

FK, tacrolimus; eGFR, estimated glomerular filtration rate; LLOQ, lower limit of quantification (LLOQ), < 1.2 log₁₀ IU/mL; ND, no data; UD, not detectable. *that of domino transplantation. †as per Metavir.

genotype 1 HCV infection (10). Currently, in Europe, treatment with ledipasvir-sofosbuvir plus ribavirin for 24 weeks is indicated for genotype 1 patients with decompensated cirrhosis and/or those who have undergone liver transplantation. Findings from the SOLAR-1 (10) and SOLAR-2 (11) trials suggest that 12 - week treatment with ledipasvir-sofosbuvir is sufficient for almost all patients with genotype 1 HCV recurrence after liver transplantation.

In the 2015 HCV treatment guidelines, the European Association for the Study of the Liver (EASL) recommend a 12 -week treatment with ledipasvir-sofosbuvir plus ribavirin as a first-line option for HCV genotype 1 patients with advanced liver disease which includes those with decompensated cirrhosis before or after liver transplantation (17). As another first-line therapy, EASL guidelines recommend a 12-week treatment with sofosbuvir plus daclatasvir with ribavirin for 12 weeks in HCV genotype 1-infected patients with decompensated cirrhosis and/or after liver transplantation (18). The Infectious Diseases Society of America and the American Association for the Study of Liver Diseases (19) have made the same recommendations.

The small size of the study cohort and the

retrospective design were limitations of the present study. This is the first study, to our knowledge, to provide such detailed insight into the combined treatment with ledipasvir and sofosbuvir for LDLT recipients.

In conclusion, combined treatment with ledipasvir and sofosbuvir is effective for recurrent HCV infection in patients after liver transplantation. The 12 -week treatment should become a standard of care for patients with recurrent genotype 1 chronic hepatitis C after liver transplantation.

References

1. Kim WR, Stock PG, Smith JM, Heimbach JK, Skeans MA, Edwards EB, Harper AM, Snyder JJ, Israni AK, Kasiske BL. OPTN/SRTR 2011 Annual Data Report: Liver. Am J Transplant. 2013;13 Suppl 1:73-102.
2. Akamatsu N, Sugawara Y. Living-donor liver transplantation and hepatitis C. HPB surgery : A world journal of hepatic, pancreatic and biliary surgery. 2013;2013:985972.
3. Guillouche P, Feray C. Systematic review: Anti-viral therapy of recurrent hepatitis C after liver transplantation. Aliment Pharmacol Ther. 2011;33:163-174.
4. Stepanova M, Wai H, Saab S, Mishra A, Venkatesan C,

- Younossi ZM. The outcomes of adult liver transplants in the United States from 1987 to 2013. *Liver Int.* 2015;35:2036-2041.
5. Roche B, Sebagh M, Canfora ML, Antonini T, Roque-Afonso AM, Delvart V, Saliba F, Duclos-Vallee JC, Castaing D, Samuel D. Hepatitis C virus therapy in liver transplant recipients: Response predictors, effect on fibrosis progression, and importance of the initial stage of fibrosis. *Liver Transpl.* 2008;14:1766-1777.
 6. Thuluvath PJ, Krok KL, Segev DL, Yoo HY. Trends in post-liver transplant survival in patients with hepatitis C between 1991 and 2001 in the United States. *Liver Transpl.* 2007;13:719-724.
 7. Kawaoka T, Takahashi S, Kawakami Y, Tsuge M, Hiramatsu A, Imamura M, Hyogo H, Aikata H, Ishiyama K, Tashiro H, Ohdan H, Tanaka J, Chayama K. Sustained virological response to antiviral therapy improves survival rate in patients with recurrent hepatitis C virus infection after liver transplantation. *Hepatol Res.* 2015;45:1047-1054.
 8. Berenguer M. Systematic review of the treatment of established recurrent hepatitis C with pegylated interferon in combination with ribavirin. *J Hepatol.* 2008;49:274-287.
 9. Suraweera D, Sundaram V, Saab S. Treatment of Hepatitis C Virus Infection in Liver Transplant Recipients. *Gastroenterol Hepatol (N Y).* 2016;12:23-30.
 10. Charlton M, Everson GT, Flamm SL, *et al.* Ledipasvir and Sofosbuvir Plus Ribavirin for Treatment of HCV Infection in Patients With Advanced Liver Disease. *Gastroenterology.* 2015;149:649-659.
 11. Manns M, Samuel D, Gane EJ, *et al.* Ledipasvir and sofosbuvir plus ribavirin in patients with genotype 1 or 4 hepatitis C virus infection and advanced liver disease: A multicentre, open-label, randomised, phase 2 trial. *Lancet Infect Dis.* 2016;16:685-697.
 12. Leroy V, Dumortier J, Coilly A, Sebagh M, *et al.* Efficacy of Sofosbuvir and Daclatasvir in Patients With Fibrosing Cholestatic Hepatitis C After Liver Transplantation. *Clin Gastroenterol Hepatol.* 2015;13:1993-2001.
 13. Harada N, Tamura S, Sugawara Y, Togashi J, Ishizawa T, Kaneko J, Aoki T, Sakamoto Y, Hasegawa K, Tanaka T, Yamashiki N, Kokudo N. Impact of donor and recipient single nucleotide polymorphisms of IL28B rs8099917 in living donor liver transplantation for hepatitis C. *PLoS One.* 2014;9:e90462.
 14. Bedossa P, Poynard T. An algorithm for the grading of activity in chronic hepatitis C. The METAVIR Cooperative Study Group. *Hepatology.* 1996;24:289-293.
 15. Lodato F, Berardi S, Gramenzi A, *et al.* Clinical trial: Peg-interferon alfa-2b and ribavirin for the treatment of genotype-1 hepatitis C recurrence after liver transplantation. *Aliment Pharmacol Ther.* 2008;28:450-457.
 16. Saab S, Oh MK, Ibrahim AB, Durazo F, Han S, Yersiz H, Farmer DG, Ghobrial RM, Goldstein LI, Tong MJ, Busuttil RW. Anemia in liver transplant recipients undergoing antiviral treatment for recurrent hepatitis C. *Liver Transpl.* 2007;13:1032-1038.
 17. EASL Recommendations on Treatment of Hepatitis C 2015. *J Hepatol.* 2015;63:199-236.
 18. Narayanan Menon KV, Poterucha JJ, El-Amin OM, Burgart LJ, Kremers WK, Rosen CB, Wiesner RH, Charlton M. Treatment of posttransplantation recurrence of hepatitis C with interferon and ribavirin: Lessons on tolerability and efficacy. *Liver Transpl.* 2002;8:623-629.
 19. Shakil AO, McGuire B, Crippin J, Teperman L, Demetris AJ, Conjeevaram H, Gish R, Kwo P, Balan V, Wright TL, Brass C, Rakela J. A pilot study of interferon alfa and ribavirin combination in liver transplant recipients with recurrent hepatitis C. *Hepatology.* 2002;36:1253-1258.

(Received November 28, 2016; Revised December 10, 2016; Accepted December 13, 2016)

A novel angiogenic peptide, Δ ADT: A truncated adrenotensin peptide revealed by secretory peptidome analysis of human retinal pericytes

Akinori Okumura, Eri Takahashi, Hiroyuki Unoki-Kubota, Yasushi Kaburagi*

Department of Diabetic Complications, Diabetes Research Center, Research Institute, National Center for Global Health and Medicine, Tokyo, Japan.

Summary Retinal pericytes play an important role in the maintenance of retinal microvascular homeostasis. We performed a secretory peptidome of primary human retinal pericytes. Using liquid chromatography-tandem mass spectrometry analysis in the culture medium of retinal pericytes, we identified 256 peptides derived from 114 proteins, and identified a novel partial fragment Leu163-His183 (termed Δ ADT) of adrenotensin (ADT). To elucidate the role of Δ ADT as a soluble mediator of pericyte-endothelial cell interactions, we investigated the bioactivity of Δ ADT in human retinal microvascular endothelial cells (HRMVECs). The cell proliferation assay indicated that the proliferation of HRMVECs was promoted by ADT or Δ ADT. Moreover, Δ ADT had a greater growth promoting effect than ADT in HRMVECs and induced migration and tube formation of HRMVECs. We also observed actin reorganization and that the levels of phosphorylated focal adhesion kinase in Δ ADT stimulated HRMVECs. These results showed that Δ ADT induces profound actin reorganization and increases the levels of phosphorylated focal adhesion kinase. Collectively, our study showed that Δ ADT has an angiogenic activity, and suggested that Δ ADT is a novel angiogenic peptide.

Keywords: Retinal pericytes, secreted peptides, peptidomics, angiogenic peptide, adrenotensin

1. Introduction

Retinal capillaries are composed of microvascular endothelial cells, pericytes, and basement membrane. Retinal pericytes fulfill important roles in a range of functions, including angiogenesis, vessel stabilization, endothelial cell regulation, and maintenance of the blood-retinal barrier. *In vitro* pericyte and endothelial cell co-culture experiments have suggested that pericytes inhibit endothelial cell proliferation in a contact-dependent manner (1) and may increase the barrier function established by endothelial cells (2), a process to which transforming growth factor β 1 (3)

and angiotensin 1 (Ang1) (4) contribute. Angiogenesis involves endothelial cell proliferation, migration, and tube formation. The pericytes provide paracrine signals that promote vascular stability. Ang1-Tie2 signaling of endothelial cells is important for angiogenesis and vascular remodeling and has been suggested to be required for vascular stabilization and maturation (5). The Tie2 receptor is specifically found on endothelial cells, whereas Ang1 is mainly expressed in pericytes. This finding demonstrated that pericyte-endothelial cell interactions are mediated by soluble factors. However, the soluble factors mediating pericyte-endothelial cell interactions are not completely understood. Further studies are required to clarify the mechanism of the interaction.

Peptidomics has been advocated for the comprehensive study of peptides cleaved from precursor proteins by endogenous proteases (6,7). These naturally occurring peptides are beyond the reach of current proteomics examining trypsin-digested peptides, and should be analyzed in their native forms. Unlike proteomics, peptidomics has the potential to uncover processing sites

Released online in J-STAGE as advance publication November 13, 2016.

*Address correspondence to:

Dr. Yasushi Kaburagi, Department of Diabetic Complications, Diabetes Research Center, Research Institute, National Center for Global Health and Medicine, 1-21-1 Toyama, Shinjuku-ku, Tokyo 162-8655, Japan.
E-mail: kaburagi@ri.ncgm.go.jp

of precursor proteins (8).

In the present study, we searched for novel peptides that may play a role in endothelial homeostasis and as a novel molecular target for retinal vascular diseases. We identified secretory peptides in human retinal pericytes using liquid chromatography-tandem mass spectrometry (LC-MS/MS) based peptidomics, and identified an angiogenic partial fragment of adrenotensin (Leu163-His183, termed Δ ADT).

2. Materials and Methods

2.1. Cell cultures

Primary human retinal pericytes (passage 2) and primary human retinal microvascular endothelial cells (HRMVECs, passage 3) were purchased from the Applied Cell Biology Research Institute (Kirkland, WA), respectively. Pericytes were cultured on poly-D-lysine-coated cell culture dishes in CSC Complete Serum-Free Medium Kit with RocketFuel. HRMVECs were cultured on type I collagen-coated cell culture dishes in EGM-2 MV medium (EBM-2 supplemented with EGM-2 MV SingleQuots; Lonza, Walkersville, MD). These cells were used at passages 7-9.

2.2. Preparation of the fraction of secreted peptides from retinal pericytes

Semi-confluent retinal pericytes were washed twice with pre-warmed Dulbecco's Modified Eagle Medium (DMEM)/Ham's F-12 medium without phenol red. Subsequently, the cells were cultured in the same medium for 24 h. After incubation, the medium was collected and filtered through a 0.22 μ m filter. The solution was then acidified to pH 3.0 with trifluoroacetic acid (TFA) and subjected to a C18 solid phase extraction cartridge (Empore 10 mm/6 mL; 3M Company, St. Paul, MN) equilibrated with 2% acetonitrile and 0.1% TFA (buffer A). The cartridge was washed with buffer A, and the fraction of crude peptides was eluted with 80% acetonitrile and 0.1% TFA (buffer B). The eluent was evaporated in a vacuum concentrator and dissolved in 100 μ L of 30% acetonitrile and 0.1% TFA (buffer C). The sample was separated by gel filtration column chromatography (TSKgel G2000SWXL; Tosoh, Tokyo, Japan) in buffer C at a flow rate of 1 mL/min. Corresponding peptide fractions (from the 8th to 11th fractions) were collected, combined, and then loaded onto a strong cation exchange spin column (MonoSpin SCX; GL Science, Tokyo, Japan). The peptide sample was washed twice with buffer B, eluted with 4% NH_4OH in MeOH, and evaporated to dryness. Samples were reconstituted in 50 mM ammonium bicarbonate and analyzed for total peptide concentration using BCA protein assay kit (ThermoFisher Pierce, Rockford, IL).

2.3. Detection and identification of peptides released from retinal pericytes

Reduction of 2 μ g of pericyte derived peptide samples was performed with 10 mM dithiothreitol for 1 h. The samples were then alkylated with 40 mM iodoacetamide in the dark for 1 h. The reaction was halted by the addition of 40 mM dithiothreitol for an additional 1 h. The reductive alkylation peptides were purified with a MonoSpin C18 spin column (GL Sciences) to remove any unreacted compounds. All reductive alkylation procedures were performed at room temperature. Nano LC-MS/MS was performed using a Paradigm MS4 system (Michrom BioResources, Auburn, CA) coupled to a QSTAR Elite Q-TOF mass spectrometer (Sciex, Framingham, MA) as described previously with minor modification at the nano liquid chromatography step (9). Peptides were eluted with mobile phases of A (2% acetonitrile, 0.1% formic acid) and B (90% acetonitrile, 0.1% formic acid) as follows: 0-30% B for 120 min, 30-40% B for 10 min, and 40-95% B for 15 min at a flow rate of 300 nL/min. Peptide identifications were acquired by matching raw spectra data against human protein from the International Protein Index (IPI) database using ProteinPilot software (version 3.0, Sciex) with the Paragon algorithm.

2.4. Synthesis of peptides

Peptides (ADT; SLPEAGPGRTLVSCKPQAHGAPAP PSGSAPHFL and Δ ADT; LVSSCKPQAHGAPAP PSGSAPH) were synthesized by Biosynthesis (Lewisville, TX) and were obtained at > 98% purity. The peptide purity was verified by analytical reverse phase high performance liquid chromatography (HPLC) and matrix-assisted laser desorption/ionization time-of-flight mass spectrometry. Peptides were solubilized in endotoxin-free water at a concentration of 10 mM and correctly diluted when used in the assays.

2.5. Endothelial cell proliferation assay

HRMVECs were seeded at a density of 1×10^4 cells/well in a 24 well plate. After 24 h incubation, different concentrations of Δ ADT and ADT (10 nM, 100 nM, and 1 μ M) were added to the wells and incubated for an additional 20 h. The cells were then trypsinized and counted against a control well.

2.6. Endothelial migration assay

For the endothelial migration assay using wound healing, transendothelial electrical resistance was measured by an electric cell-substrate impedance sensing (ECIS) Z θ instrument (Applied Biophysics, Troy, NY) as described previously (9). Briefly, HRMVECs were plated at confluence in 8W1E gold

electrode culture plates (Applied Biophysics) precoated with type I collagen in EGM-2 MV medium. On the following day, the medium was changed to serum starvation medium (EBM-2 with 0.5% fetal bovine serum), and the cells were incubated for an additional 16 h. The peptides were added to a final concentration of 1 μ M. After 1 h treatment, cells were submitted to an elevated voltage pulse frequency of 60 kHz, 1,400 μ A amplitude, and 20 s duration. This led to the death and detachment of cells present on the small active electrode, resulting in a wound that was normally healed by cells surrounding the small active electrode that had not been submitted to the elevated voltage pulse. Wound healing was then assessed by continuous impedance measurements at 16 kHz for 12 h.

2.7. *In vitro* endothelial tube formation assay

An endothelial tube formation assay used Matrigel (BD Biosciences, Bedford, MA) according to the manufacturer's protocol. Matrigel was thawed and 250 μ L aliquots were transferred into an eight well chamber slide and incubated at 37°C for 30 min. HRMVECs were seeded in quadruplicate (1×10^5 cells/well) in the presence of 100 nM Δ ADT and incubated for 16 h at 37°C. At the end of the incubation period, cells were stained with calcein AM (BD Biosciences) and imaged by the IN Cell Analyzer 6000 (GE Healthcare Biosciences, Buckinghamshire, UK). The branch point and total length of tubes for each condition were measured using the IN Cell Analyzer.

2.8. Immunoblot analysis

Serum-starved HRMVECs were exposed for 5-120 min to 100 nM Δ ADT. SDS-PAGE was performed by using standard procedures on 7.5% tris-glycine gels under reducing conditions. Proteins were transferred to Immobilon-P (Merck Millipore, Bedford, MA). The blots were incubated with rabbit anti-human focal adhesion kinase (FAK) antibody (1:1,000; Cell Signaling Technology, Beverly, MA) or rabbit anti-human phospho-FAK pTyr397 antibody (1:1,000; Cell Systems Technology). The immunoreactive protein was visualized using a SuperSignal West Femto reagent (ThermoFisher Pierce).

2.9. Filamentous actin staining

HRMVECs were plated on a type I collagen-coated eight well chamber slide (BD Biosciences) at 1×10^4 cells/well in EGM-2 MV. On the following day, the media was replaced with serum-free basal media (EBM-2, 2% BSA). After 6 h incubation, 100 nM Δ ADT was added to the wells and incubated for an additional 5, 30, or 90 min. Subsequently, cells were washed twice in PBS, fixed in 0.4 mL of 4% paraformaldehyde at

room temperature for 20 min, and washed with PBS. The cells were blocked and permeabilized with PBS containing 1% normal horse serum and 0.4% Triton X-100 overnight at 4°C. Cells were subsequently washed and incubated with Alexa Fluor 488 phalloidin (Molecular Probes, Carlsbad, CA) and 4',6-diamidino-2-phenylindole (DAPI; Dojindo, Kumamoto, Japan) in the aforementioned blocking buffer for 1 h at room temperature. The slides were washed twice in PBS, mounted on a microscope slide and FluoroSave reagent (Merk Millipore), and observed under a fluorescence microscope.

3. Results and Discussion

3.1. LC-MS/MS analysis of retinal pericytes derived from secreted peptides

To identify the secreted peptides from retinal pericytes, the peptide fractions were prepared from the culture fluid using column chromatography. We performed shotgun peptidomics experiments to investigate the bioactive peptides in the conditioned media of the cells. The LC-MS/MS data were submitted through the ProteinPilot software and searched against the human database with a decoy database to apply a false discovery rate. Using this technique, the 256 peptides originating from 114 genes could be identified with a confidence level of at least 95%. The 44 peptides originating from 15 genes that were identified at least twice in three independent experiments are listed in Table 1 (each peptide shows the results of the highest peptide score). The 42 peptides were identified with a confidence level of 99%, except for two peptides of thymosin β -10 with a confidence level of 97%. Interestingly, we identified Ala65-Ala96 and Ala65-Glu103 of reticulon-4, which play a role in inhibition of neurite outgrowth and cell spread (10). This finding indicates that since retinal pericytes are located outside retinal capillaries, they may interact with optic nerve cells. However, these 44 peptides included a fragment of cytoskeleton proteins, such as actin and vimentin. We selected five genes encoding an extracellular protein categorized as "secreted protein" in the UniProt database, namely ADM, annexin A1, annexin A2, interstitial collagenase, and vasorin.

The identified peptide of interstitial collagenase was only pro-peptide domain (11). Vasorin is predominantly expressed in vascular smooth muscle cells, and its expression is developmentally regulated. Vasorin is a transforming growth factor β -binding protein and has been shown to modulate the activity of growth factors (12). However, the peptide of vasorin identified in the present study was in the membrane spanning region. Annexin A1 is a member of the annexin family of calcium-lipid binding proteins, which are structurally defined by a highly conserved protein core domain

harboring calcium ions, phospholipid binding sites, and an N-terminal region that is unique for a given annexin (13). The anti-inflammatory activities elicited by exogenously applied annexin A1 are mediated through its unique N-terminal domain. Moreover, the identified peptide of annexin A1 was the N-terminal annexin 1 peptide, which is able to activate the human N-formyl peptide receptor (FPR) family members, FPR, FPR-like 1, or FPR-like 2 (14). All identified peptides (9-22 residues) of annexin A2 were in the N-terminal regions, for which physiological conditions have never before been reported. The N-terminal domain regulates the properties of the AnxA2 core by binding to S100A10 (15). The ADM gene encodes for a prohormone of 185 amino acid residues, which is post-translationally modified to generate four peptides: proadrenomedullin N-terminal 20 peptide (Ala22-Arg41), mid-regional pro-adrenomedullin (Glu45-Val92), adrenomedullin (Tyr95-Tyr146), and adrenotensin (ADT) (Ser153-Leu185) (16). In a search for novel regulators of retinal microvascular endothelial cells, we focused on a peptide derived from the ADT region of ADM gene products, because ADT has an endothelium-dependent vasoconstriction effect (17), and antagonizes the stimulatory effect of adrenomedullin during the generation of endothelial nitric oxide (18). Moreover, its function remains largely unknown. In particular, the identified peptide was a partial fragment of ADT lacking ten residues of the N-terminus and two residues of the C-terminus. The truncation mechanism of ADT is unknown; however, detection of this truncated peptide was reproducible in independent experiments. Therefore, we named the peptide Δ ADT. A representative Δ ADT peptide identified by LC-MS/MS is shown in Figure 1.

3.2. Δ ADT stimulates angiogenesis in cultured HRMVEC

We investigated whether Δ ADT could activate the proliferation of HRMVECs compared with ADT and control vehicle (water). To investigate the effect of Δ ADT on HRMVECs, we assayed proliferation by cell counting. Figure 2A shows that Δ ADT increases the proliferation of HRMVEC in a dose-dependent manner. Moreover, the cells that were treated with the Δ ADT showed increased cell growth compared with ADT treated cells. The maximal effect of Δ ADT was significantly lower at 100 nM than that of ADT at a concentration of 1 μ M ($p < 0.05$). This result indicates that ADT and Δ ADT are able to stimulate the proliferation of endothelial cells, and suggests that Δ ADT has a higher proliferation rate than ADT. In addition, this finding is consistent with reports showing the effects of ADT on upregulated proliferation in rat mesangial cells and pulmonary arterial smooth muscle cells (19,20).

Next, we performed HRMVEC migration assay by early wound healing using ECIS. As shown in Figure 2B, Δ ADT-treated cells exhibited nearly complete healing of the wound after 2 h, although control vehicle-treated cells remained in half recovery. This result indicates that Δ ADT increases endothelial cell migration. To evaluate the effect of Δ ADT on the ability of endothelial cells to form tube-like structures, an *in vitro* tube formation assay was performed. HRMVECs treated with Δ ADT increased compared with control vehicle angiogenic tube formation, as quantitatively evaluated by branch point numbers and total tube length (Figure 2C). Considered together, our data showed that Δ ADT derived from retinal pericytes is a novel angiogenic peptide in HRMVECs.

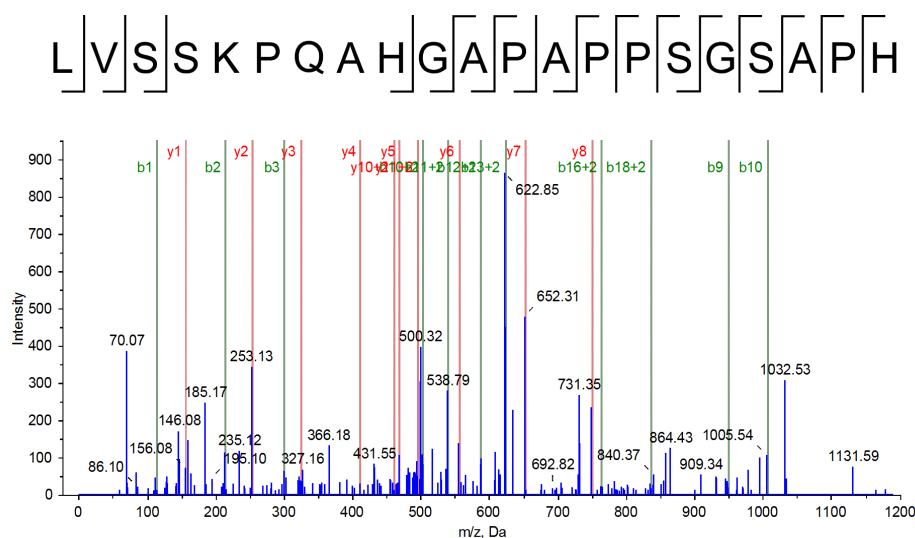


Figure 1. Typical tandem mass spectrometry (MS/MS) spectrum for the identification of a truncated peptide of adrenotensin (Leu163-His183) (Δ ADT) in culture fluid of human retinal pericytes. The MS/MS spectrum of precursor ion Δ ADT (LVSSKPKQAHGAPAPPSSGSAPH) with an identified m/z of 499.02 ($z = 4$).

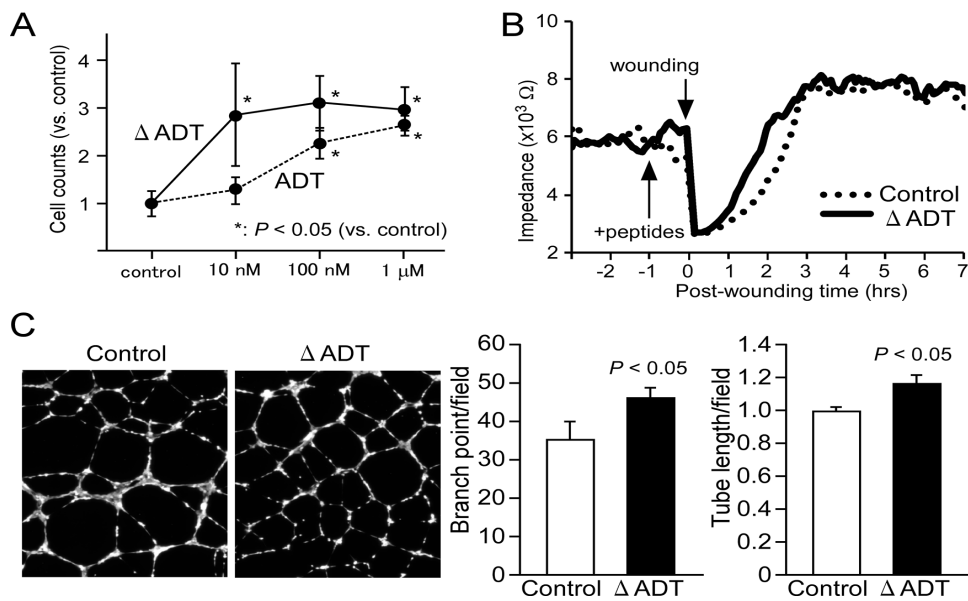


Figure 2. Promoting effect of a truncated peptide of adrenotensin (Δ ADT) on proliferation, migration, and tube formation of human retinal microvascular endothelial cells (HRMVECs). (A) Cell proliferation assay of HRMVEC incubated with Δ ADT (solid line), ADT (dashed line), and control vehicle (water) for 20 h. Cell number was determined by direct counting of trypsinized cell suspensions. **(B)** Cell migration dynamics during wound-healing assay. After 1 h treated with 1 μ M Δ ADT (solid line) or control vehicle (dotted line), HRMVECs were submitted to electrical wounding. Post-wound migration of cells was measured by real-time monitoring using electric cell-substrate impedance sensing (ECIS). **(C)** Δ ADT increases *in vitro* tube formation in HRMVECs compared with the control vehicle. Fluorescence imaging, counting of branch point number ($n = 4$; $p < 0.05$), and measurement of tube length ($n = 4$; $p < 0.05$) were conducted by IN Cell Analyzer.

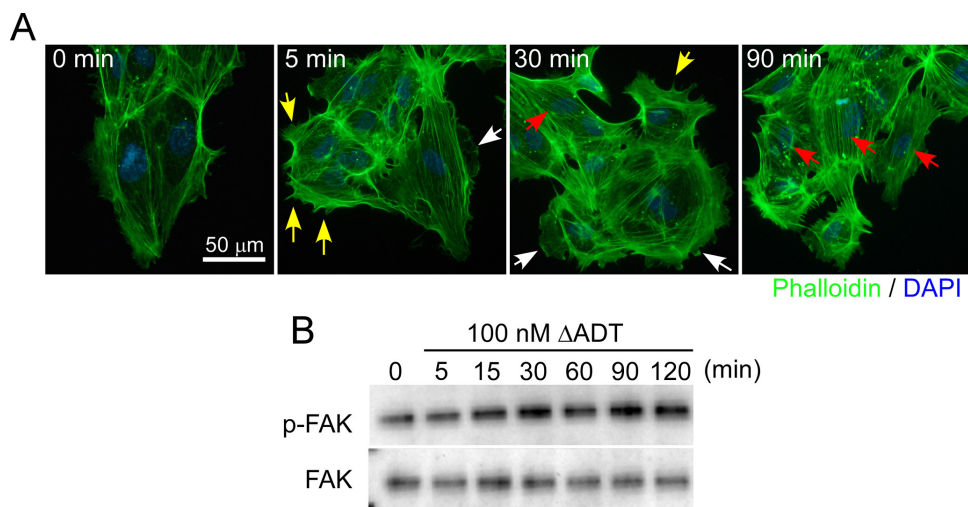


Figure 3. Δ ADT induced actin reorganization and phosphorylation of focal adhesion kinase (FAK) in HRMVEC. (A) After treatment with 100 nM truncated peptide of adrenotensin (Δ ADT) for 0, 5, 30, and 90 min, human retinal microvascular endothelial cells (HRMVECs) were representative cells at filamentous actin and nuclei were stained with Alexa Fluor 488 phalloidin and 4',6-diamidino-2-phenylindole (DAPI), respectively. Yellow arrow; filopodia, white arrow; membrane ruffling, red arrow; stress fiber. **(B)** Δ ADT induces FAK phosphorylation on Tyr397 in a time-dependent manner. Representative images of western blots are shown.

To determine whether the Δ ADT signaling pathway plays a role in regulating the polarization of the actin cytoskeleton, we evaluated the immunocytochemical location of actin in HRMVEC treated with or without Δ ADT. Figure 3A shows representative images of the reorganization of the actin cytoskeleton induced by 100 nM Δ ADT. In unstimulated serum-starved cells, actin filaments were localized mainly in the cortical region of the cells (0 min). After 5 min of stimulation with 100 nM Δ ADT, the cells

formed filopodia and membrane ruffling. Following prolonged treatment, the cells displayed prominent stress fibers related to cell contraction across the cell body (30 and 90 min). Focal adhesion kinase (FAK) is the pivotal molecule that controls the formation of focal adhesions, thereby providing the platform for cells to generate the locomotive force. Endothelial FAK is essential for vascular morphogenesis and vascular repair due to its central role in endothelial cell migration (21,22). To clarify whether FAK is

activated through autophosphorylation at Tyr397 by Δ ADT stimulation, we performed an immunoblot analysis with the HRMVECs after Δ ADT treatment. As shown in Figure 3B, tyrosine phosphorylation of FAK was increased in a time-dependent manner, and the levels of phosphorylation peaked at 30 min. This finding suggests that Δ ADT activates tyrosine phosphorylation of endothelial FAK, and implies that this leads to the formation of focal adhesion complexes. These results indicate that Δ ADT induces alterations in actin cytoskeleton dynamics and focal adhesion in endothelial cells.

In the present study, we identified Δ ADT derived from human retinal pericytes by LC-MS/MS analysis, and suggest that Δ ADT is a novel angiogenic peptide in endothelial cells. Δ ADT may play a role in angiogenesis as a novel factor of pericyte-endothelial cell interactions. At present, ADT and Δ ADT receptors remain unknown, but future research should provide further elucidation of these molecules. Within the context of retinal disease therapy, the above findings suggest that administering Δ ADT receptor antagonist or using antibodies against Δ ADT peptide may be effective for the treatment of retinal angiogenesis.

Acknowledgements

We thank Dr. Masato Kasuga for useful discussion. We also thank Ms. Keiko Kano for technical assistance. This work was supported in part by the Ministry of Health, Labour and Welfare, Japan (H20-009 and H25-016), and the National Center for Global Health and Medicine (23S104 and 24S111).

References

- Orlidge A, D'Amore PA. Inhibition of capillary endothelial cell growth by pericytes and smooth muscle cells. *J Cell Biol.* 1987; 105:1455-1462.
- Balabanov R, Dore-Duffy P. Role of the CNS microvascular pericyte in the blood-brain barrier. *J Neurosci Res.* 1998; 53:637-644.
- Dohgu S, Takata F, Yamauchi A, Nakagawa S, Egawa T, Naito M, Tsuruo T, Sawada Y, Niwa M, Kataoka Y. Brain pericytes contribute to the induction and up-regulation of blood-brain barrier functions through transforming growth factor- β production. *Brain Res.* 2005; 1038:208-215.
- Hori S, Ohtsuki S, Hosoya K, Nakashima E, Terasaki T. A pericyte-derived angiopoietin-1 multimeric complex induces occludin gene expression in brain capillary endothelial cells through Tie-2 activation *in vitro*. *J Neurochem.* 2004; 89:503-513.
- Armulik A, Abramsson A, Betsholtz C. Endothelial/pericyte interactions. *Circ Res.* 2005; 97:512-523.
- Clynen E, Baggerman G, Veelaert D, Cerstiaens A, Van der Horst D, Harthoorn L, Derua R, Waelkens E, De Loof A, Schoofs L. Peptidomics of the pars intercerebralis-corpora cardiaca complex of the migratory locust, *Locusta migratoria*. *Eur J Biochem.* 2001; 268:1929-1939.
- Schrader M, Schulz-Knappe P. Peptidomics technologies for human body fluids. *Trends Biotechnol.* 2001; 19:S55-60.
- Sasaki K, Satomi Y, Takao T, Minamino N. Snapshot peptidomics of the regulated secretory pathway. *Mol Cell Proteomics.* 2009; 8:1638-1647.
- Takahashi E, Okumura A, Unoki-Kubota H, Hirano H, Kasuga M, Kaburagi Y. Differential proteome analysis of serum proteins associated with the development of type 2 diabetes mellitus in the KK-A^y mouse model using the iTRAQ technique. *J Proteomics.* 2013; 84:40-51.
- Oertle T, van der Haar ME, Bandtlow CE, Robeva A, Burfeind P, Buss A, Huber AB, Simonen M, Schnell L, Brosamle C, Kaupmann K, Vallon R, Schwab ME. Nogo-A inhibits neurite outgrowth and cell spreading with three discrete regions. *J Neurosci.* 2003; 23:5393-5406.
- Clark IM, Cawston TE. Fragments of human fibroblast collagenase. Purification and characterization. *Biochem J.* 1989; 263:201-206.
- Ikeda Y, Imai Y, Kumagai H, Nosaka T, Morikawa Y, Hisaoka T, Manabe I, Maemura K, Nakaoka T, Imamura T, Miyazono K, Komuro I, Nagai R, Kitamura T. Vasorin, a transforming growth factor β -binding protein expressed in vascular smooth muscle cells, modulates the arterial response to injury *in vivo*. *Proc Natl Acad Sci U S A.* 2004; 101:10732-10737.
- Gerke V, Moss SE. Annexins: From structure to function. *Physiol Rev.* 2002; 82:331-371.
- Ernst S, Lange C, Wilbers A, Goebeler V, Gerke V, Rescher U. An annexin I N-terminal peptide activates leukocytes by triggering different members of the formyl peptide receptor family. *J Immunol.* 2004; 172:7669-7676.
- Rety S, Sopkova J, Renouard M, Osterloh D, Gerke V, Tabaries S, Russo-Marie F, Lewit-Bentley A. The crystal structure of a complex of p11 with the annexin II N-terminal peptide. *Nat Struct Biol.* 1999; 6:89-95.
- Hinson JP, Kapas S, Smith DM. Adrenomedullin, a multifunctional regulatory peptide. *Endocr Rev.* 2000; 21:138-167.
- Gumusel B, Chang JK, Hyman A, Lipton H. Adrenotensin: An ADM gene product with the opposite effects of ADM. *Life Sci.* 1995; 57:PL87-90.
- Li J, Ren Y, Dong X, Zhong G, Wu S, Tang C. Roles of different peptide fragments derived from proadrenomedullin in the regulation of vascular tone in isolated rat aorta. *Peptides.* 2003; 24:563-568.
- Xue H, Yuan P, Zhou L, Yao T, Huang Y, Lu LM. Effect of adrenotensin on cell proliferation is mediated by angiotensin II in cultured rat mesangial cells. *Acta Pharmacol Sin.* 2009; 30:1132-1137.
- Li W, Kong QY, Zhao CF, Zhao F, Li FH, Xia W, Wang R, Hu YM, Hua M. Adrenomedullin and adrenotensin regulate collagen synthesis and proliferation in pulmonary arterial smooth muscle cells. *Braz J Med Biol Res.* 2013; 46:1047-1055.
- Braren R, Hu H, Kim YH, Beggs HE, Reichardt LF, Wang R. Endothelial FAK is essential for vascular network stability, cell survival, and lamellipodial formation. *J Cell Biol.* 2006; 172:151-162.
- Chien S, Li S, Shiu YT, Li YS. Molecular basis of mechanical modulation of endothelial cell migration. *Front Biosci.* 2005; 10:1985-2000.

(Received October 14, 2016; Accepted November 5, 2015)

Endoscopic and surgical ampullectomy for non-invasive ampullary tumors: Short-term outcomes

Margaux Dubois^{1,§}, Ismail Labgaa^{1,§}, Gian Dorta^{2,*}, Nermin Halkic¹

¹Department of Visceral Surgery, Lausanne University Hospital (CHUV), Lausanne, Switzerland;

²Department of Gastroenterology and Hepatology, Lausanne University Hospital (CHUV), Lausanne, Switzerland.

Summary Non-invasive ampullary tumors, may be treated with endoscopic (EA) or surgical ampullectomy (SA). However, evidence on the morbidity of these techniques remains limited. This pilot study aimed to assess and compare morbidity of EA and SA. Patients undergoing EA or SA for non-invasive ampullary tumors were retrospectively analyzed and compared. Outcomes were postoperative complications graded with Clavien Classification and Comprehensive Complication Index (CCI), and length of stay (LoS). A review of the literature was performed to propose an evidence-based algorithm to treat ampullary tumors. A total of 11 EA and 19 SA were identified and analyzed. EA was associated with shorter intervention (51 vs. 191 min, $p < 0.001$) and decreased blood loss (0 vs. 100 mL, $p < 0.001$). Postoperative complications were more frequent after surgery compared to endoscopy (9% vs. 68%, $p = 0.002$). Surgical patients showed a higher CCI (0 vs. 8.7, $p < 0.001$). LoS was reduced in patients undergoing endoscopy (0 vs. 14 days, $p < 0.001$), with comparable readmissions rates ($p = 0.126$). Necessity of subsequent treatment was more frequent after endoscopic, compared to SA (5 vs. 1, $p = 0.016$). EA was associated with lower morbidity than SA and appeared as an appropriate first-line treatment for non-invasive ampullary tumors. SA remains a valuable alternative after EA failure.

Keywords: Ampulloma, ampullectomy, endoscopy, postoperative complications, morbidity

1. Introduction

Ampullary neoplasms are rare tumors accounting for 0.5% of gastrointestinal tumors, and displaying distinctive features related to their anatomical and pathological singularities (1). There is strong evidence for the risk of benign lesion to transform into malignant carcinoma (2). As a consequence, the indication to resect ampullary neoplasms, regardless of their grade, is widely accepted (1). Strikingly, no dedicated guidelines for the treatment of these tumors have been proposed so far. Although pancreaticoduodenectomy (PD) has been evidenced as the treatment of choice for invasive ampullary tumors (1,3), its high morbidity and

mortality may not be justified for non-invasive tumors. (4-6). Indeed, less invasive techniques such as surgical ampullectomy (SA) and endoscopic ampullectomy (EA) have been acknowledged as appropriate approaches for this indication (7-11). While a few studies comparing SA vs. EA have been reported, the morbidity related to these techniques has not been thoroughly assessed and compared (7,12).

This study thus aimed to provide a comprehensive assessment and comparison of the morbidity induced by EA and SA. In addition, it sought to generate a decision-making algorithm to treat ampullary neoplasms, primarily based on the available evidence from the literature.

2. Materials and Methods

This retrospective cohort study was conducted in the Departments of Visceral Surgery and Gastroenterology & Hepatology, Lausanne University Hospital (CHUV). This study was conducted in accordance with the STROBE criteria (<http://strobe-statement.org/>) and

Released online in J-STAGE as advance publication December 18, 2016.

[§]These authors contributed equally to this works.

*Address correspondence to:

Dr. Gian Dorta, Department of Gastroenterology and Hepatology, University Hospital of Lausanne (CHUV), CH-1011 Lausanne, Switzerland.

E-mail: Gian.Dorta@chuv.ch

registered under www.researchregistry.com (UIN: 577).

2.1. Patients and procedures

Patients undergoing EA or SA over the last 10 years (from 2005 to 2015) were identified from our prospective databases. Age < 18 years, immunosuppressive treatment and emergency surgery were considered as exclusion criteria. EA and SA were performed according to techniques described previously (7,12). Non-invasive ampullary tumor was defined as adenoma or in situ adenocarcinoma.

2.2. Data collection

Relevant demographics, comorbidities, preoperative assessment, details of the procedure and clinical outcomes were prospectively collected and anonymized in a computerized database. Operation duration was measured from incision to skin closure by the anesthetists. Intraoperative blood loss was estimated measuring the volume of aspirated fluid and soaked gauzes, jointly by the anesthetists and the surgeons. Postoperative complications were assessed by both the Clavien Classification (13) and the Comprehensive Complication Index (CCI) (14) within 30 postoperative days. Briefly, CCI is a score - ranging from 0 (no complication) to 100 (death) - that sums each postoperative complication. By avoiding underreported minor complications, CCI is a robust metric to assess morbidity. Length of stay (LoS) was calculated from day of surgery until discharge. Readmissions were considered

within 30 postoperative days.

Electronic search was performed using MEDLINE/ PubMed, Embase, Web of Knowledge, and The Cochrane Library. The search strategy was applied between January 1990 and June 30th 2016. Terms used were ampullectomy, ampulloma, ampullary tumor. Data from this systematic search were used to generate an algorithm for decision-making (Figure 1).

2.3. Statistical analysis

Normal continuous and categorical variables were compared using Student's *t* test and Chi-squared, respectively. A *p* value < 0.05 was considered to be statistically significant. Data analyses were performed using SPSS v20 statistical software (Chicago, IL).

3. Results and Discussion

3.1. Patients demographics and tumors characteristics

A total of 30 ampullectomies – with 11 EA and 19 SA - involving 24 patients were identified and analyzed. In term of demographics, the 2 groups were comparable for most variables (Table 1). On average, surgical patients were 4 years older than endoscopic patients (65 vs. 69 years, *p* = 0.024). None of the other demographics and comorbidities showed significant difference between the groups.

Tumors also displayed comparable characteristics in the 2 groups, with no difference in term of histological type (*p* = 0.573) or size (*p* = 0.953) (Table 1).

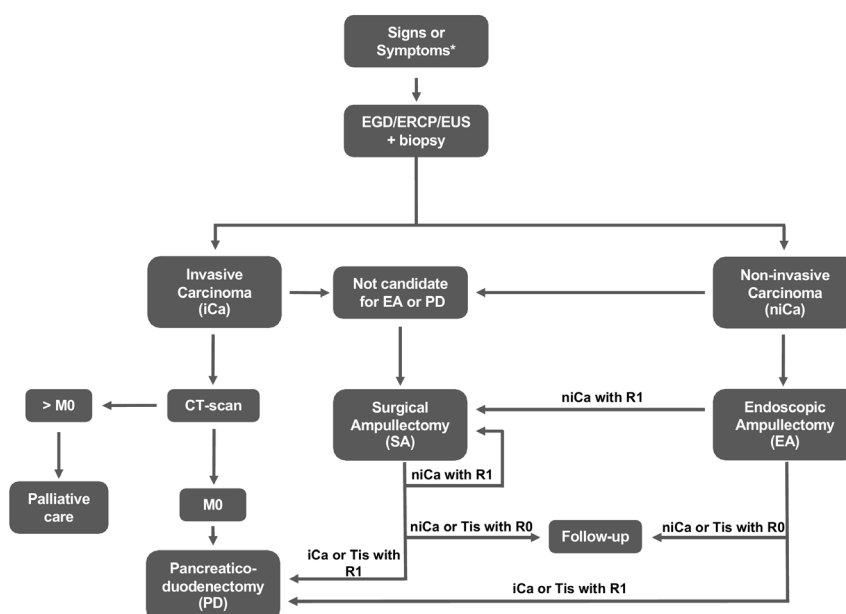


Figure 1. Decision-making of the treatment of ampullary tumors: an algorithm based on the evidence in the literature. EGD: Esophagogastroduodenoscopy. ERCP: Endoscopic Retrograde Cholangio-pancreatography. EUS: Endoscopic Ultrasound. niCa: Non-invasive Carcinoma. iCa: Invasive Carcinoma. Tis: Adenocarcinoma in situ. R0: Negative resection margins. R1: Positive resection margins. M0: Absence of distant metastasis. CT-scan: Computed Tomography. EA: Endoscopic Ampullectomy. SA: Surgical Ampullectomy. PD: Pancreaticoduodenectomy.

Table 1. Characteristics of patients and tumors

Items	Endoscopic ampullectomy (n = 11)	Surgical ampullectomy (n = 19)	p-value
Median age (years)	65 (52-74)	69 (67-81)	0.024
Gender (female)	7 (64)	12 (63)	1.000
ASA I/II	8 (80)	14 (74)	1.000
Median BMI (kg/m ²)	25 (21-27)	25 (21-28)	0.667
Diabetes	0	1 (5.3)	1.000
Smoker	3 (27)	7 (37)	0.702
Severe heart disease	3 (27)	6 (32)	1.000
Severe pulmonary disease	1 (9)	3 (16)	1.000
Immunosuppression	0	0	
FAP	3 (27)	1 (5.3)	0.126
Type of tumor			0.573
Inflammatory	1 (10)	2 (11)	
Adenoma	8 (80)	12 (63)	
Adenocarcinoma (Tis)	1 (10)	5 (26)	
Median Tumor size (mm)	15 (9-20)	14 (10-19)	0.953

EA: Endoscopic Ampullectomy. BMI: Body Mass Index. SA: Surgical Ampullectomy. FAP: Familial Adenomatous Polyposis. Tis: Adenocarcinoma *in situ*.

Table 2. Outcomes

Items	Endoscopic ampullectomy (n = 11)	Surgical ampullectomy (n = 19)	p-value
Median duration (min)	51 (29-71)	191 (181-210)	< 0.001
Median blood loss (mL)	0	100 (0-200)	< 0.001
Postoperative complications			
Overall	1 (9)	13 (68)	0.002
Minor I-II	1 (9)	10 (53)	0.023
Major III-IV	0	6 (32)	0.061
Grade V	0	0	–
CCI	0	9 (0-34)	< 0.001
Median length of stay (days)	0	14 (10-30)	< 0.001
Readmission	3 (27)	1 (5)	0.126
Further treatment requested	5 (45)	1 (5)	0.016

EA: Endoscopic Ampullectomy. SA: Surgical Ampullectomy. CCI: Comprehensive Complication Index.

3.2. Preoperative assessment

All of the patients underwent an endoscopic examination with either an Esophagogastroduodenoscopy (EGD), Endoscopic Retrograde Cholangio-pancreatography (ERCP) or Endoscopic Ultrasound (EUS) with subsequent biopsies. No further assessment is recommended for patients without invasive cancer and macroscopic features of malignancy (6). Patients who do not meet these two criteria should undergo a Computed Tomography scan (CT-scan) to exclude a metastasize disease, which will indicate the necessity of a palliative care.

Tumor size was assessed either by CT-scan or EUS. A cut-off of 2 cm was used to allocate treatment, namely EA or SA.

3.3. Outcomes

Intra- and postoperative outcomes are summarized in Table 2. Endoscopy was associated with shorter intervention (51 vs. 191 min, $p < 0.001$) and decreased blood loss (0 vs. 100 mL, $p < 0.001$). Overall, surgical patients experienced more postoperative complications

(9% vs. 68%, $p = 0.002$). Minor complications were significantly increased in the surgery group (9% vs. 53%, $p = 0.023$), whereas a trend was observed for major complications (0% vs. 32%, $p = 0.061$). Consistently, surgical patients showed a higher median CCI (0 vs. 8.7, $p < 0.001$). LoS was reduced in patients undergoing EA (0 vs. 14 days, $p < 0.001$), without increasing the readmissions (27% vs. 5%, $p = 0.126$). The proportion of patients necessitating subsequent treatment was higher in EA compared to SA (5 vs. 1, $p = 0.016$). Four patients initially treated with EA had to undergo SA for technical resectability reasons, while 1 patient underwent 2 EA procedures before necessitating SA; of note, the patient had familial adenomatous polyposis (FAP). In the SA group, 1 patient subsequently underwent PD because of recurrence.

3.4. Conclusions

EA was associated with more favorable outcomes than SA, in this cohort of patients treated for non-invasive ampullary tumors. Patients undergoing EA indeed showed lower complications rate and reduced LoS, in comparison to patients treated with SA.

Comparative studies on these less invasive alternatives reported that EA was associated with lower morbidity compared to SA (7,12). The comparison with previous studies is somehow awkward since they did not focus on postoperative complications, but rather reported overall morbidity without using a validated grading system (7,12). Notwithstanding, a landmark study by Ceppa *et al.* showed an overall morbidity of 18% for EA compared to 42% for patients undergoing surgery ($p = 0.006$) (7); these findings are indeed consistent with the present results.

Some drawbacks of the study need to be addressed. The study is mainly limited by its retrospective design and the small sample size, which may potentially influence the findings. Although it was not the aim of this study, assessing prognosis of patients undergoing EA vs. SA would enable to decipher whether one approach could offer longer survival than the other. There is an imperative need to design multicentric prospective studies in patients with ampullary tumors, to answer questions such as long-term survival, in this field. Nevertheless, the present study precisely detailed the landscape of complications after EA and SA. One could argue that the 2 groups were different for age; although significant, this difference was minor (65 vs. 69 years, $p = 0.024$) and is thus unlikely to be the only cause of the difference observed in outcomes. This report may serve as a tool to preoperatively provide precise risk rates to the patients.

Strikingly, there is a clear unmet need to define a clear consensus for the treatment of ampullary tumors. With this in mind, Figure 1 aimed to propose an algorithm to guide the decision-making for the preoperative assessment and for the treatment of ampullary neoplasms, primarily based on the evidence from the literature (3,7,8,12,15). This algorithm may be particularly pertinent to help gastroenterologists and hepatopancreatobiliary surgeons, to tailor their decision-making for the treatment of patients with non-invasive ampullary tumors. Patients frequently present with obstructive jaundice (20% in this cohort), but a variety of other unspecific symptoms may also occur, such as: abdominal pain, fatigue, weight loss or acute pancreatitis. The first step is to exclude gallstones, typically by abdominal ultrasound (US). The following measure is to perform tissue biopsies, which is critical for diagnostic purpose. This may be achieved either by ERCP/EGD or by EUS. The latter demonstrated a high sensitivity and is particularly accurate for the T staging which is key element since it determines the therapeutic modality (1,16-18). Further investigation with an abdominal CT-scan, should be performed if the pre-operative biopsies reveal an invasive carcinoma and/or if macroscopic malignant characteristics are observed during EGD/ERCP/EUS. These findings include features such as friable, ulcerative or hemorrhagic lesion, Oddi's sphincter invasion and extension to

common bile duct or pancreatic duct (1,7,15). In case of systemic disease, palliative care such as stenting could relieve patient's symptoms. The presence of invasive patterns is an indication for PD, unless the patient has contraindication for major surgery, in which case SA appears as a reasonable option (17). In case of non-invasive tumor, EA would be first considered given its lower morbidity, as confirmed by the present results. Nonetheless, SA is an alternative after EA failure or if EA is not amenable (8,15,18,19). The EA failure rate is indeed substantial, both in this series and in the literature. In this context, SA offers an appealing alternative that is efficient and safer than PD (19). If remaining malignancy is evidenced by the pathological analysis after either EA or SA, PD is further recommended. Conversely, if no evidence of malignancy is found, a follow-up with endoscopic surveillance is appropriate.

In summary, the present results suggest that EA may be associated with lower morbidity than SA, and may be considered as a first-line treatment for patients with non-invasive ampullary tumors. SA remains however a useful option after EA failure, or in patients with contraindications for EA or PD.

References

1. Panzeri F, Crippa S, Castelli P, Aleotti F, Pucci A, Partelli S, Zamboni G, Falconi M. Management of ampullary neoplasms: A tailored approach between endoscopy and surgery. *World J Gastroenterol.* 2015; 21:7970-7987.
2. Seifert E, Schulte F, Stolte M. Adenoma and carcinoma of the duodenum and papilla of Vater: A clinicopathologic study. *Am J Gastroenterol.* 1992; 87:37-42.
3. Askew J, Connor S. Review of the investigation and surgical management of resectable ampullary adenocarcinoma. *HPB (Oxford).* 2013; 15:829-838.
4. Menahem B, Guittet L, Mulliri A, Alves A, Lubrano J. Pancreaticogastrostomy is superior to pancreaticojejunostomy for prevention of pancreatic fistula after pancreaticoduodenectomy: An updated meta-analysis of randomized controlled trials. *Ann Surg.* 2015; 261:882-887.
5. Mathur A, Paul H, Ross S, Luberic K, Hernandez J, Vice M, Rosemurgy AS. Transduodenal ampullectomy for ampullary adenomas: A safe and effective procedure with long-term salutary outcomes. *Am Surg.* 2014; 80:185-190.
6. Gao Y, Zhu Y, Huang X, Wang H, Huang X, Yuan Z. Transduodenal ampullectomy provides a less invasive technique to cure early ampullary cancer. *BMC Surg.* 2016; 16:36.
7. Ceppa EP, Burbridge RA, Rialon KL, Omotosho PA, Emick D, Jowell PS, Branch MS, Pappas TN. Endoscopic versus surgical ampullectomy: An algorithm to treat disease of the ampulla of Vater. *Ann Surg.* 2013; 257:315-322.
8. Salmi S, Ezzedine S, Vitton V, Menard C, Gonzales JM, Desjeux A, Grimaud JC, Barthet M. Can papillary carcinomas be treated by endoscopic ampullectomy? *Surg Endosc.* 2012; 26:920-925.

9. Branum GD, Pappas TN, Meyers WC. The management of tumors of the ampulla of Vater by local resection. *Ann Surg.* 1996; 224:621-627.
10. de Castro SM, van Heek NT, Kuhlmann KF, Busch OR, Offerhaus GJ, van Gulik TM, Obertop H, Gouma DJ. Surgical management of neoplasms of the ampulla of Vater: Local resection or pancreatoduodenectomy and prognostic factors for survival. *Surgery.* 2004; 136:994-1002.
11. Clary BM, Tyler DS, Dematos P, Gottfried M, Pappas TN. Local ampullary resection with careful intraoperative frozen section evaluation for presumed benign ampullary neoplasms. *Surgery.* 2000; 127:628-633.
12. Onkendi EO, Naik ND, Rosedahl JK, Harmsen SW, Gostout CJ, Baron TH, Sr., Sarr MG, Que FG. Adenomas of the ampulla of Vater: A comparison of outcomes of operative and endoscopic resections. *J Gastrointest Surg.* 2014; 18:1588-1596.
13. Dindo D, Demartines N, Clavien PA. Classification of surgical complications: A new proposal with evaluation in a cohort of 6336 patients and results of a survey. *Ann Surg.* 2004; 240:205-213.
14. Slankamenac K, Graf R, Barkun J, Puhan MA, Clavien PA. The comprehensive complication index: A novel continuous scale to measure surgical morbidity. *Ann Surg.* 2013; 258:1-7.
15. Laleman W, Verreth A, Topal B, Aerts R, Komuta M, Roskams T, Van der Merwe S, Cassiman D, Nevens F, Verslype C, Van Steenberghe W. Endoscopic resection of ampullary lesions: A single-center 8-year retrospective cohort study of 91 patients with long-term follow-up. *Surg Endosc.* 2013; 27:3865-3876.
16. Skordilis P, Mouzas IA, Dimoulios PD, Alexandrakis G, Moschandrea J, Kouroumalis E. Is endosonography an effective method for detection and local staging of the ampullary carcinoma? A prospective study. *BMC Surg.* 2002; 2:1.
17. Song J, Liu H, Li Z, Yang C, Sun Y, Wang C. Long-term prognosis of surgical treatment for early ampullary cancers and implications for local ampullectomy. *BMC Surg.* 2015; 15:32.
18. Ardengh JC, Kemp R, Lima-Filho ER, Dos Santos JS. Endoscopic papillectomy: The limits of the indication, technique and results. *World J Gastrointest Endosc.* 2015; 7:987-994.
19. Schneider L, Contin P, Fritz S, Strobel O, Buchler MW, Hackert T. Surgical ampullectomy: An underestimated operation in the era of endoscopy. *HPB (Oxford).* 2016; 18:65-71.

(Received October 19, 2016; Revised November 16, 2016; Accepted November 29, 2016)

Guide for Authors

1. Scope of Articles

BioScience Trends is an international peer-reviewed journal. BioScience Trends devotes to publishing the latest and most exciting advances in scientific research. Articles cover fields of life science such as biochemistry, molecular biology, clinical research, public health, medical care system, and social science in order to encourage cooperation and exchange among scientists and clinical researchers.

2. Submission Types

Original Articles should be well-documented, novel, and significant to the field as a whole. An Original Article should be arranged into the following sections: Title page, Abstract, Introduction, Materials and Methods, Results, Discussion, Acknowledgments, and References. Original articles should not exceed 5,000 words in length (excluding references) and should be limited to a maximum of 50 references. Articles may contain a maximum of 10 figures and/or tables.

Brief Reports definitively documenting either experimental results or informative clinical observations will be considered for publication in this category. Brief Reports are not intended for publication of incomplete or preliminary findings. Brief Reports should not exceed 3,000 words in length (excluding references) and should be limited to a maximum of 4 figures and/or tables and 30 references. A Brief Report contains the same sections as an Original Article, but the Results and Discussion sections should be combined.

Reviews should present a full and up-to-date account of recent developments within an area of research. Normally, reviews should not exceed 8,000 words in length (excluding references) and should be limited to a maximum of 100 references. Mini reviews are also accepted.

Policy Forum articles discuss research and policy issues in areas related to life science such as public health, the medical care system, and social science and may address governmental issues at district, national, and international levels of discourse. Policy Forum articles should not exceed 2,000 words in length (excluding references).

Case Reports should be detailed reports of the symptoms, signs, diagnosis, treatment, and follow-up of an individual patient. Case reports may contain a demographic profile of the patient but usually describe an unusual or novel occurrence. Unreported or unusual

side effects or adverse interactions involving medications will also be considered. Case Reports should not exceed 3,000 words in length (excluding references).

News articles should report the latest events in health sciences and medical research from around the world. News should not exceed 500 words in length.

Letters should present considered opinions in response to articles published in BioScience Trends in the last 6 months or issues of general interest. Letters should not exceed 800 words in length and may contain a maximum of 10 references.

3. Editorial Policies

Ethics: BioScience Trends requires that authors of reports of investigations in humans or animals indicate that those studies were formally approved by a relevant ethics committee or review board.

Conflict of Interest: All authors are required to disclose any actual or potential conflict of interest including financial interests or relationships with other people or organizations that might raise questions of bias in the work reported. If no conflict of interest exists for each author, please state "There is no conflict of interest to disclose".

Submission Declaration: When a manuscript is considered for submission to BioScience Trends, the authors should confirm that 1) no part of this manuscript is currently under consideration for publication elsewhere; 2) this manuscript does not contain the same information in whole or in part as manuscripts that have been published, accepted, or are under review elsewhere, except in the form of an abstract, a letter to the editor, or part of a published lecture or academic thesis; 3) authorization for publication has been obtained from the authors' employer or institution; and 4) all contributing authors have agreed to submit this manuscript.

Cover Letter: The manuscript must be accompanied by a cover letter signed by the corresponding author on behalf of all authors. The letter should indicate the basic findings of the work and their significance. The letter should also include a statement affirming that all authors concur with the submission and that the material submitted for publication has not been published previously or is not under consideration for publication elsewhere. The cover letter should be submitted in PDF format. For example of Cover Letter, please visit <http://www.biosciencetrends.com/downcentre.php> (Download Centre).

Copyright: A signed JOURNAL PUBLISHING AGREEMENT (JPA) form must be provided by post, fax, or as a scanned file before acceptance of the article. Only forms with a hand-written signature are accepted. This copyright will ensure the widest possible dissemination of information. A form facilitating transfer of copyright can be downloaded by clicking the

appropriate link and can be returned to the e-mail address or fax number noted on the form (Please visit [Download Centre](#)). Please note that your manuscript will not proceed to the next step in publication until the JPA Form is received. In addition, if excerpts from other copyrighted works are included, the author(s) must obtain written permission from the copyright owners and credit the source(s) in the article.

Suggested Reviewers: A list of up to 3 reviewers who are qualified to assess the scientific merit of the study is welcomed. Reviewer information including names, affiliations, addresses, and e-mail should be provided at the same time the manuscript is submitted online. Please do not suggest reviewers with known conflicts of interest, including participants or anyone with a stake in the proposed research; anyone from the same institution; former students, advisors, or research collaborators (within the last three years); or close personal contacts. Please note that the Editor-in-Chief may accept one or more of the proposed reviewers or may request a review by other qualified persons.

Language Editing: Manuscripts prepared by authors whose native language is not English should have their work proofread by a native English speaker before submission. If not, this might delay the publication of your manuscript in BioScience Trends.

The Editing Support Organization can provide English proofreading, Japanese-English translation, and Chinese-English translation services to authors who want to publish in BioScience Trends and need assistance before submitting a manuscript. Authors can visit this organization directly at <http://www.iacmhr.com/iac-eso/support.php?lang=en>. IAC-ESO was established to facilitate manuscript preparation by researchers whose native language is not English and to help edit works intended for international academic journals.

4. Manuscript Preparation

Manuscripts should be written in clear, grammatically correct English and submitted as a Microsoft Word file in a single-column format. Manuscripts must be paginated and typed in 12-point Times New Roman font with 24-point line spacing. Please do not embed figures in the text. Abbreviations should be used as little as possible and should be explained at first mention unless the term is a well-known abbreviation (e.g. DNA). Single words should not be abbreviated.

Title Page: The title page must include 1) the title of the paper (Please note the title should be short, informative, and contain the major key words); 2) full name(s) and affiliation(s) of the author(s), 3) abbreviated names of the author(s), 4) full name, mailing address, telephone/fax numbers, and e-mail address of the corresponding author; and 5) conflicts of interest (if you have an actual or potential conflict of interest to disclose, it must be included as a footnote on the title page of the manuscript; if no conflict of

interest exists for each author, please state "There is no conflict of interest to disclose"). Please visit [Download Centre](#) and refer to the title page of the manuscript sample.

Abstract: The abstract should briefly state the purpose of the study, methods, main findings, and conclusions. For article types including Original Article, Brief Report, Review, Policy Forum, and Case Report, a one-paragraph abstract consisting of no more than 250 words must be included in the manuscript. For News and Letters, a brief summary of main content in 150 words or fewer should be included in the manuscript. Abbreviations must be kept to a minimum and non-standard abbreviations explained in brackets at first mention. References should be avoided in the abstract. Key words or phrases that do not occur in the title should be included in the Abstract page.

Introduction: The introduction should be a concise statement of the basis for the study and its scientific context.

Materials and Methods: The description should be brief but with sufficient detail to enable others to reproduce the experiments. Procedures that have been published previously should not be described in detail but appropriate references should simply be cited. Only new and significant modifications of previously published procedures require complete description. Names of products and manufacturers with their locations (city and state/country) should be given and sources of animals and cell lines should always be indicated. All clinical investigations must have been conducted in accordance with Declaration of Helsinki principles. All human and animal studies must have been approved by the appropriate institutional review board(s) and a specific declaration of approval must be made within this section.

Results: The description of the experimental results should be succinct but in sufficient detail to allow the experiments to be analyzed and interpreted by an independent reader. If necessary, subheadings may be used for an orderly presentation. All figures and tables must be referred to in the text.

Discussion: The data should be interpreted concisely without repeating material already presented in the Results section. Speculation is permissible, but it must be well-founded, and discussion of the wider implications of the findings is encouraged. Conclusions derived from the study should be included in this section.

Acknowledgments: All funding sources should be credited in the Acknowledgments section. In addition, people who contributed to the work but who do not meet the criteria for authors should be listed along with their contributions.

References: References should be numbered in the order in which they appear in the text. Citing of unpublished results, personal communications, conference abstracts, and theses in the reference list is not recommended but these sources may be mentioned in the text. In the reference list,

cite the names of all authors when there are fifteen or fewer authors; if there are sixteen or more authors, list the first three followed by *et al.* Names of journals should be abbreviated in the style used in PubMed. Authors are responsible for the accuracy of the references. Examples are given below:

Example 1 (Sample journal reference): Inagaki Y, Tang W, Zhang L, Du GH, Xu WF, Kokudo N. Novel aminopeptidase N (APN/CD13) inhibitor 24F can suppress invasion of hepatocellular carcinoma cells as well as angiogenesis. *Biosci Trends*. 2010; 4:56-60.

Example 2 (Sample journal reference with more than 15 authors): Darby S, Hill D, Auvinen A, *et al.* Radon in homes and risk of lung cancer: Collaborative analysis of individual data from 13 European case-control studies. *BMJ*. 2005; 330:223.

Example 3 (Sample book reference): Shalev AY. Post-traumatic stress disorder: diagnosis, history and life course. In: Post-traumatic Stress Disorder, Diagnosis, Management and Treatment (Nutt DJ, Davidson JR, Zohar J, eds.). Martin Dunitz, London, UK, 2000; pp. 1-15.

Example 4 (Sample web page reference): Ministry of Health, Labour and Welfare of Japan. Dietary reference intakes for Japanese. <http://www.mhlw.go.jp/houdou/2004/11/h1122-2a.html> (accessed June 14, 2010).

Tables: All tables should be prepared in Microsoft Word or Excel and should be arranged at the end of the manuscript after the References section. Please note that tables should not be image format. All tables should have a concise title and should be numbered consecutively with Arabic numerals. If necessary, additional information should be given below the table.

Figure Legend: The figure legend should be typed on a separate page of the main manuscript and should include a short title and explanation. The legend should be concise but comprehensive and should be understood without referring to the text. Symbols used in figures must be explained.

Figure Preparation: All figures should be clear and cited in numerical order in the text. Figures must fit a one- or two-column format on the journal page: 8.3 cm (3.3 in.) wide for a single column, 17.3 cm (6.8 in.) wide for a double column; maximum height: 24.0 cm (9.5 in.). Please make sure that the symbols and numbers appeared in the figures should be clear. Please make sure that artwork files are in an acceptable format (TIFF or JPEG) at minimum resolution (600 dpi for illustrations, graphs, and annotated artwork, and 300 dpi for micrographs and photographs). Please provide all figures as separate files. Please note that low-resolution images are one of the leading causes of article resubmission and schedule delays. All color figures will be reproduced in full color in the online edition of the journal at no cost to authors.

Units and Symbols: Units and symbols

conforming to the International System of Units (SI) should be used for physicochemical quantities. Solidus notation (*e.g.* mg/kg, mg/mL, mol/mm²/min) should be used. Please refer to the SI Guide www.bipm.org/en/si/ for standard units.

Supplemental data: Supplemental data might be useful for supporting and enhancing your scientific research and BioScience Trends accepts the submission of these materials which will be only published online alongside the electronic version of your article. Supplemental files (figures, tables, and other text materials) should be prepared according to the above guidelines, numbered in Arabic numerals (*e.g.*, Figure S1, Figure S2, and Table S1, Table S2) and referred to in the text. All figures and tables should have titles and legends. All figure legends, tables and supplemental text materials should be placed at the end of the paper. Please note all of these supplemental data should be provided at the time of initial submission and note that the editors reserve the right to limit the size and length of Supplemental Data.

5. Submission Checklist

The Submission Checklist will be useful during the final checking of a manuscript prior to sending it to BioScience Trends for review. Please visit [Download Centre](#) and download the Submission Checklist file.

6. Online Submission

Manuscripts should be submitted to BioScience Trends online at <http://www.biosciencetrends.com>. The manuscript file should be smaller than 5 MB in size. If for any reason you are unable to submit a file online, please contact the Editorial Office by e-mail at office@biosciencetrends.com.

7. Accepted Manuscripts

Proofs: Galley proofs in PDF format will be sent to the corresponding author via e-mail. Corrections must be returned to the editor (proof-editing@biosciencetrends.com) within 3 working days.

Offprints: Authors will be provided with electronic offprints of their article. Paper offprints can be ordered at prices quoted on the order form that accompanies the proofs.

Page Charge: Page charges will be levied on all manuscripts accepted for publication in BioScience Trends (\$140 per page for black white pages; \$340 per page for color pages). Under exceptional circumstances, the author(s) may apply to the editorial office for a waiver of the publication charges at the time of submission.

(Revised February 2013)

Editorial and Head Office:

Pearl City Koishikawa 603
2-4-5 Kasuga, Bunkyo-ku
Tokyo 112-0003 Japan
Tel: +81-3-5840-8764
Fax: +81-3-5840-8765
E-mail: office@biosciencetrends.com

JOURNAL PUBLISHING AGREEMENT (JPA)

Manuscript No.:

Title:

Corresponding Author:

The International Advancement Center for Medicine & Health Research Co., Ltd. (IACMHR Co., Ltd.) is pleased to accept the above article for publication in BioScience Trends. The International Research and Cooperation Association for Bio & Socio-Sciences Advancement (IRCA-BSSA) reserves all rights to the published article. Your written acceptance of this JOURNAL PUBLISHING AGREEMENT is required before the article can be published. Please read this form carefully and sign it if you agree to its terms. The signed JOURNAL PUBLISHING AGREEMENT should be sent to the BioScience Trends office (Pearl City Koishikawa 603, 2-4-5 Kasuga, Bunkyo-ku, Tokyo 112-0003, Japan; E-mail: office@biosciencetrends.com; Tel: +81-3-5840-8764; Fax: +81-3-5840-8765).

1. Authorship Criteria

As the corresponding author, I certify on behalf of all of the authors that:

- 1) The article is an original work and does not involve fraud, fabrication, or plagiarism.
- 2) The article has not been published previously and is not currently under consideration for publication elsewhere. If accepted by BioScience Trends, the article will not be submitted for publication to any other journal.
- 3) The article contains no libelous or other unlawful statements and does not contain any materials that infringes upon individual privacy or proprietary rights or any statutory copyright.
- 4) I have obtained written permission from copyright owners for any excerpts from copyrighted works that are included and have credited the sources in my article.
- 5) All authors have made significant contributions to the study including the conception and design of this work, the analysis of the data, and the writing of the manuscript.
- 6) All authors have reviewed this manuscript and take responsibility for its content and approve its publication.
- 7) I have informed all of the authors of the terms of this publishing agreement and I am signing on their behalf as their agent.

2. Copyright Transfer Agreement

I hereby assign and transfer to IACMHR Co., Ltd. all exclusive rights of copyright ownership to the above work in the journal BioScience Trends, including but not limited to the right 1) to publish, republish, derivate, distribute, transmit, sell, and otherwise use the work and other related material worldwide, in whole or in part, in all languages, in electronic, printed, or any other forms of media now known or hereafter developed and the right 2) to authorize or license third parties to do any of the above.

I understand that these exclusive rights will become the property of IACMHR Co., Ltd., from the date the article is accepted for publication in the journal BioScience Trends. I also understand that IACMHR Co., Ltd. as a copyright owner has sole authority to license and permit reproductions of the article.

I understand that except for copyright, other proprietary rights related to the Work (e.g. patent or other rights to any process or procedure) shall be retained by the authors. To reproduce any text, figures, tables, or illustrations from this Work in future works of their own, the authors must obtain written permission from IACMHR Co., Ltd.; such permission cannot be unreasonably withheld by IACMHR Co., Ltd.

3. Conflict of Interest Disclosure

I confirm that all funding sources supporting the work and all institutions or people who contributed to the work but who do not meet the criteria for authors are acknowledged. I also confirm that all commercial affiliations, stock ownership, equity interests, or patent-licensing arrangements that could be considered to pose a financial conflict of interest in connection with the article have been disclosed.

Corresponding Author's Name (Signature):

Date:

